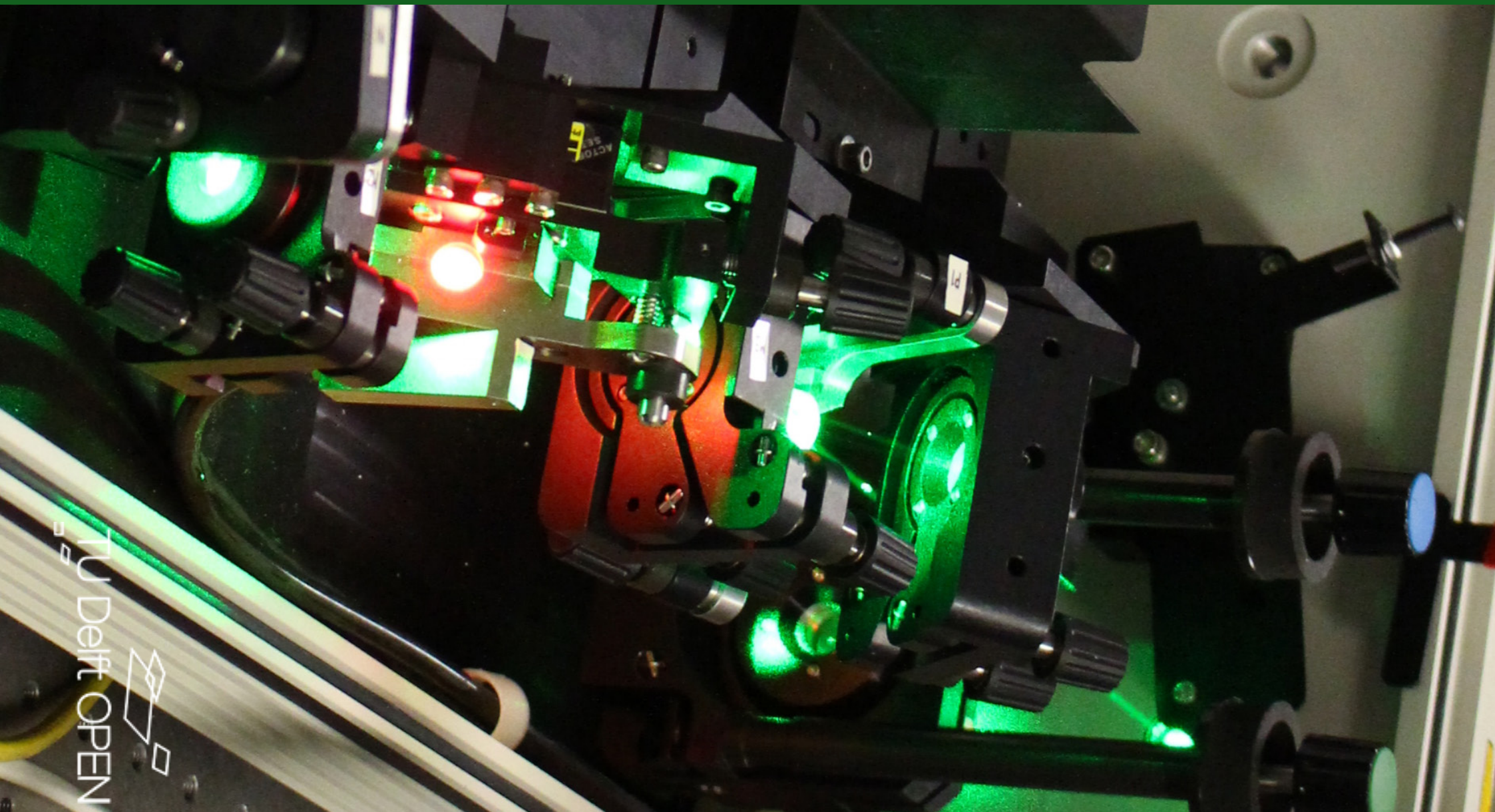
BSc Optics - 2nd edition

Sander Konijnenberg, Aurèle J.L. Adam & H. Paul Urbach



TU Delft OPEN

Contents

Preface	14
Basic Electromagnetic and Wave Optics	16
Electromagnetic Theory of Optics and Quantum Optics	17
The Maxwell Equations in Vacuum	17
Maxwell Equations in Matter	18
The Scalar and Vector Wave Equation	20
Time-Harmonic Solutions of the Wave Equation	21
Time-Harmonic Maxwell Equations in Matter	26
Electromagnetic Energy	31
Time-Averaged Energy of Time-Harmonic Fields	33
Reflection and Transmission at an Interface	34
Fiber Optics	45
Problems	46
Geometrical Optics	48
Introduction	48
Principle of Fermat	50
Some Consequences of Fermat's Principle	51
Perfect Imaging by Conic Sections	53
Gaussian Geometrical Optics	55
Beyond Gaussian Geometrical Optics	75
Problems	77
Optical Instruments	86
The Camera Obscura	86
The Camera	86
Camera in a Smart Phone	88

Contents (continued)

The Human Eye	88
The Magnifying Glass	92
Eyepieces	95
The Compound Microscope	96
The Telescope	97
Problems	98
Polarisation	102
Polarisation States and Jones Vectors	102
Creating and Manipulating Polarisation States	105
Linear Polariser or Wave Plate?	111
Decomposition of polarisation	112
Problems	113
Interference and Coherence	116
Introduction	116
Interference of Monochromatic Fields of the Same Frequency	117
Coherence	119
Temporal Coherence and the Michelson Interferometer	123
Spatial Coherence and Young's Experiment	126
More on Spatial Coherence	129
Stellar Interferometry	132
Fringe contrast	133
Fabry-Perot resonator	134
Interference and polarisation	139
Problems	141
Scalar Diffraction Optics	144

Contents (continued)

Introduction	144
Propagation of light through a homogeneous medium	145
Intuition for the Spatial Fourier Transform in Optics	149
Fresnel and Fraunhofer Approximations	151
Fraunhofer Diffraction Revisited	164
Fourier Optics	166
Super-resolution	173
Problems	177
Lasers	182
Unique Properties of Lasers	182
Optical Resonator	185
Amplification	187
Cavities	191
Problems with Laser Operation	192
Types of Lasers	196
Problems	198
About the Authors	200
References	202
Vector Calculus	208
The Lorentz Model for Material Dispersion	210
About the Conservation of Electromagnetic Energy	212
Electromagnetic Momentum	214
The Fourier Transform	216
Definitions	216
General Equations	216

Contents (continued)

Some Fourier transforms 216
Basis transformations 218
Algebraic Distance in Geometrical Optics 224
Definition 224
Properties 224
Algebraic distance in Optics 225
One Spherical Surface 225
Mirror 227
Spherical lens 228
Thin spherical lens 228



Delft University of Technology

Bachelor Applied Physics

BSc Optics

A.P.Konijnenberg
A.J.L.Adam
H.P.Urbach

Optics Research Group
Delft University of Technology

March-April 2024
Wednesday 13th March, 2024, 09:14



This Open Textbook is licensed under a Creative Commons Attribution 4.0 International (CC-BY-4.0), except where otherwise noted.

Cover image CC-BY TU Delft is a photograph of the inside of a femto-laser taken by Roland Horsten, Delft University of Technology. The final cover design was made by Marco Neeleman, Delft University of Technology Library.

The above copyright license which TU Delft Open uses for their original content does not extend to or include any special permissions which were granted to us by the rights holders for our use of their content.

Creative Commons conditions are not applicable to figures 1.13 down right (p. 36), 3.6 (p. 81), 2.24 (p. 67), 6.20 (p. 167), 6.21 (p. 169).

Every attempt has been made to ascertain the correct source of images and other potentially copyrighted material and ensure that all materials included in this book have been attributed and used according to their license. If you believe that a portion of the material infringes someone else's copyright, please contact the author a.j.l.adam@tudelft.nl

An electronic version of this Book is available at:
https://textbooks.open.tudelft.nl/textbooks

Title Open Textbook: BSc Optics
Authors: A.P. Konijnenberg, A.J.L. Adam, H.P. Urbach
Publisher: TU Delft Open
Second Edition
Year of publication: 2024
ISBN (softback/paperback): 978-94-6366-847-7
ISBN (e-book/PDF): 978-94-6366-846-0
DOI https://doi.org/10.59490/tb.91

Contents

Preface **5**

1 Basic Electromagnetic and Wave Optics **7**
1.1 Electromagnetic Theory of Optics and Quantum Optics . . . 8
1.2 The Maxwell Equations in Vacuum . . . 8
1.3 Maxwell Equations in Matter . . . 9
1.4 The Scalar and Vector Wave Equation . . . 11
1.5 Time-Harmonic Solutions of the Wave Equation . . . 12
1.5.1 Time-Harmonic Plane Waves . . . 12
1.5.2 Complex Notation for Time-Harmonic Functions . . . 13
1.5.3 Time-Harmonic Spherical Waves . . . 16
1.6 Time-Harmonic Maxwell Equations in Matter . . . 17
1.6.1 Time-Harmonic Electromagnetic Plane Waves . . . 18
1.6.2 Field of an Electric Dipole . . . 20
1.7 Electromagnetic Energy . . . 22
1.8 Time-Averaged Energy of Time-Harmonic Fields . . . 24
1.9 Reflection and Transmission at an Interface . . . 25
1.9.1 Boundary Conditions at an Interface . . . 26
1.9.2 Snell's Law . . . 28
1.9.3 Fresnel Coefficients . . . 29
1.9.4 Properties of the Fresnel Coefficients . . . 32
1.9.5 Total Internal Reflection and Evanescent Waves . . . 35
1.10 Fiber Optics . . . 36
Problems . . . 37

2 Geometrical Optics **39**
2.1 Introduction . . . 39
2.2 Principle of Fermat . . . 41
2.3 Some Consequences of Fermat's Principle . . . 42
2.4 Perfect Imaging by Conic Sections . . . 44
2.5 Gaussian Geometrical Optics . . . 46
2.5.1 Gaussian Imaging by a Single Spherical Surface . . . 46
2.5.2 Virtual Images and Virtual Objects of a Single Spherical Surface . . . 49
2.5.3 Ray Vectors and Ray Matrices . . . 50
2.5.4 The Lens Matrix . . . 54
2.5.5 Focusing with a Thin Lens . . . 56
2.5.6 Imaging with a Thin Lens . . . 56
2.5.7 Two Thin Lenses . . . 60
2.5.8 The Thick Lens . . . 63
2.5.9 Stops . . . 65
2.6 Beyond Gaussian Geometrical Optics . . . 66

2.6.1 Aberrations . . . 66
2.6.2 Diffraction . . . 67
Problems . . . 68

3 Optical Instruments **77**
3.1 The Camera Obscura . . . 77
3.2 The Camera . . . 77
3.3 Camera in a Smart Phone . . . 79
3.4 The Human Eye . . . 79
3.4.1 Anatomy . . . 79
3.4.2 Working of the eye . . . 79
3.4.3 Retina . . . 82
3.4.4 Dioptric Power of thin lenses. . . . 82
3.4.5 Eyeglasses . . . 82
3.4.6 New Correction Technique . . . 83
3.5 The Magnifying Glass . . . 83
3.5.1 Magnifying Power . . . 85
3.6 Eyepieces . . . 86
3.7 The Compound Microscope . . . 87
3.8 The Telescope . . . 88
Problems . . . 89

4 Polarisation **93**
4.1 Polarisation States and Jones Vectors . . . 93
4.2 Creating and Manipulating Polarisation States . . . 96
4.2.1 Jones Matrices . . . 98
4.2.2 Linear Polarisers . . . 99
4.2.3 Degree of Polarisation . . . 100
4.2.4 Quarter-Wave Plates . . . 100
4.2.5 Half-Wave Plates . . . 101
4.2.6 Full-Wave Plates . . . 102
4.3 Linear Polariser or Wave Plate? . . . 102
4.4 Decomposition of polarisation . . . 103
Problems . . . 104

5 Interference and Coherence **107**
5.1 Introduction . . . 107
5.2 Interference of Monochromatic Fields of the Same Frequency . . . 108
5.3 Coherence . . . 110
5.3.1 Coherence of Light Sources . . . 111
5.3.2 Polychromatic Light . . . 112
5.4 Temporal Coherence and the Michelson Interferometer . . . 114
5.5 Spatial Coherence and Young's Experiment . . . 117
5.6 More on Spatial Coherence . . . 120
5.7 Stellar Interferometry . . . 123
5.8 Fringe contrast . . . 124
5.9 Fabry-Perot resonator . . . 125
5.10 Interference and polarisation . . . 130
Problems . . . 132

6 Scalar Diffraction Optics **135**
6.1 Introduction . . . 135
6.2 Propagation of light through a homogeneous medium . . . 136
6.2.1 Angular Spectrum Method . . . 136
6.2.2 Rayleigh-Sommerfeld Diffraction Integral . . . 139
6.3 Intuition for the Spatial Fourier Transform in Optics . . . 140
6.4 Fresnel and Fraunhofer Approximations . . . 142
6.4.1 Fresnel Approximation . . . 146
6.4.2 Fraunhofer Approximation . . . 147
6.4.3 Examples of Fresnel and Fraunhofer approximations . . . 149
6.4.3.1 Fresnel approximation of the field of two point sources. . . . 149
6.4.3.2 Fraunhofer approximation of a rectangular aperture in a screen. 150
6.4.3.3 Fresnel approximation of a rectangular aperture in a mask . . . 151
6.4.3.4 Fraunhofer approximation of a periodic array of slits . . . 151
6.5 Fraunhofer Diffraction Revisited . . . 155
6.6 Fourier Optics . . . 157
6.6.1 Focusing of a Parallel Beam . . . 157
6.6.2 Imaging by a lens . . . 162
6.6.3 Spatial Light Modulators and Optical Fourier Filtering . . . 164
6.7 Super-resolution . . . 164
Problems . . . 168

7 Lasers **173**
7.1 Unique Properties of Lasers . . . 173
7.1.1 Narrow Spectral Width; High Temporal Coherence . . . 174
7.1.2 Highly Collimated Beam . . . 174
7.1.3 Diffraction-Limited Focused Spot; High Spatial Coherence . . . 175
7.1.4 High Power . . . 175
7.1.5 Wide Tuning Range . . . 176
7.2 Optical Resonator . . . 176
7.3 Amplification . . . 178
7.3.1 The Einstein Coefficients . . . 179
7.3.2 Relation Between the Einstein Coefficients . . . 179
7.3.3 Population Inversion . . . 181
7.4 Cavities . . . 182
7.5 Problems with Laser Operation . . . 183
7.6 Types of Lasers . . . 187
7.6.1 Optical Pumping . . . 187
7.6.2 Electron-Collision Pump . . . 187
7.6.3 Atomic Collision . . . 188
7.6.4 Chemical Pump . . . 188
7.6.5 Semiconductor Laser . . . 189
Problems . . . 189

About the Authors **191**

References **193**

Appendices

A Vector Calculus **199**

B The Lorentz Model for Material Dispersion **201**

C About the Conservation of Electromagnetic Energy **203**

D Electromagnetic Momentum **205**

E The Fourier Transform **207**
E.1 Definitions . . . 207
E.2 General Equations . . . 207
E.3 Some Fourier transforms . . . 207

F Basis transformations **209**

G Algebraic Distance in Geometrical Optics **215**
G.1 Definition . . . 215
G.2 Properties . . . 215
G.3 Algebraic distance in Optics . . . 216
G.4 One Spherical Surface . . . 216
G.5 Mirror . . . 218
G.6 Spherical lens . . . 219
G.7 Thin spherical lens . . . 219

Preface

This book is about optics for advanced undergraduate and beginning graduate students of physics, electrical engineering and related fields. As a student of these subjects you are probably already familiar with many concepts of optics and the nature of light. You may remember Snell's law of refraction, the lens formula, ray tracing and interference fringes as observed in the double-slit experiment. By now you have also learned that from Maxwell's equations one can derive that light consists of electromagnetic waves, that its speed c was found to be constant, which resulted in the development of the theory of relativity, and that light exhibits a wave-particle duality that is explained by the De Broglie hypothesis in quantum mechanics. Although this is already a rather sizeable body of knowledge, there is still a lot to learn about optics. However, many of the important topics of optics do not require knowledge of quantum mechanics or even Maxwell's equations. Instead, they concern approximate theories and models of the behaviour of light which are sufficiently advanced to explain the phenomena and sufficiently simple so that explicit computations of (approximate) solutions are possible. Using simplified models such a geometrical optics to study problems leads to approaches that differ quite substantially from applying more rigorous theories such as Maxwell's equations. However, the simplified model give in many circumstances more insight in the physical phenomena and furthermore Maxwell's equations are much too complicated to apply to macroscopic imaging systems in microscopy, lithography or astronomy. This will remain the case for a long time to come in spite of increasing computer resources. When studying different approximate models it is essential to understand their hierarchy and the limits of validity of the approximations made.

Maybe you wonder why you will learn to apply theories which are from the fundamental point of view not correct. But remember that in the end all of physics is merely a model that tries to describe reality. Some models, which tend to be more complex, are more accurate than others, but depending on the phenomena we want to predict, a simpler, less accurate model may suffice. For example in many practical cases, such as the modelling of imaging formation in cameras, geometrical optics is already sufficiently accurate and a model based on Maxwell's equations or even a model based on the scalar wave equation would be too computationally demanding. From a pedagogical point of view, it surely seems preferable to learn the simpler model prior to learning the more accurate model.

We remark that what you will learn from this book applies to a much larger part of physics than only optics. In fact, optics refers strictly speaking only to electromagnetic fields of visible wavelengths from 390 nm to 780 nm. However, everything we will discuss applies to electromagnetic radiation of any wavelength, from γ radiation of 10^{-13} nm wavelength to long radio waves of more than 10^3 m wavelength. Since the approximate theories that we will discuss, such as geometrical optics, are valid provided the wavelength is sufficiently small compared to the size of the objects in the problem, these theories apply also to any of the above-mentioned wavelengths, provided the same ratio of wavelength to typical size of the objects holds.

We summarize the content of the book. In Chapter 1 we recall some basic facts about Maxwell's equations and show in particular how the wave equation is derived from these equations. Then we discuss some special solutions of Maxwell's equations, such as plane waves and the field emitted by an electric dipole. The use of complex notation for the important case of time-harmonic fields is reviewed. The derivation of the Fresnel reflection and transmission coeffi-

cients of a plane wave incident on an interface is so general that the results apply also to materials with absorption. Evanescent waves are studied in the context of total internal reflection.
In subsequent chapters of the book it is assumed that the reader is familiar with the main part of the topics treated in Chapter 1.

In Chapter 2, we study light from the point of view of **Geometrical Optics**. This model of optics applies to cases where the wavelength of light can be considered to be much smaller than other lengths in the problem. In geometrical optics, light is considered to travel as rays. With this concept we can explain phenomena observed in for example the pinhole camera or simple microscopes and telescopes. As the basis of geometrical optics we use the Principle of Fermat. Next, the paraxial theory is introduced. Ray matrices are used extensively, in particular in the study of a thick lens.

In Chapter 3 geometrical optics is applied to some imaging systems such as the pinhole camera, an ordinary camera, the human eye, the microscope and the telescope.

Then in Chapter 4 different kinds of **polarisation of light** are studied and how these can be manipulated. Here Jones matrices and Jones vectors are used.

In Chapter 5, the theory of time and spatial coherence is explained. The superposition of light waves is discussed and the phenomenon of interference of light and how this is linked to the degree of coherence is explained. The change of the degree of coherence during the propagation of light is derived and applied to stellar interferometry.

In Chapter 6 we treat **Diffraction Optics**. In this model light is described as a wave. With this theory one can explain phenomena such as interference fringes caused by the interaction of light with structures of finite size such as a slit or aperture in a screen. Furthermore, diffraction gratings and applications to spectroscopy are studied and the limit of resolution of a diffraction limited imaging system is derived.

Finally, in Chapter 7 the unique properties of **lasers and their applications** are discussed. In the treatment of lasers, many of the properties of light discussed in previous chapters will play a role, in particular coherence. A laser contains an optical resonator with a medium which amplifies the light by stimulated emission. To understand the mechanism of stimulated emission, the theory of Einstein is discussed.

All chapters are followed by Problems. Advanced problems are noted by a *. Finally, in the Appendix some background such as vector calculus, the Lorentz Model for material dispersion and a list of Fourier transformations is given.

The digital version of the book contains links to websites with useful demonstrations and is freely available at https://textbooks.open.tudelft.nl/textbooks.

A upcoming version augmented with questions and interactive graphs is available freely at https://textbooks.open.tudelft.nl/textbooks/catalog/book/90

The book has profited from constructive criticisms of many students that have attended the course over the years. The authors like to thank in particular the teaching assistants Yifeng Shao, Marco Mout, Paulo Ansuinelli, Po-Ju Chen, Thomas van den Hooven, Xukang Wei, Alex Heemels, Thomas Kotte and Luuk Zonneveld for their help in pointing out mistakes and inconsistencies. For the third version, we thank the following lecturers Tom van der Reep, Martijn Anthonissen, Rob Harr and Miriam Menzel. For the remaining errors solely the authors are responsible.

Delft, 2022-2024 A.P.K., A.J.L.A., H.P.U.

Chapter 1

Basic Electromagnetic and Wave Optics

What you should know and be able to after studying this chapter

This chapter is about Maxwell's equations and is a prerequisite for the rest of the book. It is assumed that the reader is already familiar with electromagnetism at the bachelor level. Therefore the treatments of Maxwell's equations in matter, boundary conditions at interfaces, electromagnetic energy, the field of an electric dipole and the reflection and transmission at an interface are rather concise.

After studying this chapter you should know and be able to

- Derive the scalar wave equation for the electromagnetic field components from Maxwell's equations.
- Work with the complex notation of time harmonic fields.
- Understand time harmonic plane waves, spherical waves and the concept of wave fronts.
- Know the main properties of the field radiated by a time-harmonic electric dipole and understand that it is the fundamental solution of Maxwell's equations from which the radiation of any time-harmonic source can be derived.
- Qualitatively understand the far field radiation pattern of a time-harmonic electric dipole (you do not need to know the formulas).
- Derive long-time averages of products of time-harmonic functions.
- Compute the rate of energy flow using the Poynting vector and its long-time average. The derivation of the law of conservation of electromagnetic energy is not part of the exam.
- Understand the method of deriving the reflection and transmission of an incident plane wave at an interface by separating in s- and p-polarised states. The formulas for the Fresnel coefficients do not have to be known by heart.
- Understand the Brewster angle, total internal reflection and evanescent waves.
- Understand the principle of the guiding of electromagnetic waves.

1.1 Electromagnetic Theory of Optics and Quantum Optics

Maxwell's equations provide a very complete description of light which includes diffraction, interference and polarisation. Yet it is strictly speaking not fully accurate, because it allows monochromatic electromagnetic waves to carry any amount of energy, whereas according to quantum optics the energy is quantised. According to quantum optics, light is a flow of massless particles, the photons, which each carry an extremely small quantum of energy: $\hbar\omega$, where $\hbar = 6.63\times10^{-34}/(2\pi)$ Js and ω is the frequency, which for visible light is of the order 5×10^{14} Hz. Hence for visible light $\hbar\omega \approx 3.3\times10^{-19}$ J.

Quantum optics is mainly important in experiments involving a small number of photons, i.e. at very low light intensities and for specially prepared photons states (e.g. entangled states) for which there is no classical description. In almost all applications of optics the light sources emit so many photons that quantum effects are irrelevant (see Fig. 1.1).

Light Source	Number of photons/(s×m^2)
Laserbeam (10 mW, He-Ne, focused to 20 μm)	10^{26}
Laserbeam (1 mW, He-Ne)	10^{21}
Bright sunlight on earth	10^{18}
Indoor light level	10^{16}
Twilight	10^{14}
Moonlight on earth	10^{12}
Starlight on earth	10^{10}

Table 1.1: The mean photon flux density for some common sources.

The visible light spectrum is only a small part of the overall electromagnetic spectrum (see Fig. 1.1). The results we will derive are however generally valid for electromagnetic waves of any frequency.

1.2 The Maxwell Equations in Vacuum

In vacuum, an electromagnetic field, and hence also visible light, is described by the vector fields $\boldsymbol{\mathcal{E}}(\mathbf{r},t)$ [Volt/m][1] and $\boldsymbol{\mathcal{B}}(\mathbf{r},t)$ [Tesla=Weber/m^2= kg/(C s)], which in general vary with position $\mathbf{r}$ and time t. These vector fields are traditionally called the electric field strength and the magnetic induction, respectively, and together they are referred to as "the electromagnetic field". This terminology is explained by the fact that when the field vaires with time (as is always the case in optics), the electric and magnetic fields always occur together, i.e. one does not exist without the other. Only when the fields are independent of time, an electric field can exist without a magnetic field and conversely. The first case is called electrostatics, the second magnetostatics.

Time-dependent electromagnetic fields are generated by moving electric charges, called the sources. Let the source have charge density $\rho(\mathbf{r},t)$ [C/m^3] and current density $\boldsymbol{\mathcal{J}}(\mathbf{r},t)$ [C/(s m^3)]. Since charge can neither be created nor destroyed, the rate of increase of charge inside a volume

[1] Units of physical quantities are written between brackets [.].

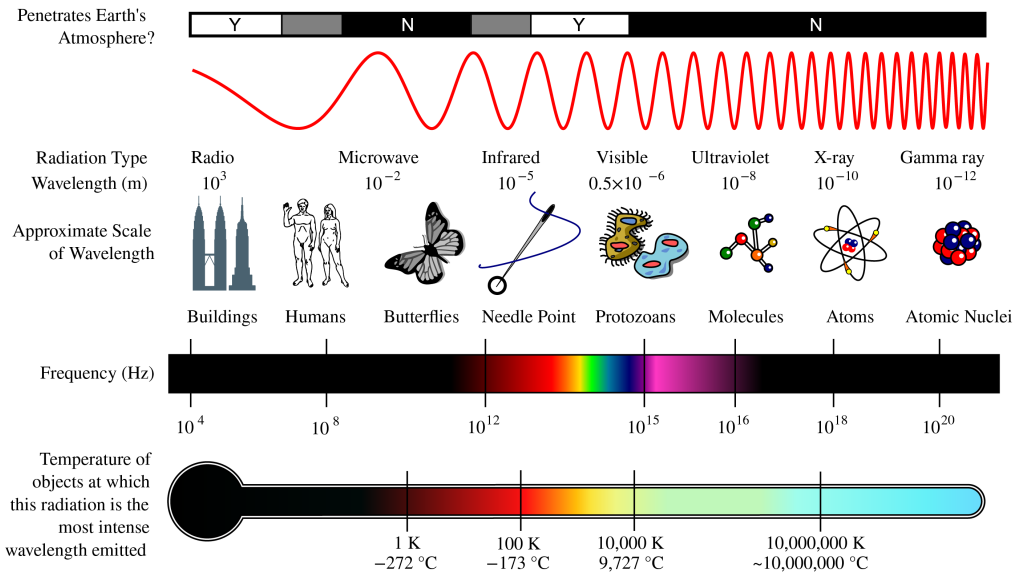


Figure 1.1: The electromagnetic spectrum (from Wikimedia Commons by NASA/ CC BY-SA).

V must be equal to the net flux of charges passing through the surface S bounding V from the outside to the inside, i.e.:

$$\frac{d}{dt}\int_V \varrho \, \mathrm{d}V = -\int_S \boldsymbol{\mathcal{J}} \cdot \hat{\mathbf{n}} \, \mathrm{d}S, \tag{1.1}$$

where $\hat{\mathbf{n}}$ is the outward-pointing unit normal on S. Using the Gauss divergence theorem (A.13), the right-hand side of (1.1) can be converted to a volume integral from which follows the differential form of the law of conservation of charge:

$$-\nabla \cdot \boldsymbol{\mathcal{J}} = \frac{\partial \rho}{\partial t}. \tag{1.2}$$

At every point in vacuum and at every time, the field vectors $\boldsymbol{\mathcal{E}}$ and $\boldsymbol{\mathcal{B}}$ satisfy Maxwell's equations[2,3]:

$$\nabla \times \boldsymbol{\mathcal{E}} = -\frac{\partial \boldsymbol{\mathcal{B}}}{\partial t}, \qquad \text{Faraday's Law,} \tag{1.3}$$

$$\nabla \times \frac{\boldsymbol{\mathcal{B}}}{\mu_0} = \epsilon_0 \frac{\partial \boldsymbol{\mathcal{E}}}{\partial t} + \boldsymbol{\mathcal{J}}, \qquad \text{Maxwell's Law,} \tag{1.4}$$

$$\nabla \cdot \epsilon_0 \boldsymbol{\mathcal{E}} = \varrho, \qquad \text{Gauss's Law,} \tag{1.5}$$

$$\nabla \cdot \boldsymbol{\mathcal{B}} = 0, \qquad \text{no magnetic charge.} \tag{1.6}$$

where $\epsilon_0 = 8.8544\times10^{-12}\ \mathrm{C^2N^{-1}\,m^{-2}}$ is the dielectric permittivity and $\mu_0 = 1.2566\times10^{-6}\ \mathrm{m\,kg\,C^{-2}}$ is the magnetic permeability of vacuum. The quantity $c = (1/\epsilon_0\mu_0)^{1/2} = 2.997\,924\,58 \times 10^8$ m/s is the speed of light in vacuum and $Z = \sqrt{\mu_0/\epsilon_0}$=377 Ω =377 V s/C is the impedance of vacuum.

1.3 Maxwell Equations in Matter

Atoms are neutral and consist of a positively charged nucleus surrounded by a cloud of negatively charged electrons. In an electric field, the centre of the positive charges and the centre of the

[2]Khan Academy - Faraday's Law Introduction
[3]Khan Academy - Magnetic field created by a current carrying wire (Ampere's Law)

negative charges get displaced with respect to each other. Therefore, an atom in an electric field behaves like an electric dipole. In polar molecules, the centres of charge of the positive and negative charges are permanently separated, even without an electric field. But without an electric field, they are randomly orientated and therefore have no net effect, while in the presence of an electric field they line up parallel to the field. Whatever the precise mechanism, an electric field induces a certain net dipole moment density per unit volume $\boldsymbol{\mathcal{P}}(\mathbf{r})$ [C/m^2] in matter which is proportional to the *local* electric field $\boldsymbol{\mathcal{E}}(\mathbf{r})$:

$$\boldsymbol{\mathcal{P}}(\mathbf{r},t) = \epsilon_0 \chi_e \boldsymbol{\mathcal{E}}(\mathbf{r},t), \tag{1.7}$$

where χ_e is the electric susceptibility of the material (a dimensionless quantity). A dipole moment which varies with time radiates an electromagnetic field. It is important to realize that in (1.7) $\boldsymbol{\mathcal{E}}$ is the total local electric field at the position of the dipole, i.e. it contains the contribution of all other dipoles which are excited and hence also radiate an electromagnetic field. Only in the case of dilute gasses, the electromagnetic interaction between dipoles can be neglected. Then the local electric field is simply given by the field emitted by a source external to the matter under consideration.

A dipole moment density that changes with time corresponds to a current density $\boldsymbol{\mathcal{J}}_p$ [Ampere/m^2=C/(m^2 s)] and a charge density ϱ_p [C/m^3] given by

$$\begin{aligned} \boldsymbol{\mathcal{J}}_p(\mathbf{r},t) &= \frac{\partial \boldsymbol{\mathcal{P}}(\mathbf{r},t)}{\partial t} = \epsilon_0 \chi_e \frac{\partial \boldsymbol{\mathcal{E}}(\mathbf{r},t)}{\partial t}, & (1.8)\\ \varrho_p(\mathbf{r},t) &= -\nabla \cdot \boldsymbol{\mathcal{P}}(\mathbf{r},t) = -\nabla \cdot (\epsilon_0 \chi_e \boldsymbol{\mathcal{E}}). & (1.9) \end{aligned}$$

All materials conduct electrons to a certain extent, although the conductivity σ [Ampere/(Volt.m) =C/(Volt.s)] differs greatly between dielectrics, semi-conductors and metals (the conductivity of copper is 10^7 times that of a good conductor such as sea water and 10^{19} times that of glass). The current density $\boldsymbol{\mathcal{J}}_c$ and the charge density corresponding to the conduction electrons satisfy:

$$\begin{aligned} \boldsymbol{\mathcal{J}}_c &= \sigma \boldsymbol{\mathcal{E}}, & (1.10)\\ \frac{\partial \varrho_c}{\partial t} &= -\nabla \cdot \boldsymbol{\mathcal{J}}_c = -\nabla \cdot (\sigma \boldsymbol{\mathcal{E}}), & (1.11) \end{aligned}$$

where (1.10) is Ohm's Law. The total current density on the right-hand side of Maxwell's Law (1.4) is the sum of $\boldsymbol{\mathcal{J}}_p$, $\boldsymbol{\mathcal{J}}_c$ and an external current density $\boldsymbol{\mathcal{J}}_{ext}$. The latter we assume to be known. Similarly, the total charge density at the right of (1.5) is the sum of ϱ_p, ϱ_c and a given external charge density ϱ_{ext}. The latter is linked to the external current density by the law of conservation of charge (1.2). Hence, (1.4) and (1.5) become

$$\begin{aligned} \nabla \times \frac{\boldsymbol{\mathcal{B}}}{\mu_0} &= \epsilon_0 \frac{\partial \boldsymbol{\mathcal{E}}}{\partial t} + \boldsymbol{\mathcal{J}}_p + \boldsymbol{\mathcal{J}}_c + \boldsymbol{\mathcal{J}}_{ext} \\ &= \epsilon_0 (1+\chi_e) \frac{\partial \boldsymbol{\mathcal{E}}}{\partial t} + \sigma \boldsymbol{\mathcal{E}} + \boldsymbol{\mathcal{J}}_{ext} & (1.12)\\ \nabla \cdot \epsilon_0 \boldsymbol{\mathcal{E}} &= \varrho_p + \varrho_c + \varrho_{ext}, \\ &= -\nabla \cdot (\epsilon_0 \chi_e \boldsymbol{\mathcal{E}}) + \varrho_c + \varrho_{ext}. & (1.13) \end{aligned}$$

We define the permittivity ϵ in matter by

$$\epsilon = \epsilon_0 (1+\chi_e). \tag{1.14}$$

Then (1.12) and (1.13) can be written as

$$\begin{aligned} \nabla \times \frac{\boldsymbol{\mathcal{B}}}{\mu_0} &= \epsilon \frac{\partial \boldsymbol{\mathcal{E}}}{\partial t} + \sigma \boldsymbol{\mathcal{E}} + \boldsymbol{\mathcal{J}}_{ext}, & (1.15)\\ \nabla \cdot (\epsilon \boldsymbol{\mathcal{E}}) &= \varrho_c + \varrho_{ext}. & (1.16) \end{aligned}$$

It is the purpose of Problem 1 of the problem section of this chapter to demonstrate that in a conductor any accumulation of charge is extremely quickly reduced to zero. Therefore we may assume that

$$\varrho_c = 0. \tag{1.17}$$

If the material is magnetic, the magnetic permeability is different from vacuum and is written as $\mu = \mu_0(1 + \chi_m)$, where χ_m is the (dimensionless) magnetic susceptibility. In Maxwell's equations, one should then replace μ_0 by μ. However, at optical frequencies magnetic effects are negligible (except in ferromagnetic materials, which are rare). **We will therefore always assume that the magnetic permeability is that of vacuum:** $\mu = \mu_0$.

It is customary to define the magnetic field by $\boldsymbol{\mathcal{H}} = \boldsymbol{\mathcal{B}}/\mu_0$ [Ampere/m=C/(ms)]. By using the magnetic field $\boldsymbol{\mathcal{H}}$ instead of the magnetic induction $\boldsymbol{\mathcal{B}}$, Maxwell's equations become more symmetric:

$$\nabla \times \boldsymbol{\mathcal{E}} = -\mu_0 \frac{\partial \boldsymbol{\mathcal{H}}}{\partial t}, \qquad \text{Faraday's Law,} \tag{1.18}$$

$$\nabla \times \boldsymbol{\mathcal{H}} = \epsilon \frac{\partial \boldsymbol{\mathcal{E}}}{\partial t} + \sigma \boldsymbol{\mathcal{E}} + \boldsymbol{\mathcal{J}}_{ext}, \qquad \text{Maxwell's Law,} \tag{1.19}$$

$$\nabla \cdot \epsilon \boldsymbol{\mathcal{E}} = \varrho_{ext}, \qquad \text{Gauss's Law,} \tag{1.20}$$

$$\nabla \cdot \boldsymbol{\mathcal{H}} = 0. \qquad \text{no magnetic charge.} \tag{1.21}$$

This form of Maxwell's equations in matter will be used in this book. It is seen that the Maxwell equations in matter are identical to those in vacuum, with ϵ substituted for ϵ_0.

We end this section by remarking that our derivations are valid for non-magnetic materials which are electrically isotropic. This means that the magnetic permeability is that of vacuum and that the permittivity ϵ is a scalar. In an anisotropic dielectric the induced dipole vectors are in general not parallel to the local electric field. Then χ_e and therefore also ϵ become matrices. Throughout the major part of this book matter is assumed to be non-magnetic and electrically isotropic. The only exception is wave plates. which are discussed in Chapter 4. These devices are made of an anisotropic material and are used to change the polarisation of light.

1.4 The Scalar and Vector Wave Equation

We consider a homogeneous insulator (i.e. ϵ is independent of position and σ=0) in which there are no external sources:

$$\boldsymbol{\mathcal{J}}_{ext} = 0, \quad \varrho_{ext} = 0. \tag{1.22}$$

In optics the external source, e.g. a laser, is normally spatially separated from the objects of interest with which the light interacts. Therefore the assumption that the external source vanishes in the region of interest is often justified. Take the curl of (1.18) and the time derivative of (1.19) and add the equations obtained. This gives

$$\nabla \times \nabla \times \boldsymbol{\mathcal{E}} + \epsilon\mu_0 \frac{\partial^2 \boldsymbol{\mathcal{E}}}{\partial t^2} = \mathbf{0}. \tag{1.23}$$

Now for any vector field $\boldsymbol{\mathcal{A}}$ there holds:

$$\nabla \times \nabla \times \boldsymbol{\mathcal{A}} = -\nabla^2 \boldsymbol{\mathcal{A}} + \nabla\nabla \cdot \boldsymbol{\mathcal{A}}. \tag{1.24}$$

where $\nabla^2 \boldsymbol{\mathcal{A}}$ is the vector:

$$\nabla^2 \boldsymbol{\mathcal{A}} = \nabla^2 \mathcal{A}_x \, \hat{\mathbf{x}} + \nabla^2 \mathcal{A}_y \, \hat{\mathbf{y}} + \nabla^2 \mathcal{A}_z \, \hat{\mathbf{z}}, \tag{1.25}$$

with

$$\nabla^2 = \frac{\partial^2}{\partial x^2} + \frac{\partial^2}{\partial y^2} + \frac{\partial^2}{\partial z^2}. \tag{1.26}$$

Because Gauss's law (1.20) with $\varrho_{ext} = 0$ and ϵ constant implies that $\nabla \cdot \boldsymbol{\mathcal{E}} = 0$, (1.24) applied to $\boldsymbol{\mathcal{E}}$ yields

$$\nabla \times \nabla \times \boldsymbol{\mathcal{E}} = -\nabla^2 \boldsymbol{\mathcal{E}}. \tag{1.27}$$

Hence, (1.23) becomes

$$\nabla^2 \boldsymbol{\mathcal{E}} - \epsilon\mu_0 \frac{\partial^2 \boldsymbol{\mathcal{E}}}{\partial t^2} = \mathbf{0}. \tag{1.28}$$

By a similar derivation it is found that also $\boldsymbol{\mathcal{H}}$ satisfies (1.28). Hence in a homogeneous dielectric without external sources, every component of the electromagnetic field satisfies the scalar wave equation:

$$\nabla^2 \mathcal{U} - \epsilon\mu_0 \frac{\partial^2 \mathcal{U}}{\partial t^2} = 0. \tag{1.29}$$

The **refractive index** is the dimensionless quantity defined by

$$n = \sqrt{\frac{\epsilon}{\epsilon_0}}. \tag{1.30}$$

The scalar wave equation can then be written as

$$\nabla^2 \mathcal{U} - n^2 \epsilon_0 \mu_0 \frac{\partial^2 \mathcal{U}}{\partial t^2} = 0. \tag{1.31}$$

The speed of light in matter is

$$\frac{c}{n} = \frac{1}{\sqrt{\epsilon\mu_0}}. \tag{1.32}$$

1.5 Time-Harmonic Solutions of the Wave Equation

The fact that in the frequently occurring case that light interacts with a homogeneous dielectric, all components of the electromagnetic field satisfy the scalar wave equation, justifies a detailed study of solutions of this equation. Since in optics usually so-called monochromoatic or time-harmonic fields are considered which depend on time by a cosine function, we will focus attention on time-harmonic solutions of the wave equation.

1.5.1 Time-Harmonic Plane Waves

By definition functions that depend on time by a cosine or a sine function are called time-harmonic. One can easily verify by substitution that

$$\mathcal{U}(\mathbf{r}, t) = \mathcal{A}\cos(kx - \omega t + \varphi), \tag{1.33}$$

where $\mathcal{A} > 0$ and φ are constants, is a solution of (1.31), provided that

$$k = \omega(\epsilon\mu_0)^{1/2} = \omega n\sqrt{\epsilon_0\mu_0} = nk_0, \tag{1.34}$$

where $k_0 = \omega/c = \omega\sqrt{\epsilon_0\mu_0}$ is the *wave number* in vacuum. The frequency $\omega > 0$ can be chosen arbitrarily. The wave number k in the material is then determined by (1.34). We define $T = 2\pi/\omega$ and $\lambda = 2\pi/k$ as the period and the *wavelength in the material*, respectively. Furthermore, $\lambda_0 = 2\pi/k_0$ is the wavelength in vacuum.

Remark. When speaking about "the wavelength", we always mean the wavelength in vacuum.

We can write (1.33) in the form

$$\mathcal{U}(x,t) = \mathcal{A}\cos\left[k\left(x - \frac{c}{n}t\right) + \varphi\right], \tag{1.35}$$

where $c/n = 1/\sqrt{\epsilon\mu_0}$ is the speed of light in the material, $\mathcal{A}$ is the amplitude and the argument under the cosine: $k\left(x - \frac{c}{n}t\right) + \varphi$ is called the phase at position x and time t. A wave front is a set of space-time points where the phase is constant:

$$x - \frac{c}{n}t = \text{constant}. \tag{1.36}$$

At any fixed time t the wave fronts are planes (in this case perpendicular to the x-axis), and therefore the wave is called a plane wave. As time proceeds, the wave fronts move with velocity c/n in the positive x-direction.

A time-harmonic plane wave propagating in an arbitrary direction is given by

$$\mathcal{U}(\mathbf{r},t) = \mathcal{A}\cos(\mathbf{k}\cdot\mathbf{r} - \omega t + \varphi), \tag{1.37}$$

where $\mathcal{A}$ and φ are again constants and $\mathbf{k} = k_x\hat{\mathbf{x}} + k_y\hat{\mathbf{y}} + k_z\hat{\mathbf{z}}$ is the wave vector. The wave fronts are given by the set of all space-time points $(\mathbf{r},t)$ for which the phase $\mathbf{k}\cdot\mathbf{r} - \omega t + \varphi$ is constant, i.e. for which

$$\mathbf{k}\cdot\mathbf{r} - \omega t = \text{constant}. \tag{1.38}$$

At fixed times the wave fronts are planes perpendicular to the direction of $\mathbf{k}$ as shown in Fig. 1.2. Equation (1.37) is a solution of (1.31) provided that

$$k_x^2 + k_y^2 + k_z^2 = \omega^2\epsilon\mu_0 = \omega^2 n^2\epsilon_0\mu_0 = k_0^2 n^2. \tag{1.39}$$

The direction of the wave vector can be chosen arbitrarily, but its length is determined by the frequency ω.

1.5.2 Complex Notation for Time-Harmonic Functions

We consider a general time-harmonic solution of the wave equation (1.29):

$$\mathcal{U}(\mathbf{r},t) = \mathcal{A}(\mathbf{r})\cos(\varphi(\mathbf{r}) - \omega t), \tag{1.40}$$

where the amplitude $\mathcal{A}(\mathbf{r}) > 0$ and the phase $\varphi(\mathbf{r})$ are functions of position $\mathbf{r}$. The wave fronts consist of sets of space-time points $(\mathbf{r},t)$ where the phase is equal to some constant:

$$\varphi(\mathbf{r}) - \omega t = \text{constant}. \tag{1.41}$$

At fixed time t, the sets of constant phase: $\varphi(\mathbf{r}) = \omega t + \text{constant}$ are surfaces which in general are not planes, hence the solution in general is not a plane wave. Equation (1.40) could for example be a wave with spherical wave fronts, as discussed below.

Remark. A plane wave is infinitely extended and transports an infinite amount of electromagnetic energy. A plane wave can not exist in reality, but it is nevertheless an usual and convenient idealisation. As will be demonstrated in Section 7.1, *every time-harmonic solution of the wave equation* can always be expanded in terms of plane waves of the form (1.37).

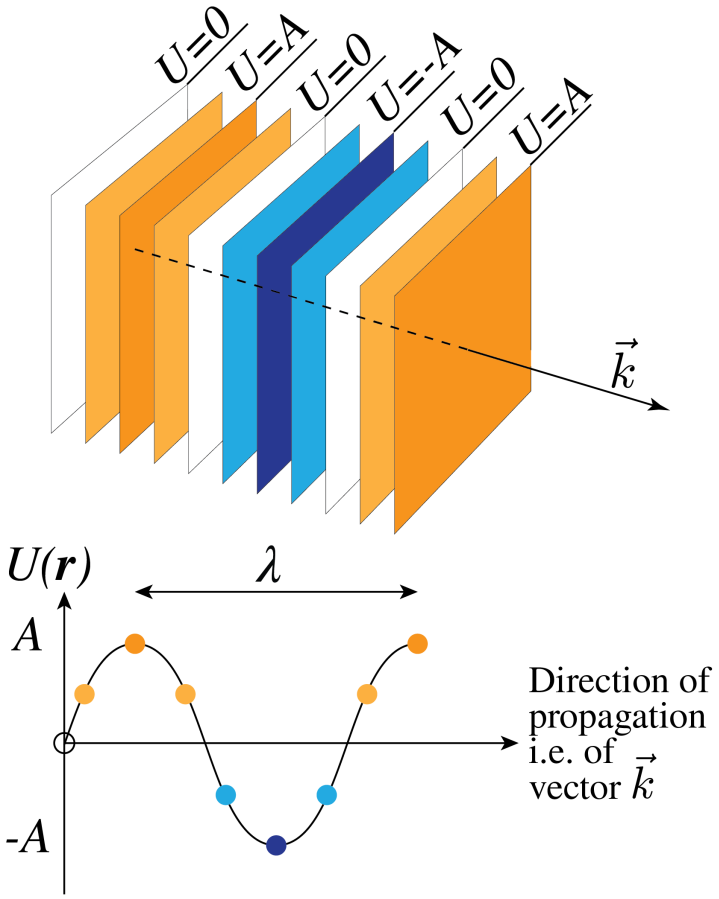


Figure 1.2: Planes of constant phase.

For time-harmonic solutions it is often convenient to use **complex notation**. Define the **complex amplitude** by:

$$U(\mathbf{r}) = \mathcal{A}(\mathbf{r})e^{i\varphi(\mathbf{r})}, \tag{1.42}$$

i.e. the modulus of the complex number $U(\mathbf{r})$ is the amplitude $\mathcal{A}(\mathbf{r})$ and the argument of $U(\mathbf{r})$ is the phase $\varphi(\mathbf{r})$ at $t = 0$. The time-dependent part of the phase: $-\omega t$ is thus separated from the space-dependent part of the phase. Then (1.40) can be written as

$$\mathcal{U}(\mathbf{r}, t) = \mathrm{Re}\left[U(\mathbf{r})e^{-i\omega t}\right]. \tag{1.43}$$

Hence $\mathcal{U}(\mathbf{r}, t)$ is the real part of the complex time-harmonic function

$$U(\mathbf{r})e^{-i\omega t}. \tag{1.44}$$

Remark. The complex amplitude $U(\mathbf{r})$ is also called the complex field. In the case of vector fields such as $\mathbf{E}$ and $\mathbf{H}$ we speak of complex vector fields, or simply complex fields. Complex amplitudes and complex (vector) fields are only functions of position $\mathbf{r}$; the time dependent factor $\exp(-i\omega t)$ is omitted. To get the physical meaningful real quantity, the complex amplitude or complex field first has to be multiplied by $\exp(-i\omega t)$ and then the real part must be taken.

The following convention is used throughout this book:
Real-valued physical quantities (whether they are time-harmonic or have more general time dependence) are denoted by a calligraphic letter, e.g. $\mathcal{U}$, $\mathcal{E}_x$, or $\mathcal{H}_x$. The symbols are bold when we are dealing with a vector, e.g. $\boldsymbol{\mathcal{E}}$ or $\boldsymbol{\mathcal{H}}$. The complex amplitude of a time-harmonic function is linked to the real physical quantity by (1.43) and is written as an ordinary letter such as U and $\mathbf{E}$.

It is easier to calculate with complex amplitudes (complex fields) than with trigonometric functions (cosine and sine). As long as all the operations carried out on the functions are *linear*, the operations can be carried out on the complex quantities. To get the real-valued physical quantity of the result (i.e. the physical meaningful result), multiply the finally obtained complex amplitude by $\exp(-i\omega t)$ and take the real part. The reason that this works is that taking the real part commutes with all linear operations, i.e. taking first the real part to get the real-valued physical quantity and then operating on this real physical quantity gives the same result as operating on the complex scalar and taking the real part at the end.

By substituting (1.43) into the wave equation (1.31) we get

$$\begin{aligned} \nabla^2\mathcal{U}(\mathbf{r}, t) - n^2\epsilon_0\mu_0\frac{\partial^2\mathcal{U}(\mathbf{r}, t)}{\partial t^2} &= \mathrm{Re}\left[\nabla^2 U(\mathbf{r})e^{-i\omega t}\right] - n^2\epsilon_0\mu_0\mathrm{Re}\left[U(\mathbf{r})\frac{\partial^2 e^{-i\omega t}}{\partial t^2}\right] \\ &= \mathrm{Re}\left\{\left[\nabla^2 U(\mathbf{r}) + \omega^2 n^2\epsilon_0\mu_0 U(\mathbf{r})\right]e^{-i\omega t}\right\}. \end{aligned} \tag{1.45}$$

Since this must be zero for all times t, it follows that the complex expression between the brackets [.] must vanish. To see this, consider for example the two instances $t = 0$ and $t = \pi/(2\omega)$. We conclude that the complex amplitude satisfies

$$\nabla^2 U(\mathbf{r}) + k_0^2 n^2 U(\mathbf{r}) = 0, \qquad \text{Helmholtz Equation}, \tag{1.46}$$

where $k_0 = \omega\sqrt{\epsilon_0\mu_0}$ is the wave number in vacuum.

Remark. The complex quantity of which the real part has to be taken is: $U\exp(-i\omega t)$. As explained above, it is not necessary to drag the time-dependent factor $\exp(-i\omega t)$ along in the computations: it suffices to calculate only with the complex amplitude U, then multiply by $\exp(-i\omega t)$ and then take the real part. However, when a derivative with respect to time has to be taken: $\partial/\partial t$, the complex field must be multiplied by $-i\omega$. This is also done in the time-harmonic Maxwell's equations in Section 1.6 below.

1.5.3 Time-Harmonic Spherical Waves

A spherical wave depends on position only by the distance to a fixed point which is the source or sink of the wave. For simplicity we choose the origin of our coordinate system at this point. We thus seek a solution of the form $\mathcal{U}(r,t)$ with $r=\sqrt{x^2+y^2+z^2}$. For spherical symmetric functions we have

$$\nabla^2\mathcal{U}(r,t)=\frac{1}{r}\frac{\partial^2}{\partial r^2}[r\mathcal{U}(r,t)]. \tag{1.47}$$

It is easy to see that outside of the origin

$$\mathcal{U}(r,t)=\frac{f(\pm r-ct/n)}{r}, \tag{1.48}$$

satisfies (1.47) for any choice for the function f, where as before $c=1/\sqrt{\epsilon_0\mu_0}$ is the speed of light and $n=\sqrt{\epsilon/\epsilon_0}$. Of particular interest are time-harmonic spherical waves:

$$\mathcal{U}(r,t)=\frac{\mathcal{A}}{r}\cos\left[k\left(\pm r-\frac{c}{n}t\right)+\varphi\right]=\frac{\mathcal{A}}{r}\cos\left(\pm kr-\omega t+\varphi\right) \tag{1.49}$$

where $\mathcal{A}$ is a constant

$$k=n\omega/c. \tag{1.50}$$

and $\pm kr-\omega t+\varphi$ is the phase at $\mathbf{r}$ and at time t. A wave front is a set of space-time points $(\mathbf{r},t)$ where the phase is equal to a constant:

$$\pm kr-\omega t=\text{constant}. \tag{1.51}$$

Wave fronts are thus spheres which move with the speed of light in the radial direction. When the + sign is chosen, the wave propagates outwards, i.e. away from the origin. The wave is then radiated by a **source** at the origin. Indeed, if the + sign holds in (1.49), then if time t increases, (1.51) implies that a surface of constant phase moves outwards. Similarly, if the − sign holds, the wave propagates towards the origin which then acts as a **sink**. The amplitude of the wave $\mathcal{A}/r$ is proportional to the inverse distance to the source sink. Since the time average of the local flux of energy is proportional to $\mathcal{A}^2/r^2$, the time averaged total flux through the surface of any sphere with centre at the origin is independent of the radius of the sphere. Since there is a source or a sink at the origin, (1.49) satisfies (1.47) only outside of the origin. There is a δ-function as source density on the right-hand side:

$$\epsilon\mu_0\frac{\partial^2}{\partial t^2}\mathcal{U}(r,t)-\nabla^2\mathcal{U}(r,t)=4\pi\mathcal{A}\,\delta(r), \tag{1.52}$$

where the right-hand side corresponds to either a source or sink at the origin, depending on the sign chosen in the phase.

Using complex notation we have for the outwards propagating spherical wave:

$$\mathcal{U}(r,t)=\text{Re}\left[U(\mathbf{r})e^{-i\omega t}\right]=\text{Re}\left[\frac{A}{r}e^{i(kr-i\omega t)}\right] \tag{1.53}$$

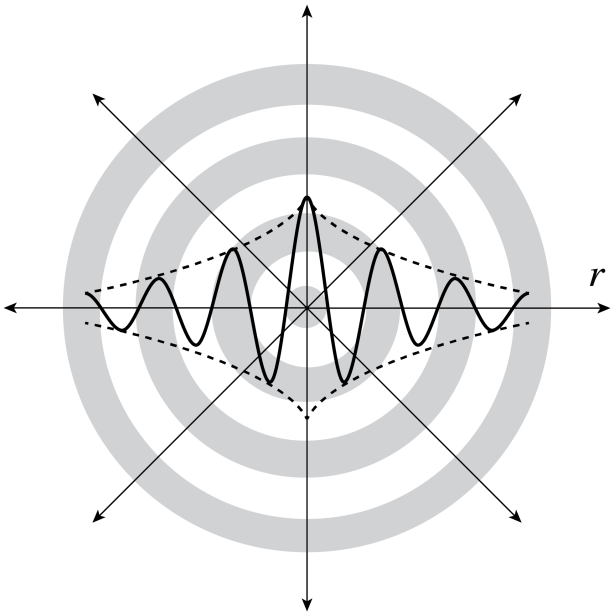


Figure 1.3: Spherical wave fronts and amplitude which is proportional to the reciprocal of the distance to the centre.

with $U(\mathbf{r}) = A\exp(ikr)/r$ and $A = \mathcal{A}\exp(i\varphi)$, where φ is the argument and $\mathcal{A}$ is the modulus of the complex number A.

In Fig. 1.3 and Fig. 1.4 spherical wave fronts are shown. For an observer who is at a large distance from the source, the spherical wave looks like a plane wave which propagates from the source towards the observer (or in the opposite direction, if there is a sink).

1.6 Time-Harmonic Maxwell Equations in Matter

We now return to Maxwell's equations and consider time-harmonic electromagnetic fields, because these are by far the most important fields in optics. Using complex notation we have

$$\boldsymbol{\mathcal{E}}(\mathbf{r},t) = \mathrm{Re}\left[\mathbf{E}(\mathbf{r})e^{-i\omega t}\right], \tag{1.54}$$

with $\mathbf{E}(\mathbf{r}) = E_x(\mathbf{r})\hat{\mathbf{x}} + E_y(\mathbf{r})\hat{\mathbf{y}} + E_z(\mathbf{r})\hat{\mathbf{z}}$ and

$$\begin{aligned} E_x(\mathbf{r}) &= |E_x(\mathbf{r})|e^{i\varphi_x(\mathbf{r})}, \\ E_y(\mathbf{r}) &= |E_y(\mathbf{r})|e^{i\varphi_y(\mathbf{r})}, \\ E_z(\mathbf{r}) &= |E_z(\mathbf{r})|e^{i\varphi_z(\mathbf{r})}, \end{aligned}$$

where $\varphi_x(\mathbf{r})$ is the argument of the complex number $E_x(\mathbf{r})$ etc. With similar notations for the magnetic field, we obtain by substitution into Maxwell's equations (1.18), (1.19), (1.20) and (1.21), the time-harmonic Maxwell equations for the **complex fields**:

$$\nabla \times \mathbf{E} = i\omega\mu_0\mathbf{H}, \qquad \text{Faraday's Law,} \tag{1.55}$$

$$\nabla \times \mathbf{H} = -i\omega\epsilon\mathbf{E} + \sigma\mathbf{E} + \mathbf{J}_{ext}, \qquad \text{Maxwell's Law,} \tag{1.56}$$

$$\nabla \cdot \epsilon\mathbf{E} = \varrho_{ext}, \qquad \text{Gauss's Law,} \tag{1.57}$$

$$\nabla \cdot \mathbf{H} = 0, \qquad \text{no magnetic charge,} \tag{1.58}$$

where the time derivative has been replaced by multiplication of the complex fields by $-i\omega$.

In the time-harmonic Maxwell equations, the conductivity is sometimes included in the imaginary part of the permittivity:

$$\epsilon = \epsilon_0 \left[1 + \chi_e + i\frac{\sigma}{\omega}\right]. \tag{1.59}$$

Although it is convenient to do this in Maxwell's Law (1.56), one should remember that in Gauss's Law (1.57), the original permittivity: $\epsilon = 1 + \chi_e$ should still be used. When there are no external sources: $\varrho_{ext} = 0$ and the material is homogeneous (i.e. χ_e and σ are independent of position), then (1.57) is equivalent to

$$\nabla \cdot \mathbf{E} = 0. \tag{1.60}$$

Hence in this (important) special case, definition (1.59) for the permittivity can safely be used without the risk of confusion.

We see that when we use definition (1.59), the conductivity makes the permittivity complex and dependent on frequency. But actually, also for insulators ($\sigma = 0$), the permittivity ϵ depends in general on frequency and is complex with a positive imaginary part. The positive imaginary part of ϵ is a measure of the absorption of the light by the material. The property that the permittivity depends on the frequency is called **dispersion**. Except close to a resonance frequency, the imaginary part of $\epsilon(\omega)$ is small and the real part is a slowly increasing function of frequency. This is called normal dispersion and is illustrated in Fig. 1.5. Near a resonance, the real part is rapidly changing and *decreases* when ω increases (this behaviour is called anomalous dispersion), while the imaginary part has a maximum at the resonance frequency of the material, which means that absorption is maximum at the resonance. For light with a narrow frequency band such as for laser light, it is often sufficiently accurate to use the value of the permittivity and the conductivity at the centre frequency of the band.

In the literature the following notation is often used: $\epsilon/\epsilon_0 = (n + i\kappa)^2$, where n and κ ("kappa", not to be confused with the wave number k) are both real and positive, with n the refractive index and κ linked to the absorption. We then have $\mathrm{Re}(\epsilon) = n^2 - \kappa^2$ and $\mathrm{Im}(\epsilon) = 2n\kappa$. At optical frequencies, mostly normal dispersion applies to optical materials like glass as seen in Fig. 1.6. Note that although n and κ are both positive, $\mathrm{Re}(\epsilon)$ can be negative for certain frequencies. This happens for metals in the visible part of the spectrum.

> **Remark.** When ϵ depends on frequency, Maxwell's equations in the form (1.19) and (1.20) for fields that are not time-harmonic can strictly speaking not be valid, because it is not clear which value of ϵ corresponding to which frequency should be chosen. In fact, in the case of strong dispersion, the products $\epsilon\boldsymbol{\mathcal{E}}$ should in the time domain be replaced by a convolution. Since we will almost always consider fields with a narrow-frequency band, we shall not elaborate on this issue further.

1.6.1 Time-Harmonic Electromagnetic Plane Waves

In this section we assume that for the frequencies of interest the material in which the wave propagates is non-conducting ($\sigma = 0$), does not absorb the light and is homogeneous, i.e. the permittivity ϵ is a real constant. Furthermore, we assume that in the region of space of interest there are no sources. These assumptions imply in particular that (1.60) holds. The electric field of a time-harmonic plane wave is given by

$$\boldsymbol{\mathcal{E}}(\mathbf{r}, t) = \mathrm{Re}\left[\mathbf{E}(\mathbf{r})e^{-i\omega t}\right], \tag{1.61}$$

with

$$\mathbf{E}(\mathbf{r}) = \mathbf{A}e^{i\mathbf{k}\cdot\mathbf{r}}, \tag{1.62}$$

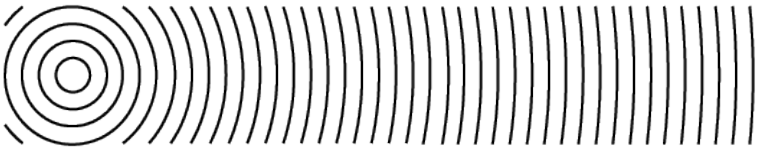


Figure 1.4: Planes of constant phase in cross-section. For an observer at large distance to the source the spherical wave looks similar to a plane wave.

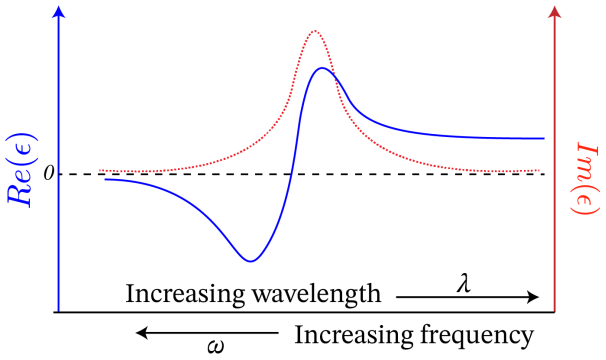


Figure 1.5: Real and imaginary part of the permittivity $\epsilon =$, as function of wavelength and of frequency near a resonance.

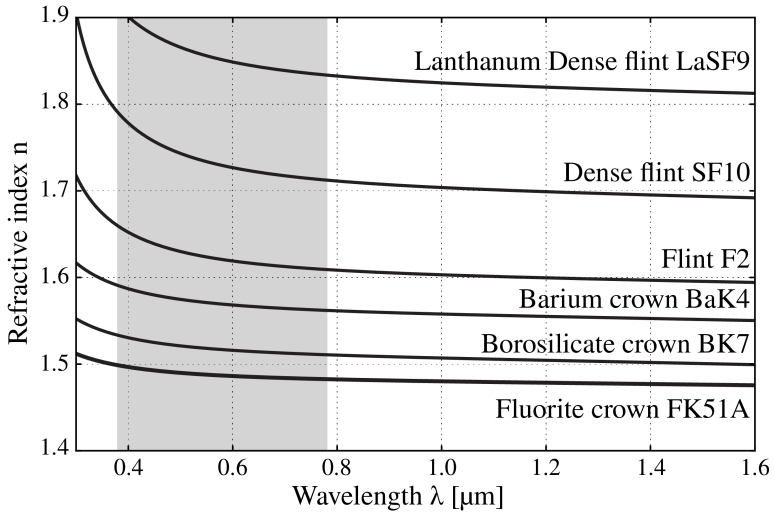


Figure 1.6: Refractive index as function of wavelength for several types of glass (from Wikimedia Commons by Geek3 / CC BY-SA).

where $\mathbf{A}$ is a constant complex vector (i.e. it is independent of position and time):

$$\mathbf{A} = A_x\hat{\mathbf{x}} + A_y\hat{\mathbf{y}} + A_z\hat{\mathbf{z}}, \tag{1.63}$$

with $A_x = |A_x|e^{i\varphi_x}$ etc.. The wave vector $\mathbf{k}$ satisfies (1.39). Substitution of (1.62) into (1.60) implies that

$$\mathbf{E}(\mathbf{r}) \cdot \mathbf{k} = 0, \tag{1.64}$$

for all $\mathbf{r}$ and hence (1.61) implies that also the physical real electric field is at every point $\mathbf{r}$ perpendicular to the wave vector: $\boldsymbol{\mathcal{E}}(\mathbf{r}, t) \cdot \mathbf{k} = 0$. For simplicity we now choose the wave vector in the direction of the z-axis and we assume that the electric field vector is parallel to the x-axis. This case is called an x-polarised electromagnetic wave. The complex field is then written as

$$\mathbf{E}(z) = Ae^{ikz}\hat{\mathbf{x}}, \tag{1.65}$$

where $k = \omega\sqrt{\epsilon\mu_0}$ and $A = |A|\exp(i\varphi)$. It follows from Faraday's Law (1.55)) that

$$\mathbf{H}(z) = \frac{k}{\omega\mu_0}\hat{\mathbf{z}} \times \hat{\mathbf{x}}Ae^{ikz} = \sqrt{\frac{\epsilon}{\mu_0}}Ae^{ikz}\hat{\mathbf{y}}. \tag{1.66}$$

The real electromagnetic field is thus:

$$\boldsymbol{\mathcal{E}}(z,t) = \mathrm{Re}\left[\mathbf{E}(z)e^{-i\omega t}\right] = |A|\cos(kz - \omega t + \varphi)\hat{\mathbf{x}}, \tag{1.67}$$

$$\boldsymbol{\mathcal{H}}(z,t) = \mathrm{Re}\left[\mathbf{H}(z)e^{-i\omega t}\right] = \sqrt{\frac{\epsilon}{\mu_0}}|A|\cos(kz - \omega t + \varphi)\hat{\mathbf{y}}. \tag{1.68}$$

We conclude that *in a lossless medium, the electric and magnetic field of a plane wave are in phase, and at every point and at every instant are perpendicular to the wave vector and to each other*. As illustrated in Fig. 1.7, at any given time the electric and the magnetic fields achieve their maximum and minimum values in the same points.

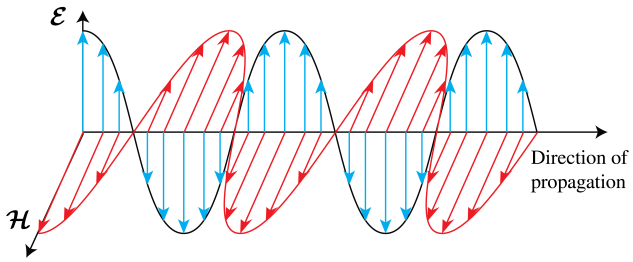


Figure 1.7: The time-harmonic vectors $\boldsymbol{\mathcal{E}}$ and $\boldsymbol{\mathcal{H}}$ of a plane polarised wave in a lossless medium are perpendicular to each other and to the direction of the wave vector which is also the direction of $\boldsymbol{\mathcal{E}} \times \boldsymbol{\mathcal{H}}$.

1.6.2 Field of an Electric Dipole

Another important solution of Maxwell's equations is the field radiated by a time-harmonic electric dipole, i.e. two opposite charges with equal strength that move time-harmonically around their centre of mass. In this section the medium is homogeneous, but it may absorb part of the light, i.e. the permittivity is a constant with non-negative imaginary part. An electric dipole is the classical electromagnetic model for an atom or molecule. Because the optical wavelength is

much larger than an atom and molecule, the atomic charges may be considered to be concentrated both in the same point $\mathbf{r}_0$. The charge and current densities of such an elementary dipole are

$$\rho = -\mathbf{p}\cdot\nabla\delta(\mathbf{r}-\mathbf{r}_0), \tag{1.69}$$
$$\mathbf{J} = -i\omega\mathbf{p}\delta(\mathbf{r}-\mathbf{r}_0), \tag{1.70}$$

where $\delta(\mathbf{r})$ is Dirac's delta function and $\mathbf{p}$ is the dipole vector which is defined by

$$\mathbf{p} = q\mathbf{a}, \tag{1.71}$$

where $q>0$ is the positive charge and $\mathbf{a}$ is the position vector of the positive with respect to the negative charge.

The field radiated by an electric dipole is very important. It is the fundamental solution of Maxwell's equations, in the sense that the field radiated by an arbitrary distribution of sources can always be written as a superposition of the fields of elementary electric dipoles. This follows from the fact that Maxwell's equations are linear and any current distribution can be written as a superposition of elementary dipole currents.

The field radiated by an elementary dipole at $\mathbf{r}_0$ in homogeneous matter is given by[9]

$$\mathbf{E}(\mathbf{r}) = \left\{k^2\hat{\mathbf{R}}\times\left(\mathbf{p}\times\hat{\mathbf{R}}\right)+\left(3\hat{\mathbf{R}}\cdot\mathbf{p}\,\hat{\mathbf{R}}-\mathbf{p}\right)\left(\frac{1}{R^2}-\frac{ik}{R}\right)\right\}\frac{e^{ikR}}{4\pi\epsilon R}, \tag{1.72}$$
$$\mathbf{H}(\mathbf{r}) = \frac{k^2c}{n}\left(1+\frac{i}{kR}\right)\hat{\mathbf{R}}\times\mathbf{p}\frac{e^{ikR}}{4\pi R}, \tag{1.73}$$

where $k=k_0n$, k_0 the wave number in vacuum,$n=\sqrt{\epsilon/\epsilon_0}$, and $\mathbf{R}=\mathbf{r}-\mathbf{r}_0$, $\hat{\mathbf{R}}=\mathbf{R}/R$. It is seen that the complex electric and magnetic fields are proportional to the complex spherical wave:

$$\frac{e^{ikR}}{R}$$

discussed in Section 1.5.3, but that these fields contain additional position dependent factors. At large distance from the dipole ($R\to\infty$) there holds:

$$\mathbf{H}(\mathbf{r}) \approx \frac{k^2c}{n}\hat{\mathbf{R}}\times\mathbf{p}\frac{e^{ikR}}{4\pi R}, \tag{1.74}$$
$$\mathbf{E}(\mathbf{r}) \approx k^2\hat{\mathbf{R}}\times\left(\mathbf{p}\times\hat{\mathbf{R}}\right)\frac{e^{ikR}}{4\pi\epsilon R} = -\sqrt{\frac{\mu_0}{\epsilon}}\hat{\mathbf{R}}\times\mathbf{H}(\mathbf{r}). \tag{1.75}$$

In Fig. 1.8 the electric and magnetic field lines are shown of a radiating dipole with dipole vector parallel to the z-axis. For an observer at large distance from the dipole, the electric and magnetic fields are perpendicular to each other and perpendicular to the direction of the line of sight $\hat{\mathbf{R}}$ from the dipole to the observer. Furthermore, the electric field is in the plane through the dipole vector $\mathbf{p}$ and the vector $\hat{\mathbf{R}}$, while the magnetic field is perpendicular to this plane. So, for a distant observer the field radiated by a dipole is similar to that of a plane wave which propagates from the dipole towards the observer and has an electric field parallel to the plane through the dipole and the line of sight $\hat{\mathbf{R}}$ and perpendicular to $\hat{\mathbf{R}}$. Furthermore, the amplitudes of the electric and magnetic fields depend on the direction of the line of sight, with the field vanishing when the line of sight $\hat{\mathbf{R}}$ is parallel to the dipole vector $\mathbf{p}$ and with maximum amplitude when $\hat{\mathbf{R}}$ is in the plane perpendicular to the dipole vector. This result agrees with the well-known radiation pattern of an antenna when the current of the dipole is in the same direction as that of the antenna.

[9]For a derivation see D.J. Griffiths, *Introduction to Electrodynamics*, Pearson.

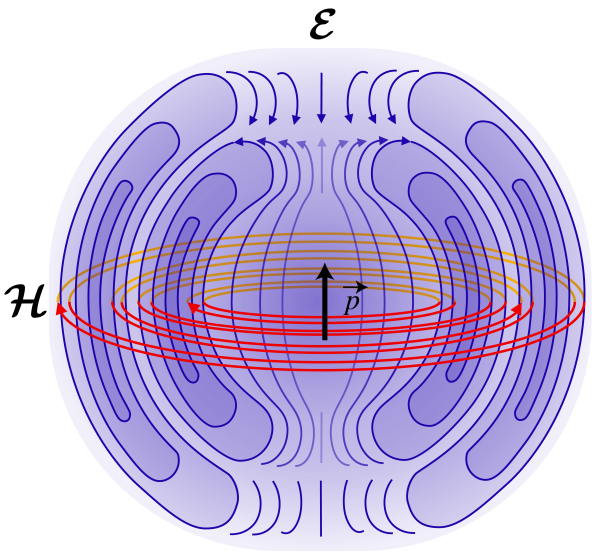


Figure 1.8: Electric and magnetic field lines radiated by a radiating dipole (from Wikimedia Commons, original JPG due to Averse, SVG by Maschen. / CC0).

1.7 Electromagnetic Energy

The total energy stored in the electromagnetic field per unit of volume at a point $\mathbf{r}$ is equal to the sum of the electric and the magnetic energy densities. We postulate that the results for the energy densities derived in electrostatics and magnetostatics are also valid for the fast-oscillating fields in optics; hence we assume that the total electromagnetic energy density is given by:

$$U_{em}(\mathbf{r},t) = \frac{\epsilon}{2}\boldsymbol{\mathcal{E}}(\mathbf{r},t)\cdot\boldsymbol{\mathcal{E}}(\mathbf{r},t) + \frac{\mu_0}{2}\boldsymbol{\mathcal{H}}(\mathbf{r},t)\cdot\boldsymbol{\mathcal{H}}(\mathbf{r},t). \tag{1.76}$$

It is to be noticed that we assume in this section that the permittivity is real, i.e. there is no absorption and the permittivity does not include the conductivity.

Time dependent electromagnetic fields propagate energy. The flow of electromagnetic energy at a certain position $\mathbf{r}$ and time t is given by the Poynting vector, which is defined by

$$\boldsymbol{\mathcal{S}}(\mathbf{r},t) = \boldsymbol{\mathcal{E}}(\mathbf{r},t)\times\boldsymbol{\mathcal{H}}(\mathbf{r},t). \tag{1.77}$$

More precisely, the flow of electromagnetic energy through a small surface $\mathrm{d}S$ with normal $\hat{\mathbf{n}}$ at point $\mathbf{r}$ and in the direction of $\hat{\mathbf{n}}$ is given by

$$\boldsymbol{\mathcal{S}}(\mathbf{r},t)\cdot\hat{\mathbf{n}}\,\mathrm{d}S. \tag{1.78}$$

If the scalar product is positive, the energy flow is in the direction of $\hat{\mathbf{n}}$, otherwise it is in the direction of $-\hat{\mathbf{n}}$. Hence the direction of the vector $\boldsymbol{\mathcal{S}}(\mathbf{r},t)$ is the direction of the flow of energy at point $\mathbf{r}$ and the length $\|\boldsymbol{\mathcal{S}}(\mathbf{r},t)\|$ is the amount of the flow of energy, per unit of time and per unit of area perpendicular to the direction of $\boldsymbol{\mathcal{S}}$. This quantity has unit $\mathrm{J}/(\mathrm{s}\times\mathrm{m}^2)$.

That the Poynting vector gives the flow of energy can be seen in a dielectric for which dispersion may be neglected by the following derivation. Consider the rate of change with time of the total electromagnetic energy in a volume V:

$$\frac{d}{dt}\iiint_V U_{em}(\mathbf{r},t)\,\mathrm{d}V = \iiint_V \epsilon\frac{\partial\boldsymbol{\mathcal{E}}(\mathbf{r},t)}{\partial t}\cdot\boldsymbol{\mathcal{E}}(\mathbf{r},t) + \mu_0\frac{\partial\boldsymbol{\mathcal{H}}(\mathbf{r},t)}{\partial t}\cdot\boldsymbol{\mathcal{H}}(\mathbf{r},t)\,\mathrm{d}V. \tag{1.79}$$

By substituting (1.18), (1.19) and using

$$-\boldsymbol{\mathcal{A}}\cdot\nabla\times\boldsymbol{\mathcal{B}} + \boldsymbol{\mathcal{B}}\cdot\nabla\times\boldsymbol{\mathcal{A}} = \nabla\cdot(\boldsymbol{\mathcal{A}}\times\boldsymbol{\mathcal{B}}), \tag{1.80}$$

which holds for any two vector fields, we find

$$\begin{aligned}
&\iiint_V \epsilon\boldsymbol{\mathcal{E}}(\mathbf{r},t)\cdot\frac{\partial}{\partial t}\boldsymbol{\mathcal{E}}(\mathbf{r},t)+\mu_0\boldsymbol{\mathcal{H}}(\mathbf{r},t)\cdot\frac{\partial}{\partial t}\boldsymbol{\mathcal{H}}(\mathbf{r},t)\,\mathrm{d}V\\
&=\iiint_V \boldsymbol{\mathcal{E}}(\mathbf{r},t)\cdot\nabla\times\boldsymbol{\mathcal{H}}(\mathbf{r},t)-\boldsymbol{\mathcal{H}}(\mathbf{r},t)\cdot\nabla\times\boldsymbol{\mathcal{E}}(\mathbf{r},t)\,\mathrm{d}V-\iiint_V \sigma\boldsymbol{\mathcal{E}}(\mathbf{r},t)\cdot\boldsymbol{\mathcal{E}}(\mathbf{r},t)\,\mathrm{d}V\\
&\qquad-\iiint_V \boldsymbol{\mathcal{E}}(\mathbf{r},t)\cdot\boldsymbol{\mathcal{J}}_{ext}(\mathbf{r},t)\,\mathrm{d}V\\
&=-\iiint_V \nabla\cdot(\boldsymbol{\mathcal{E}}\times\boldsymbol{\mathcal{H}})\,\mathrm{d}V-\iiint_V \sigma\boldsymbol{\mathcal{E}}(\mathbf{r},t)\cdot\boldsymbol{\mathcal{E}}(\mathbf{r},t)\,\mathrm{d}V-\iiint_V \boldsymbol{\mathcal{E}}(\mathbf{r},t)\cdot\boldsymbol{\mathcal{J}}_{ext}(\mathbf{r},t)\,\mathrm{d}V\\
&=-\iint_S(\boldsymbol{\mathcal{E}}\times\boldsymbol{\mathcal{H}})\cdot\hat{\mathbf{n}}\,\mathrm{d}S-\iiint_V \sigma\boldsymbol{\mathcal{E}}(\mathbf{r},t)\cdot\boldsymbol{\mathcal{E}}(\mathbf{r},t)\,\mathrm{d}V-\iiint_V \boldsymbol{\mathcal{E}}(\mathbf{r},t)\cdot\boldsymbol{\mathcal{J}}_{ext}(\mathbf{r},t)\,\mathrm{d}V,
\end{aligned}\tag{1.81}$$

where in the last step the divergence theorem was used with S the surface bounding volume V and $\hat{\mathbf{n}}$ the unit normal on S pointing out of V. Hence,

$$\begin{aligned}
\frac{d}{dt}\iiint_V U_{em}(\mathbf{r},t)\;\mathrm{d}V+\iiint_V \sigma\boldsymbol{\mathcal{E}}(\mathbf{r},t)\cdot\boldsymbol{\mathcal{E}}(\mathbf{r},t)\,\mathrm{d}V+\iiint_V \boldsymbol{\mathcal{E}}(\mathbf{r},t)\cdot\boldsymbol{\mathcal{J}}(\mathbf{r},t)\,\mathrm{d}V\\
=-\iint_S \boldsymbol{\mathcal{S}}(\mathbf{r},t)\cdot\hat{\mathbf{n}}\,\mathrm{d}S.
\end{aligned}\tag{1.82}$$

This equation says that the rate of change with time of the electromagnetic energy in a volume V plus the work done by the field on the conduction and external currents inside V is equal to the net influx of electromagnetic energy through the boundary of V.

Remark. The energy flux $\boldsymbol{\mathcal{S}}$ and the energy density U_{em} depend quadratically on the field. For U_{em} the quadratic dependence on the electric and magnetic fields is clear. To see that the Poynting vector is also quadratic in the electromagnetic field, one should realise that the electric and magnetic fields are inseparable: they together form the electromagnetic field. Stated differently: if the amplitude of the electric field is doubled, then also that of the magnetic field is doubled and hence the Poynting vector is increased by the factor 4. Therefore, when computing the Poynting vector or the electromagnetic energy density of a time-harmonic electromagnetic field, the real-valued vector fields should be used, i.e. the complex fields should **NOT** be used.

If we substitute the real fields (1.65), (1.66) of the plane wave in the Poynting vector and the electromagnetic energy density we get:

$$\boldsymbol{\mathcal{S}}(z,t)=\boldsymbol{\mathcal{E}}(z,t)\times\boldsymbol{\mathcal{H}}(z,t)=\sqrt{\frac{\epsilon}{\mu_0}}|A|^2\cos^2(kz-\omega t+\varphi)\,\hat{\mathbf{z}},\tag{1.83}$$

$$U_{em}(z,t)=\epsilon|A|^2\cos^2(kz-\omega t+\varphi).\tag{1.84}$$

We see that the energy flow of a plane wave is in the direction of the wave vector, which is also the direction of the phase velocity. Furthermore, it changes with time at frequency 2ω. Furthermore, for a plane wave the energy flow and the energy density are both proportional to the squared amplitude of the electric field.

1.8 Time-Averaged Energy of Time-Harmonic Fields

Optical frequencies are in the range of 5×10^{14} Hz and the fastest detectors working at optical frequencies have integration times larger than 10^{-10} s. Hence there is no detector which can measure the time fluctuations of the electromagnetic fields at optical frequencies and every detector always measures an average value, taken over an interval of time that is very large compared to the period $2\pi/\omega$ of the light wave. We therefore compute averages over such time intervals of the Poynting vector and of the electromagnetic energy. Because the Poynting vector and energy density depend nonlinearly (quadratically) on the field amplitudes, we can *not* perform the computations using the complex amplitudes and take the real part afterwards, but have instead to start from the real quantities. Nevertheless, it turns out that the final result can be conveniently expressed in terms of the complex field amplitudes.

Consider two time-harmonic functions:

$$\mathcal{A}(t) = \mathrm{Re}\left[Ae^{-i\omega t}\right] = |A|\cos(\varphi_A - \omega t) \tag{1.85}$$

$$\mathcal{B}(t) = \mathrm{Re}\left[Be^{-i\omega t}\right] = |B|\cos(\varphi_B - \omega t), \tag{1.86}$$

with $A = |A|\exp(i\varphi_A)$ and $B = |B|\exp(i\varphi_B)$ the complex amplitudes. For a general function of time $f(t)$ we define the time average over an interval T at a certain time t, by

$$\frac{1}{T}\int_{t-T/2}^{t+T/2} f(t')\mathrm{d}t', \tag{1.87}$$

where T is much larger (say a factor of 10^5) than the period of the light. It is obvious that for time-harmonic fields the average does not depend on the precise time t at which it is computed. and we therefore take $t = 0$ and write

$$\langle f(t)\rangle = \lim_{T\to\infty}\frac{1}{T}\int_{-T/2}^{T/2} f(t)\mathrm{d}t. \tag{1.88}$$

With

$$\mathcal{A}(t) = \mathrm{Re}\left[Ae^{-i\omega t}\right] = \frac{1}{2}\left[Ae^{-i\omega t} + A^* e^{i\omega t}\right],$$

where A^* is the complex conjugate of A, and with a similar expression for $\mathcal{B}(t)$, it follows that

$$\begin{aligned}\lim_{T\to\infty}\frac{1}{T}\int_{-T/2}^{T/2}\mathcal{A}(t)\mathcal{B}(t)\,\mathrm{d}t &= \lim_{T\to\infty}\frac{1}{4T}\int_{-T/2}^{T/2}\left[AB^* + A^*B + ABe^{-2i\omega t} + A^*B^*e^{2i\omega t}\right]\mathrm{d}t \\ &= \lim_{T\to\infty}\frac{1}{4}\left[AB^* + A^*B + AB\frac{e^{i\omega T} - e^{-i\omega T}}{2iT\omega} + A^*B^*\frac{e^{i\omega T} - e^{-i\omega T}}{2iT\omega}\right] \\ &= \frac{1}{2}\mathrm{Re}\left[AB^*\right]. \end{aligned} \tag{1.89}$$

This important result will be used over and over again. In words:

> The average of the product of two time-harmonic quantities taken over a long time interval compared with the period, is half the real part of the product of the complex amplitude of one quantity and the complex conjugate of the other.

If we apply this to the Poynting vector of a general time-harmonic electromagnetic field:

$$\begin{aligned}\boldsymbol{\mathcal{E}}(\mathbf{r},t) &= \mathrm{Re}\left[\mathbf{E}(\mathbf{r})e^{-i\omega t}\right],\\ \boldsymbol{\mathcal{H}}(\mathbf{r},t) &= \mathrm{Re}\left[\mathbf{H}(\mathbf{r})e^{-i\omega t}\right],\end{aligned}$$

we find that the time-averaged energy flow denoted by $\mathbf{S}(\mathbf{r})$ is given by

$$\mathbf{S}(\mathbf{r}) = \lim_{T\to\infty}\frac{1}{T}\int_{-T/2}^{T/2}\boldsymbol{\mathcal{S}}(\mathbf{r},t)dt = \frac{1}{2}\mathrm{Re}\left[\mathbf{E}\times\mathbf{H}^*\right]. \tag{1.90}$$

Similarly, the time-averaged electromagnetic energy density is:

$$\begin{aligned}\langle U_{en}(\mathbf{r})\rangle &= \lim_{T\to\infty}\frac{1}{T}\int_{-T/2}^{T/2}U_{en}(\mathbf{r},t)\,\mathrm{d}t = \frac{1}{2}\epsilon\mathbf{E}(\mathbf{r})\cdot\mathbf{E}(\mathbf{r})^* + \frac{\mu_0}{2}\mathbf{H}(\mathbf{r})\cdot\mathbf{H}(\mathbf{r})^*\\ &= \frac{1}{2}\epsilon|\mathbf{E}(\mathbf{r})|^2 + \frac{\mu_0}{2}|\mathbf{H}(\mathbf{r})|^2.\end{aligned} \tag{1.91}$$

For the special case of plane wave (1.65), (1.66) in a medium without absorption, we get:

$$\mathbf{S} = \frac{1}{2}\sqrt{\frac{\epsilon}{\mu_0}}\mathrm{Re}\left[AA^*\right]\hat{\mathbf{z}} = \frac{1}{2}\sqrt{\frac{\epsilon}{\mu_0}}|A|^2\hat{\mathbf{z}}. \tag{1.92}$$

The length of vector (1.92) is the time-averaged flow of energy per unit of area in the direction of the plane wave and is commonly called the **intensity** of the wave. For the time-averaged electromagnetic energy density of the plane wave, we get:

$$< U_{en} >= \frac{1}{2}\epsilon|A|^2 + \frac{1}{2\mu_0}\mu_0\epsilon|A|^2 = \epsilon|A|^2. \tag{1.93}$$

For a plane wave both the time-averaged energy flux and the time-averaged energy density are proportional to the squared modulus of the complex electric field.

1.9 Reflection and Transmission at an Interface

When an electromagnetic field is incident on an interface between different media, it is partially reflected and partially transmitted. An important special case is that of a monochromatic plane wave which is incident on a planar interface as in Fig. 1.10.

Let $z = 0$ be the interface between materials in $z < 0$ and $z > 0$ with permittivities ϵ_i and ϵ_t, respectively. We first assume that the materials are lossless, i.e. that the permittivities are real. The plane wave is incident from medium $z < 0$ and the incident electromagnetic field is given by:

$$\boldsymbol{\mathcal{E}}^i(\mathbf{r},t) = \mathrm{Re}\left[\mathbf{E}^i(\mathbf{r})e^{-i\omega t}\right] = \mathrm{Re}\left[\mathbf{A}^i e^{i(\mathbf{k}^i\cdot\mathbf{r}-\omega t)}\right], \tag{1.94}$$

$$\boldsymbol{\mathcal{H}}^i(\mathbf{r},t) = \mathrm{Re}\left[\mathbf{H}^i(\mathbf{r})e^{-i\omega t}\right] = \mathrm{Re}\left[\frac{\mathbf{k}^i}{\omega\mu_0}\times\mathbf{A}^i e^{i(\mathbf{k}^i\cdot\mathbf{r}-\omega t)}\right], \tag{1.95}$$

where $\mathbf{k}^i = k_x^i\hat{\mathbf{x}} + k_y^i\hat{\mathbf{y}} + k_z^i\hat{\mathbf{z}}$, with

$$k_z^i = \sqrt{\omega^2\epsilon_i\mu_0 - (k_x^i)^2 - (k_y^i)^2}. \tag{1.96}$$

Because the time dependence is given by $\exp(-i\omega t)$ with $\omega > 0$ and the incident wave propagates in the positive z-direction, the positive square root is chosen for k_z^i. Part of the incident field is reflected into $z < 0$ and part is transmitted into $z > 0$. The reflected field is written as

$$\boldsymbol{\mathcal{E}}^r(\mathbf{r},t) = \mathrm{Re}\left[\mathbf{E}^r(\mathbf{r})e^{-i\omega t}\right] = \mathrm{Re}\left[\mathbf{A}^r e^{i(\mathbf{k}^r\cdot\mathbf{r}-\omega t)}\right], \tag{1.97}$$

$$\boldsymbol{\mathcal{H}}^r(\mathbf{r},t) = \mathrm{Re}\left[\mathbf{H}^r(\mathbf{r})e^{-i\omega t}\right] = \mathrm{Re}\left[\frac{\mathbf{k}^r}{\omega\mu_0}\times\mathbf{A}^r e^{i(\mathbf{k}^r\cdot\mathbf{r}-\omega t)}\right], \tag{1.98}$$

where $\mathbf{k}^r = k_x^r\hat{\mathbf{x}} + k_y^r\hat{\mathbf{y}} + k_z^r\hat{\mathbf{z}}$, with

$$k_z^r = -\sqrt{\omega^2\epsilon_i\mu_0 - (k_x^r)^2 - (k_y^r)^2}, \tag{1.99}$$

where the minus sign is chosen because the reflected wave propagates in the negative z-direction. The transmitted field is for $z > 0$

$$\boldsymbol{\mathcal{E}}^t(\mathbf{r},t) = \mathrm{Re}\left[\mathbf{E}^t(\mathbf{r})e^{-i\omega t}\right] = \mathrm{Re}\left[\mathbf{A}^t e^{i(\mathbf{k}^t\cdot\mathbf{r}-\omega t)}\right], \tag{1.100}$$

$$\boldsymbol{\mathcal{H}}^t(\mathbf{r},t) = \mathrm{Re}\left[\mathbf{H}^t(\mathbf{r})e^{-i\omega t}\right] = \mathrm{Re}\left[\frac{\mathbf{k}^t}{\omega\mu_0}\times\mathbf{A}^t e^{i(\mathbf{k}^t\cdot\mathbf{r}-\omega t)}\right], \tag{1.101}$$

where $\mathbf{k}^t = k_x^t\hat{\mathbf{x}} + k_y^t\hat{\mathbf{y}} + k_z^t\hat{\mathbf{z}}$, with

$$k_z^t = \sqrt{\omega^2\epsilon_t\mu_0 - (k_x^t)^2 - (k_y^t)^2}. \tag{1.102}$$

Our aim is to determine $\mathbf{A}^r$ and $\mathbf{A}^t$ for given $\mathbf{A}^i$.

1.9.1 Boundary Conditions at an Interface

There exist conditions for the continuity of the tangential and the normal components of both the electric and magnetic fields at an interface between different media. The boundary conditions for the tangential components follow from the Maxwell equations that contain the curl-operator, i.e. (1.55) and (1.56). There holds for the interface $z = 0$ with the incident, reflected and transmitted plane waves introduced above:

$$\hat{\mathbf{z}}\times(\mathbf{E}^i + \mathbf{E}^r) = \hat{\mathbf{z}}\times\mathbf{E}^t, \tag{1.103}$$

$$\hat{\mathbf{z}}\times(\mathbf{H}^i + \mathbf{H}^r) = \hat{\mathbf{z}}\times\mathbf{H}^t, \tag{1.104}$$

where $\hat{\mathbf{z}}$ is the unit normal on the interface. This means that the tangential components of the *total* electric and *total* magnetic field are continuous across the interface, or explicitly:

$$E_x^i(x,y,0) + E_x^r(x,y,0) = E_x^t(x,y,0), \tag{1.105}$$

$$E_y^i(x,y,0) + E_y^r(x,y,0) = E_y^t(x,y,0), \tag{1.106}$$

and similarly for the magnetic field.

We will only demonstrate that the tangential components of the electric field are continuous. By choosing a thin closed loop in the (x,z)-plane which is intersected by the interface $z = 0$ as shown in Fig. 1.9, and integrating the y-component of Faraday's Law (1.18) for the total electromagnetic field over the area A bounded by the loop $\mathcal{L}$, we obtain:

$$-\mu_0\frac{d}{dt}\iint_A \hat{\mathbf{y}}\cdot\boldsymbol{\mathcal{H}}\,\mathrm{d}A = \iint_A \hat{\mathbf{y}}\cdot\nabla\times\boldsymbol{\mathcal{E}}\,\mathrm{d}A = \oint_{\mathcal{L}}\boldsymbol{\mathcal{E}}\cdot\mathrm{d}\mathbf{l}, \tag{1.107}$$

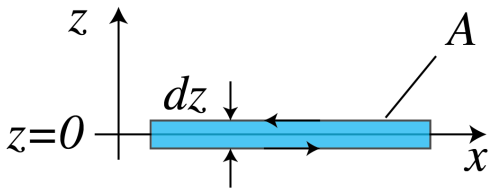


Figure 1.9: Thin closed losed loop in the (x, z)-plane enclosing the area A and surrounding part of the interface $z = 0$, as used in Stokes' Law to derive the continuity of the electric and magnetic components which are tangential to the interface and parallel to the plane through the loop.

where in the last step we used Stokes' theorem with the direction of integration over the loop given by that of the direction of rotation of a screw driver when it moves in the direction of the normal $\hat{\mathbf{y}}$. In words: the rate of change of the magnetic flux through the surface A is equal to the integral of the tangential electric field over the bounding closed loop $\mathcal{L}$.

By taking the limit $\mathrm{d}z \to 0$, the surface integral and the integrals over the vertical parts of the loop vanish and there remain only the integrals of the tangential electric field over the horizontal parts parallel to the x-axis of the loop on both sides of the interface $z = 0$. Since these integrals are traversed in opposite directions and the lengths of these parts are the same and arbitrary, we conclude for the loop as shown in Fig. 1.9 that

$$\lim_{z\uparrow 0} \boldsymbol{\mathcal{E}}_x(x, y, z, t) = \lim_{z\downarrow 0} \boldsymbol{\mathcal{E}}_x(x, y, z, t), \tag{1.108}$$

where $\boldsymbol{\mathcal{E}}$ is the total electric field, i.e. it is equal to the sum of the incident and the reflected field for $z < 0$, and equal to the transmitted field in $z > 0$. By choosing the closed loop in the (y, z)-plane instead of the (x, z)-plane one finds similarly that the y-component of the electric field is continuous. The continuity of the tangential components of the magnetic field are derived in a similar manner.

Our derivation holds for electromagnetic fields of arbitrary time dependence. Furthermore, the derivation used above for the planar interface $z = 0$ can easily be generalized for curved surfaces. Therefore we conclude:

> The tangential electric and magnetic field components are continuous across any interface.

By integrating Maxwell's equations that contain the div-operator (1.20), (1.21) over a pill box with height $\mathrm{d}z$ and top and bottom surfaces on either side and parallel to the interface, and considering the limit $\mathrm{d}z \to 0$, we find continuity relations for the normal components of the fields:

$$\lim_{z\uparrow 0} \epsilon_i\, \hat{\mathbf{z}} \cdot \boldsymbol{\mathcal{E}}(x, y, z, t) = \lim_{z\downarrow 0} \epsilon_t\, \hat{\mathbf{z}} \cdot \boldsymbol{\mathcal{E}}(x, y, z, t), \tag{1.109}$$

$$\lim_{z\uparrow 0} \hat{\mathbf{z}} \cdot \boldsymbol{\mathcal{H}}(x, y, z, t) = \lim_{z\downarrow 0} \hat{\mathbf{z}} \cdot \boldsymbol{\mathcal{H}}(x, y, z, t), \tag{1.110}$$

> The normal components of $\epsilon\boldsymbol{\mathcal{E}}$ and $\boldsymbol{\mathcal{H}}$ are continuous across an interface.

Remarks.

1. Since the derived boundary conditions hold for all times t, it follows that for time-harmonic fields they also hold for the complex fields. Hence (1.103) and (1.104) hold and similarly we find that the normal components of $\epsilon\mathbf{E}$ and $\mathbf{H}$ are continuous.

2. When the magnetic permeability is discontinuous, we have that the normal component of $\mu\boldsymbol{\mathcal{H}}$ is continuous across the interface. But as has been remarked before, at optical frequencies the magnetic permeability is often that of vacuum and we assume this to be the case in this book.

1.9.2 Snell's Law

By substituting the complex electric fields derived from (1.94), (1.97) and (1.100) into equation (1.103), we get

$$\hat{\mathbf{z}} \times \left[\mathbf{A}^i e^{i(k_x^i x + k_y^i y)} + \mathbf{A}^r e^{i(k_x^r x + k_y^r y)}\right] = \hat{\mathbf{z}} \times \mathbf{A}^t e^{i(k_x^t x + k_y^t y)}, \tag{1.111}$$

Since this equation must be satisfied for all points (x, y), it follows that

$$k_x^i = k_x^r = k_x^t, \tag{1.112}$$

$$k_y^i = k_y^r = k_y^t. \tag{1.113}$$

Hence, the tangential components of the wave vectors of the incident, reflected and transmitted waves are identical. In fact, if (1.112) would not hold, then by keeping y fixed, the exponential functions in (1.111) would not all have the same periodicity as functions of x and then (1.111) could never be satisfied for all x. The same argument with x kept fixed leads to the conclusion (1.113).

Without restricting the generality, we will from now on assume that the coordinate system is chosen such that

$$k_y^i = k_y^r = k_y^t = 0. \tag{1.114}$$

The plane through the incident wave vector and the normal to the interface is called the **plane of incidence**. Hence in the case of (1.114) the plane of incidence is the (x, z)-plane.

Since the length of the wave vectors $\mathbf{k}^i$ and $\mathbf{k}^r$ is $k_0 n_i$, with k_0 the wave number in vacuum and $n_i = \sqrt{\epsilon_i/\epsilon_0}$ the refractive index, and since the length of $\mathbf{k}^t$ is $k_0 n_t$, with $n_t = \sqrt{\epsilon_t/\epsilon_0}$, it follows from (1.112)

$$\sin\theta_i = \frac{k_x^i}{k_0 n_i} = \frac{k_x^r}{k_0 n_i} = \sin\theta_r, \tag{1.115}$$

and

$$n_i \sin\theta_i = \frac{k_x^i}{k_0} = \frac{k_x^t}{k_0} = n_t \sin\theta_t, \tag{1.116}$$

where the angles are as in Fig. 1.10. Hence,

$$\theta_i = \theta_r, \qquad \text{angle of reflection} = \text{angle of incidence}, \tag{1.117}$$

$$n_i \sin\theta_i = n_t \sin\theta_t, \qquad \text{Snell's Law}. \tag{1.118}$$

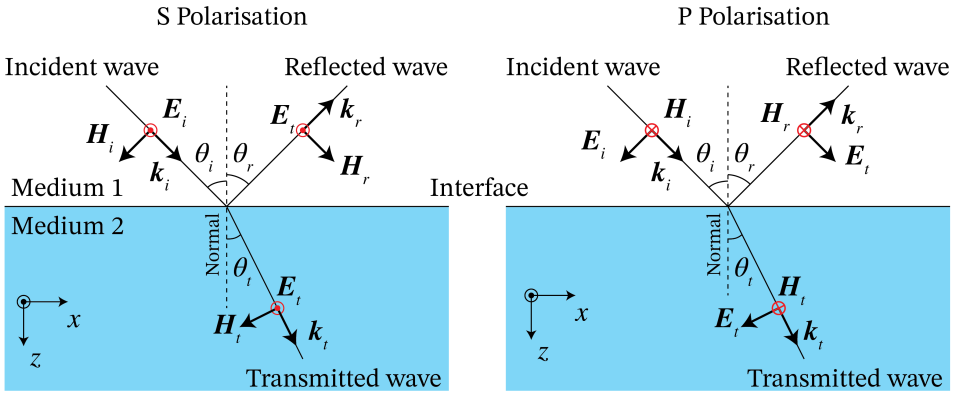


Figure 1.10: The incident, reflected, and transmitted wave vectors with the electric and magnetic vectors for s- and p-polarisation. Note that the positive z-axis is pointing downwards and hence that the positive y-axis points out of the paper. For s-polarisation the electric field points in the positive y-direction at the instant shown while for p-polarisation the magnetic field points in the positive y-direction at the instant shown.

Snell's Law[12] implies that when the angle of incidence θ_i increases, the angle of transmission increases as well. When the medium in $z < 0$ is air with refractive index $n_i = 1$ and the other medium is glass with refractive index $n_t = 1.5$, the maximum angle of transmission occurs when $\theta_i = 90°$ with

$$\theta_{t,max} = \arcsin(n_i/n_t) = 41.8°. \tag{1.119}$$

In case the light is incident from glass, i.e. $n_i = 1.5$ and $n_t = 1.0$, the angle of incidence θ_i cannot be larger than 41.8° because otherwise there is no real solution for θ_t. It turns out that when $\theta_i > 41.8°$, the wave is totally reflected and there is no *propagating* transmitted wave in air. As explained in Section 1.9.5, this does however not mean that there is no field in $z > 0$. In fact there is a non-propagating so-called evanescent wave in $z > 0$. The angle $\theta_{i,crit} = 41.8°$ is called the **critical angle of total internal reflection**. It exists only if a wave is incident from a medium with larger refractive index on a medium with lower refractive index ($n_t < n_i$). The critical angle is independent of the polarisation of the incident wave.

1.9.3 Fresnel Coefficients

Because of (1.112) and (1.114), we write $k_x = k_x^i = k_x^r = k_x^t$ and therefore $k_z^i = \sqrt{\omega^2\epsilon_i\mu_0 - k_x^2} = -k_z^r$ and $k_z^t = \sqrt{\omega^2\epsilon_t\mu_0 - k_x^2}$. Hence,

$$\mathbf{k}^i = k_x\hat{\mathbf{x}} + k_z^i\hat{\mathbf{z}}, \quad \mathbf{k}^r = k_x\hat{\mathbf{x}} - k_z^i\hat{\mathbf{z}}, \tag{1.120}$$

and

$$\mathbf{k}^t = k_x\hat{\mathbf{x}} + k_z^t\hat{\mathbf{z}}. \tag{1.121}$$

According to (1.64), for the incident, reflected and transmitted plane waves there must hold:

$$\mathbf{A}^i \cdot \mathbf{k}^i = \mathbf{A}^r \cdot \mathbf{k}^r = \mathbf{A}^t \cdot \mathbf{k}^t = 0. \tag{1.122}$$

We choose an orthonormal basis perpendicular to $\mathbf{k}^i$ with unit vectors:

$$\hat{\mathbf{s}} = \hat{\mathbf{y}}, \quad \hat{\mathbf{p}}^i = \frac{1}{|\mathbf{k}^i|}\left(-k_z^i\hat{\mathbf{x}} + k_x\hat{\mathbf{z}}\right), \tag{1.123}$$

[12]Named after Willebrord Snellius 1580-1626, mathematics professor in Leiden

where

$$|\mathbf{k}^i| = \sqrt{\mathbf{k}^i \cdot (\mathbf{k}^i)^*} = \sqrt{k_x^2 + |k_z^i|^2}, \tag{1.124}$$

and where in writing the complex conjugate we anticipate the case the k_z^i is complex, which may happen for example when ϵ_i is complex (a case that has been excluded so far but which later will be considered) or in the case of evanescent waves discussed in Section 1.9.5. Note that when k_z^i is real, $|\mathbf{k}^i| = \sqrt{k_x^2 + (k_z^i)^2} = k_0 n_i$. It is easy to see that the basis (1.123) is orthonormal in the space of two-dimensional complex vectors and that $\hat{\mathbf{s}} \cdot \mathbf{k}^i = \hat{\mathbf{p}}^i \cdot \mathbf{k}^i = 0$. The vector $\hat{\mathbf{s}}$ is perpendicular to the plane of incidence, therefore the electric field component in this direction is polarised perpendicular to the plane of incidence and is called *s*-polarised ("Senkrecht" in German). The other basis vector $\hat{\mathbf{p}}^i$ is (for real $\mathbf{k}^i$) parallel to the plane of incidence. When the electric component is along this direction, it is called *p*-polarised. The complex vector $\mathbf{A}^i$ can be expanded on this basis:

$$\mathbf{A}^i = A_s^i\, \hat{\mathbf{y}} + A_p^i\, \hat{\mathbf{p}}^i. \tag{1.125}$$

Since

$$\mathbf{k}^i \times \hat{\mathbf{y}} = |\mathbf{k}^i| \hat{\mathbf{p}}^i, \quad \mathbf{k}^i \times \hat{\mathbf{p}}^i = -\frac{k_0^2 \epsilon_i}{|\mathbf{k}^i|} \hat{\mathbf{y}}, \tag{1.126}$$

it follows that the electric and magnetic field of the incident plane wave can be written as

$$\mathbf{E}^i(\mathbf{r}) = \left(A_s^i\, \hat{\mathbf{y}} + A_p^i\, \hat{\mathbf{p}}^i\right) e^{i\mathbf{k}^i \cdot \mathbf{r}}, \tag{1.127}$$

$$\mathbf{H}^i(\mathbf{r}) = \left(\frac{|\mathbf{k}^i|}{\omega \mu_0} A_s^i\, \hat{\mathbf{p}}^i - \frac{\omega \epsilon_0 \epsilon_i}{|\mathbf{k}^i|} A_p^i\, \hat{\mathbf{y}}\right) e^{i\mathbf{k}^i \cdot \mathbf{r}}. \tag{1.128}$$

The reflected field is similarly expanded on the basis $\hat{\mathbf{y}}$ and $\hat{\mathbf{p}}^r$ with

$$\hat{\mathbf{p}}^r = -\frac{1}{|\mathbf{k}^i|} \left(k_z^i \hat{\mathbf{x}} + k_x \hat{\mathbf{z}}\right). \tag{1.129}$$

The sign in front of the unit vector $\hat{\mathbf{p}}^r$ is chosen such that its x-component is the same as that of $\hat{\mathbf{p}}^i$. Since

$$\mathbf{k}^r \times \hat{\mathbf{y}} = -|\mathbf{k}^i| \hat{\mathbf{p}}^r, \quad \mathbf{k}^r \times \hat{\mathbf{p}}^r = \frac{k_0^2 \epsilon_i}{|\mathbf{k}^i|} \hat{\mathbf{y}}, \tag{1.130}$$

it follows that

$$\mathbf{E}^r(\mathbf{r}) = \left(A_s^r\, \hat{\mathbf{y}} + A_p^r\, \hat{\mathbf{p}}^r\right) e^{i\mathbf{k}^r \cdot \mathbf{r}}, \tag{1.131}$$

$$\mathbf{H}^r(\mathbf{r}) = \left(-\frac{|\mathbf{k}^i|}{\omega \mu_0} A_s^r\, \hat{\mathbf{p}}^r + \frac{\omega \epsilon_0 \epsilon_i}{|\mathbf{k}^i|} A_p^r\, \hat{\mathbf{y}}\right) e^{i\mathbf{k}^r \cdot \mathbf{r}}, \tag{1.132}$$

where we used that $\mathbf{k}^r \cdot \mathbf{k}^r = k_0^2 n_i^2$ and $|\mathbf{k}^r| = \sqrt{k_x^2 + |k_z^r|^2} = \sqrt{k_x^2 + |k_z^i|^2} = |\mathbf{k}^i|$. For the transmitted plane wave we use the basis $\hat{\mathbf{y}}$ and $\hat{\mathbf{p}}^t$ with

$$\hat{\mathbf{p}}^t = \frac{1}{|\mathbf{k}^t|} \left(-k_z^t \hat{\mathbf{x}} + k_x \hat{\mathbf{z}}\right), \tag{1.133}$$

where $\hat{\mathbf{p}}^t$ is chosen such that the x-component of $\hat{\mathbf{p}}^t$ has the same sign as the x-component of $\hat{\mathbf{p}}^i$. Since

$$\mathbf{k}^t \times \hat{\mathbf{y}} = |\mathbf{k}^t| \hat{\mathbf{p}}^t, \quad \mathbf{k}^t \times \hat{\mathbf{p}}^t = -\frac{k_0^2 \epsilon_t}{|\mathbf{k}^t|} \hat{\mathbf{y}}, \tag{1.134}$$

we get

$$\mathbf{E}^t(\mathbf{r}) = \left(A_s^t\,\hat{\mathbf{y}} + A_p^t\,\hat{\mathbf{p}}^t\right) e^{i\mathbf{k}^t\cdot\mathbf{r}}, \tag{1.135}$$

$$\mathbf{H}^t(\mathbf{r}) = \left(\frac{|\mathbf{k}^t|}{\omega\mu_0}A_s^t\,\hat{\mathbf{p}}^t - \frac{\omega\epsilon_0\epsilon_t}{|\mathbf{k}^t|}A_p^t\,\hat{\mathbf{y}}\right) e^{i\mathbf{k}^t\cdot\mathbf{r}}. \tag{1.136}$$

We now consider an s-polarised incident plane wave, i.e. $A_p^i = 0$. We will show that all boundary conditions can be satisfied by $A_p^r = A_p^t = 0$ and by appropriately expressing A_s^r and A_s^t in terms of A_s^i. This implies that if the incident plane wave is s-polarised, the reflected and transmitted waves are s-polarised as well. For s-polarisation, the electric field has only a y-component and this component is tangential to the interface $z = 0$. This leads to the condition

$$A_s^i + A_s^r = A_s^t. \tag{1.137}$$

The only tangential component of the magnetic field is the x-component and requiring it to be continuous for $z = 0$ leads to

$$-k_z^i A_s^i + k_z^i A_s^r = -k_z^t A_s^t. \tag{1.138}$$

Solving (1.137), (1.138) for A_s^r and A_s^t gives the following formula for the reflection and transmission coefficients:

$$r_s = \frac{A_s^r}{A_s^i} = \frac{k_z^i - k_z^t}{k_z^i + k_z^t}, \tag{1.139}$$

$$t_s = \frac{A_s^t}{A_s^i} = \frac{2k_z^i}{k_z^i + k_z^t}. \tag{1.140}$$

Only the magnetic field has a z-component and it easy to verify that $H_z^i + H_z^r = H_z$ for $z = 0$.

By looking at the case of a p-polarised incident wave: $A_s^i = 0$, we see that the expressions for the magnetic field in the p-polarised case become similar (except for the chosen signs) to that of the electric field for s-polarisation and conversely. Enforcing the continuity of the tangential components at $z = 0$ gives for p-polarisation:

$$r_p = \frac{A_p^r}{A_p^i} = -\frac{\frac{k_z^i}{\epsilon_i} - \frac{k_z^t}{\epsilon_t}}{\frac{k_z^i}{\epsilon_i} + \frac{k_z^t}{\epsilon_t}}, \tag{1.141}$$

$$t_p = \frac{A_p^t}{A_p^i} = \frac{\epsilon_i|\mathbf{k}^t|}{\epsilon_t|\mathbf{k}^i|}\frac{\frac{2k_z^i}{\epsilon_i}}{\frac{k_z^i}{\epsilon_i} + \frac{k_z^t}{\epsilon_t}}. \tag{1.142}$$

It is easy to verify that E_z is the only normal component and that $\epsilon_i(E_z^i + E_z^r) = \epsilon_t E_z^t$ for $z = 0$.

The reflection and transmission coefficients r_s, r_p, t_s and t_p are called **Fresnel coefficients**. As follows from the derivation, there is no cross talk between s- and p-polarised plane waves incident on a planar interface. A generally polarised incident plane wave can always be written as a linear combination of s- and a p-polarised incident plane waves. Because in general $r_s \neq r_p$ and $t_s \neq t_p$, it follows that the reflected and transmitted fields are also linear combinations of s- and p-polarised fields, but with different coefficients (weights) of these two fundamental polarisation states than for the incident wave.

Remarks.

1. In the derivation of the Fresnel coefficients the continuity of the normal field components was not used and was automatically satisfied. The reason is that the electromagnetic fields of the plane waves were chosen from the start to be perpendicular to the wave vectors. This implies that the divergence of $\epsilon\boldsymbol{\mathcal{E}}$ and of $\boldsymbol{\mathcal{H}}$ vanishes which in turn implies that the normal components are automatically continuous across the interface.

2. When k_z^i and k_z^t are both real, we have $|\mathbf{k}^i| = k_0 n_i$ and $|\mathbf{k}^t| = k_0 n_t$ and the Fresnel coefficients can be expressed in the angles θ_i, θ_r and θ_t and the refractive indices $n_i = \sqrt{\epsilon_i/\epsilon_0}$ and $n_t = \sqrt{\epsilon_t/\epsilon_0}$. Because $k_z^i = k_0 n_i \cos\theta_i$ and $k_z^t = k_0 n_t \cos\theta_t$, we find

$$r_s = \frac{n_i\cos\theta_i - n_t\cos\theta_t}{n_i\cos\theta_i + n_t\cos\theta_t} = -\frac{\sin(\theta_i-\theta_t)}{\sin(\theta_i+\theta_t)}, \tag{1.143}$$

$$t_s = \frac{2n_i\cos\theta_i}{n_i\cos\theta_i + n_t\cos\theta_t} = \frac{2\cos\theta_i\sin\theta_t}{\sin(\theta_i+\theta_t)}, \tag{1.144}$$

and

$$r_p = -\frac{\frac{\cos\theta_i}{n_i} - \frac{\cos\theta_t}{n_t}}{\frac{\cos\theta_i}{n_i} + \frac{\cos\theta_t}{n_t}} = -\frac{\tan(\theta_i-\theta_t)}{\tan(\theta_i+\theta_t)}, \tag{1.145}$$

$$t_p = \frac{\frac{2\cos\theta_i}{n_i}}{\frac{\cos\theta_i}{n_i} + \frac{\cos\theta_t}{n_t}} = \frac{2\cos\theta_i\sin\theta_t}{\sin(\theta_i+\theta_t)\cos(\theta_i-\theta_t)}. \tag{1.146}$$

To obtain the expressions at the far right in (1.143)-(1.146) Snell's Law has been used.

3. The big advantage of the expressions (1.139), (1.140), (1.141), (1.142) in terms of the wave vector components k_z^i and k_z^t is that these also apply when k_z^i and/or k_z^t are complex. The components k_z^i and/or k_z^t are complex when there is absorption in $z < 0$ and/or in $z > 0$. When the materials are lossless and $\epsilon_i > \epsilon_t$ and the incident angle is above the critical angle, k_z^t is imaginary (see Section 1.9.5). In all these cases (1.139), (1.140), (1.141), (1.142) apply.

1.9.4 Properties of the Fresnel Coefficients

For normal incidence: $\theta_i = 0$, Snell's Law implies: $\theta_t = 0$. Hence, (1.143), (1.145) give:

$$r_s(\theta_i = 0) = r_p(\theta_i = 0) = \frac{n_i - n_t}{n_i + n_t}, \tag{1.147}$$

So for normal incidence: $r_p = r_s$, as expected. Note however that if we would not have defined $\hat{\mathbf{p}}^r$ such that its tangential components are the same as those of $\hat{\mathbf{p}}^i$, the two reflection coefficients for normal incidence would have had the opposite signs (as is the case in some books). If the incident medium is air and the other medium is glass ($n_i = 1.0$, $n_t = 1.5$), we get

$$r_s(\theta_i = 0) = r_p(\theta_i = 0) = -0.2, \tag{1.148}$$

and since the flow of energy is proportional to the square of the field, it follows that 4% of the light incident in the direction of the normal is reflected at the interface between air and glass. Hence a lens of glass without anti-reflection coating reflects approximately 4% of the light at normal incidence. The transmission coefficient for normal incidence is:

$$t_s(\theta_i = 0) = t_p(\theta_i = 0) = \frac{2n_i}{n_i + n_t}, \tag{1.149}$$

which for air-glass becomes 0.8.

Remark. Energy conservation requires that the time-averaged normal component $\langle S_z \rangle$ of the energy flux through the interface is continuous. By using the formula for the time-averaged Poynting vector of a plane wave (1.92), it can be verified that the Fresnel coefficients are such that the energy flux is indeed conserved.

It follows from Snell's Law (1.118) that when both refractive indices n_i and n_t are real, $\sin\theta_t = (n_i/n_t)\sin\theta_i$. Hence θ_t monotonically increases with θ_i and therefore there exists some θ_i such that

$$\theta_i + \theta_t = 90^\circ. \tag{1.150}$$

For this particular angle of incidence, the denominator of (1.145) is infinite and hence $r_p = 0$, i.e. the p-polarised wave is not reflected at all. This angle of incidence is called the **Brewster angle**θ_B[15]. It is easy to see from (1.143) that the reflection is never zero for s-polarisation.

If unpolarised light is incident at the Brewster angle, the reflected light will be purely s-polarised.

Since at the Brewster angle s-polarised light is only partially reflected and the rest is transmitted, the transmitted light at the Brewster angle is a mixture of s- and p-polarisation. We have $\theta_t = 90^\circ - \theta_i$, hence $\sin\theta_t = \cos\theta_i$ and by Snell's Law (writing $\theta_i = \theta_B$):

$$\tan(\theta_B) = \frac{n_t}{n_i}. \tag{1.151}$$

We see that there is always a Brewster angle when both refractive indices are real, independent of whether the wave is incident from the material with the smallest or largest refractive index. For the air-glass interface we have $\theta_B = 56.3^\circ$ and $\theta_t = 33.7^\circ$. By (1.143):

$$r_s(\theta_B = 56.3^\circ) = -0.38, \tag{1.152}$$

so that $(0.38)^2/2 = 0.07$, or 7 % of the unpolarised light is reflected as purely s-polarised light at the air glass interface at the Brewster angle. For a wave incident from glass, $\theta_B = 33.7^\circ$.

In Fig. 1.11 the Fresnel reflection and transmission coefficients of s- and p-polarised waves are shown as functions of the angle of incidence for the case of incidence from air to glass. There is no critical angle of total reflection in this case. The Brewster angle is indicated. It is seen that the reflection coefficients decrease from the values -0.2 for $\theta_i = 0^\circ$ to -1 for $\theta_i = 90^\circ$. The transmission coefficients monotonically decrease to 0 at $\theta_i = 90^\circ$.

Fig. 1.12 shows the Fresnel coefficients when the wave is incident from glass to air. The critical angle is $\theta_{i,crit} = 41.8^\circ$ as derived earlier. At the angle of total internal reflection the absolute values of the reflection coefficients are identical to 1. There is again an angle where the reflection of p-polarised light is zero $\theta_B = 33.7^\circ$.

Depending on the refractive indices and the angle of incidence, the Fresnel reflection coefficients can be negative. The reflected electric field then has an additional π phase shift compared to the incident wave. In contrast, provided that the materials are lossless and the angle of incidence is below the critical angle, the transmitted field is always in phase with the incident field, i.e. the transmission coefficients are always positive under the mentioned conditions.

[15] MIT OCW - Reflection at The Air-glass Boundary: demonstration of reflection of polarised light and the Brewster angle.

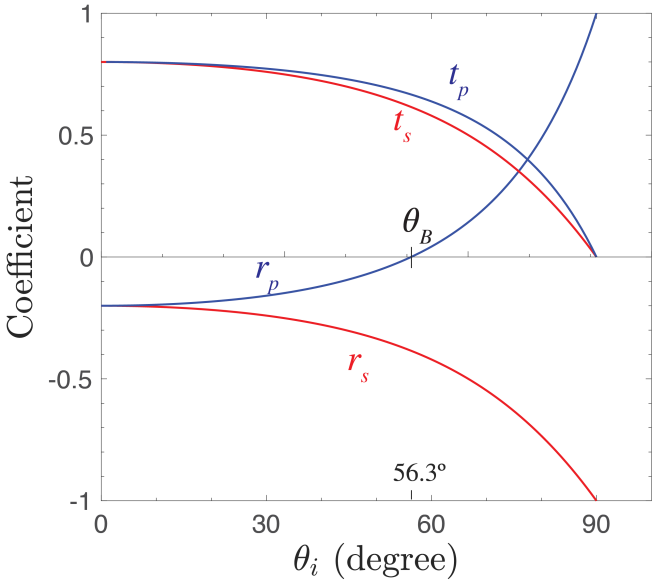


Figure 1.11: Reflection and transmission coefficients as function of the angle of incidence of s- and p-polarised waves incident from air to glass. The Brewster angle θ_B is indicated.

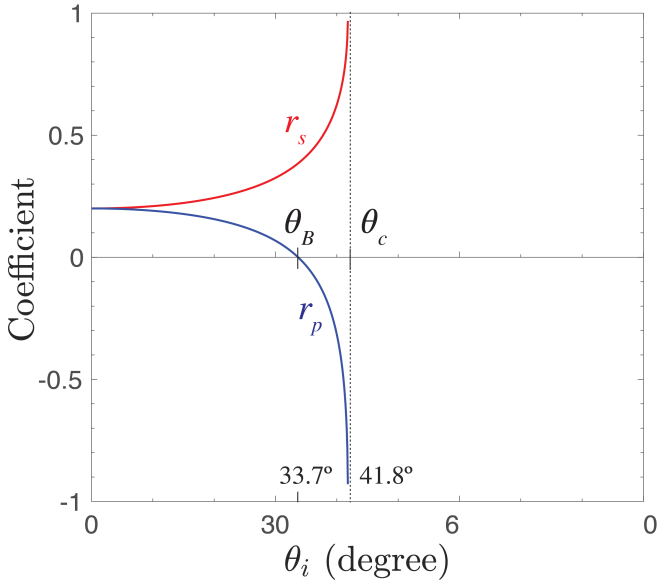


Figure 1.12: Reflection and transmission coefficients as function of the angle of incidence of s- and p-polarised waves incident from glass to air.

1.9.5 Total Internal Reflection and Evanescent Waves

We return to the case of a wave incident from glass to air, i.e. $n_i = 1.5$ and $n_t = 1$. As has been explained, there is then a critical angle, given by

$$\sin\theta_{i,crit} = \frac{n_t}{n_i}.$$

This is equivalent to

$$k_x^t = k_0 n_i \sin\theta_{i,crit} = k_0 n_t. \tag{1.153}$$

The wave vector $\mathbf{k}^t = k_x^t\hat{\mathbf{x}} + k_z^t\hat{\mathbf{z}}$ in $z > 0$ always satisfies:

$$(k_x^t)^2 + (k_z^t)^2 = k_0^2 n_t^2, \tag{1.154}$$

and hence at the critical angle there holds

$$k_z^t = 0. \tag{1.155}$$

For angles of incidence above the critical angle we have: $k_x^t > k_0 n_t$ and it follows from (1.154) that $(k_z^t)^2 = k_0^2 n_t^2 - (k_x^t)^2 < 0$, hence k_z^t is **imaginary**:

$$k_z^t = \pm\sqrt{k_0^2 n_t^2 - (k_x^t)^2} = \pm i\sqrt{(k_x^t)^2 - k_0^2 n_t^2}, \tag{1.156}$$

where the last square root is a positive real number. It can be shown that above the critical angle the reflection coefficients are **complex** numbers with modulus 1: $|r_s| = |r_p| = 1$. This implies that the reflected intensity is identical to the incident intensity, while at the same time the transmission coefficients are not zero! For example, for s-polarisation we have according to (1.139), (1.140):

$$t_s = 1 + r_s \neq 0, \tag{1.157}$$

because $r_s \neq -1$ (although $|r_s| = 1$). Therefore there is an electric field in $z > 0$, given by

$$\mathbf{E}(x,z)e^{-i\omega t} = t_s e^{ik_x^t x + ik_z^t z - i\omega t}\hat{\mathbf{y}} = t_s e^{i(k_x^t x - \omega t)} e^{-z\sqrt{(k_x^t)^2 - k_0^2 n_t^2}}\hat{\mathbf{y}}, \quad z > 0, \tag{1.158}$$

where we have chosen the + sign in (1.156) to prevent the field from blowing up for $z \to \infty$. Since k_x^t is real, the wave propagates in the x-direction. In the z-direction, however, the wave is **not** propagating. Its amplitude decreases exponentially as a function of distance z to the interface and therefore the wave is confined to a thin layer adjacent to the interface. Such a wave is called an **evanescent wave**. The Poynting vector of the evanescent wave can be computed and is found to be parallel to the interface. Hence,

> The flow of energy of an evanescent wave propagates parallel to the interface, namely in the direction in which k_x^t is positive.

Hence, above the critical angle, no energy is transported away from the interface into the air region. We shall return to evanescent waves in the chapter on diffraction theory.

External sources in recommended order

1. Youtube video - 8.03 - Lect 18 - Index of Refraction, Reflection, Fresnel Equations, Brewster Angle - Lecture by Walter Lewin
2. MIT OCW - Reflection at The Air-glass Boundary: demonstration of reflection of polarised light and the Brewster angle.

1.10 Fiber Optics

We will show in Chapter 6 on diffraction that a light beam ultimately always becomes broader for increasing propagation distance. The divergence means that the energy density in the beam decreases with propagation distance. This divergence can be prevented by letting the light propagate inside a fiber. The guiding of light inside a fiber is based on the phenomenon of total internal reflection. The principle has been known for a long time, but the topic was greatly boosted by the invention of the laser.

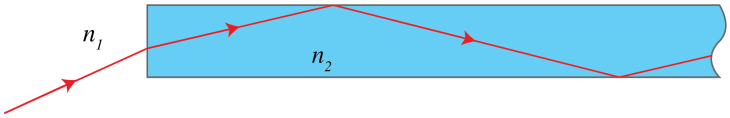




Figure 1.13: Top: schematic of a light ray entering a glass fiber (blue). Inside the fiber the light is totally reflected and is guided by the fiber. The lower left figure shows light guided within a piece of glass (from Wikimedia Commons by Keerthi - CC BY) while the lower right figure shows the end of a glass fiber where the light distribution that exits the fiber has been twisted by 180 degrees due to the propragation through the fiber relative to distribution at the input side of the fiber (Image:©SCHOTT)

.

Consider a straight glass cylinder of refractive index n_2, surrounded by air with refractive index $n_1 = 1 < n_2$. The core of the cylinder has a cross section approximately the size of a human hair and hence, although quite small, it is still many optical wavelengths thick. This implies that when light strikes the cylindrical surface, we can locally consider the cylinder as a flat surface. By focusing a laser beam at the entrance plane of the fiber, light can be coupled into the fiber. The part of the light inside the fiber that strikes the cylinder surface at an angle with the normal that is larger than the critical angle of total reflection will be totally reflected. As it hits the opposite side of the cylinder surface, it will again be totally reflected and so on (Fig. 1.13 top).

Since visible light has such high frequencies (order 10^{15} Hz), roughly a hundred thousand times more information can be carried through a fiber using visible light than using microwave frequencies. Today fibers with very low losses are fabricated so that signals can be sent around the earth with hardly any attenuation. Abraham van Heel, professor of optics at Delft University of Technology, showed for the first time in a paper published in Nature in 1954[16] that by packing

[16]Van Heel, A. A, New Method of transporting Optical Images without Aberrations. Nature 173, 39 (1954)

thousands of fibers into a cable, images can be transferred, even if the bundle is bent (Fig. 1.13 right).

External sources in recommended order

1. MIT OCW - Single Mode Fiber: Demonstration of a single-mode fiber.
2. MIT OCW - Multi-mode Fiber: Demonstration of a multimode fiber.

Problems

1. In a homogeneous medium with permittivity ϵ and conductivity σ and without external sources ($\boldsymbol{\mathcal{J}}_{ext} = \mathbf{0}$, $\varrho_{ext} = 0$), derive from (1.11) and (1.16) that for $t > 0$

$$\varrho_c(t) = -\varrho_c(0)e^{-t/\tau}, \tag{1.159}$$

where $\varrho_c(0)$ is the charge at time $t = 0$ and $\tau = \sigma/\epsilon$ is the relaxation time. Even for a moderate conductor such as sea water, τ is only 2×10^{-10} s.
This shows that the charge density corresponding to conduction currents becomes very quickly negligible.

2. In a medium with constant permittivity ϵ, magnetic permeability μ_0 and conductivity $\sigma = 0$ derive that every component of the magnetic field $\boldsymbol{\mathcal{H}}$ satisfies the wave equation.

3. In a medium with constant ϵ, magnetic permeability μ_0 and conductivity σ, derive that in a region without external sources the electric field satisfies:

$$\nabla^2 \boldsymbol{\mathcal{E}} - \epsilon\mu_0 \frac{\partial^2 \boldsymbol{\mathcal{E}}}{\partial t^2} - \mu_0\sigma \frac{\partial \boldsymbol{\mathcal{E}}}{\partial t} = \mathbf{0}. \tag{1.160}$$

4. Write the expressions for the real and the complex electric and magnetic field of a time-harmonic plane wave with frequency ω and wave number k which propagates in the (x, z)-plane with angle of 45°with the positive x-axis and has electric field parallel to the y-direction with unit amplitude and such that it is maximum for $x = z = 0$ at time $t = 0$.

5. Derive the Fresnel equations (1.141), (1.142) for a p-polarised plane wave.

6. Derive the Fresnel equation (1.143), (1.144), (1.145) and (1.146) for the case that k_z^i and k_z^t are real.

7. Let a p-polarised plane wave be incident on an interface $z = 0$ from $z < 0$. Let there be vacuum in $z < 0$: $\epsilon_i = \epsilon_0$ and let the permittivity in $z > 0$ be $\epsilon_t > 0$. The reflected field can be considered to be radiated in vacuum by dipoles in $z > 0$ with dipole density given by (2.31):

$$\boldsymbol{\mathcal{P}}(\mathbf{r}) = (\epsilon - \epsilon_0)\boldsymbol{\mathcal{E}}^t(\mathbf{r}), \tag{1.161}$$

where $\boldsymbol{\mathcal{E}}^t(\mathbf{r})$ is the transmitted electric field in point $\mathbf{r}$ with $z > 0$.

   a) According to (1.75) the field radiated by a dipole vanishes in the line of sight parallel to the direction of the dipole. Derive from this the relationship between the angle of reflection θ_r and the incident angle θ_i for which the reflected field vanishes.

   b) Show that this relationship is satisfied by the Brewster angle for a p-polarised incident wave but that it can not be satisfied for an s-polarised incident wave.

8. **Two plane waves.** Consider two electromagnetic plane waves with wave vectors $\mathbf{k}_1 = k_x\hat{\mathbf{x}} + k_z\hat{\mathbf{z}}$ and $\mathbf{k}_2 = k_x\hat{\mathbf{x}} - k_z\hat{\mathbf{z}}$, where $k_z = \sqrt{k_0^2\epsilon - k_x^2}$, where k_0 is the wave number in vacuum and ϵ is the permittivity which is assumed to be real. These plane waves are both polarised parallel to the y-direction, i.e. the electric field is along the y-direction. They real amplitudes A_1 and A_2 and are in phase for $\mathbf{r} = \mathbf{0}$ at $t = 0$.

   a) Write the expressions for the total complex and real electric field $\mathbf{E}$, $\boldsymbol{\mathcal{E}}$ and magnetic field $\mathbf{H}$ and $\boldsymbol{\mathcal{H}}$.

   b) Compute the square modulus $|\boldsymbol{\mathcal{E}}|^2$ of the total electric field.

   c) There is a standing wave as function of z. What is the period of this standing wave as function of the angle $\theta = 2\arctan(k_z/k_x)$ between the wave vectors? Make a sketch of this period as function of θ. Note: the standing wave occurs in the direction in which the wave vectors are opposite, i.e. in this case the z-direction.

   d) Compute the time-averaged Poynting vector. Show that its z-component is the sum of the z-components of the time-averaged Poynting vectors of the individual plane waves. This result proves that the net energy flow in the z-direction for the case of an incident plane wave that is partially reflected at an interface is the difference between the incident and the reflected intensities.

link

e) The x-component of the Poynting vector is a function of z. Show that nevertheless the total flux through the boundary of any cube with faces that are perpendicular to one of the unit vectors $\hat{\mathbf{x}}$, $\hat{\mathbf{y}}$ and $\hat{\mathbf{z}}$, vanishes.

9. **Evanescent wave.** Consider a wave in $z < 0$ that is incident on an interface $z = 0$ between glass with $n_i = 1.5$ in $z < 0$ and air with $n_t = 1$ in $z > 0$. Let the wave vector of the incident wave be $\mathbf{k}^i = k_x\hat{\mathbf{x}} + k_z^i\hat{\mathbf{z}}$ and let $k_x > k_0 n_i$, so that the angle of incidence is above the critical angle.

   a) If the incident wave is s-polarised, derive expressions for the complex electric $\boldsymbol{\mathcal{E}}^t$ and magnetic $\boldsymbol{\mathcal{H}}^t$ field in $z > 0$.

   b) Compute the time averaged Poynting vector in a point $\mathbf{r}$ with $z > 0$.

   c) What is the direction of the energy flow in $z > 0$?

   d) Explain that when the Poynting vector would have a nonzero z-component, this would contradict the conservation of energy.

10. * **Electric dipole.**
    Let an electric dipole be at the origin and let its dipole vector be parallel to the z-direction: $\mathbf{p} = p\hat{\mathbf{z}}$. Then $\hat{\mathbf{R}} = \hat{\mathbf{r}}$ and $R = r$ in (1.74) and (1.75). Let the frequency be ω and let the surrounding medium have real permittivity ϵ.

    a) Show that at large distance to the dipole, the time-averaged Poynting vector is given by

$$\mathbf{S}(\mathbf{r}) = \left(\frac{\mu_0}{\epsilon_0}\right)^{\frac{1}{2}} n\frac{\omega^4 p^2}{32\pi^2 c^2}\,|\hat{\mathbf{r}} \times \hat{\mathbf{z}}|^2\,\frac{\hat{\mathbf{r}}}{r^2}, \tag{1.162}$$

    where $n = \sqrt{\epsilon}$ is the refractive index.

    b) Show that the totally radiated power is:

$$P = \left(\frac{\mu_0}{\epsilon_0}\right)^{1/2} n\frac{\omega^4 p^2}{12\pi c^2}. \tag{1.163}$$

    Hint: integrate over a sphere $r =$ constant using spherical coordinates $\mathbf{r} = r\sin\theta\cos\varphi\hat{\mathbf{x}} + r\sin\theta\sin\varphi\hat{\mathbf{y}} + r\cos\theta\hat{\mathbf{z}}$.

    c) For a given dipole vector, the radiated power increases with the fourth power of the frequency. Explain with this property why the clear sky is blue.

Chapter 2

Geometrical Optics

What you should know and be able to do after studying this chapter

- Principle of Fermat.
- Know how to derive the law of reflection and Snell's law of refraction from the Principle of Fermat.
- Be able to explain what in geometrical optics is a perfect image.
- Understand the approximation made in Gaussian geometrical optics.
- Know how to work with the sign convention of the Lens Maker's Formula (not the derivation of the formula).
- Understand how the Lens Maker's Formula of a single lens follows from the formula for a single interface.
- Understand how the image of two and more lenses is derived from that of a single lens by construction and by computing intermediate images. You do not need to know the imaging equation and the formulae for the focal distances of two thin lenses.
- Understand the matrix method (you do not need to know the matrices by hart).
- Understand the limitations of geometrical optics, in particular when diffraction optics is needed.

Nice software for practicing geometrical optics:
https://www.geogebra.org/m/X8RuneVy

2.1 Introduction

Geometrical optics is an old subject but it is still essential to understand and design optical instruments such as camera's, microscopes, telescopes etc. Geometrical optics started long before it was discovered that light is an electromagnetic wave and that optics is part of electromagnetism.

In this chapter we go back in history and treat geometrical optics. That may seem strange now that we have a much more accurate and better theory at our disposal. However, the predictions of geometrical optics are under quite common circumstances very useful and also very accurate. In fact, for many optical systems and practical instruments there is no alternative for geometrical optics because more accurate theories are much too complicated to use.

When a material is illuminated by monochromatic light, its molecules start to radiate spherical waves (more precisely, they radiate like tiny electric dipoles) with the same frequency as that of the illumination. The total wave scattered by the material is time-harmonic and equal to the sum of all the spherical waves. A time-harmonic wave has at every point in space and at every instant of time a well defined phase. A **wave front** is a set of space-time points where the phase has the same value. At any fixed time, the wave front is called a surface of constant phase. This surface moves with the phase velocity in the direction of its local normal.

For plane waves we have shown in the previous chapter that the surfaces of constant phase are planes and that the normal to these surfaces is in the direction of the wave vector which coincides with the direction of the phase velocity as well as with the direction of the flow of energy (the direction of the Poynting vector). For general waves, the local direction of energy flow is given by the direction of the Poynting vector. Provided that the radius of curvature of the surfaces of constant phase is much larger than the wavelength, the normal to these surfaces may still be considered to be in the direction of the local flow of energy. Such waves behave locally as plane waves and their effect can be accurately described by the methods of geometrical optics.

Geometrical optics is based on the intuitive idea that light consists of a bundle of rays. But what is a ray?

A ray is an oriented curve which is everywhere perpendicular to the surfaces of constant phase and points in the direction of the flow of energy.

Consider a point source at some distance before an opaque screen with an aperture. According to the ray picture, the light distribution on a second screen further away from the source and parallel to the first screen is simply an enlarged copy of the aperture (see Fig. 2.1). The copy is enlarged due to the fanning out of the straight rays. However, this description is only accurate when the wavelength of the light is very small compared to the diameter of the aperture. If the aperture is only ten times the wavelength, the pattern is much broader due to the bending of the rays around the edge of the aperture. This phenomenon is called **diffraction**. Diffraction can not be explained by geometrical optics and will be studied in Chapter 6.

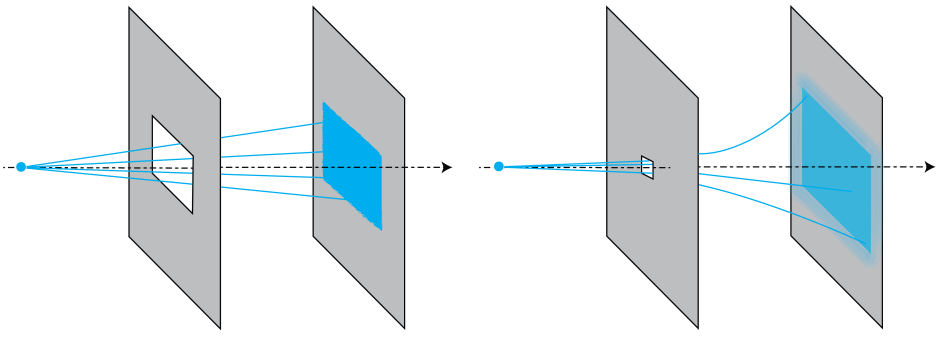


Figure 2.1: Light distribution on a screen due to a rectangular aperture illuminated by a point source. Left: for a large aperture, we get an enlarged copy of the aperture. Right: for an aperture that is of the order of the wavelength there is strong bending (diffraction) of the light.

Geometrical optics is accurate when the sizes of the objects in the system are large compared to the wavelength. It is possible to derive geometrical optics from Maxwell's equations by formally expanding the electromagnetic field in a power series in the wavelength and retaining only the first term of this expansion [1]. However, this derivation is not rigorous because the power series

[1] See Chapter 1 of M. Born & E. Wolf, "Principles of Optics", Cambridge University Press (2013)

generally does not converge (it is a so-called asymptotic series).

Although it is possible to incorporate polarisation into geometrical optics [2], this is not standard theory and we will not consider polarisation effects in this chapter.

2.2 Principle of Fermat

The starting point of the treatment of geometrical optics is the

Principle of Fermat (1657). The path followed by a light ray between two points is the one that takes the least amount of time.

The speed of light in a material with refractive index n, is c/n, where $c = 3 \times 10^8$ m/s is the speed of light in vacuum. At the time of Fermat it was the conviction that the speed of light must be finite, but nobody could suspect how incredibly large it actually is. In 1676 the Danish astronomer Ole Römer computed the speed from inspecting the eclipses of a moon of Jupiter and arrived at an estimate that was only 30% too low.

Let $\mathbf{r}(s)$, be a ray with s the length parameter. The ray links two points S and P. Suppose that the refractive index varies with position: $n(\mathbf{r})$. Over the infinitesimal distance from s to $s + \mathrm{d}s$, the speed of the light is

$$\frac{c}{n(\mathbf{r}(s))}. \tag{2.1}$$

Hence the time it takes for light to go from $\mathbf{r}(s)$ to $\mathbf{r}(s + \mathrm{d}s)$ is:

$$\mathrm{d}t = \frac{n(\mathbf{r}(s))}{c}\,\mathrm{d}s, \tag{2.2}$$

and the total total time to go from S to P is:

$$t_{S\to P} = \int_0^{s_P} \frac{n(\mathbf{r}(s))}{c}\,\mathrm{d}s, \tag{2.3}$$

where s_P is the distance along the ray from S to P. The **optical path length** [m] of the ray between S and P is defined by:

$$\mathrm{OPL} = \int_0^{s_P} n(\mathbf{r}(s))\,\mathrm{d}s, \tag{2.4}$$

So the OPL is the distance weighted by the refractive index.

Fermat's principle is thus equivalent to the statement that a ray follows the path with shortest OPL.

[2] R.K. Luneburg, Mathematical Theory of Optics, University of California Press, Berkeley and Los Angeles, 1964

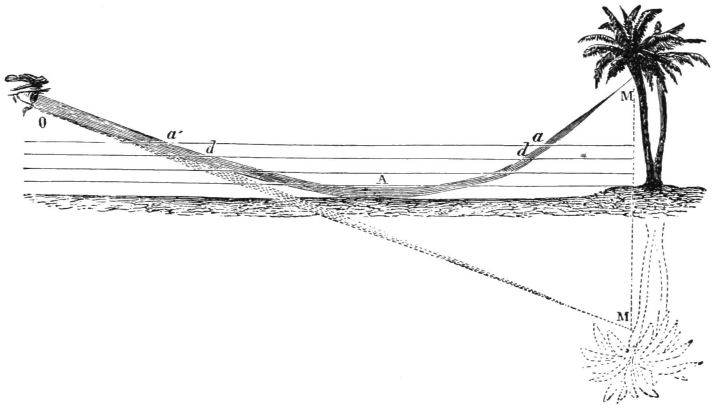


Figure 2.2: Because the temperature close to the ground is higher, the refractive index is lower there. Therefore the rays bend upwards, creating a mirror image of the tree below the ground. (From Popular Science Monthly Volume 5, Public Domain , link).

Remark. Actually, Fermat's principle as formulated above is not complete. There are circumstances that a ray can take two paths between two points that have different travel times. Each of these paths then corresponds to a minimum travel time compared to nearby paths, so the travel time is in general a *local minimum*. An example is the reflection by a mirror discussed in the following section.

2.3 Some Consequences of Fermat's Principle

1. Homogeneous matter.
In homogeneous matter, the refractive index is constant and therefore paths of shortest OPL are straight lines. Hence in homogeneous matter rays are straight lines.
2. Inhomogeneous matter.
When the refractive index is a function of position such as in air when there is a temperature gradient, the rays bend towards regions of higher refractive index. In the case of Fig. 2.2 for example, the ray from the top of the tree to the eye of the observer passes on a warm day close to the ground because there the temperature is higher and hence the refractive index is smaller. Although the curved path is longer than the straight path, the total travel time of the light is less because near the ground the light speed is higher (since the refractive index is smaller). The observer gets the impression that the tree is upside down under the ground.
3. Law of reflection.
Consider the mirror shown in Fig. 2.3. Since the medium above the mirror is homogeneous, a ray from point P can end up in Q in two ways: by going along a straight line directly form P to Q or alternatively by straight lines via the mirror. Both possibilities have different path lengths and hence different travel times and hence both are local minima mentioned at the end of the previous section. We consider here the path by means of reflection by the mirror. Let the x-axis be the intersection of the mirror and the plane through the points P and Q and perpendicular to the mirror. Let the y-axis be normal to the mirror. Let (x_P, y_P) and (x_Q, y_Q) be the coordinates of P and Q, respectively. If $(x, 0)$ is the point where a ray from P to Q hits the mirror, the travel time of that ray is

$$\frac{n}{c}d_1(x) + \frac{n}{c}d_2(x) = \frac{n}{c}\sqrt{(x - x_P)^2 + y_P^2} + \frac{n}{c}\sqrt{(x_Q - x)^2 + y_Q^2}, \tag{2.5}$$

where n is the refractive index of the medium in $y > 0$. According to Fermat's Principle, the

point $(x, 0)$ should be such that the travel time is minimum , i.e.

$$\frac{d}{dx}[d_1(x) + d_2(x)] = \frac{(x - x_P)}{d_1(x)} - \frac{(x_Q - x)}{d_2(x)} = 0. \tag{2.6}$$

Hence

$$\sin\theta_i = \sin\theta_r, \tag{2.7}$$

or

$$\theta_r = \theta_i. \tag{2.8}$$

where θ_i and θ_r are the angles of incidence and reflection as shown in Fig. 2.3.

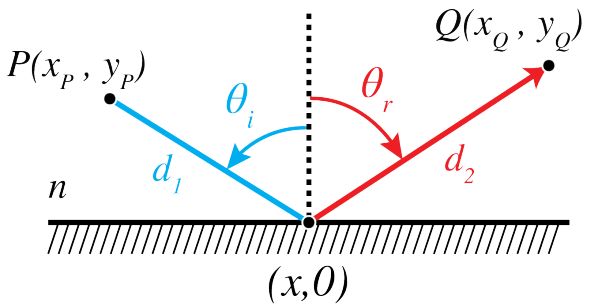


Figure 2.3: Ray from P to Q via the mirror.

4. Snell's law of refraction.
Next we consider refraction at an interface. Let $y = 0$ be the interface between a medium with refractive index n_i in $y > 0$ and a medium with refractive index n_t in $y < 0$. We use the same coordinate system as in the case of reflection above. Let (x_P, y_P) and (x_Q, y_Q) with $y_P > 0$ and $y_Q < 0$ be the coordinates of two points P and Q as shown in Fig. 2.4. What path will a ray follow that goes from P to Q? Since the refractive index is constant in both half spaces, the ray is a straight line in both media. Let $(x, 0)$ be the coordinate of the intersection point of the ray with the interface. Then the travel time is

$$\frac{n_i}{c}d_1(x) + \frac{n_t}{c}d_2(x) = \frac{n_i}{c}\sqrt{(x - x_P)^2 + y_P^2} + \frac{n_t}{c}\sqrt{(x_Q - x)^2 + y_Q^2}. \tag{2.9}$$

The travel time must be minimum, hence there must hold

$$\frac{d}{dx}\left[n_i d_1(x) + n_t d_2(x)\right] = n_i\frac{(x - x_P)}{d_1(x)} - n_t\frac{(x_Q - x)}{d_2(x)} = 0. \tag{2.10}$$

where the travel time has been multiplied by the speed of light in vacuum. Eq. (2.10) implies

$$n_i \sin\theta_i = n_t \sin\theta_t, \tag{2.11}$$

where θ_i and θ_t are the angles shown in Fig. 2.4 between the ray and the normal to the surface in the upper half space and the lower half space, respectively.

Hence we have derived the law of reflection and Snell's law from Fermat's principle. In Chapter 1 the same reflection law and Snell's law have been derived by a different method, namely from the continuity of the tangential electromagnetic field components at the interface.

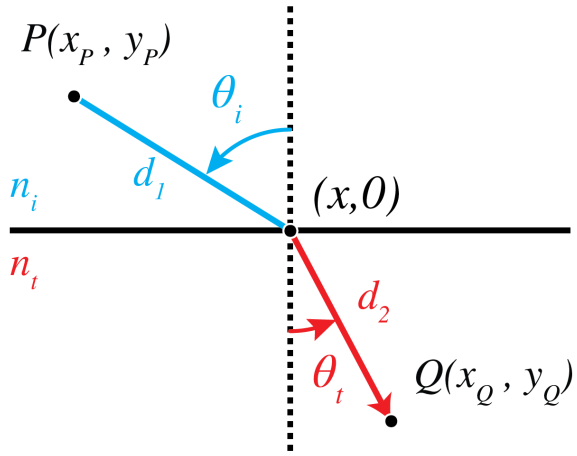


Figure 2.4: Ray from P to Q refracted by an interface.

2.4 Perfect Imaging by Conic Sections

In this section the conic sections ellipse, hyperbole and parabola are mentioned. In Fig. 2.6 their definitions are shown as a quick reminder[4].

We first explain what in geometrical optics is meant by **perfect imaging**. Let S be a point source. The rays perpendicular to the spherical wave fronts emitted by S radially fan out from S. Due to optical components such as lenses etc. the spherical wave fronts are deformed and the direction of the rays are made to deviate from the radial propagation direction. When there is a point P and a cone of rays coming from point S and all rays in that cone intersect in point P, then by Fermat's principle, all these rays have traversed paths of minimum travel time. In particular, their travel times are equal and therefore they **all add up in phase** when they arrive in P. Hence at P there is a high light intensity. Hence, if there is a cone of rays from point S which all intersect in a point P as shown in Fig. 2.5, point P is called a **perfect image** of S. By reversing the direction of the rays, S is similarly a perfect image of P. The optical system in which this happens is called **stigmatic for the two points S and P**.

> **Remark.** The concept of a perfect image point exists only in geometrical optics. As we will explain in Chapter 6, in reality finite apertures of lenses and other imaging systems cause diffraction due to which image points are never perfect but are blurred.

We briefly discuss the main examples of stigmatic systems.

1. Perfect focusing and imaging by refraction.

A parallel bundle of rays propagating in a medium with refractive index n_2 can be focused into a point F in a medium n_1. If $n_2 > n_1$, the interface between the media should be a hyperbole with focus F, whereas if $n_2 < n_1$ the interface should be an ellipse with focus F (see Figs. 2.27 and 2.28). By reversing the rays we obtain perfect collimation. Therefore, a point S in air can be perfectly imaged onto a point F in air by inserting a piece of glass in between them with hyperbolic surfaces as shown in Fig. 2.28. These properties are derived in Problem 2.2.

2. Perfect focusing of parallel rays by a mirror.

A bundle of parallel rays in air can be focused into a point F by a mirror of parabolic shape with F as focus (see Fig. 2.29). This is derived in Problem 2.3. By reversing the arrows, we get (within geometrical optics) a perfectly parallel beam. Parabolic mirrors are used everywhere, from automobile headlights to radio telescopes.

[4]See also https://en.wikipedia.org/wiki/Conic_section

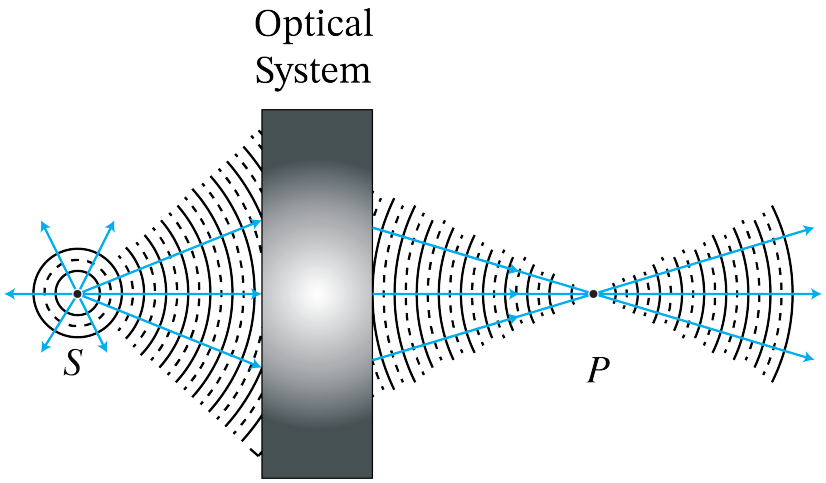
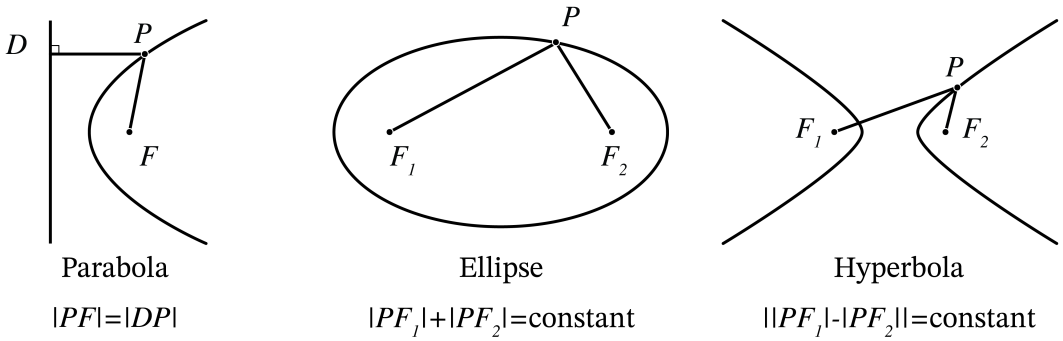


Figure 2.5: Perfect imaging: a cone of rays which diverge from S and all intersect in point P. The rays continue after P.



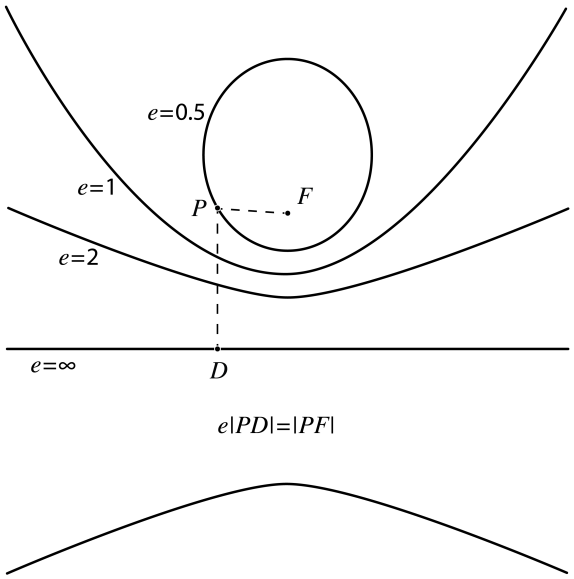


Figure 2.6: Overview of conic sections. The lower figure shows a definition that unifies the three definitions in the figure above by introducing a parameter called the eccentricity e. The point F is the focus and the line $e = \infty$ is the directrix of the conic sections.

Remark. Although we found that conic surfaces give perfect imaging for a certain pair of points, other points and planes do in general *not* have perfect images in the sense that for a certain cone of rays from the object points, all rays are refracted (or reflected) to the same point. For example, Maxwell[6] proved that if two distinct flat planes are imaged perfectly and the refractive indices in object and image space are the same, the transverse magnification for both planes is unity. Perfect imaging of two flat or two curved planes is for some special lens shapes possible but then only for a particular magnifications [Walther [6]].

External sources in recommended order

- KhanAcademy - Geometrical Optics: Playlist on elementary geometrical optics.
- Yale Courses - 16. Ray or Geometrical Optics I - Lecture by Ramamurti Shankar
- Yale Courses - 17. Ray or Geometrical Optics II - Lecture by Ramamurti Shankar

2.5 Gaussian Geometrical Optics

We have seen that, although by using lenses or mirrors which have surfaces that are conic sections we can perfectly image a certain pair of points, for other points the image is not perfect. The imperfections are caused by the rays which angle with the **optical axis**, i.e. with the symmetry axis of the system, is large. Rays for which these angles are small are called **paraxial rays**. Because for paraxial rays the angles of incidence and transmission at the surfaces of the lenses are small, the sine of the angles in Snell's Law are replaced by the angles themselves:

$$n_i\theta_i = n_t\theta_t \qquad \text{(paraxial rays only)}. \tag{2.12}$$

This approximation greatly simplifies the calculations. Furthermore, when only paraxial rays are considered, one may replace any surface by a sphere with the same curvature at its vertex. Errors caused by replacing a surface by a sphere are of second order in the angles which the ray makes with the optical axis and hence are insignificant for paraxial rays. Spherical surfaces are not only more simple in the derivations but they are also much easier to manufacture. Hence in the optical industry spherical surfaces are used a lot. To reduce imaging errors caused by non-paraxial rays one applies two strategies: 1. adding more spherical surfaces (more lenses); 2 replacing one of the spherical surfaces (typically the last before image space) by a non-sphere.

In Gaussian geometrical optics only paraxial rays and spherical surfaces are considered.
In Gaussian geometrical optics every point has a perfect image.

2.5.1 Gaussian Imaging by a Single Spherical Surface

We will first show that within Gaussian optics a single spherical surface between two media with refractive indices $n_1 < n_2$ images all points perfectly (Fig. 2.7). The sphere has radius R and centre C which is inside medium 2. We consider a point object S to the left of the surface. We draw a ray from S perpendicular to the surface. The point of intersection is V. Since for this ray the angle of incidence with the local normal on the surface vanishes, the ray continues into the second medium without refraction and then passes through the centre C of the sphere. Next

[6] J.C. Maxwell, "On the general laws of optical instruments", Q. J. Pure PPL. Math. II, 271-285 (1885)
[6] A. Walther, "Irreducible aberration of a lens used for a range of magnifications", JOSA A, vol. 6, issue 3, pp 415-422 (1989)

we draw a ray that hits the spherical surface in some point A and draw the refracted ray in medium 2 using Snell's law in the paraxial form (2.12). Note that the angles of incidence and transmission must be measured with respect to the local normal at A, i.e. with respect to CA. We assume that this refracted ray intersects the first ray in point P. We will show that within the approximation of Gaussian geometrical optics, all rays from S pass through P. Furthermore, with respect to a coordinate system (y, z) with origin at V, the z-axis pointing from V to C and the y-axis positive upwards as shown in Fig. 2.7, we have:

$$-\frac{n_1}{s_o} + \frac{n_2}{s_i} = \mathfrak{P}, \tag{2.13}$$

where

$$\mathfrak{P} = \frac{n_2 - n_1}{R}, \tag{2.14}$$

is called the power of the surface and where s_o and s_i are the z-**coordinates** of S and P, respectively, hence $s_0 < 0$ and $s_i > 0$ in Fig. 2.7. We use calligraphic $\mathfrak{P}$ for the power of the surface to distinguish it from point P. It unit is $1/\text{meter}$, which is also called Diopter $\mathcal{D} = 1\text{meter}$.

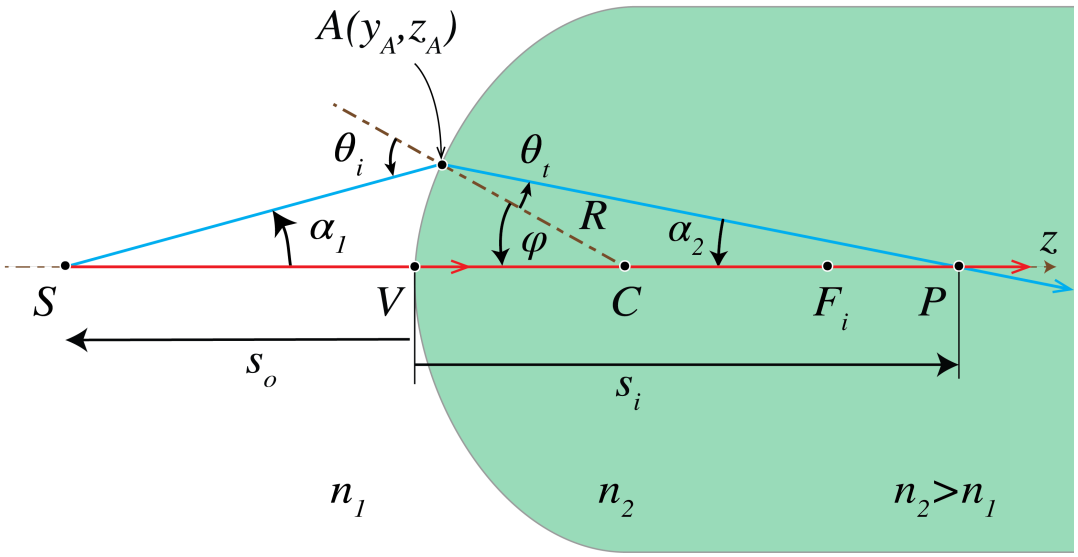


Figure 2.7: Imaging by a spherical interface between two media with refractive indices $n_2 > n_1$.

Proof.
(Note: the proof is **not** part of the exam). It suffices to show that P is independent of the ray, i.e. of A. We will do this by expressing s_i into s_o and showing that the result is independent of A. Let α_1 and α_2 be the angles of the rays SA and AP with the z-axis as shown in Fig. 2.7. Let θ_i be the angle of incidence of ray SA with the local normal CA on the surface and θ_t be the angle of refraction. By considering the angles in triangle ΔSCA we find

$$\theta_i = \alpha_1 + \varphi. \tag{2.15}$$

Similarly, from ΔCPA we find

$$\theta_t = -\alpha_2 + \varphi. \tag{2.16}$$

By substitution into the paraxial version of Snell's Law (2.12), we obtain

$$n_1\alpha_1 + n_2\alpha_2 = (n_2 - n_1)\varphi. \tag{2.17}$$

Let y_A and z_A be the coordinates of point A. Since $s_o < 0$ and $s_i > 0$ we have

$$\alpha_1 \approx \tan(\alpha_1) = \frac{y_A}{z_A - s_o}, \qquad \alpha_2 \approx \tan(\alpha_2) = \frac{y_A}{s_i - z_A}. \tag{2.18}$$

Furthermore, for the angle φ between CA and SC we have

$$\varphi \approx \sin\varphi \approx \frac{y_A}{R}. \tag{2.19}$$

which is small for paraxial rays. Hence,

$$z_A = R - R\cos\varphi = R - R\left(1 - \frac{\varphi^2}{2}\right) = \frac{R}{2}\varphi^2 \approx 0, \tag{2.20}$$

because it is second order in y_A and therefore is neglected in the paraxial approximation. Then, (2.18) becomes

$$\alpha_1 = -\frac{y_A}{s_o}, \qquad \alpha_2 = \frac{y_A}{s_i}. \tag{2.21}$$

By substituting (2.21) and (2.19) into (2.17) we find

$$-\frac{n_1}{s_o}y_A + \frac{n_2}{z_i}y_A = \frac{n_2 - n_1}{R}y_A,$$

or

$$-\frac{n_1}{s_o} + \frac{n_2}{s_i} = \frac{n_2 - n_1}{R},$$

which is (2.13). It is seen that s_i, and hence P, is indeed independent of y_A, i.e. of the ray chosen. Therefore, P is a perfect image within the approximation of Gaussian geometrical optics.

> **Remark.** Snell's law is applied to determine the direction of propagation of the ray which is transmitted by a spherical surface (or surface of more general shape) of a lens. Because in practice anti-reflective coatings are used on these surfaces, the reflection of the rays may be neglected.

When $s_o \to -\infty$, the incident rays are parallel to the z-axis in medium 1 and the corresponding image point F_i is called the **second focal point** or **image focal point**. With (2.13) it follows that its z-coordinate is given by:

$$f_i = \frac{n_2}{\mathfrak{P}} = \frac{n_2 R}{n_2 - n_1}, \tag{2.22}$$

and its absolute value (it is negative when $n_2 < n_1$) is called the **second focal length** or **image focal length**.

When $s_i \to \infty$, all rays after refraction are parallel to the z-axis and (2.13) implies that $s_o \to -n_1 R/(n_2 - n_1)$. The object point for which all rays in the medium 2 are parallel to the z-axis is called the **first focal point** or **object focal point** F_o. Its z-coordinate is:

$$f_o = -\frac{n_1}{\mathfrak{P}} = -\frac{n_1 R}{n_2 - n_1}. \tag{2.23}$$

The absolute value $|f_o|$ of f_o is called the **front focal length** or **object focal length**. With (2.22) and (2.23), we can rewrite (2.13) as:

$$-\frac{n_1}{s_o}+\frac{n_2}{s_i}=\mathfrak{P}=\frac{n_2}{f_i}=-\frac{n_1}{f_o}. \tag{2.24}$$

2.5.2 Virtual Images and Virtual Objects of a Single Spherical Surface

If we adopt the sign convention listed in Table 2.1 below, it turns out that (2.13) holds generally. So far we have considered a convex surface of which the centre C is to the right of the surface, but (2.13) applies also to a concave surface of which the centre is to the left of the surface, provided that the radius R is chosen negative. The convention for the sign of the radius is illustrated in Fig. 2.8.

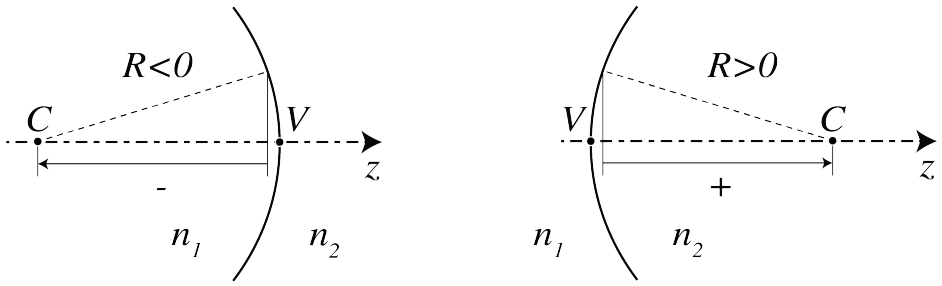


Figure 2.8: Sign convention for the radius R of a spherical surface

If the power $\mathfrak{P}$ given by (2.14) is positive, then the surface makes bundles of incident rays convergent or less divergent. If the power is negative, incident bundles are made divergent or less convergent. The power of the surface can be negative because of two reasons: 1) $R>0$ and $n_1 > n_2$, or 2) $R<0$ and $n_1 < n_2$. The effect of the two cases is the same. For any object to the left of the surface: $s_o < 0$, (2.24) and a negative power imply that $s_i < 0$, which suggests that the image is to the left of the surface. Indeed, in Figs. 2.9 the diverging ray bundle emitted by S is made more strongly divergent by the surface. By extending these rays in image space back to object space (without refraction at the surface), they are seen to intersect in a point P to the left of the surface. This implies that for an observer at the right of the surface it looks as if the diverging rays in image space are emitted by P. Because there is no actual concentration of light intensity at P, it is called a **virtual image**, in contrast with the **real images** that occur to the right of the surface and where there is an actual concentration of light energy. We have in this case $f_o > 0$ and $f_i < 0$, which means that the object and image focal points are to the right and left, respectively, of the surface.

Note that also when the power is positive, a virtual image can occur, namely when the object S is between the object focal point F_o and the surface. Then the bundle of rays from S is so strongly diverging that the surface can not convert it into a convergent bundle and hence again the rays in image space seem to come from a point P to the left of the surface. This agrees with the fact that when $\mathfrak{P} > 0$ and $f_o < s_o < 0$, (2.24) implies that $s_i < 0$.

Finally we look at a case that there is a bundle of convergent rays incident from the left on the surface which, when extended into the right medium without refraction at the surface, would intersect in a point S. Since this point is not actually present, it is called a **virtual object point**, in contrast to **real object points** which are to the left of the surface. The coordinate of a virtual object point is positive: $s_o > 0$. One may wonder why we look at this case. The reason is that if we have several spherical surfaces behind each other, we can compute the image

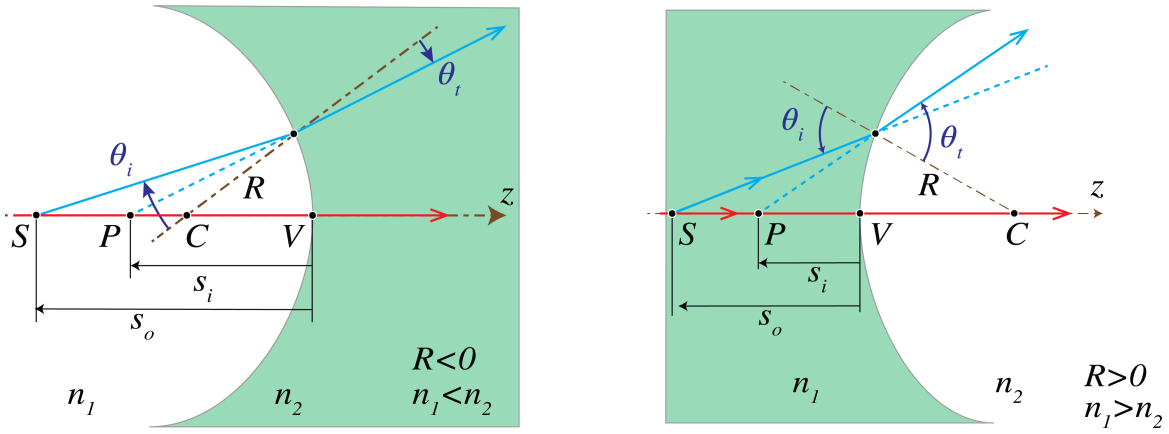


Figure 2.9: Left: imaging by a concave surface ($R < 0$) with $n_2 > n_1$. Right: imaging by a convex surface ($R > 0$) with $n_1 > n_2$ All image points P are to the left of the surface, i.e. are virtual ($s_i < 0$).

of an object point by first determining the intermediate image by the most left surface and then use this intermediate image as object for the next surface and so on. In such a case it can easily happen that an intermediate image is to the right of the next surface and hence is a virtual object for that surface. In the case of Fig. 2.10 at the left, the power is positive, hence the convergent bundle of incident rays is made even more convergent which leads to a real image point. Indeed when $s_o > 0$ and $\mathfrak{P} > 0$ then (2.13) implies that always $s_i > 0$. At the right of Fig. 2.10 the power is negative but is not sufficiently strong to turn the convergent incident bundle into a divergent bundle. So the image is still real. However, the image will be virtual when the virtual object S is to the right of F_o (which is to the right of the surface) since then the incident bundle of rays converges so weakly that the surface turns it into a divergent bundle.

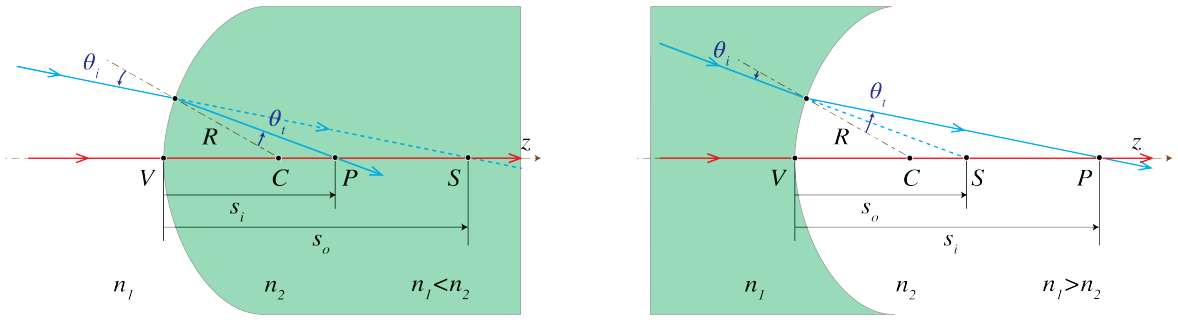


Figure 2.10: Imaging of a virtual object S by a spherical interface with $R > 0$ between two media with refractive indices $n_1 < n_2$ (left) and $n_1 > n_2$ (right).

In conclusion: provided the sign convention listed in Table 2.1 is used, formula (2.13) can always be used to determine the image of a given object by a spherical surface.

2.5.3 Ray Vectors and Ray Matrices

Now that we know that within Gaussian geometrical optics a single spherical surface images every object point to a perfect (real or virtual) image point, it is easy to see that any sequence of spherical surfaces separated by homogeneous materials will also image any point perfectly. We first determine the intermediate image of the object point under the most left spherical surface as if the other surfaces were not present and use this intermediate image point as object point for

quantity	positive	negative
s_o, s_i. f_0, f_i	corresponding point is to the right of vertex	corresponding point is to left of vertex
y_o, y_i	object, image point above optical axis	object, image point below optical axis
R	centre of curvature right of vertex	centre of curvature left of vertex
Refractive index n ambient medium of a mirror	before reflection	after reflection

Table 2.1: Sign convention for spherical surfaces and thin lenses. The convention for s_o, f_o, s_i, f_i follows from the fact that these are z-coordinates with the origin at vertex V of the spherical surface (or the centre of the thin lens) and the positive z-axis is pointing to the right. The convention for the y-coordinate follows from the fact that the y-axis is positive upwards. The convention for the sign of the refractive index of the ambient medium in the case of a mirror is convenint to take account of the reversal of the direction of the rays by the mirror.

imaging by the next spherical surface and so on. Of course, the intermediate image and object points can be virtual.

Although this procedure is in principle simple, it is convenient to introduce in Gaussian geometrical optics the concept of ray vectors and ray matrices to deal with optical systems consisting of several spherical surfaces. With ray matrices it is easy to derive how the distance of a given ray to the optical axis and its direction change during propagation through an optical system. This in turn can be used to determine the image plane in an optical system for a given object plane.

In any plane perpendicular to the z-axis, a ray is determined by the y-coordinate of the point of intersection of the ray with the plane and the angle α with the optical (z)-axis. This angle has a sign and is defined as follows. Let (y_1, z_1) and (y_2, z_2) be the coordinates of two points on the ray and let the light propagate from point 1 to point 2. Then we define

$$\alpha = \frac{y_2 - y_1}{z_2 - z_1}. \tag{2.25}$$

Examples of positive and negative α are given in Fig.2.11. The case $z_2 - z_1 < 0$ occurs when a ray propagates in the negative z-direction after it has been reflected by a mirror. According to Table 2.1 the refractive index of the ambient medium should after the reflection be taken negative. After a second reflection due to which the ray propagates again in the positive z-direction the refractive index should be chosen positive again.

We define the ray vector

$$\begin{pmatrix} n\alpha \\ y \end{pmatrix}, \tag{2.26}$$

where n is the local refractive index. The definition with the refractive index as factor in the first element of the ray vector turns out to be convenient.

The ray vectors of a ray in any two planes $z = z_1$, $z = z_2$, with $z_2 > z_1$, are related by a

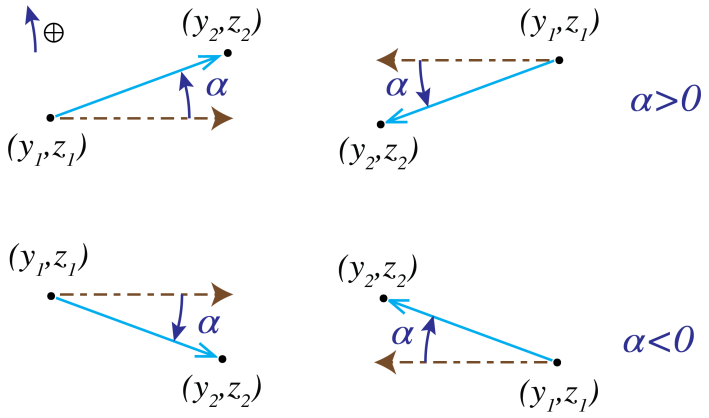


Figure 2.11: Sign convention for the ray angle. In the upper two figures $\alpha > 0$ while in the lower two figures $\alpha < 0$.

so-called ray matrix:

$$\begin{pmatrix} n_2\alpha_2 \\ y_2 \end{pmatrix} = \mathcal{M} \begin{pmatrix} n_1\alpha_1 \\ y_1 \end{pmatrix}. \tag{2.27}$$

where

$$\mathcal{M} = \begin{pmatrix} A & B \\ C & D \end{pmatrix}. \tag{2.28}$$

The elements of matrix $\mathcal{M}$ depend on the optical components and materials between the planes $z = z_1$ and $z = z_2$.

As an example consider the ray matrix that relates a ray vector in the plane immediately before the spherical surface in Fig. 2.7 to the corresponding ray vector in the plane immediately behind that surface. By multiplying (2.13) by $y_1 = y_A$ and substituting the angles $\alpha_1 = -y_A/s_o$ and $\alpha_2 = -y_A/s_i$, it follows

$$n_1\alpha_1 - n_2\alpha_2 = \frac{(n_2 - n_1)y_1}{R}. \tag{2.29}$$

Note that according to the sign convention, the angle α_1 in Fig. 2.7 should be taken positive whereas α_2 is negative. Because furthermore $y_2 = y_1$, we conclude

$$\begin{aligned} \begin{pmatrix} n_2\alpha_2 \\ y_2 \end{pmatrix} &= \begin{pmatrix} n_1\alpha_1 - \frac{(n_2-n_1)y_1}{R} \\ y_1 \end{pmatrix} \\ &= \begin{pmatrix} 1 & -\mathfrak{P} \\ 0 & 1 \end{pmatrix} \begin{pmatrix} n_1\alpha_1 \\ y_1 \end{pmatrix}, \quad \textbf{spherical surface,} \end{aligned} \tag{2.30}$$

where

$$\mathfrak{P} = \frac{n_2 - n_1}{R}, \tag{2.31}$$

is as before the **power** of the surface.

Next we consider a spherical mirror with radius of curvature R. We will show that the ray matrix between the planes just before and after the mirror is given by:

$$\begin{pmatrix} n_2\alpha_2 \\ y_2 \end{pmatrix} = \begin{pmatrix} 1 & -\mathfrak{P} \\ 0 & 1 \end{pmatrix} \begin{pmatrix} n_1\alpha_1 \\ y_1 \end{pmatrix}, \quad \textbf{spherical reflector,} \tag{2.32}$$

where

$$\mathfrak{P} = \frac{2n}{R}, \tag{2.33}$$

is the power of the mirror, $n_1 = n$ but $n_2 = -n$, because the convention mentioned in Table 2.1 is used that if a ray propagates from **right to left** (i.e. in the negative z-direction), the refractive index in the ray vectors and ray matrices is chosen **negative**. Note that when the mirror is flat: $R = \infty$, the ray matrix of the reflector implies

$$n_2\alpha_2 = n_1\alpha_1,$$

which agrees with the fact that $n_2 = -n_1$ and according to definition (2.25) α_2 and α_1 have opposite sign for a mirror.

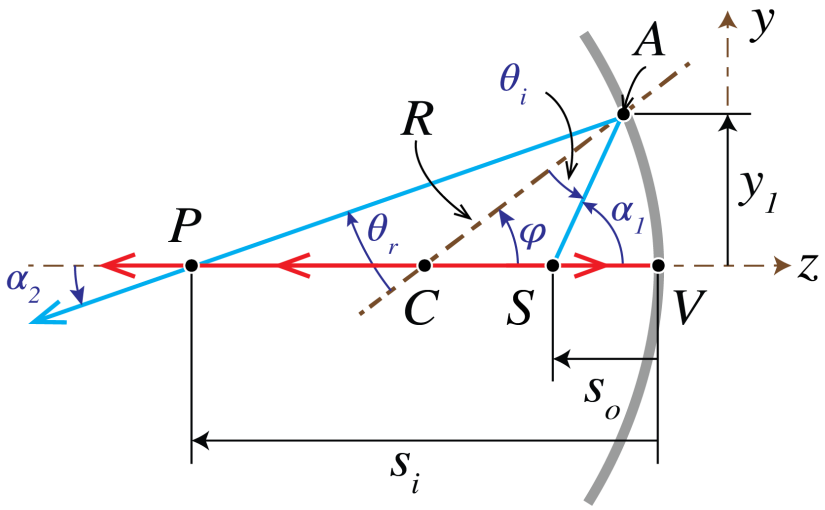


Figure 2.12: Reflection by a mirror.

With all angles positive for the moment, it follows from Fig. 2.12

$$\alpha_1 = \theta_i + \varphi, \tag{2.34}$$
$$\alpha_2 = \varphi - \theta_r = \varphi - \theta_i. \tag{2.35}$$

Hence,

$$\alpha_2 = -\alpha_1 + 2\varphi. \tag{2.36}$$

Now

$$\varphi \approx \frac{y_1}{R} \tag{2.37}$$

In the situation drawn in Fig. 2.12, it follows from (2.25) that both α_2 and α_1 are positive. By choosing the refractive index negative after reflection, we conclude from (2.36) and (2.37):

$$n_2\alpha_2 = -n\alpha_2 = n\alpha_1 - \frac{2n}{R}y_1 = n_1\alpha_1 - \frac{2n}{R}. \tag{2.38}$$

This proves Eq. (2.32).

We next consider the ray matrix when a ray propagates from a plane z_1 to a plane z_2 through a medium with refractive index n. In that case we have $\alpha_2 = \alpha_1$ and $y_2 = y_1 + \alpha_1(z_2 - z_1)$, hence

$$\mathcal{M} = \begin{pmatrix} 1 & 0 \\ \frac{z_2 - z_1}{n} & 1 \end{pmatrix}, \quad \textbf{homogeneous space}. \tag{2.39}$$

Note that if the light propagates from the left to the right: $z_2 > z_1$ and hence $z_2 - z_1$ in the first column and second row of the matrix is positive, i.e. it is the distance between the planes.

For two planes between which there are a number of optical components, possibly separated by regions with homogeneous material, the ray matrix can be obtained by multiplying the matrices of the individual components and of the homogeneous regions. The order of the multiplication of the matrices is such that the **right-most matrix corresponds to the first component that is encountered while propagating**, and so on.

In the ray matrix approach all rays stay in the same plane, namely the plane through the ray and the z-axis. These rays are called **meridional rays**. By considering only meridional rays, the imaging by optical systems is restricted to two dimensions. Non-meridional rays are called **skew rays**. Skew rays do not pass through the optical axis and are not considered in the paraxial theory.

Remarks.

1. In matrix (2.39) z_1 and z_2 are **coordinates**, i.e. they have a sign.

2. Instead of choosing the refractive index negative in ray vectors of rays that propagate from right to left, one can reverse the direction of the positive z-axis after every reflection. The convention to make the refractive index negative is however more convenient in ray tracing software.

3. The determinant of the ray matrices (2.30), (2.32) and (2.39) are all 1. Since all ray matrices considered below are products of these elementary matrices, the determinant of every ray matrix considered is unity.

2.5.4 The Lens Matrix

We apply ray matrices to a lens. Fig. 2.13 shows a lens with two spherical surfaces. The refractive index of the lens is n_l and that of the media to the left and to the right of the lens is n_1 and n_2, respectively. Let the distance between the vertices be d. We will first derive the matrix

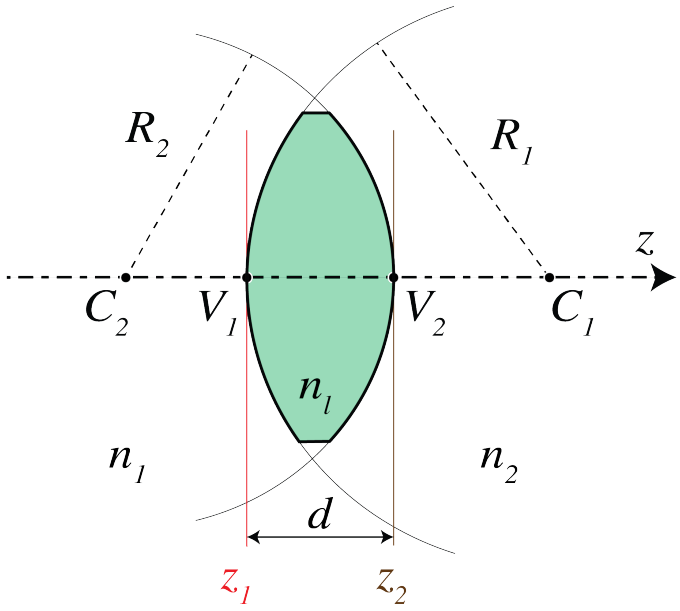


Figure 2.13: A lens with thickness d. The ray matrix is defined between the planes immediately before and after the lens.

which maps the ray vector in the plane **immediately in front** of the lens to that in the plane

immediately behind the lens. Let

$$\begin{pmatrix} n_1\alpha_1 \\ y_1 \end{pmatrix} \quad \text{and} \quad \begin{pmatrix} n_2\alpha_2 \\ y_2 \end{pmatrix} \tag{2.40}$$

be two vectors in the two planes which correspond to the same ray. The ray is first refracted by the spherical surface with radius R_1 and centre C_1. Using (2.30) and (2.31) it follows that the matrix between the ray vectors just before and just behind the spherical surface with radius R_1 and centre C_1 is given by

$$\mathcal{M}_1 = \begin{pmatrix} 1 & -\mathfrak{P}_1 \\ 0 & 1 \end{pmatrix}, \tag{2.41}$$

where

$$\mathfrak{P}_1 = \frac{n_l - n_1}{R_1}. \tag{2.42}$$

The ray propagates then over the distance d through the material of which the lens is made. The matrix that maps ray vectors from the plane inside the lens immediately behind the left spherical surface to a ray vector in the plane immediately before the right spherical surface follows from (2.39):

$$\mathcal{M}_2 = \begin{pmatrix} 1 & 0 \\ \frac{d}{n_l} & 1 \end{pmatrix}. \tag{2.43}$$

Finally, the matrix that maps ray vectors from the plane in the lens immediately before the second spherical surface to vectors in the plane immediately behind it is

$$\mathcal{M}_3 = \begin{pmatrix} 1 & -\mathfrak{P}_2 \\ 0 & 1 \end{pmatrix}. \tag{2.44}$$

with

$$\mathfrak{P}_2 = \frac{n_2 - n_l}{R_2}. \tag{2.45}$$

Hence the matrix that maps ray vectors in the plane immediately before the lens to ray vectors in the plane immediately behind the lens is given by the matrix product:

$$\begin{aligned} \mathcal{M} &= \mathcal{M}_3\mathcal{M}_2\mathcal{M}_1 \\ &= \begin{pmatrix} 1 - \frac{d}{n_l}\mathfrak{P}_2 & -\mathfrak{P}_1 - \mathfrak{P}_2 + \frac{d}{n_l}\mathfrak{P}_1\mathfrak{P}_2 \\ \frac{d}{n_l} & 1 - \frac{d}{n_l}\mathfrak{P}_1 \end{pmatrix}, \quad \textbf{thick lens}. \end{aligned} \tag{2.46}$$

The quantity

$$\mathfrak{P} = \mathfrak{P}_1 + \mathfrak{P}_2 - \frac{d}{n_l}\mathfrak{P}_1\mathfrak{P}_2 \tag{2.47}$$

is called the **power** of the lens. Similarly to a single spherical surface, it has dimension 1/length and is given in diopter ($\mathcal{D}$), where $1\ \mathcal{D} = \mathrm{m}^{-1}$. The power can be positive and negative. The space to the left of the lens is called the **object space** and that to the right of the lens is called the **image space**.

2.5.5 Focusing with a Thin Lens

For a thin lens $d = 0$ and the vertices V_1 and V_2 coincide, hence (2.46) becomes

$$\mathcal{M} = \begin{pmatrix} 1 & -\mathfrak{P} \\ 0 & 1 \end{pmatrix}, \quad \textbf{thin lens}, \tag{2.48}$$

where

$$\mathfrak{P} = \mathfrak{P}_1 + \mathfrak{P}_2 = \left(\frac{n_l - n_1}{R_1} + \frac{n_2 - n_l}{R_2} \right), \tag{2.49}$$

The origin of the coordinate system is chosen in the common vertex $V_1 = V_2$.

By considering a ray in medium 1 which is parallel to the optical axis ($\alpha_1 = 0$) and at height y_1, we get $n_2\alpha_2 = -\mathfrak{P}y_1$ and $y_2 = y_1$. Hence, when $\mathfrak{P} > 0$, the angle α_2 of the ray has sign opposite to y_2 and therefore the ray in image space is bent back to the optical axis, yielding a **second focal point** or **image focal point** F_i. Its z-coordinate f_i is:

$$f_i = \frac{y_2}{-\alpha_2} = \frac{n_2}{\mathfrak{P}}. \tag{2.50}$$

For a ray emerging in image space at height y_2 and parallel to the optical axis: $\alpha_2 = 0$, we have $y_1 = y_2$ and

$$n_1\alpha_1 = \mathfrak{P}y_1. \tag{2.51}$$

If the power is positive: $\mathfrak{P} > 0$, the angle α_1 has the same sign as y_1, which implies that the ray in object space has intersected the optical axis in a point F_o with z-coordinate: $z = f_o$

$$f_o = -\frac{y_1}{\alpha_1} = -\frac{n_1}{\mathfrak{P}}. \tag{2.52}$$

The point F_o is called the **first focal point** or **object focal point**.

We conclude that when the power $\mathfrak{P}$ of the lens is positive, $f_i > 0$ and $-f_o > 0$, which means that the image and object focal points are in the image and object space, respectively, hence they are both real. A lens with positive power is called **convergent** or **positive**. It makes incident bundles of rays convergent or less divergent.

A lens with negative power is called divergent and has $f_i < 0$, $-f_o < 0$. It makes incident rays more divergent or less convergent. Incident rays which are parallel to the optical axis are refracted away from the optical axis and seem to come from a point in front of the lens with z-coordinate $f_i < 0$. Hence the image focal point does not correspond to a location where there is an actual concentration of light intensity, i.e. it is virtual. The object focal point is a virtual object point, because only a bundle of incident rays that are converging to a certain point behind the negative lens can be turned into a bundle of rays parallel to the optical axis.

With the results obtained for the focal coordinates we can rewrite the lens matrix of a thin lens as

$$\mathcal{M} = \begin{pmatrix} 1 & -\frac{n_2}{f_i} \\ 0 & 1 \end{pmatrix}, \quad \textbf{thin lens}. \tag{2.53}$$

2.5.6 Imaging with a Thin Lens

We first consider a general ray matrix (2.27), (2.28) between two planes $z = z_1$ and $z = z_2$ and ask the following question: what are the properties of the ray matrix such that the two planes are images of each other, or (as this is also called) are each other's conjugate? Clearly for these planes to be each other's image, we should have that for every point with coordinate y_1, say, in the plane $z = z_1$ there is a point with some coordinate y_2 in the plane $z = z_2$ such that any ray

through (y_1, z_1) (within some cone of rays) will pass through point (y_2, z_2). Hence for any angle α_1 (in some interval of angles) there is an angle α_2 such that (2.27) is valid. This means that for any y_1 there is a y_2 such that for all angles α_1:

$$y_2 = Cn_1\alpha_1 + Dy_1, \tag{2.54}$$

This requires that

$$C = 0, \quad \textbf{condition for imaging}. \tag{2.55}$$

The ratio of y_2 and y_1 is the magnification M. Hence,

$$M = \frac{y_2}{y_1} = D, \tag{2.56}$$

is the **magnification** of the image (this quantity has sign).

We consider now imaging by a thin lens. The refractive index in object and image space n_1 and n_2, respectively may differ. The eye lens is an important example of a lens for which this is true. Furthermore, in microscopy the object is frequently immersed in a fluid so that the refractive index in object space is increased, thereby increasing the resolution.

First we derive the ray matrix between two planes $z = z_1 < 0$ and $z = z_2 > 0$ on either side of the thin lens. The origin of the coordinate system is again at the vertex of the thin lens. This ray matrix is the product of the matrix for propagation from $z = z_1$ to the plane immediately in front of the lens, the matrix of the thin lens and the matrix for propagation from the plane immediately behind the lens to the plane $z = z_2$:

$$\begin{aligned} \mathcal{M} &= \begin{pmatrix} 1 & 0 \\ \frac{z_2}{n_2} & 1 \end{pmatrix} \begin{pmatrix} 1 & -\mathfrak{P} \\ 0 & 1 \end{pmatrix} \begin{pmatrix} 1 & 0 \\ \frac{-z_1}{n_1} & 1 \end{pmatrix} \\ &= \begin{pmatrix} 1 + \frac{z_1}{n_1}\mathfrak{P} & -\mathfrak{P} \\ -\frac{z_1}{n_1} + \frac{z_2}{n_2} + \frac{z_1 z_2}{n_1 n_2}\mathfrak{P} & 1 - \frac{z_2}{n_2}\mathfrak{P} \end{pmatrix}. \end{aligned} \tag{2.57}$$

The imaging condition (2.55) implies :

$$-\frac{n_1}{s_o} + \frac{n_2}{s_i} = \mathfrak{P}, \quad \textbf{Lensmaker's Formula}, \tag{2.58}$$

where we have written $s_o = z_1$ and $s_i = z_2$ for the z-coordinates of the object and the image. Because for the matrix (2.57): $D = 1 - z_2/f_i = 1 - s_i/f_i$, it follows by using (2.58) and (2.50) that the magnification (2.56) is given by

$$M = \frac{y_i}{y_o} = 1 - \frac{s_i}{f_i} = \frac{n_1 s_i}{n_2 s_o}. \tag{2.59}$$

Remark. The Lensmaker's formula for imaging by a thin lens can alternatively be derived by using the imaging formula (2.13) of the two spherical surfaces of the lens. We first image a given point S by the left spherical surface using (2.13) as if the second surface were absent. The obtained intermediate image P' is then imaged by the second spherical surface as if the first surface were absent. P' can be a real or virtual object for the second surface. The derivation is carried out in Problem 2.5.

Analogous to the case of a single spherical surface, an image is called a **real image** if it is to the right of the lens ($s_i > 0$) and is called a **virtual image** if when observed from image space it seems to be to the left of the lens ($s_i < 0$). An object is called a **real object** if it is to the left of the lens ($s_o < 0$) and is a **virtual object** if when observed from the object space it seems to be to the right of the lens ($s_o > 0$). For a positive lens: $\mathfrak{P} > 0$, (2.58) implies that $s_i > 0$ provided $|s_o| > |f_o|$ which means that the image by a convergent lens is real if the object is further from the lens than the object focal point F_o. The case $s_o > 0$ corresponds to a virtual object, i.e. to the case of a converging bundle of incident rays, which for an observer in object space seems to converge to a point at distance s_o behind the lens. A convergent lens ($f_i > 0$) will then make an image between the lens and the second focal point. In contrast, a diverging lens ($f_i < 0$) can turn the incident converging bundle into a real image only if the virtual object point is between the lens and the focal point. If the virtual object point has larger distance to the lens, the convergence of the incident bundle is too weak and the diverging lens then refracts this bundle into a diverging bundle of rays which seem to come from a virtual image point in front of the lens ($s_i < 0$).

Instead of using ray matrices, one can construct the image with a ruler. Consider the imaging of a finite object S_1S_2 as shown in Fig. 2.14. Let y_o be the y-coordinate of S_2. We have $y_o > 0$ when the object is above the optical axis.

Draw the ray through the focal point F_o in object space and draw the so-called chief ray through the centre V of the lens. The first ray becomes parallel in image space. The chief ray intersects both surfaces of the lens almost in their (almost coinciding) vertices where the surfaces are perpendicular to the optical axis. In the upper figure of Fig. 2.14 the refractive indices of the medium to the left and right of the lens are different. At the first surface the refractive index at the left and right of the surface are n_1 and n_l and the chief ray is refracted according to the paraxial version of Snell's Law. At the second surface the chief ray is refracted corresponding to refractive indices at the left and right of the surface n_l and n_2, respectively. Because the lens is thin we neglect the lateral displacement (i.e. perpendicular to the z-axis) of the chief ray as it propagates through the lens. The chief ray is then approximately refracted by the lens as at an interface between a medium with refractive index n_1 and n_2:

$$n_2\alpha_2 = n_1\alpha_1, \tag{2.60}$$

where the angles α_1 and α_2 are as shown in Fig. 2.14. In particular, in the important case, shown in the lower figure of Fig. 2.14, that the refractive indices in object and image space are the same: $n_2 = n_1$, the chief ray passes through the centre of the thin lens without refraction.

The intersection of the ray through the object focal point and the chief ray gives the location of the image point P_2 of S_2. The image is real if the intersection occurs in image space and is virtual otherwise. For the case of a convergent lens with a real object with $y_o > 0$ as shown in Fig. 2.14, it follows from the similar triangles $\Delta\,\mathrm{BVF}_i$ and $\Delta\,\mathrm{P_2P_1F}_i$ that

$$\frac{y_o}{|y_i|} = \frac{f_i}{s_i - f_i}. \tag{2.61}$$

From the similar triangles $\Delta\,\mathrm{S_2S_1F}_o$ and $\Delta\,\mathrm{AVF}_o$:

$$\frac{|y_i|}{y_o} = \frac{f_o}{f_o - s_o} = \frac{\frac{n_1}{n_2}f_i}{f_i - s_o}. \tag{2.62}$$

(The absolute value of y_i is taken because according to our sign convention y_i in Fig. 2.14 is negative, whereas (2.62) is a ratio of lengths). By multiplying these two equations, using (2.50) and 2.52, we get the **Newtonian form** of the lens equation

$$x_o x_i = -\frac{n_1}{n_2}f_i^2 = -\frac{n_2}{n_1}f_o^2, \tag{2.63}$$

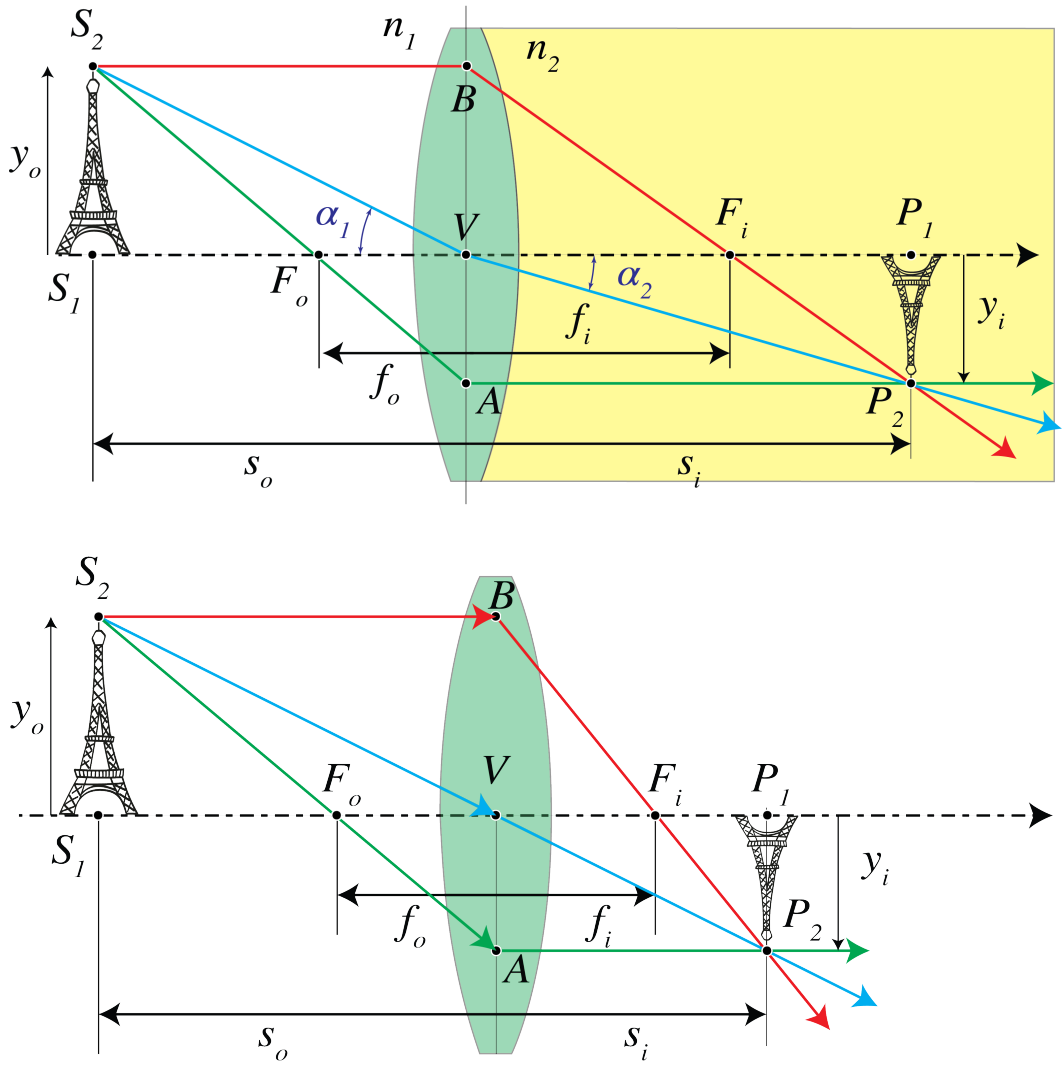


Figure 2.14: Construction with a ruler of imaging by a thin lens with different refractive indices n_1 and n_2 in object and image space in the top figure and for the case that these refractive indices are the same in the bottom figure. In the first case the ray through V is diffracted according to the paraxial version of Snell's law, in the second case this ray is straight, i.e. not refracted ($\alpha_2 = \alpha_1$).

where x_o and x_i are the z-coordinates of the object and image relative to those of the first and second focal point, respectively:

$$x_o = s_o - f_o, \quad x_i = s_i - f_i. \tag{2.64}$$

Hence x_o is negative if the object is to the left of F_o and x_i is positive if the image is to the right of F_i.

The **transverse magnification** is

$$M = \frac{y_i}{y_o} = \frac{n_1 s_i}{n_2 s_o} = -\frac{x_i}{f_i}, \tag{2.65}$$

where the second identity follows from ((2.59)) and the third from considering similar triangles $\Delta \mathrm{P_2P_1F}_i$ and $\Delta \mathrm{BVF}_i$ in Fig. 2.14. A positive M means that the image is erect, a negative M means that the image is inverted.

All equations are also valid for virtual objects and images. Examples of real and virtual object and image points for a positive and a negative lens are shown in Figs. 2.15 and 2.16.

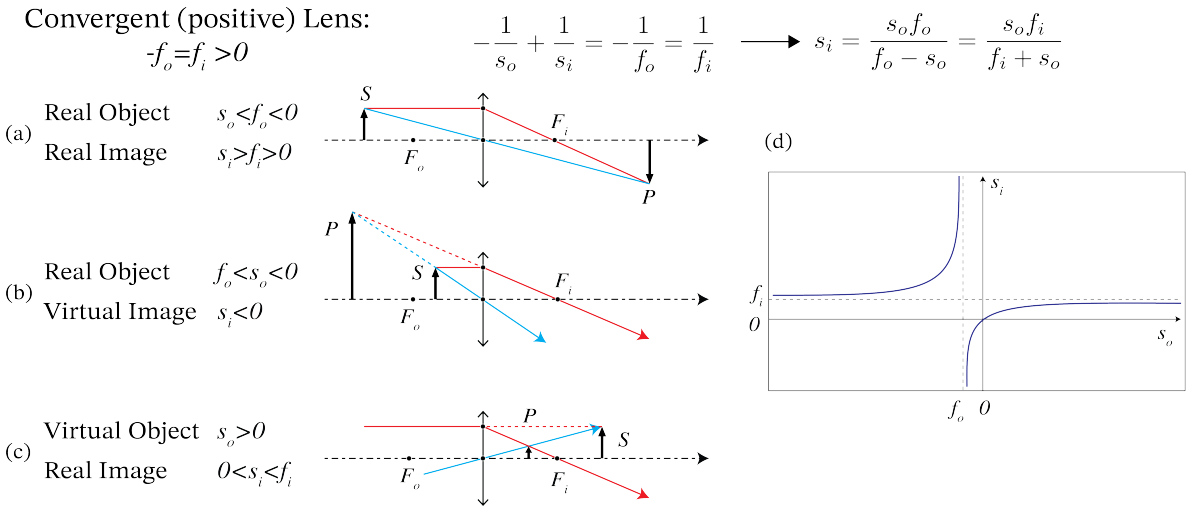


Figure 2.15: Real and virtual objects and images for a convergent thin lens with the same refractive index left and right of the lens, i.e. $-f_o = f_i > 0$. In (a) the object is real with $s_o < f_o$ and the image is real as well ($s_i > 0$). In (b) the object is between the front focal point and the lens: $f_o < s_o < 0$. Then the rays from the object are too divergent for the lens to make them convergent in image space and hence the image is virtual: $s_i < 0$. In (c) there is a cone of converging rays incident on the lens from the left which, in the absence of the lens, would converge to point S behind the lens. Therefore S is a virtual object ($s_0 > 0$). The image is real and can be constructed with the two rays shown. In (d) s_i is shown as function of s_o for a convergent lens (see Eq. (2.58)).

2.5.7 Two Thin Lenses

The ray matrix is a suitable method to study the imaging of a system consisting of several thin lenses. For two thin lenses however, the imaging can still easily be obtained by construction. We simply construct the image obtained by the first lens as if the second lens were not present and use this image as (possibly virtual) object for the second lens. In Fig. 2.17 an example is shown where surrounding the lenses the refractive index is 1 and the distance between the lenses is larger than the sum of their focal lengths. First the image P' of S is constructed as obtained by L_1 as if L_2 were not present. We construct the intermediate image P' due to lens L_1 using

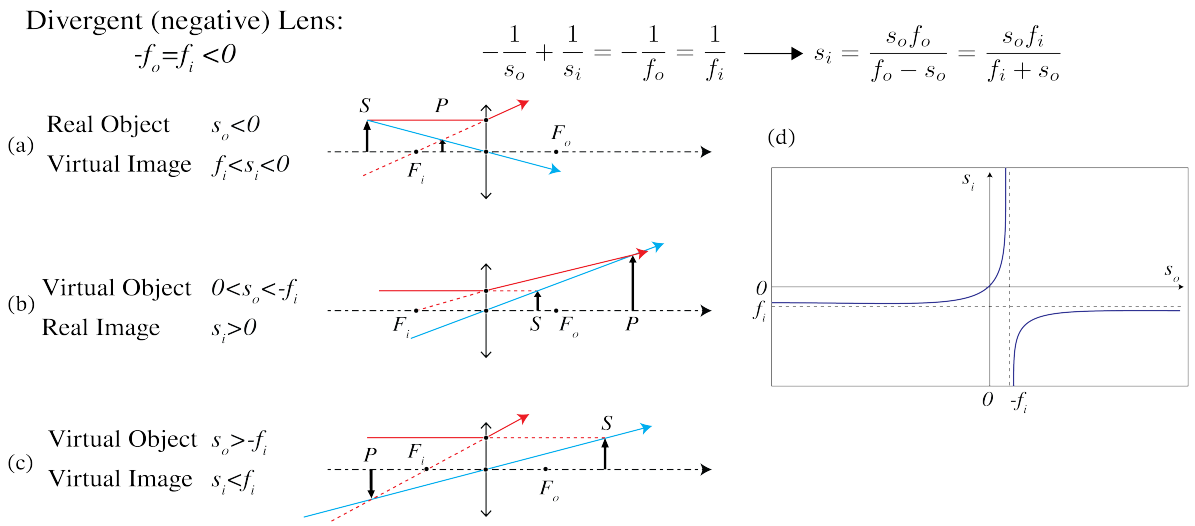


Figure 2.16: Real and virtual objects and images for a divergent thin lens with the same refractive index to the left and right of the lens, i.e. $-f_o = f_i < 0$. In (a) the object is real, i.e. $s_o < 0$. The diverging lens makes the cone of rays from the object more divergent so that the image is virtual: $s_i < 0$. When the object is virtual, there is a cone of converging rays incident from the left which after extension to the right of the lens (as if the lens is not present) intersect in the virtual object S ($s_o > 0$). It depends on how strong the convergence is whether the diverging lens turns this cone into converging rays or whether the rays keep diverging. In (b) $0 < s_o < -f_i$, and the image is real. In c) $s_o > -f_i$ and the image is virtual ($s_i < 0$). In (d) s_i is shown as function of s_o for a divergent lens ($f_i < 0$ (see Eq. (2.58)).

rays 2 and 3. P' is a real image for lens L_1 and also a real object for lens L_2. Ray 3 is parallel to the optical axis between the two lenses and is thus refracted by lens L_2 through its back focal point F_{2i}. Ray 4 is the ray from P' through the centre of lens L_2. The image point P is the intersection of rays 3 and 4.

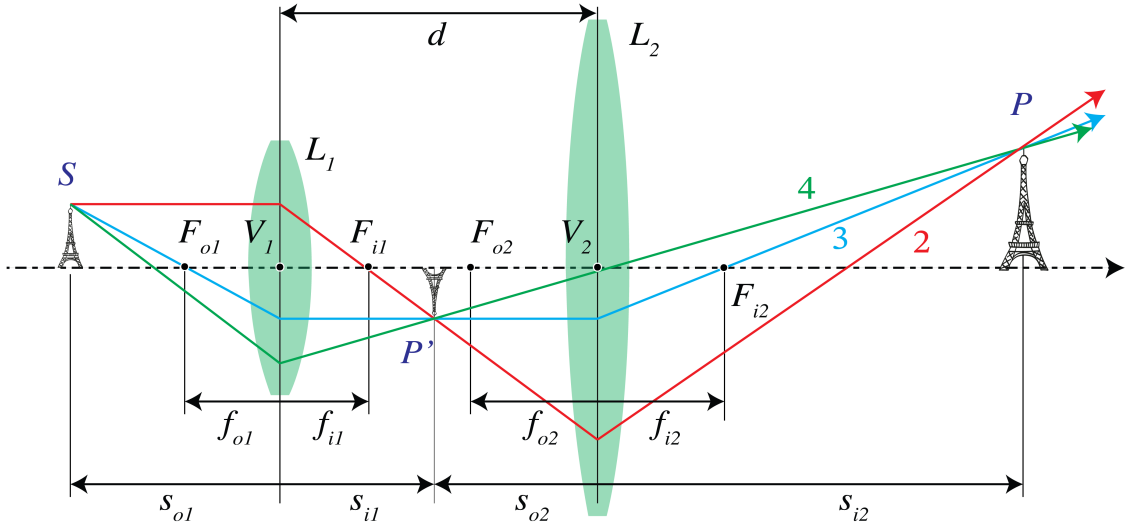


Figure 2.17: Two thin lenses separated by a distance that is larger than the sum of their focal lengths.

In the case of Fig. 2.18 the distance d between the two positive lenses is smaller than the sum of their focal lengths. The intermediate image P' is a real image for L_1 obtained as the

intersection of rays 2 and 3 passing through the object and image focal points F_{o1} and F_{i1} of lens L_1. P' is now a virtual object for lens L_2. To find its image by L_2, draw ray 4 from P' through the centre of lens L_2 back to S (this ray is refracted by lens L_1 but not by L_2) and draw ray 3 as refracted by lens L_2. Since ray 3 is parallel to the optical axis between the lenses, it passes through the back focal point F_{2i} of lens L_2. The intersection point of rays 3 and 4 is the final image point P.

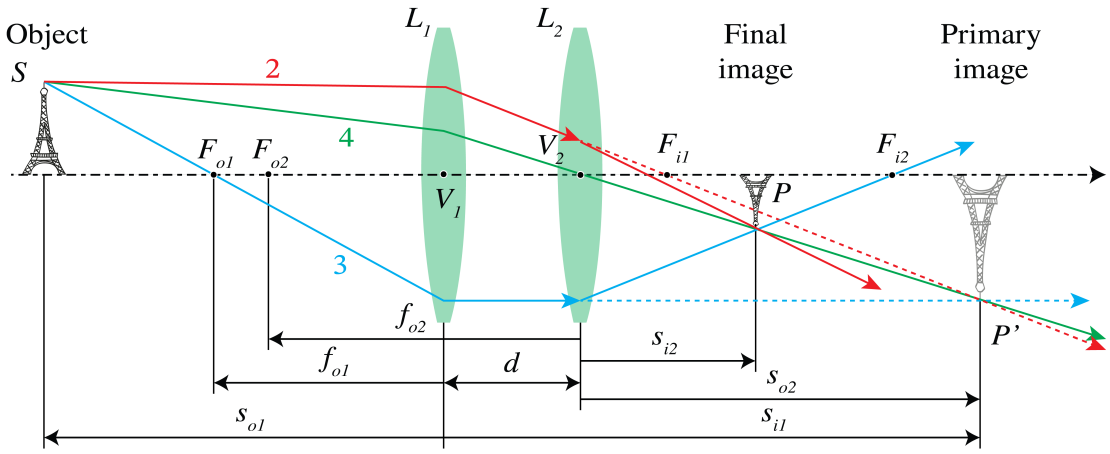


Figure 2.18: Two thin lenses at a distance smaller than the sum of their focal lengths.

It is easy to express the z-coordinate s_i with respect to the coordinate system with origin at the vertex of L_2 of the final image point, in the z-component s_o with respect to the origin at the vertex of lens L_1 of the object point. We use the Lensmaker's Formula for each lens while taking care that the proper local coordinate systems are used. The intermediate image P' due to lens L_1 has z-coordinate s_{1i} with respect to the coordinate system with origin at the vertex V_1, which satisfies:

$$-\frac{1}{s_o}+\frac{1}{s_{1i}}=\frac{1}{f_{1i}}. \tag{2.66}$$

As object for lens L_2, P' has z-coordinate with respect to the coordinate system with origin at V_2 given by: $s_{2o}=s_{1i}-d$, where d is the distance between the lenses. Hence, with $s_i=s_{2i}$ the Lensmaker's Formula for lens L_2 implies:

$$-\frac{1}{s_{1i}-d}+\frac{1}{s_i}=\frac{1}{f_{2i}}. \tag{2.67}$$

By solving (2.66) for s_{1i} and substituting the result into (2.67), we find

$$s_i=\frac{-df_{1i}f_{2i}+f_{2i}(f_{i1}-d)s_o}{f_{1i}(f_{2i}-d)+(f_{1i}+f_{2i}-d)s_o}, \qquad \textbf{two thin lenses.} \tag{2.68}$$

By taking the limit $s_o\to-\infty$, we obtain the z-coordinate f_i of the image focal point of the two lenses, while $s_i\to\infty$ gives the z-coordinate f_o of the object focal point:

$$f_i = \frac{(f_{1i}-d)f_{2i}}{f_{1i}+f_{2i}-d}, \tag{2.69}$$

$$f_o = -\frac{(f_{2i}-d)f_{1i}}{f_{1i}+f_{2i}-d}, \tag{2.70}$$

We found in Section 2.5.5 that when the refractive indices of the media before and after the lens are the same, the object and image focal lengths of a thin lens are the identical. However, as

follows from (2.69) and (2.70) the object and image focal lengths (as measured from the vertices of the first and last lens, respectively) are in general different when there are several lenses.

By construction using the intermediate image, it is clear that the magnification of the two-lens system is the product of the magnifications of the two lenses:

$$M = M_1 M_2. \tag{2.71}$$

Remarks.

1. In the limit where the lenses are very close together: $d \to 0$, (2.68) becomes

$$-\frac{1}{s_o} + \frac{1}{s_i} = \frac{1}{f_{1i}} + \frac{1}{f_{2i}}. \tag{2.72}$$

The focal length f_i of the system of two lenses in contact thus satisfies:

$$\frac{1}{f_i} = \frac{1}{f_{1i}} + \frac{1}{f_{2i}}. \tag{2.73}$$

In particular, by using two identical lenses in contact, the focal length is halved.

2. Although for two lenses the image coordinate can still be expressed relatively easily in the object coordinate, for systems with more lenses finding the overall ray matrix and then using the image condition (2.55) is a much better strategy.

2.5.8 The Thick Lens

At the left of Fig. 2.19 a thick lens is shown. The object focal point is defined as the point whose rays are refracted such that the emerging rays are parallel to the optical axis. By extending the incident and emerging rays by straight segments, the points of intersection are found to be on a curved surface, which close to the optical axis (i.e. in the paraxial approximation) is in good approximation a plane perpendicular to the optical axis. This plane is called the **primary principal plane** and its intersection with the optical axis is called the primary principal point H_1. By considering incident rays which are parallel to the optical axis and therefore focused in

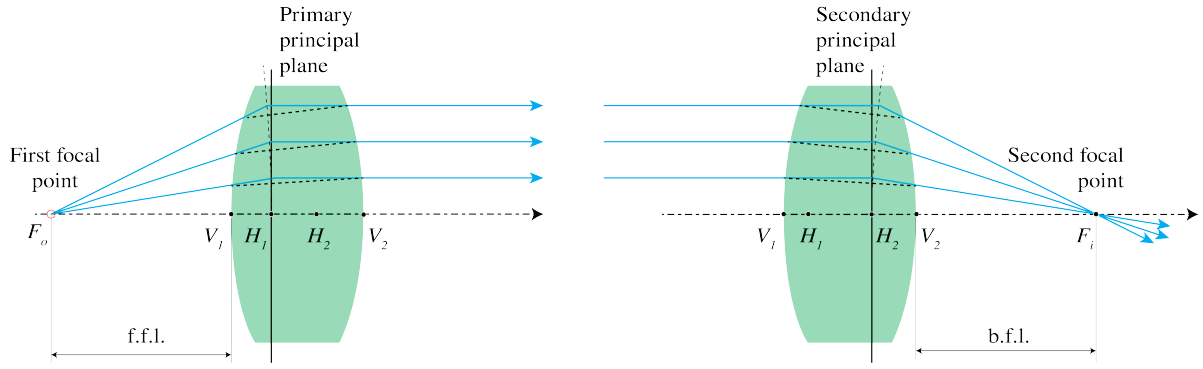


Figure 2.19: Principal planes of a thick lens, with front and back focal lengths: f.f.l and b.f.l.

the image focal point, the **secondary principal plane** and secondary principal point H_2 are defined in a similar way (see the drawing at the right in Fig. 2.19). The principal planes can be outside the lens. For meniscus lenses, this is usually the case as shown in Fig. 2.20. It can be seen from Fig. 2.19 that the principal planes are images of each other, with unit magnification. Hence, if an object is placed in the primary principal plane (hypothetically if this plane is inside the lens), its image is in the secondary principal plane. The image is erect and has unit magnification.

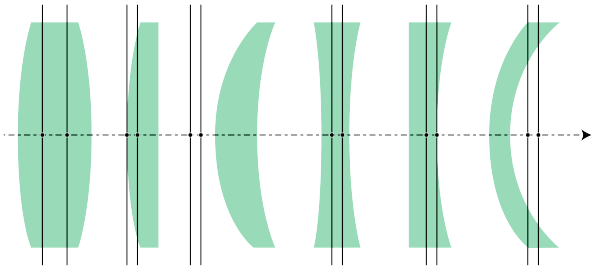


Figure 2.20: Position of the principal planes for several lenses.

Now, if the object coordinates and object focal point are defined with respect to the origin at H_1 and the image coordinates and image focal point are defined with respect to the origin in H_2, the Lensmaker's formula (2.58) can also be used for a thick lens.

Proof
We recall result (2.46) for the ray matrix between the planes through the front and back vertices V_1, V_2 of a thick lens with refractive index n_l and thickness d:

$$\mathcal{M}_{V_1V_2} = \begin{pmatrix} 1-\frac{d}{n_l}\mathfrak{P}_2 & -\mathfrak{P} \\ \frac{d}{n_l} & 1-\frac{d}{n_l}\mathfrak{P}_1 \end{pmatrix}, \qquad \textbf{thick lens}, \tag{2.74}$$

where

$$\mathfrak{P}_1 = \frac{n_l - n_1}{R_1}, \qquad \mathfrak{P}_2 = \frac{n_2 - n_l}{R_2}, \tag{2.75}$$

and n_1, n_2 are the refractive indices to the left and the right of the lens, respectively, and where

$$\mathfrak{P} = \mathfrak{P}_1 + \mathfrak{P}_2 - \frac{d}{n_l}\mathfrak{P}_1\mathfrak{P}_2. \tag{2.76}$$

If h_1 is the z-coordinate of the first principal point H_1 with respect to the coordinate system with origin at vertex V_1, we have according to (2.39) for the ray matrix between the primary principal plane and the plane through vertex V_1

$$\mathcal{M}_1 = \begin{pmatrix} 1 & 0 \\ \frac{h_1}{n_1} & 1 \end{pmatrix}. \tag{2.77}$$

Similarly, if h_2 is the coordinate of the secondary principal point H_2 with respect to the coordinate system with V_2 as origin, the ray matrix between the plane through vertex V_2 and the secondary principal plane is

$$\mathcal{M}_2 = \begin{pmatrix} 1 & 0 \\ \frac{h_2}{n_2} & 1 \end{pmatrix}. \tag{2.78}$$

The ray matrix between the two principle planes is then

$$\mathcal{M}_{H_1H_2} = \mathcal{M}_2\mathcal{M}_{V_1V_2}\mathcal{M}_1. \tag{2.79}$$

The coordinates h_1 and h_2 can be found by imposing to the resulting matrix the imaging condition (2.55): $C = 0$ and the condition that the magnification should be unity: $D = 1$, which follows from (2.56). We omit the details and only give the resulting expressions here:

$$h_1 = \frac{n_1}{n_l}\frac{\mathfrak{P}_2}{\mathfrak{P}}d, \tag{2.80}$$

$$h_2 = -\frac{n_2}{n_l}\frac{\mathfrak{P}_1}{\mathfrak{P}}d. \tag{2.81}$$

With these results, (2.79) becomes

$$\mathcal{M}_{H_1H_2} = \begin{pmatrix} 1 & -\mathfrak{P} \\ 0 & 1 \end{pmatrix}. \tag{2.82}$$

We see that **the ray matrix between the principal planes is identical to the ray matrix of a thin lens** (2.48). We therefore conclude that if the coordinates in object space are chosen with respect to the origin in the primary principal point H_1, and the coordinates in image space are chosen with respect to the origin in the secondary principal point H_2, the expressions for the first and second focal points and for the coordinates of the image point in terms of that of the object point are identical to those for a thin lens. An example of imaging by a thick lens is shown in Fig. 2.21.

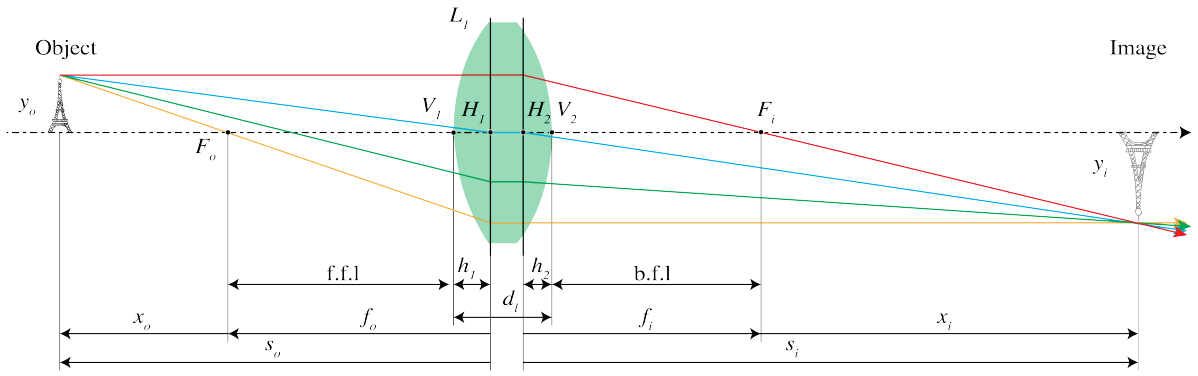


Figure 2.21: Thick-lens geometry. There holds $|f_i| = |f_o|$ if the ambient medium left of the lens is the same as to the right of the lens. All coordinates in object and image space are with respect to the origin in H_1 and H_2, respectively.

2.5.9 Stops

An element such as the rim of a lens or a diaphragm which determines the set of rays that can contribute to the image, is called the **aperture stop**. An ordinary camera has a variable diaphragm.

The **entrance pupil** is the image of the aperture stop by all elements to the left of the aperture stop. In constructing the entrance pupil, rays are used which propagate from the right to the left. The image can be real or virtual. If there are no lenses between object and aperture stop, the aperture stop itself is the entrance pupil. Similarly, the **exit pupil** is the image of the aperture stop by all elements to the right of it. This image can be real or virtual. The entrance pupil determines for a given object the cone of rays in object space that contribute to the image, while the cone of rays leaving the exit pupil are those taking part in the image formation pupil (see Fig. 2.22).

For any object point, the **chief ray** is the ray in the cone that passes through the centre of the entrance pupil, and hence also through the centres of the aperture stop and the exit pupil. A marginal ray is the ray that for an object point on the optical axis passes through the rim of the entrance pupil (and hence also through the rims of the aperture stop and the exit pupil).

For a fixed diameter D of the exit pupil and for given x_o, the magnification of a single lens is according to (2.65) and (2.63) given by $M = -x_i/f_i = f_i/x_o$. It follows that when f_i is increased, the magnification increases. A larger magnification means a lower energy density, hence a longer exposure time, i.e. **the speed of the lens is reduced**. Camera's often consist of several lenses and the optical system is then usually specified by two numbers: the focal length f, measured with respect to the exit pupil and the diameter D of the exit pupil. The **f-number** is the ratio of the focal length to this diameter:

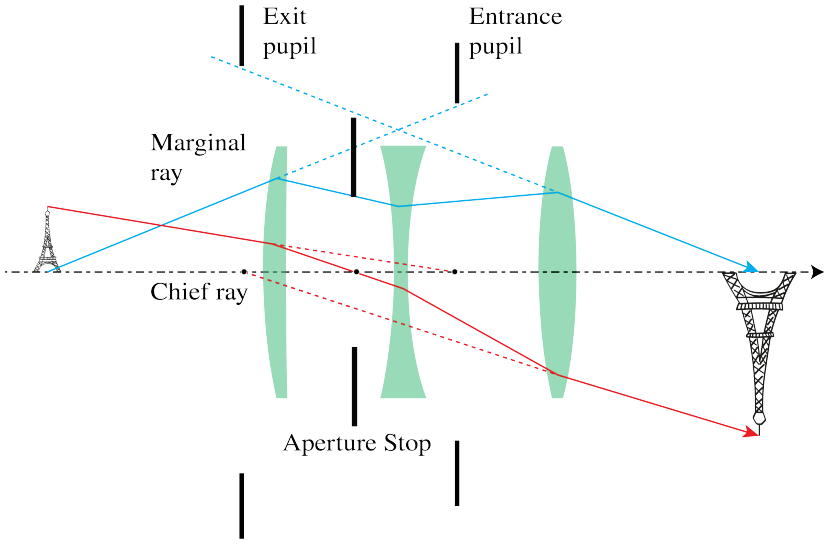


Figure 2.22: Aperture stop (A.S.) between the second and third lens, with entrance pupil and exit pupil (in this case these pupils are virtual images of the aperture stop). Also shown are the chief ray and the marginal ray.

$$\text{f-number} = f/D. \tag{2.83}$$

For example, "f-number = 2" means "$f = 2D$". Since the exposure time is proportional to the square of the f-number, a lens with f-number 1.4 is twice as fast as a lens with f-number 2.

2.6 Beyond Gaussian Geometrical Optics

2.6.1 Aberrations

For designing advanced optical systems Gaussian geometrical optics is not sufficient. Instead non-paraxial rays, and among them also non-meridional rays, must be traced using software based on Snell's Law with the sine of the angles of incidence and refraction. Often many thousands of rays are traced to evaluate the quality of an image. It is then found that in general the non-paraxial rays do not intersect at the ideal Gaussian image point. Instead of a single spot, a spot diagram is found which is more or less confined. The deviation from an ideal point image is quantified in terms of **aberrations**. One distinguishes between monochromatic and chromatic aberrations. The latter are caused by the fact that the refractive index depends on wavelength. Recall that in paraxial geometrical optics Snell's Law (2.11) is replaced by: $n_i\theta_i = n_t\theta_t$, i.e. $\sin\theta_i$ and $\sin\theta_t$ are replaced by the linear terms. If instead one retains the first two terms of the Taylor series of the sine, the errors in the image can be quantified by five monochromatic aberrations, the so-called **primary** or **Seidel aberrations**. The best known is **spherical aberration**, which is caused by the fact that for a convergent spherical lens, the rays that make a large angle with the optical axis are focused closer to the lens than the paraxial rays (see Fig. 2.23). **Distortion** is one of the other five primary aberrations. It causes deformation of images due to the fact that the magnification depends on the distance of the object point to the optical axis.

For high-quality imaging the aberrations have to be reduced by adding more lenses and optimising the curvatures of the surfaces, the thicknesses of the lenses and the distances between them. Sometimes a lens with an aspherical surface is used. Systems with very small aberrations are extremely expensive, in particular if the field of view is large, as is the case in lithographic

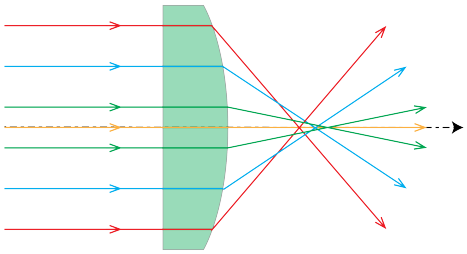


Figure 2.23: Spherical aberration of a planar-convex lens.

imaging systems used in the manufacturing of integrated circuits as shown in the lithographic system in Fig. 2.24.

A comprehensive treatment of aberration theory can be found in Braat et al.[11].

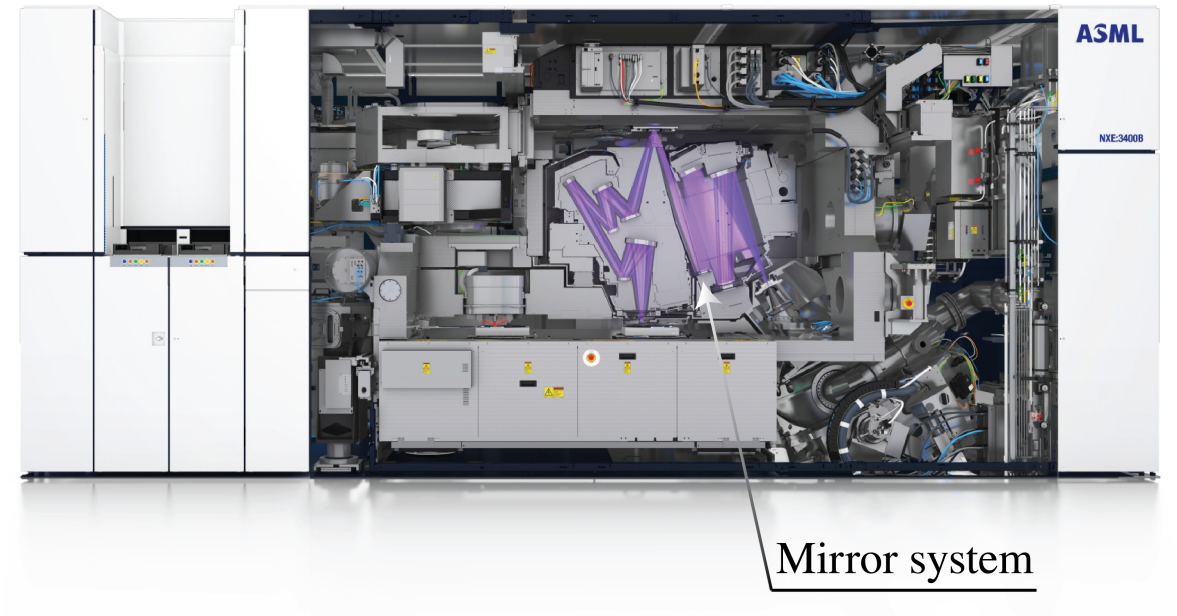


Figure 2.24: The EUV stepper TWINSCAN NXE:3400B.Lithographic system for wavelength of 13.5 nm). Ray paths are shown in purple. The optical system consists of mirrors since there are no lenses for light at this wavelength because is absorbed by all materials. High reflection of the mirrors is achieved by using coatings consisting of many layers. (Courtesy of ASML).

2.6.2 Diffraction

According to a generally accepted criterion formulated first by Rayleigh, aberrations start to deteriorate images considerably if they cause path length differences of more than a quarter of the wavelength. When the aberrations are less than this, the system is called **diffraction limited**.

Even if the wave transmitted by the exit pupil would be perfectly spherical (no aberrations), the wave front consists of only a circular section of a sphere since the field is limited by the aperture. An aperture always causes **diffraction**, i.e. bending and spreading of the light. When one images a point object, diffraction causes inevitable blurring given by the so-called Airy spot,

[11] J. Braat, P. Török, *Imaging Optics*, Cambridge University Press (2019)

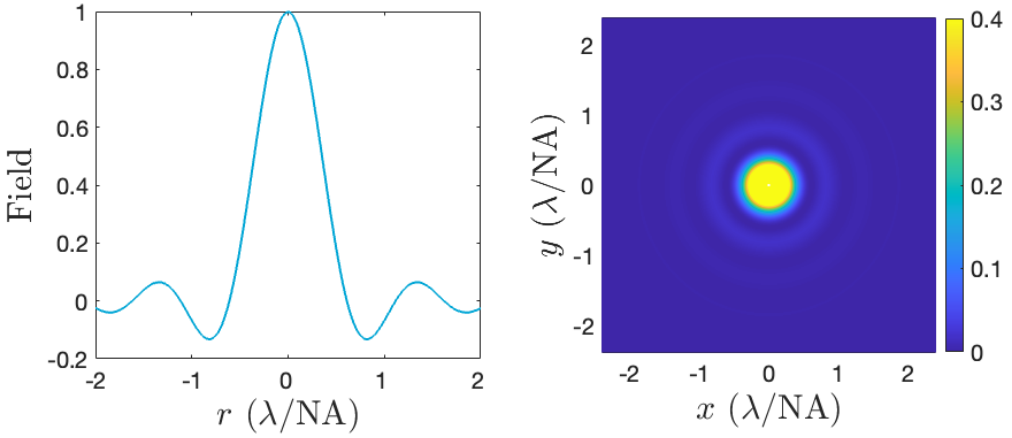


Figure 2.25: Left: cross-section of the amplitude (not the square of the amplitude) of the field of the Airy pattern. Right: circular symmetric intensity of the Airy pattern. The maximum is set to 0.4 instead of 1 in order to observe the rings.

as shown in Fig. 2.25. The Airy spot has full-width at half maximum:

$$\text{FWHM} = 0.6\frac{\lambda}{\text{NA}}, \tag{2.84}$$

where NA$=$ arcsin(a/s_i) is the numerical aperture (i.e. 0$<$NA$<$1) with a the radius of the exit pupil and s_i the image distance as predicted by Gaussian geometrical optics. Diffraction depends on the wavelength and hence it cannot be described by geometrical optics, which applies in the limit of vanishing wavelength. We will treat diffraction by apertures in Chapter 6.

Problems

1. **Principle of Fermat and Snell's Law.** Consider a layer of thickness d and refractive index n_2 which is sandwiched between two half spaces with refractive index n_1 and n_3 as shown in Fig. 2.26. A ray from point $P = (x_P, y_P)$ with $y_P > d$ passes through point $Q = (x_Q, y_Q)$ with $y_Q < 0$.

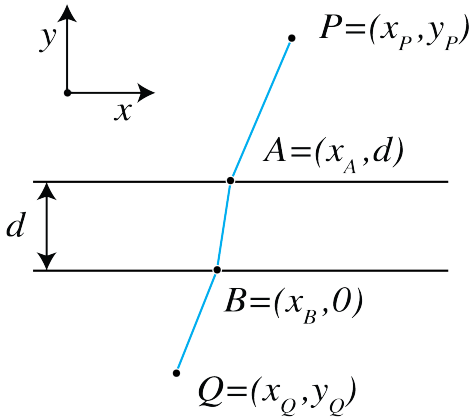


Figure 2.26: A ray through points P and Q.

a) Write a formula for the OPL of the ray from P to Q as shown in Fig. 2.26.

b) Find the equations to be satisfied by x_A and x_B such that the OPL is minimum. Hint: set the partial derivatives of the OPL with respect to x_A and x_B equal to zero.

c) Express the equations derived under b) in terms of $\sin\theta_1$, $\sin\theta_2$ and $\sin\theta_3$ and derive that Snell's Law holds for the angles θ_1 and θ_3:

$$n_1 \sin\theta_1 = n_3 \sin\theta_3. \tag{2.85}$$

Note that the relationship between θ_3 and θ_1 is independent of the refractive index n_2 and the thickness d of the middle layer.

d) Does Snell's Law (2.85)) hold irrespective of the number of layers and their thicknesses in between the two half spaces? Explain your answer.

e) Derive (2.85) by using the boundary conditions for the tangential components of the electromagnetic field, as described in Section 1.9.1.

2. **Perfect focusing by an ellipsoid and a hyperboloid.** Suppose that there are two media with refractive indices $n_1 > n_2$ and that point S is at infinity in the medium with refractive index n_2. We will construct a surface (interface) between the two media such that all rays from S are focused into the same point F (see Fig. 2.27a). Because S is at very large distance, the rays entering from the right are parallel. Since all parallel rays have travelled the same distance when they hit the surface DD' perpendicular to the rays, all parallel rays have the same phase at their intersection points with the plane DD'.

a) If point A is on the interface sought, derive that

$$\frac{n_2}{c}|DA| + \frac{n_1}{c}|AF| = \text{constant}, \tag{2.86}$$

the constant is the same for all points A on the interface.

b) Show that by moving the plane DD' parallel to itself we can achieve that for the new plane DD' we get:

$$e|DA| + |AF| = 0, \tag{2.87}$$

where $e = n_2/n_1 < 1$. Hence the interface is an ellipsoid.

c) Suppose next that $n_2 > n_1$ as shown at the right of Fig. 2.27. Show that now, by the same argument as above, the interface is a hyperboloid with F as one of its focal points.

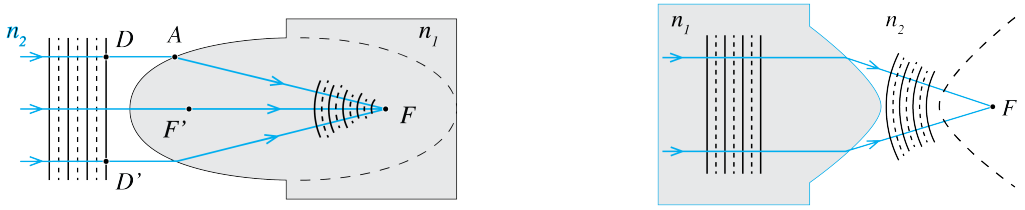


Figure 2.27: (a) Ellipsoid ($n_2 < n_1$) and (b) hyperboloid ($n_2 > n_1$) to perfectly focus a parallel beam incident from the medium with refractive index n_2 into a point in a medium with refractive index n_1.

d) Use the previous results to describe a lens with refractive index $n_2 > n_1$ and having hyperboloid surfaces which perfectly image two given points S and P in the ambient medium with refractive index n_1.

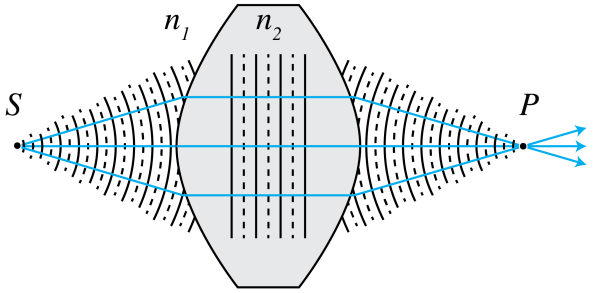


Figure 2.28: Lens with hyperboloid surfaces for perfect imaging of a pair of points.

3. **Perfect focusing by a parabolic mirror.** Next we consider perfect focusing of parallel rays in air ($n = 1$) by a mirror. Let there be a parallel bundle of rays in air ($n = 1$) and suppose we want to focus all rays in point F.

   a) We draw a plane Σ_1 perpendicular to the rays as shown in Fig. 2.29. The rays that hit Σ_1 have traversed the same optical path length. Draw a second surface Σ_2 parallel to Σ_1. Consider rays hitting the mirror in A_1 and A_2. Derive that

   $$\text{OPL} = |W_1A_1| + |A_1F| = |W_2A_2| + |A_2F|. \tag{2.88}$$

   b) Derive that

   $$|W_1A_1| + |A_1D_1| = |W_2A_2| + |A_2D_2|. \tag{2.89}$$

   c) Show that (2.88) is satisfied for points A for which $|AF| = |AD|$, and conclude that the mirror is a paraboloid with f as focus and Σ_2 as diretrix (i.e. line perpendicular to the axis of the parabola).

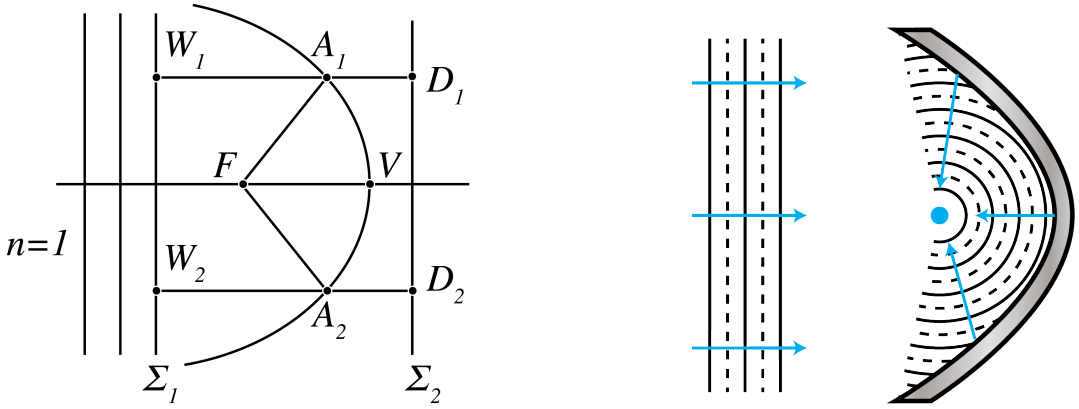


Figure 2.29: A paraboloid mirror.

4. **Imaging of a virtual object.** A virtual object is at a distance d_0 behind a converging lens. The converging incident rays to the left of the lens, that correspond to the virtual object, are shown in Fig. 2.30. The lens has focal length f.

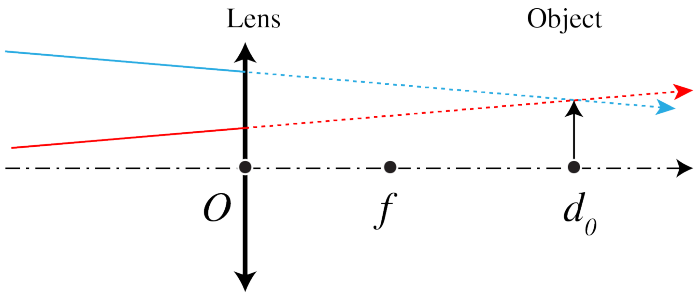


Figure 2.30: An object is created by incoming rays.

   a) Construct the image when $f = 2$ cm, $d_0 = 4$ cm and the height of the object 1 cm.

   b) Is the image real or virtual? Inverted or upright?

   c) Calculate the location of the image using the lens formula and compare it with your drawing. What is the magnification?

5. **Two thin lenses.** Suppose we have two thin lenses $\mathcal{L}_1$ and $\mathcal{L}_2$. Lens $\mathcal{L}_1$ is convergent (i.e. positive) with focal distance $f_1 > 0$ and lens $\mathcal{L}_2$ is divergent (i.e. negative) with focal distance $f_2 < 0$. The distance between the lenses is d. Let there be an object at distance $2f_1$ in front of lens $\mathcal{L}_1$, as shown in Fig. 2.31.

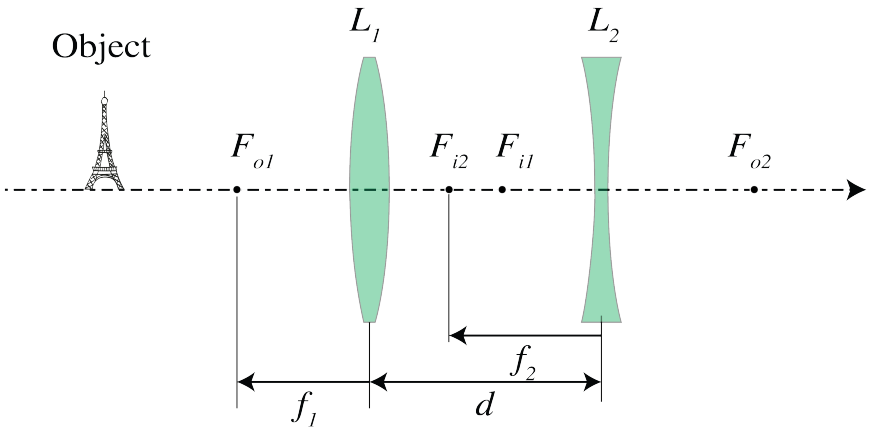


Figure 2.31: Figure corresponding to Exercise "A convergent and divergent lens".

a) Derive the condition on the distance d between the lenses such that the final image is real.

b) Let $f_1 = 3$ cm and $f_2 = -2$ cm. What should be the distance d such that the final image is real and the magnification is 2?

6. **System matrix for imaging by a spherical surface.** Consider a spherical surface with radius of curvature R with to the left (right) of the surface a medium with refractive index n_1 (n_2).

a) Derive the ray matrix between a plane to the left of the surface and at distance d_1 to the vertex, and a plane to the right of the surface with distance of d_2 to the vertex. (As always the rays are assumed to propagate from the left to the right).

b) Derive the conditions such that the plane at distance d_2 is the image of the plane at distance d_1. Express the formula in coordinates $s_o = -d_1$, $s_i = d_2$ with respect to the vertex as origin and show that the result is identical to formula (2.24)

c) Assume that $n_1 = 1$, $n_2 = 2$ and $R = 2$ cm. Show by construction using the paraxial version of Snell's Law that when the object is virtual with $s_o = -4$ cm, the coordinate of the image point is given by $s_i = 8$ cm, in agreement with the formula derived in b).

d) Construct again the image when $s_o = -4$ cm but now for the case that $R = -2$ cm and verify that the coordinate s_i of the image point agrees with the formula derived in b).

7. 'bf Derivation of the Lensmaker's formula. The purpose of this problem is to derive the Lensmaker's formula for a thin lens by applying the imaging formula of a spherical surface twice. The image P of a point S as shown in Fig. 2.32 is computed in two steps. First the intermediate image P' of S by the spherical surface with vertex V_1 is computed and then this intermediate image is imaged by the spherical surface with vertex V_2.

a) Use (2.24) to deduce that when S is imaged by the first spherical surface as if the second spherical surface were absent, the image P' with z-coordinate s_{i1} with respect to the origin in V, of S, satisfies:

$$-\frac{n_m}{s_{o1}} + \frac{n_l}{s_{i1}} = \frac{n_l - n_m}{R_1}, \tag{2.90}$$

where s_{o1} is the z-coordinate of S with respect to the origin in V.

b) Show that with respect to the origin at V_2 the z-coordinate of P' is

$$s_{o2} = s_{i1} - d. \tag{2.91}$$

c) Show that the z-coordinate s_{i2} of P with respect to the origin at V_2 satisfies

$$-\frac{n_l}{s_{o2}} + \frac{n_m}{s_{i2}} = \frac{n_m - n_l}{R_2}. \tag{2.92}$$

d) Add the results of a) and c) to derive

$$-\frac{n_m}{s_{o1}} + \frac{n_m}{s_{i2}} = (n_l - n_m)\left(\frac{1}{R_1} - \frac{1}{R_2}\right) + \frac{n_l d}{(s_{i1} - d)s_{i1}}. \tag{2.93}$$

e) Derive the Lensmaker's formula for the thin lens (2.58) by taking the limit $d \to 0$ in d).

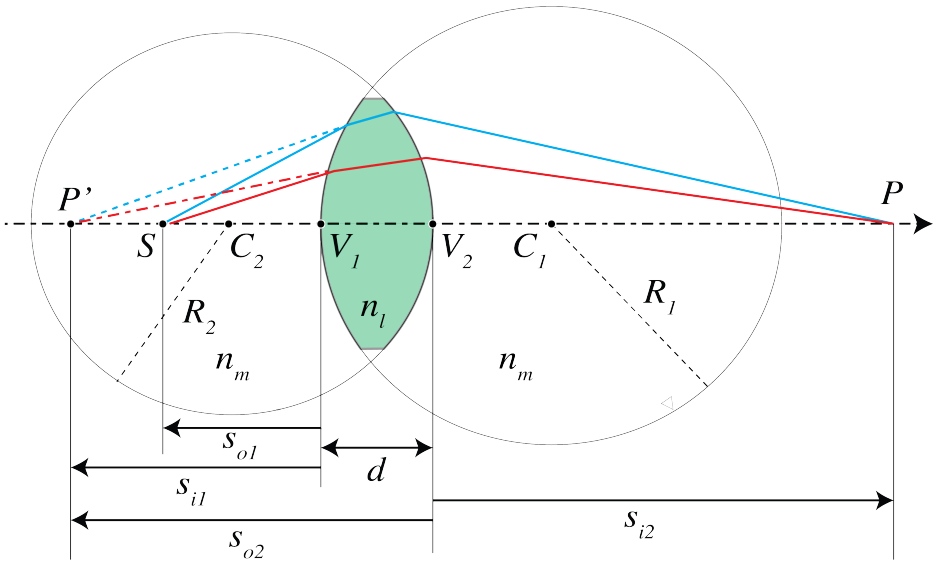


Figure 2.32: A spherical lens made of glass of index n_l in a medium of index n_m. The point S is imaged in P.

8. **System matrix for focusing.** Consider a ray transfer matrix

$$\begin{pmatrix} A & B \\ C & D \end{pmatrix} \tag{2.94}$$

between two planes.

a) Suppose that any ray that is parallel to the optical axis in the first plane goes through a point on the optical axis in the second plane. This means that the second plane is the image focal plane of the system. What does this imply for the elements of the transfer matrix?

b) Suppose that the first plane is the object focal plane, so that any ray emitted by the point on the optical axis in the first plane becomes collimated in the second plane. What does this imply for the elements for the transfer matrix?

c) Consider two thin lenses with distance d and focal distances f_{1i} and f_{2i}. Derive the transfer matrix linking the plane immediately before the first lens with the plane immediately behind the second lens. You may assume that the lenses are in air with refractive index $n = 1$.

d) Use the condition that you found in a) to derive the image focal distance of a system consisting of two thin lenses with image focal distances f_{1i} and f_{2i} and distance d. Verify that the result agrees with the distance for the image focal plane (2.69). Hint: let f_i be the distance of the image focal point of the two-lens system to the second lens. Write the transfer matrix between the lens immediately before the first lens and the plane through the image focal point.

e) Add a third thin lens with image focal distance f_{3i} is in contact to the second lens. Derive the ray matrix of this system.

f) Let f_i be the distance from the image focal plane to the third lens. Use the condition derived in a) and the ray matrix derived in e) to derive f_i.

9. **Matrix for two thin lenses.**

a) Consider two thin lenses which are surrounded by a medium with refractive index n. Let the left and right lens have power $\mathfrak{P}_1$ and $\mathfrak{P}_2$, respectively and let the distance between their vertices be d. Derive that the matrix between the planes immediately to the left of the first lens and the plane immediately to the right of the second lens is given by

$$\begin{pmatrix} 1 - \frac{d}{n}\mathfrak{P}_1 & -\mathfrak{P}_1 - \mathfrak{P}_2 - \frac{d}{n}\mathfrak{P}_1\mathfrak{P}_2 \\ \frac{d}{n} & 1 - \frac{d}{n}\mathfrak{P}_2 \end{pmatrix}. \tag{2.95}$$

b) Show that the coordinates of the image and object focal points are given by:

$$f_i = \frac{\mathfrak{P}_1 + \mathfrak{P}_2 + \frac{d}{n}\mathfrak{P}_1\mathfrak{P}_2}{n\left(1 - \frac{d}{n}\right)\mathfrak{P}_2} \tag{2.96}$$

$$f_o = \frac{\mathfrak{P}_1 + \mathfrak{P}_2 + \frac{d}{n}\mathfrak{P}_1\mathfrak{P}_2}{n\left(1 - \frac{d}{n}\right)\mathfrak{P}_1}. \tag{2.97}$$

c) Verify that these formulae are equivalent to (2.70),(2.69).

10. **Entrance pupil of a system of two lenses.** Consider a system of two lenses L_1 and L_2 with distance d. The left lens L_1 has image focal distance f_{1i} and a_1, a_2 are the radii of the lens apertures of L_1 and L_2.

a) Let lens L_1 be convergent with $f_{1i} = 2$ cm and let the distance be $d = 1$cm. Furthermore, let $a_1 = 2$cm and $a_2 = 1$cm. Determine by construction with a ruler the entrance pupil. Compute also its position and radius using the Lensmakers' formula and derive the tangent of the angle that the marginal ray makes with the optical axis for an object on the optical axis at 4 cm to the left of L_1.

b) Same question when L_1 is a divergent lens with $f_{1i} = -6$ cm, $d = 3$ cm and $a_1 = a_2 = 1$cm.

11. **Diaphragm in a system of two thin lenses.** The purpose of this problem is to determine the entrance and exit apertures of a system consisting of two thin lenses with a diaphragm using three methods: construction, applying the Lensmaker's formula and the matrix method. The situation is as shown in Fig. 2.33. The focal distances of the two thin lenses are $f_1 = 10$ cm and $f_2 = 12$ cm and their distance $d = 6$ cm. Suppose that the aperture stop is as shown in Fig. 2.33. It is at a distance of 1.5 cm in front of the lens L_1 and has a diameter $D_a = 5$ cm.

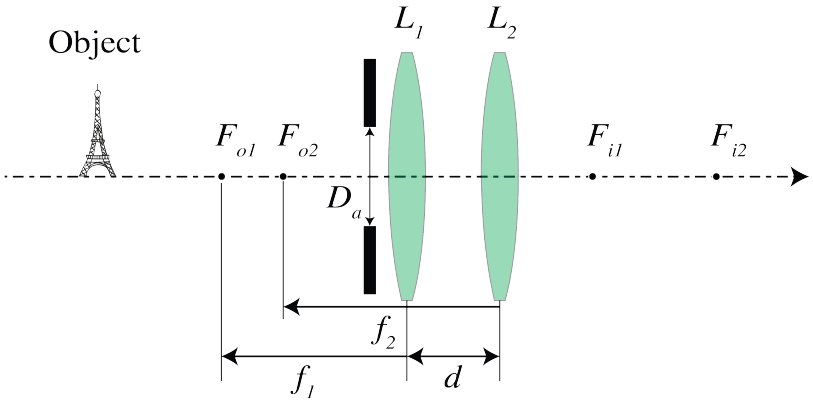


Figure 2.33: Two thin lenses

a) Determine the position of the entrance pupil and its diameter D_e by the mentioned three methods.

b) Determine the position of the exit pupil and its diameter D_{exit} by the mentioned three methods.

c) Compute the f-number of the system.

12. * **Principal planes for a thick lens.**
In this problem the transfer matrix for a thick lens is derived. By finding the positions of the principal planes, you will derive that the transfer matrix has the same form as for a thin lens when object, image and focal distances are measured with respect to principle planes.
The transfer matrices which you should use are those for refraction through a spherical interface between two media with refractive indices n, n' to the left and right of the interface, respectively, and with radius of curvature R:

$$\mathcal{S} = \begin{pmatrix} 1 & -\mathfrak{P} \\ 0 & 1 \end{pmatrix}$$

where $\mathfrak{P} = (n' - n)/R$, and secondly the matrix $\mathcal{M}_d$ for propagation through a medium with refractive index n over a distance d .

Consider a thick lens made of a glass of refractive index n with thickness d. For paraxial rays, the thickness can be identified with the distance between the vertices V_1 and V_2 of the surfaces of the lens.

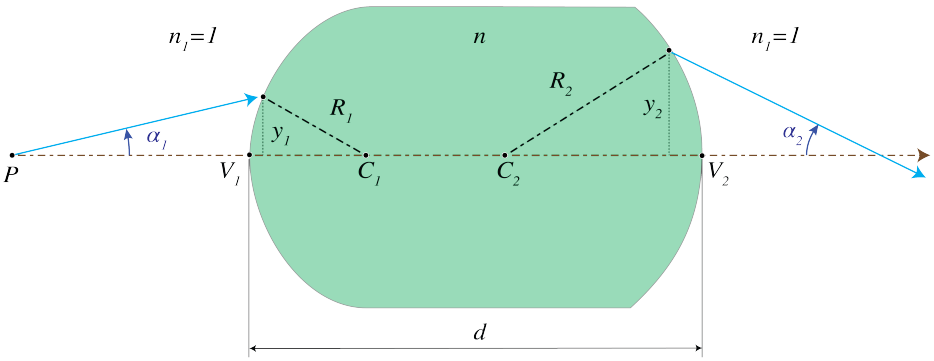


Figure 2.34: Thick lens.

a) Derive that the transfer matrix between the surfaces through the two vertices of the thick lens is given by:

$$\mathcal{L}_{V_2V_1} = \begin{pmatrix} 1-\mathfrak{P}_2\frac{d}{n} & -\mathfrak{P}_1-\mathfrak{P}_2+\mathfrak{P}_1\mathfrak{P}_2\frac{d}{n} \\ \frac{d}{n} & 1-\mathfrak{P}_1\frac{d}{n} \end{pmatrix} \tag{2.98}$$

where $\mathfrak{P}_1 = (n-1)/R_1$ and $\mathfrak{P}_2 = (1-n)/R_2$.

b) Show that for $d = 0$ the transfer matrix is identical to that for a thin lens given by Eq. (2.48).
In Section 3.5.7 of the Lecture Notes the primary and secondary principle planes were defined. Let the distance between the primary principle plane $\mathcal{H}_1$ and vertex V_1 be T_1, and let the distance of the second principle plane $\mathcal{H}_2$ to vertex V_2 be T_2 as shown in Fig. 2.35). $T_1 > 0$ and $T_2 > 0$ if the first principle plane is to the left of V_1 and the second principle plane is to the right of V_2, respectively, while T_1 and T_2 are negative otherwise.

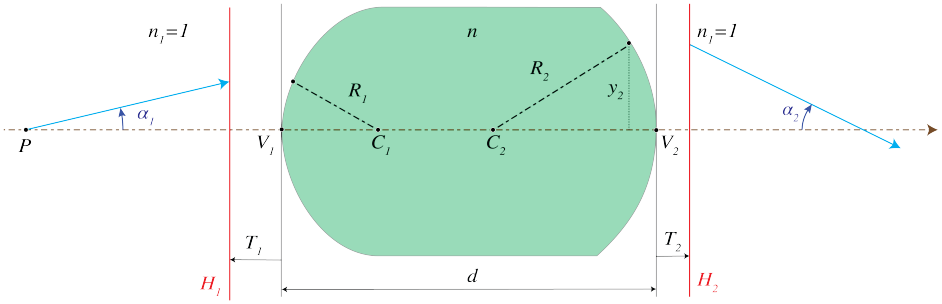


Figure 2.35: Thick lens with principle planes.

The transformation of a ray from the primary principle plane $\mathcal{H}_1$ to the secondary principle plane $\mathcal{H}_2$ is:

$$\begin{pmatrix} \alpha_1 \\ y_1 \end{pmatrix} = \mathcal{L}_{\mathcal{H}_1\mathcal{H}_2} \begin{pmatrix} \alpha_2 \\ y_2 \end{pmatrix}, \tag{2.99}$$

where

$$\mathcal{L}_{\mathcal{H}_2\mathcal{H}_1} = \mathcal{M}_{T_2}\mathcal{L}_{V_2V_1}\mathcal{M}_{T_1} \tag{2.100}$$

c) By using the following abbreviation for the matrix (2.98):

$$\begin{pmatrix} 1-\mathfrak{P}_2\frac{d}{n} & -\mathfrak{P}_1-\mathfrak{P}_2+\mathfrak{P}_1\mathfrak{P}_2\frac{d}{n} \\ \frac{d}{n} & 1-\mathfrak{P}_1\frac{d}{n} \end{pmatrix} = \begin{pmatrix} a_{11} & a_{12} \\ a_{21} & a_{22} \end{pmatrix}, \tag{2.101}$$

derive that:

$$\mathcal{L}_{\mathcal{H}_2\mathcal{H}_1} = \begin{pmatrix} a_{11}+T_1a_{12} & a_{12} \\ T_2(a_{11}+T_1a_{12})+a_{21}+T_1a_{22} & a_{22}+T_2a_{12} \end{pmatrix} \tag{2.102}$$

d) The principle planes are conjugate (i.e. they are each other images) with unit magnification. Derive from this fact that the locations of the principle planes are given by:

$$T_2 = \frac{1 - a_{22}}{a_{12}}$$
$$T_1 = \frac{1 - a_{11}}{a_{12}}$$

With the solutions for T_1 and T_2 the system matrix between the principal planes becomes:

$$\mathcal{L}_{\mathcal{H}_2\mathcal{H}_1} = \begin{pmatrix} 1 & a_{12} \\ 0 & 1 \end{pmatrix} \tag{2.103}$$

which has the same shape as the transfer matrix for a thin lens.

e) Show that the back focal point is at distance $1/a_{12}$ from the secondary principle plane and that the front focal plane is at distance $1/a_{12}$ from the primary principle plane.

Chapter 3

Optical Instruments

What you should know and be able to do after studying this chapter

- Understand the working principle of a camera.
- Understand the optics of the eye and its accommodation with the near and far point.
- The working of eye glasses.
- Understand the principle of the magnifier and the eyepiece and its use in the microscope and the telescope.
- Understand the microscope and the telescope concept and the (angular) magnification in both cases.

After the treatment in the preceding chapter of the laws of Gaussian geometrical optics, more complex systems based on lenses and reflectors can now be considered.

3.1 The Camera Obscura

The camera obscura or pinhole camera is the simplest image forming system. It consists of a closed box with a pinhole on one side. An inverted image is cast on the opposite side of the box as shown in Fig. 3.1. If the hole is too large, the image is very blurred. At the cost of less light, the image can be made sharper by reducing the aperture. The camera obscura can form images of objects across an extremely wide angular field due to great depth of focus and over a large range of distances (great depth of field) as you can see in Fig. 3.1. If a film would be used to record the image, very long exposure times would be needed because only a small amount of light enters the pinhole, (f-number= 500). It is believed that painters such as Johannes Vermeer have used the camera obscura to make paintings of external scenes.

3.2 The Camera

In Fig. 3.2 a single-lens reflex (SLR) camera is shown. The name does not mean that there is only one lens in the optical system, but that the photographer looks through the same lenses that the picture is taken with, instead of looking through a separate parallel optical system as in the twin reflex camera. After traversing the first few lens elements, the light passes through an iris diaphragm with adjustable diameter with which the f-number can be changed. After the lenses the light is reflected by a movable mirror tilted at 45°, passes through a prism and exits the camera through the finder eyepiece. When the shutter is released, the diaphragm closes to a preset value, the mirror swings up and the CCD is exposed. To focus the camera, the entire lens is

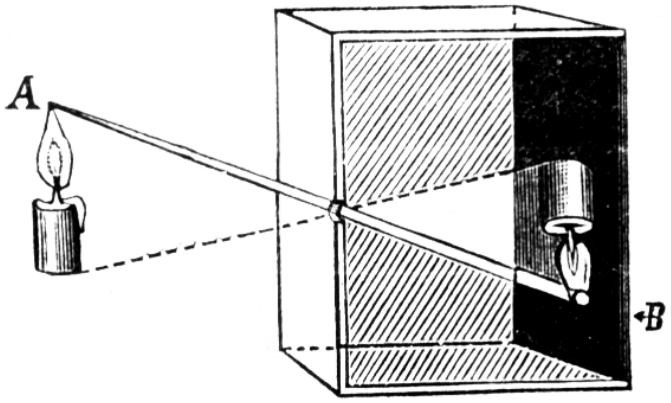


Figure 3.1: The principle of the camera obscura (from Wikimedia Commons in Fizyka z. (1910) / Public Domain). Examples of pictures made with a camera obscura can be found here.

moved toward or away from the detection plane. Autofocus is based on maximising the contrast of the images. The **angular field of view** (AFOV) is defined for scenes at large distances

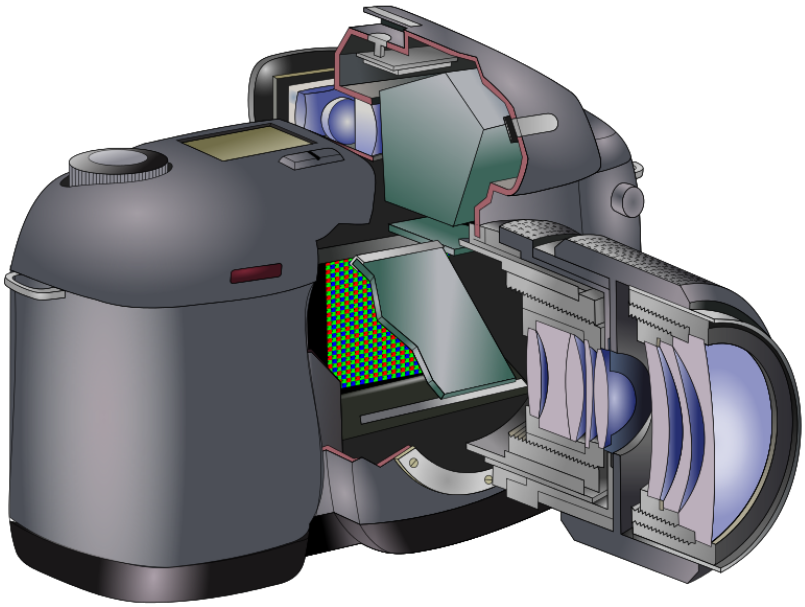


Figure 3.2: Digital SLR camera. The pixelated digital sensor is behind a movable mirror at angle of 45 degrees with the optical axis. (from Wikimedia Commons by Jean François WITZ / CC BY-SA 3.0).

and is equal to the angle subtended at the lens by the detector when the image distance is the focal length f, i.e. the object is at infinity (Fig. 3.3). The AFOV decreases when f increases. A standard SLR has a focal length of around 6 cm with AFOV between 40° and 50°. More complex

systems can have a variable focal length by changing the distance between the lenses, i.e. they are able to *zoom* into a scene.
The **depth of focus** is a range of object distances around a given distance for which the images on the sensor are sharp. The depth of focus depends on the diaphragm. When the aperture is wide open, rays forming the image will make larger angles with the optical axis. When these rays come from objects at various distances they will for a large diaphragm cause more blurred images on the sensor (see Fig. 3.4). When the aperture is reduced, this effect is less and therefore a smaller diaphragm implies a larger depth of focus. The drawback is that less light reaches the sensor, therefore a longer exposure time is needed.

3.3 Camera in a Smart Phone

A camera in a smart phone can contain standard **double Gauss** or **Cook triplet** lenses and sometimes more advanced aspheres. The image sensor is CMOS device. Nowadays smart phones have auto-focus systems where the lens is moved towards or away from the sensor using different criteria. In the standard contrast detection auto-focus the lens is moved until the contrast in the image is largest. This trial-and-error method is relatively slow: it usually takes 1 second to focus. In high-end cameras so-called phase detection auto-focus is used where the relative position of two spots obtained by focusing of two small diaphragms on either side of the optical axis is analysed. A third auto-focus system is similar to radar. An infrared laser pulse is emitted and the distance of the object of interest is determined from the return time of the reflected pulse. The method works very well under low light conditions, but is not accurate for objects at distances of more than 5 m. In all smart phone cameras, blurry images are sharpened by post-processing using software.

3.4 The Human Eye

The eye is an adaptive imaging system.

3.4.1 Anatomy

The human eye is made of an almost spherical (24 mm long and 22 mm across) gelatinous substance called the **vitreous humor** with refractive index $n_{vh} = 1.337$ for green light, surrounded by a white shell, the **sclera** (Fig. 3.5). At the front, the sclera has an opening with a transparent lens called the **cornea**, with for green light an index of refraction of 1.376. Most of the bending of the rays takes place at the air-cornea interface and this is why it is difficult to see under water ($n_{water} = 1.33$). After passing the cornea, the rays reach the **aqueous humour** ($n \approx 1.336$) with the **iris** or pupil. It can expand or contract from a 2 mm (bright sun) to 8 mm (low light) diameter to adapt to the light intensity. The iris gives colour to the eye. After the iris, the rays reach the flexible **crystalline lens** which has the size of a bean (9 mm in diameter, and 4 mm thick in relaxed condition). Its index of refraction varies from 1.406 in the centre to 1.386 at the edge.

3.4.2 Working of the eye

The entire eye can accurately be treated as two lenses in contact, of which the second lens can change its focal length. But often the system is approximated by only a single lens and this is also what we will do below. In relaxed condition, the object focal distance of the lens system is $f_o = 16$ mm as measured from the cornea while the image focal distance is equal to the length of the eye: $f_i = 24$ mm. These focal distances are different, because the refractive indices of

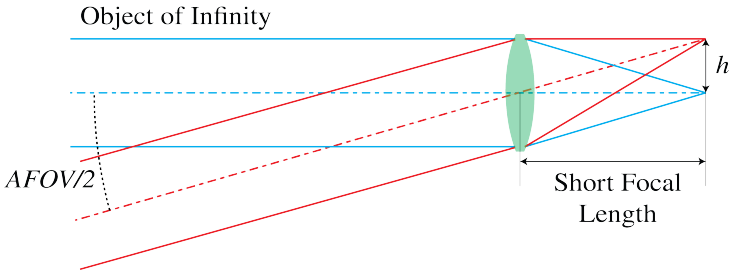


Figure 3.3: Angular field of view

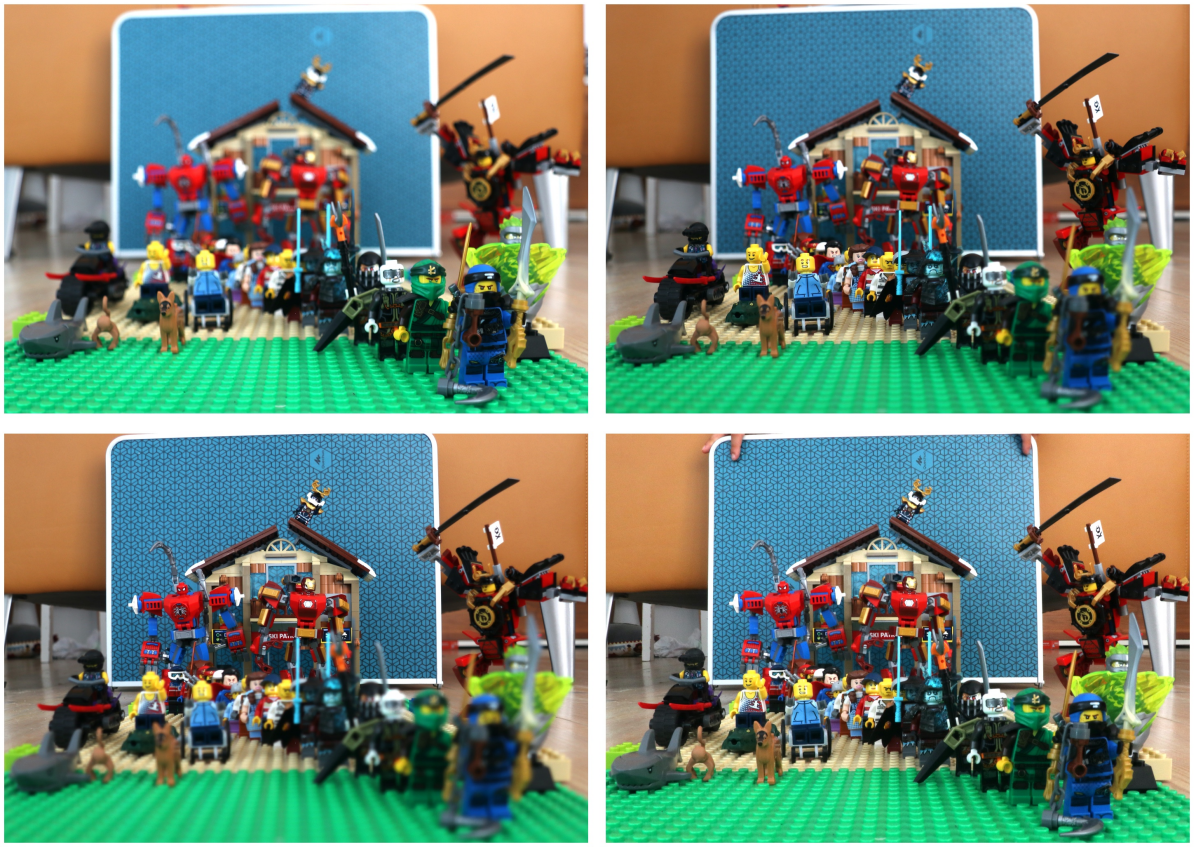


Figure 3.4: Four images taken with different diaphragm and different focal plane. The image on bottom right is taken with a small diaphragm and the entire image appears clear (photos taken by Aurèle J.L. ADAM / CC BY-SA).

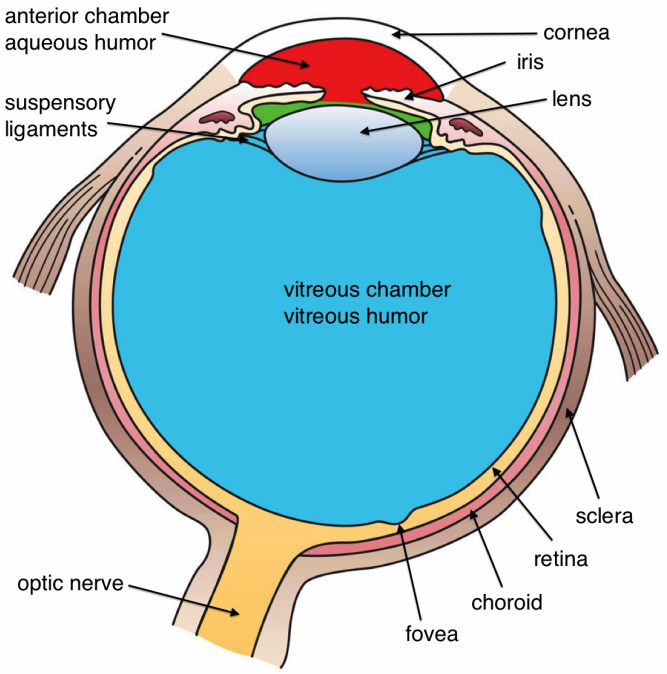


Figure 3.5: Cross section of a human eye (from Wikimedia Commons by Holly Fischer / CC BY).

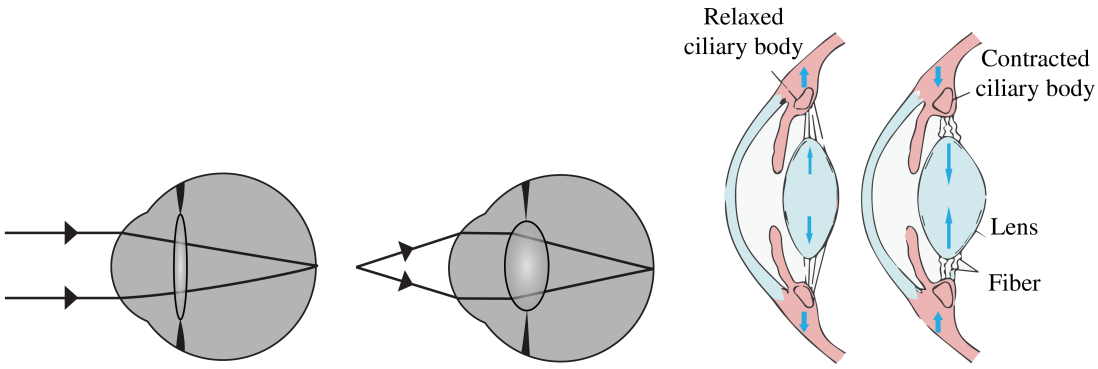


Figure 3.6: Left: Optical rays showing how an eye accommodates by changing its focal length. Right: Relaxed and contracted muscle at the crystalline lens needed for this accommodation.(Left: adapted from Wikimedia Commons Erin Silversmith / BY-NC-SA 2.5 Generic. Right: adapted from Sjaastad O.V., Sand O. and Hove K. (2010) Physiology of domestic animals, 2nd edn., Oslo: Scandinavian Veterinary Press).

the surrounding media (air and vitreous humour) differ. The power of the healthy relaxed eye is according to (2.48), (2.53):

$$\mathfrak{P} = \frac{n_{vh}}{f_i} = \frac{1.337}{0.024} = 55 \text{ Diopter}. \tag{3.1}$$

In relaxed condition the lens focuses light coming from infinity on the retina. When the object is closer, the eye muscles contract due to which the crystalline lens becomes more convex and the focal length of the system decreases, as seen on the right of Fig. 3.6. At a certain point, the object will be too close to be focused on the retina. This is called the **near point** of the eye. Due to the loss of elasticity of the muscle, the near point moves from 7 cm for teens to 100 cm for a 60-year-old. Fig. 3.6 shows the optical rays entering the eyes, for two configurations: an object at infinity and an object nearby. The **normal near point** is defined to be at the distance of 25 cm from the eye. The **far point** is the furthest object which is imaged on the retina by the relaxed eye. For a normal eye the far point is at infinity.

3.4.3 Retina

The retina is composed of approximately 125 million photoreceptor cells: the **rods** and the **cones**. The rods are highly sensitive black and white (intensity) sensors, while the cones are colour sensitive for the wavelengths 390 nm - 780 nm. UV light is absorbed by the lens (people whose lens is removed because of cataract can "see" UV light). The **fovea centralis** is the most sensitive centre of the retina with a high density of cones. The eyes move continuously to focus the image on this area. The information is transferred by the optical nerve, placed at the back of the eye, where it causes a blind spot.

3.4.4 Dioptric Power of thin lenses.

Recall that for a single thin lens the dioptric power $\mathfrak{P}$ is defined by

$$\mathfrak{P} = \frac{n_2}{f_i} = \frac{n_l - n_1}{R_1} + \frac{n_2 - n_l}{R_2}, \tag{3.2}$$

with R_1 and R_2 the radii of curvature of the first and second surface of the thin lens measured in meter, n_l the index of refraction of the lens and n_1 and n_2 the refractive indices in the media to the left and the right of the lens, respectively. For two thin lenses in contact, the total focal length is given by:

$$\frac{1}{f_i} = \frac{1}{f_{1i}} + \frac{1}{f_{2i}}, \tag{3.3}$$

hence the combined power of the two lenses in contact is the sum of the individual powers:

$$\mathfrak{P} = \mathfrak{P}_1 + \mathfrak{P}_2 \tag{3.4}$$

A positive lens of focal length f_1=10 cm in air has a dioptric power $\mathfrak{P}_1 = 10$ diopter. If it is in contact with a negative lens of dioptric power $\mathfrak{P}_2 = -10$ diopter, the resulting power is $\mathfrak{P} = 0$, equivalent to a parallel sheet of glass.

3.4.5 Eyeglasses

The eye can suffer from imperfections as seen in Fig. 3.7. We discuss the most common imperfections and their solutions, for the case that the eye is modelled by a single thin lens.

a. Myopia or nearsightedness. A myopic eye has too short focal distances (has too high power). Distant objects are focused in front of the retina by the relaxed eye. The far point is

thus not at infinity, but closer. This can be corrected by a negative lens. Suppose the far point is at 2 m. If the concave lens makes a virtual image of a distant object at distance 2 m in front of the cornea, the relaxed eye can see it clearly. The lens Law (2.58), with $s_o = -\infty$ implies then $f_i = s_i = -2$ m. Hence the required power of the lens is:

$$\mathfrak{P} = \frac{1}{f_i} = -0.5 \text{ diopter}. \tag{3.5}$$

The lens is best put in the front focal plane of the relaxed eye, i.e. at approximately 16 mm in front of the cornea. This follows from (2.58) and the fact that the distance of the retina to the eye lens is roughly 22 mm while the refractive index of the vitrous humor is 1.337. Hence, the focal distance in air of the relaxed eye is $22/1.337 \approx 16$ mm. The reason for putting the lens at the focal distance is that in this case the magnification of the eye and the negative lens together are the same as for the uncorrected eye. To see this, draw a ray from the top of the object through the centre of the negative lens. This will then be made parallel to the optical axis by the eye lens; the distance of this ray to the optical axis is the image size on the retina. This ray will end up at the same point of the retina as when the negative lens is taken out, because it is not refracted by this negative lens.

Contact lenses are very close to the eye lens and hence the total power of the eye with a contact lens is simply the sum of the power of the eye and the contact lens.

b. Hyperopia or farsightedness. In this case a distant object is imaged by the relaxed eye behind the retina, i.e. the back focal distance of the relaxed eye is larger than the depth of the eye. Close objects can not be imaged on the retina, hence the near point is relatively far from the cornea. In order to bend the rays more, a positive lens is placed in front of the eye. Suppose that a hyperopic eye has near point at distance 125 cm. For an object at the normal near point $s_o = -25$ cm to have virtual image at $s_i = -125$ cm so that it can be seen, the focal length of the positive lens must satisfy

$$\frac{1}{f_i} = -\frac{1}{s_o} + \frac{1}{s_i} = \frac{1}{0.25} - \frac{1}{1.25} = \frac{1}{0.31}, \tag{3.6}$$

hence the power must be $\mathfrak{P} = 1/f_i = +3.2$ diopter.

c. Presbyopia. This is the lack of accommodation of the eye as is common in people over 40. It results in an increase in the distance between the near point and the cornea. This defect affects all images. Presbyopia is usually corrected by glasses with progressive correction, the upper part of glass used for distance vision and the lower part for near vision.

d. Astigmatism. In this case the focal distances for two directions perpendicular to the optical axis are different. It is attributed to a lack of symmetry of revolution of the cornea. This is compensated by using glasses which themselves are astigmatic.

3.4.6 New Correction Technique

In recent years, to correct eye defects such as myopia and astigmatism, technology has been developed to change the local curvatures of the surface of the cornea using an excimer laser. The laser is computer-controlled and causes photo-ablation in parts of the cornea.

3.5 The Magnifying Glass

A magnifying glass causes an image on the retina which is larger than without the magnifier. In principle, the image on the retina can be increased by simply bringing the object closer to the

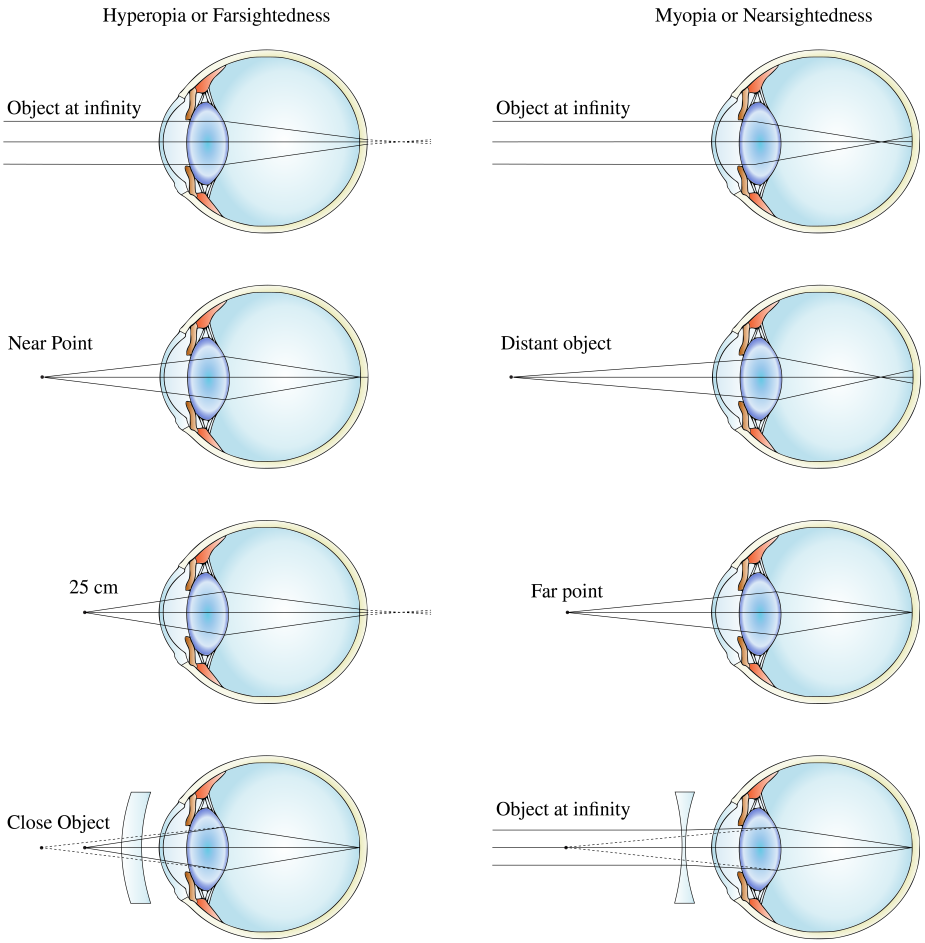


Figure 3.7: Correction of farsighted (left) and nearsighted (right) eye (adapted from Wikimedia Commons by Gumenyuk I.S. / CC BY-SA 4.0).

eye (reduce $|s_o|$ at fixed s_i). But $|s_o|$ can not be smaller than the near point d_o, which we take here to be 25 cm. It is desirable to use a lens that makes a magnified erect image at a distance to the eye greater than d_o. This can be achieved by a positive lens with the object closer to the lens than the first focal point, thereby producing a magnified virtual image. An example is given in Fig. 3.8.



Figure 3.8: Example of a positive lens used as a magnifying glass (picture taken by A.J.L. Adam / CC-BY-SA 4.0).

3.5.1 Magnifying Power

The **magnifying power** MP or **angular magnification** M_a is defined as the ratio of the size of the retinal image obtained with the instrument and the maximum possible size of the retinal image as seen by the unaided eye. The maximum retinal image for the unaided eye occurs for the closest possible viewing distance d_o which is the distance from the near point to the eye. To estimate the size of the retinal image, we compare in both cases where **the chief ray through the top of the object and the centre of the pupil of the eye hits the retina**. Since the distance between the eye lens and the retina is fixed, the ratio of the image size on the retina for the eye with and without magnifying glass is:

$$\text{MP} = \frac{\alpha_a}{\alpha_u}, \tag{3.7}$$

where α_a and α_u are the angles between the optical axis and the chief rays for the aided and the unaided eye, respectively, as shown in Fig. 3.9. Working with these angles instead of distances is in particular useful when the virtual image of the magnifying glass is at infinity. Using $\alpha_a \approx y_i/L$ and $\alpha_u \approx y_o/d_o$ with y_i and y_0 positive and L the positive distance from the image to the eye (with as requirement : $L \geq d_o$), we find

$$\text{MP} = \frac{y_i d_o}{y_o L}. \tag{3.8}$$

Since $s_i < 0$ and $f_o < 0$ we have,

$$\frac{y_i}{y_o} = \frac{s_i}{s_o} = 1 + \frac{s_i}{f_o},$$

where we used the lens equation for the magnifying glass. We have $s_i = -|s_i| = -(L - \ell)$, where ℓ is the distance between the magnifying glass and the eye. Hence, (3.8) becomes:

$$\begin{aligned} \text{MP} &= \frac{d_o}{L}\left[1 + \frac{L-\ell}{|f_o|}\right] \\ &= \frac{d_o}{L}\left[1 + \mathfrak{P}\,(L-\ell)\right], \end{aligned} \tag{3.9}$$

where $\mathfrak{P}$ is the power of the magnifying glass.

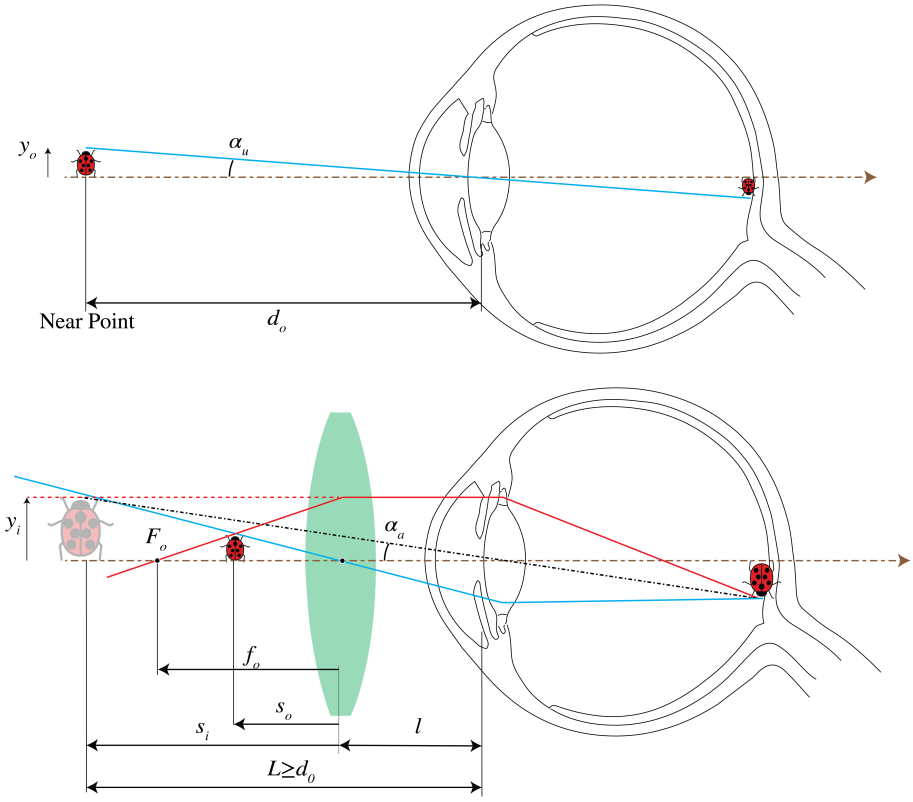


Figure 3.9: An unaided view (top) and an aided view using a magnifier.

We distinguish three situations:

1. $\ell = |f_o|$: the magnifying power is then MP $= d_o\mathfrak{P}$.
2. $\ell = 0$ and $L = d_o$. Then MP is maximum:

$$\text{MP}|_{\ell=0, L=d_o} = d_o\mathfrak{P} + 1. \tag{3.10}$$

3. The object is at the focal point of the magnifier ($s_0 = f_o$), so that the virtual image is at infinity ($L = \infty$) and hence

$$\text{MP}|_{L=\infty} = d_o\mathfrak{P}, \tag{3.11}$$

for every distance ℓ between the eye and the magnifying glass. The rays are parallel, so that the eye views the object in a relaxed way. This is the most common use of the magnifier.

In practice $d_o\mathfrak{P} = d_o/|f_o|$ is much larger than 1, so that MP has similar value for the three cases.

Normally magnifiers are expressed in terms of the magnifying power when $L = \infty$ (case 3 above). For example, a magnifier with a power of 10 Diopter has a MP equal to 2.5 or 2.5×. In other words, the image is 2.5 times larger than it would be if the object would be at the near point of the unaided eye.

3.6 Eyepieces

An **eyepiece** or **ocular** is a magnifier used before the eye at the end of an other optical instrument such as a microscope or a telescope. The eye looks into the ocular and the ocular "looks" into

the optical instrument. The ocular provides a magnified virtual image of the image produced by the optical instrument. Similar to the magnifying glass, the virtual image should preferably be at or near infinity to be viewed by a relaxed eye. Therefore, for the magnifying power (3.11) holds. Several types of eye pieces exist and most of them are made out of two lenses: 1. the field lens, which is the first lens in the ocular; 2. the eye-lens, which is closest to the eye at a fixed distance called the **eye relief**. The aperture of the eyepiece is controlled by a field stop. An example is given in Fig. 3.10.

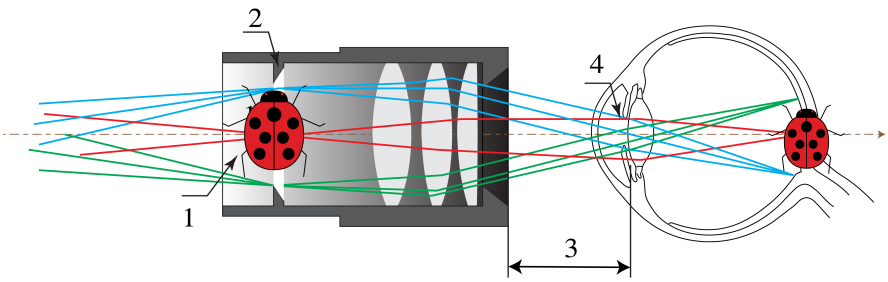


Figure 3.10: Example of an eyepiece consisting of three lenses. 1) Real image, 2) field diaphragm, 3) eye relief, 4) eye pupil (adapted from Wikimedia Commons by Tamas-flex / CC BY-SA 3.0).

3.7 The Compound Microscope

A magnifier alone can provide very high magnification only at the cost of intolerable aberrations. The **compound microscope** is a magnifier of close objects with a high angular magnification, generally more than 30×. It was invented by Zacharias Janssen in Middelburg in 1590 (but this claim is disputed). The first element of the compound microscope is an objective (in Fig. 3.11 a simple positive lens, but in practice consisting of several high quality lenses) which makes a real, inverted and magnified image of the object in the front focal plane of an eyepiece (where there is also the field stop). The eyepiece will make a virtual image at infinity, as explained above in situation 3 for the magnifying glass of Section 3.5.1. As explained there, the magnifying power of the eyepiece is the ratio of the size of the image on the retina when the object is in the front focal plane of the eyepiece and the size of the image without the eyepiece when the object would be at the near point. This angular magnification is given by (3.11). However, first the object lens makes a magnified image of the object in the focal plane of the eyepiece. Therefore, the magnifying power of the entire system is the product of the transverse linear magnification of the objective M_T and the angular magnification of the eyepiece M_{Ae}:

$$\text{MP} = M_T M_{Ae}. \tag{3.12}$$

According to (2.65): $M_T = \text{-}x_i/f_i^{obj}$, where x_i is the distance of the image made by the objective to its back focal plane with focal distance f_i^{obj}. We have $x_i = L$ which is the tube length, i.e. the distance between the second focal point of the objective and the first focal point of the eyepiece. The tube length is standardised at 16 cm. Furthermore, according to (3.11), the angular magnification for a virtual image at infinity is : $M_{Ae} = d_o/f_i^e$. Hence, we obtain:

$$\text{MP} = \frac{\text{-}x_i}{f_i^{obj}} \frac{d_o}{f_i^e} = \frac{\text{-}16}{f_o} . \frac{25}{f_e}, \tag{3.13}$$

with the standard near-point d_o =25 cm. As an example, an Amici objective gives 40× and combined with a 10× eye piece one gets $MP = 400$.

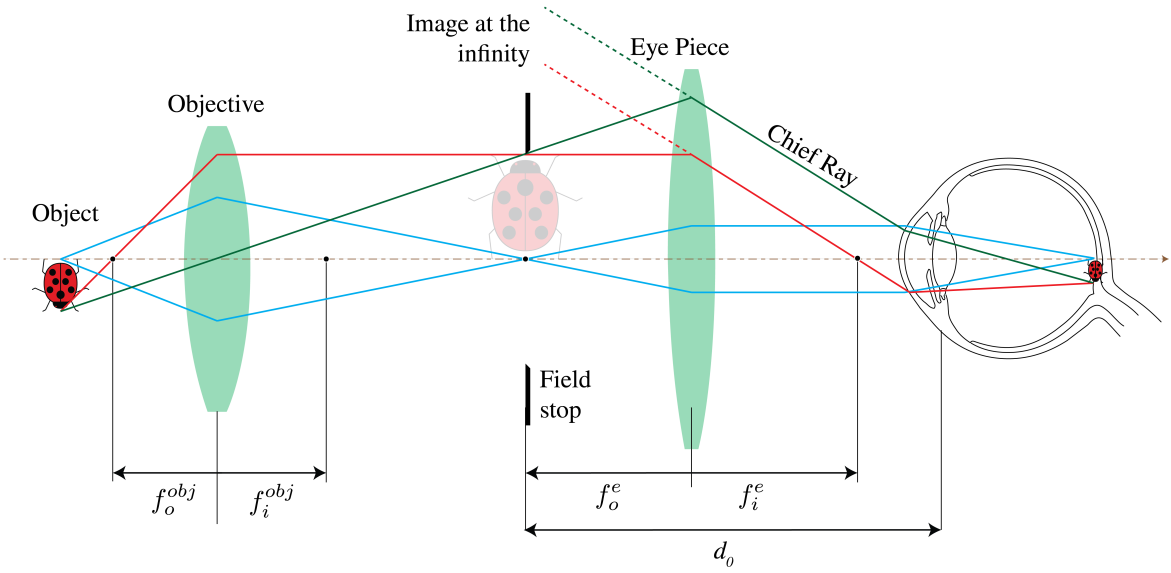


Figure 3.11: Simple compound microscope. The objective forms a real image of a nearby object. The eyepiece enlarges this intermediate image. The final image can be bigger than the barrel of the device, since it is virtual.

The **numerical aperture** of a microscope is a measure of the capability to gather light from the object. It is defined by:

$$\text{NA} = n_{im} \sin \theta_{max} \tag{3.14}$$

with n_{im} the refractive index of the immersing medium, often air but it could be water or oil, and θ_{max} the half-angle of the maximum cone of light accepted by the lens which, as has been explained in Subsection 2.5.9, is the cone with top the object point on the optical axis and base the entrance pupil of the microscope. The numerical aperture is the second number etched in the barrel of the objective. It ranges from 0.07 (low-power objectives) to 1.4 for high-power objectives. Note that it depends on the object distance. In Chapter 7 it will be explained that NA is, for a given object distance, proportional to the resolving power which is the minimum transverse distance between two object points that can be resolved in the image.

3.8 The Telescope

A telescope enlarges the retinal image of a distant object. Like a compound microscope, it is also composed of an objective and an eyepiece as seen in Fig. 3.12.

The object in this figure is at very large distance, therefore an image is formed by the objective approximately in the second focal plane of the objective. The eyepiece makes a virtual magnified image, to be viewed with a relaxed eye as the magnifying glass does. We choose the front focal point of the eyepiece with focal length f_o^e to coincide with the image focal point of the objective f_i^{obj}. So the distance between the two lenses is equal to the sum of their image focal lengths. Suppose that the edge of the object subtends angle α at the objective (see Fig. 3.12). Since the object distance is very large, this is in good approximation also the angle α_u that the object would subtend at the unaided eye. The angular magnification is: MP $= \alpha_a/\alpha_u$ where α_a is the half angle of the apparent cone of rays coming from the virtual image of the eye piece. Note that the ray trough the front focal point of the objective also passes through the second focal point of the eyepiece. Since, AB=CD, we find by considering the triangles $F_o^{obj}AB$ and F_i^eCD

in Fig. 3.12 that

$$\mathrm{MP} = -\frac{f_i^{obj}}{f_i^e}. \tag{3.15}$$

The minus sign is because the image is inverted. An erect system can be obtained by inserting an additional lens between the objective and the eyepiece.

The aperture stop is immediately in front of the objective. One can derive that the exit pupil coincides with the second focal plane of the eyepiece.

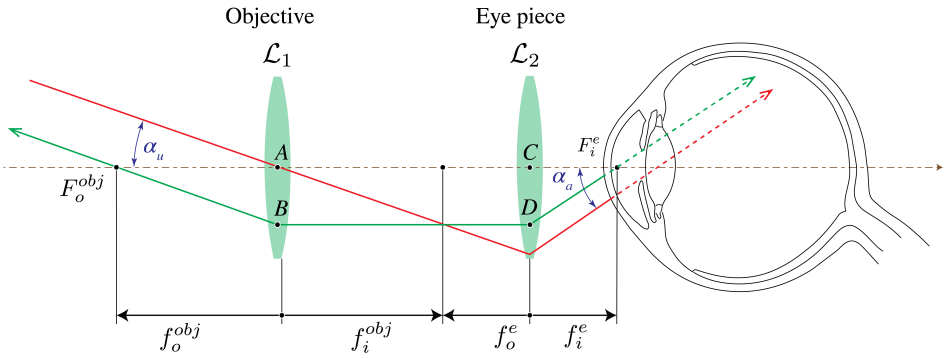


Figure 3.12: Ray angles for a telescope

Remark. The telescope is an optical system of which both the object and image focal points are at infinite distance. Systems with this property are called **telescopic**.

Problems

1. **Lenses in combination.** Consider a ray transfer matrix

$$\begin{pmatrix} A & B \\ C & D \end{pmatrix} \tag{3.16}$$

between two planes.

a) Suppose that any ray that is parallel to the optical axis in the first plane goes through a point on the optical axis in the second plane. This means that the second plane is the focal plane of the system. What does this imply for the elements of the transfer matrix?

b) Suppose that the first plane is a focal plane so that any ray emitted by the point on the optical axis in this plane becomes collimated in the second plane. What does this imply for the elements for the transfer matrix?

c) Consider two thin lenses with distance d and focal distances f_1 and f_2. Derive the transfer matrix linking the plane immediately before the first lens with the plane immediately behind the second lens. You may assume that the lenses are in air with refractive index $n = 1$.

d) Use the condition that you found in a) to derive the back focal distance of a system consisting of two thin lenses with refractive index f_1 and f_2 and distance d. Verify that the result agrees with the distance for the back focal plane in Section 3.5.4. Hint: let f_b be the distance of the back focal point of the two-lens system to the second lens. Write the transfer matrix between the lens immediately before the first lens and the plane through the back focal point.

e) Add a third thin lens with refractive index f_3 in contact to the second lens. Answer question c) for this system.

2. **The eye and the magnifying glass.**
In this problem the eye is modelled as a single thin lens that creates an image on the retina.
The distance between the retina and the lens is d_r. Let us call the focal length of the lens f_{eye}. The eye is capable of varying f_{eye}.

a) Suppose that the relaxed eye can see far-away objects sharply. How are f_{eye} and d_r related for a relaxed eye?

b) Suppose we want to see an object that is nearby, with coordinate s_o, say. What should f_{eye} be to obtain a sharp image on the retina?

c) We introduce a magnifying glass, i.e. we put a thin lens with focal length f in front of the eye. In front of the magnifying glass, there is a nearby object. We want to place the object such that a completely relaxed eye can see it sharply. Where should the object be? Verify your answer using the applet found here: http://www.geogebra.org/m/977919 .

d) Calculate the magnification of the system by using the transfer matrices. Assume for simplicity that throughout the entire system $n = 1$. How does the magnification of the object depend on f? Verify your answer with the applet.

3. **Increasing the angular field of view.**
Patients with tunnel vision have only a limited field of view because only the central region of their retina is light sensitive. Suppose that the sensitive region of the retina is circular and has radius $r = 2$cm. The length of the eye is 24 cm and the cornea and crystaline lens are together treated as a single thin lens.

a) Show that the angular field of view of distant objects is

$$\alpha_u = 6.4^o. \tag{3.17}$$

(take into account that the ray which enters the centre of the eye lens is refracted because the vitreous humor has refractive index $n = 1.337$).

b) Use a negative lens with focal distance $f < 0$ at a distance d in front of the eye. Show that when

$$d = 9|f|,$$

the angular field of view is increased by a factor 10.

c) We require that the virtual images of all distant objects are at distance of at least the distance of the normal near point. This implies that we require that $d + |f_2| > 25$cm. Derive d and the strength of the negative lens in diopter.

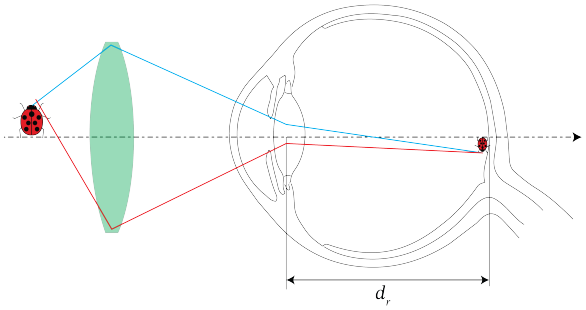


Figure 3.13: Angular view α_u without and with the use of a negative lens.

4. * **Imaging with a planar interface.**
In this problem we investigate whether it is possible to image an object with a single planar interface.

a) We have two media with refractive indices n_1 and n_2, separated by a planar interface. Give the transfer matrix $\mathcal{T}$ for refraction at a planar interface using the paraxial approximation.

b) Suppose we have an object that is a distance d from the interface. Give the system matrix that describes a ray propagating from the object to the plane that is a distance d behind the interface (see Fig. 3.14).

c) Assuming that $d > 0$, what condition has to be fulfilled in order to create an image in the plane behind the interface? Such an imaging system is called a **Veselago lens**.

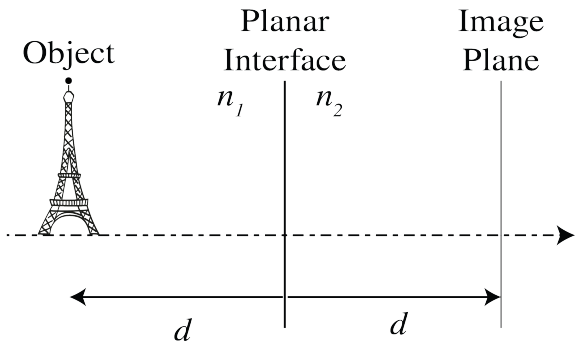


Figure 3.14

Chapter 4

Polarisation

What you should know and be able to do after studying this chapter

- Understand how different states of polarisation are related to the ratio of the amplitudes and the difference in phase between two orthogonal components of the electric field.
- Know that elliptical polarisation is the most general state of polarisation.
- Know that linear polarisation and circular polarisation are special cases.
- Know how to compute the degree of polarisation.
- Be able to work with Jones vectors and Jones matrices.
- Know how birefringence is exploited to create wave plates and know the types of wave plates.
- Know how to rotate a state of linear polarisation over a given angle.
- Know how to change linear polarisation into circular polarisation and conversely.
- Be able to show that elliptical polarisation can be written as the sum of two orthogonal linear polarisations and as the sum of two circular polarisations.

4.1 Polarisation States and Jones Vectors

We have seen in Chapter 1 that light is an electromagnetic wave which satisfies Maxwell's equations and the wave equation derived therefrom. Since the electric field is a vector which oscillates as function of time in a certain direction, we say that the wave has a certain polarisation. In this chapter we look at the different types of polarisation and how the polarisation of a light beam can be manipulated.

We start with Eqs. (1.61), (1.62) and (1.64) which show that the (real) electric field $\boldsymbol{\mathcal{E}}(\mathbf{r}, t)$ of a time-harmonic plane wave is always perpendicular to the direction of propagation, which is the direction of the wave vector $\mathbf{k}$ as well as the direction of the Poynting vector (the direction

of the power flow). Let the wave propagate in the z-direction:

$$\mathbf{k} = \begin{pmatrix} 0 \\ 0 \\ k \end{pmatrix}. \tag{4.1}$$

Then the electric field vector does not have a z-component and hence the real electric field at z and at time t can be written as

$$\boldsymbol{\mathcal{E}}(z,t) = \begin{pmatrix} \mathcal{A}_x \cos(kz - \omega t + \varphi_x) \\ \mathcal{A}_y \cos(kz - \omega t + \varphi_y) \\ 0 \end{pmatrix}. \tag{4.2}$$

where $\mathcal{A}_x$ and $\mathcal{A}_y$ are positive amplitudes and φ_x, φ_y are the phases of the electric field components. While k and ω are fixed, we can vary $\mathcal{A}_x$, $\mathcal{A}_y$, φ_x and φ_y. This degree of freedom is why different states of polarisation exist: **the state of polarisation is determined by the ratio of the amplitudes and by the phase difference $\varphi_y - \varphi_x$ between the two orthogonal components of the light wave**. Varying the quantity $\varphi_y - \varphi_x$ means that we are 'shifting' $\mathcal{E}_y(\mathbf{r},t)$ with respect to $\mathcal{E}_x(\mathbf{r},t)$ [1]. Consider the electric field in a fixed plane $z = 0$:

$$\begin{aligned} \begin{pmatrix} \mathcal{E}_x(0,t) \\ \mathcal{E}_y(0,t) \end{pmatrix} &= \begin{pmatrix} \mathcal{A}_x \cos(-\omega t + \varphi_x) \\ \mathcal{A}_y \cos(-\omega t + \varphi_y) \end{pmatrix} \\ &= \mathrm{Re}\left\{ \begin{pmatrix} \mathcal{A}_x e^{i\varphi_x} \\ \mathcal{A}_y e^{i\varphi_y} \end{pmatrix} e^{-i\omega t} \right\} \\ &= \mathrm{Re}\left\{ \begin{pmatrix} E_x(0) \\ E_y(0) \end{pmatrix} e^{-i\omega t} \right\}, \end{aligned} \tag{4.3}$$

The complex vector

$$\mathbf{J} = \begin{pmatrix} E_x(0) \\ E_y(0) \end{pmatrix} = \begin{pmatrix} \mathcal{A}_x e^{i\varphi_x} \\ \mathcal{A}_y e^{i\varphi_y} \end{pmatrix}, \tag{4.4}$$

is called the **Jones vector**. It is used to characterise the polarisation state. Let us see how, at a fixed position in space, the electric field vector behaves as a function of time for different choices of $\mathcal{A}_x$, $\mathcal{A}_y$ and $\varphi_y - \varphi_x$.

a) Linear polarisation: $\varphi_y - \varphi_x = 0$ or $\varphi_y - \varphi_x = \pi$. When $\varphi_y - \varphi_x = 0$ we have

$$\mathbf{J} = \begin{pmatrix} \mathcal{A}_x \\ \mathcal{A}_y \end{pmatrix} e^{i\varphi_x}. \tag{4.5}$$

Equality of the phases: $\varphi_y = \varphi_x$, means that the field components $\mathcal{E}_x(z,t)$ and $\mathcal{E}_y(z,t)$ are in phase: when $\mathcal{E}_x(z,t)$ is large, $\mathcal{E}_y(z,t)$ is large, and when $\mathcal{E}_x(z,t)$ is small, $\mathcal{E}_y(z,t)$ is small. We can write

$$\begin{pmatrix} \mathcal{E}_x(0,t) \\ \mathcal{E}_y(0,t) \end{pmatrix} = \begin{pmatrix} \mathcal{A}_x \\ \mathcal{A}_y \end{pmatrix} \cos(\omega t - \varphi_x), \tag{4.6}$$

[1] KhanAcademy - Polarisation of light, linear and circular: Explanation of different polarisation states and their applications.

which shows that for $\varphi_y - \varphi_x = 0$ the electric field simply oscillates in one direction given by the real vector $\mathcal{A}_x\hat{\mathbf{x}} + \mathcal{A}_y\hat{\mathbf{y}}$. See Fig. 4.1a.

If $\varphi_y - \varphi_x = \pi$ we have

$$\mathbf{J} = \begin{pmatrix} \mathcal{A}_x \\ -\mathcal{A}_y \end{pmatrix} e^{i\varphi_x}. \tag{4.7}$$

In this case $\mathcal{E}_x(z,t)$ and $\mathcal{E}_y(z,t)$ are out of phase and the electric field oscillates in the direction given by the real vector $\mathcal{A}_x\hat{\mathbf{x}} - \mathcal{A}_y\hat{\mathbf{y}}$.

b) Circular polarisation: $\varphi_y - \varphi_x = \pm\pi/2$, $\mathcal{A}_x = \mathcal{A}_y$. In this case the Jones vector is:

$$\mathbf{J} = \begin{pmatrix} 1 \\ \pm i \end{pmatrix} \mathcal{A}_x e^{i\varphi_x}. \tag{4.8}$$

The field components $\mathcal{E}_x(z,t)$ and $\mathcal{E}_y(z,t)$ are $\pi/2$ radian (90°) out of phase: when $\mathcal{E}_x(z,t)$ is large, $\mathcal{E}_y(z,t)$ is small, and when $\mathcal{E}_x(z,t)$ is small, $\mathcal{E}_y(z,t)$ is large. We can write for $z = 0$ and with $\varphi_x = 0$:

$$\begin{aligned} \begin{pmatrix} \mathcal{E}_x(0,t) \\ \mathcal{E}_y(0,t) \end{pmatrix} &= \begin{pmatrix} \mathcal{A}_x \cos(-\omega t) \\ \mathcal{A}_x \cos(-\omega t \pm \pi/2) \end{pmatrix} \\ &= \mathcal{A}_x \begin{pmatrix} \cos(\omega t) \\ \mp \sin(\omega t) \end{pmatrix}. \end{aligned} \tag{4.9}$$

At a given position, the electric field vector moves along a circle as time proceeds. When for an observer looking towards the source, the electric field is rotating anti-clockwise, the polarisation is called **left-circularly polarised** (+ sign in (4.9)), while if the electric vector moves clockwise, the polarisation is called **right-circularly polarised** (- sign in (4.9)).

c) Elliptical polarisation: $\varphi_y - \varphi_x = \pm\pi/2$, $\mathcal{A}_x$ **and** $\mathcal{A}_y$ **arbitrary.** The Jones vector is:

$$\mathbf{J} = \begin{pmatrix} \mathcal{A}_x \\ \pm i\mathcal{A}_y \end{pmatrix} e^{i\varphi_x}. \tag{4.10}$$

In this case we get instead of (4.9) (again taking $\varphi_x = 0$):

$$\begin{pmatrix} \mathcal{E}_x(0,t) \\ \mathcal{E}_y(0,t) \end{pmatrix} = \begin{pmatrix} \mathcal{A}_x \cos(\omega t) \\ \pm\mathcal{A}_y \sin(\omega t) \end{pmatrix}. \tag{4.11}$$

which shows that the electric vector moves along an ellipse with major and minor axes parallel to the x- and y-axis. When the + sign applies, the field is called left-elliptically polarised, otherwise it is called right-elliptically polarised.

d) Elliptical polarisation: $\varphi_y - \varphi_x =$ **anything else,** $\mathcal{A}_x$ **and** $\mathcal{A}_y$ **arbitrary.** The Jones vector is now the most general one:

$$\mathbf{J} = \begin{pmatrix} \mathcal{A}_x e^{i\varphi_x} \\ \mathcal{A}_y e^{i\varphi_y} \end{pmatrix}. \tag{4.12}$$

It can be shown that the electric field vector moves always along an ellipse. The exact shape and orientation of this ellipse varies with the difference in phase $\varphi_y - \varphi_x$ and the ratio of the amplitude $\mathcal{A}_x, \mathcal{A}_y$ and, except when $\varphi_y - \varphi_x = \pm\pi/2$, the major and minor axis of the ellipse are not parallel to the x- and y-axis. See Fig. 4.1c.

Remarks.

1. Frequently the Jones vector is normalised such that

$$|J_x|^2 + |J_y|^2 = 1. \tag{4.13}$$

The normalized vector represents of course the same polarisation state as the non-normalised one. In general, multiplying the Jones vector by a complex number does not change the polarisation state. If we multiply for example by $e^{i\theta}$, this has the same result as changing the instant that $t = 0$, hence it does not change the polarisation state. In fact:

$$\boldsymbol{\mathcal{E}}(0,t) = \mathrm{Re}\left[e^{i\theta}\mathbf{J}e^{-i\omega t}\right] = \mathrm{Re}\left[\mathbf{J}e^{-i\omega(t-\theta/\omega)}\right] \tag{4.14}$$

2. We will show in Section 6.2.1 that a general time-harmonic electromagnetic field, is a superposition of plane waves with wave vectors of the same length determined by the frequency of the wave but with different directions. An example is the electromagnetic field near the focal plane of a strongly converging lens. There is then no particular direction of propagation to which the electric field should be perpendicular. In other words, there is no obvious choice for a plane in which the electric field oscillates as function of time. It can nevertheless be shown that for every point in space such a plane exists, but the orientation of the plane varies in general with position. Furthermore, the electric field in a certain point moves along an ellipse in the corresponding plane, but the shape of the ellipse and the orientation of its major axis can be arbitrary. We can conclude that in any point of an arbitrary time-harmonic electromagnetic field, the electric (and in fact also the magnetic) field vector prescribes as function of time an ellipse in some plane which depends on position[2]. In this chapter we only consider the field and polarisation state of a single plane wave.

External source

- KhanAcademy - Polarization of light, linear and circular: Explanation of different polarisation states and their applications.

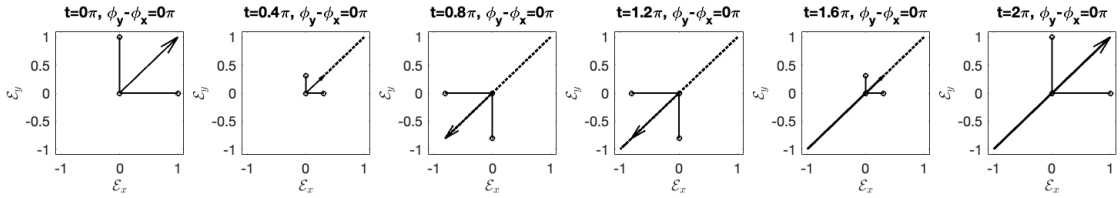
4.2 Creating and Manipulating Polarisation States

We have seen how Maxwell's equations allow the existence of plane waves with many different states of polarisation. But how can we create these states, and how do these states manifest themselves?

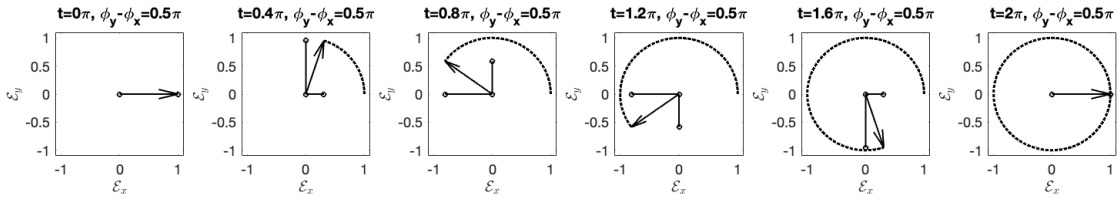
Natural light often does not have a definite polarisation. Instead, the polarisation fluctuates rapidly with time. To turn such randomly polarised light into linearly polarised light in a certain direction, we must extinguish the light polarised in the perpendicular direction. The remaining light is then linearly polarised along the desired direction. One could do this by using light reflected under the Brewster angle (which extinguishes p-polarised light), or one could let light pass through a dichroic crystal, which is a material which absorbs light polarised perpendicular to its so-called optic axis. A third method is sending the light through a wire grid polariser, which consists of a metallic grating with sub-wavelength slits. Such a grating only transmits the electric field component that is perpendicular to the slits.

So suppose that with one of these methods we have obtained linearly polarised light. Then the question rises how the state of linear polarisation can be changed into circularly or elliptically polarised light? Or how the state of linear polarisation can be rotated over a certain angle?

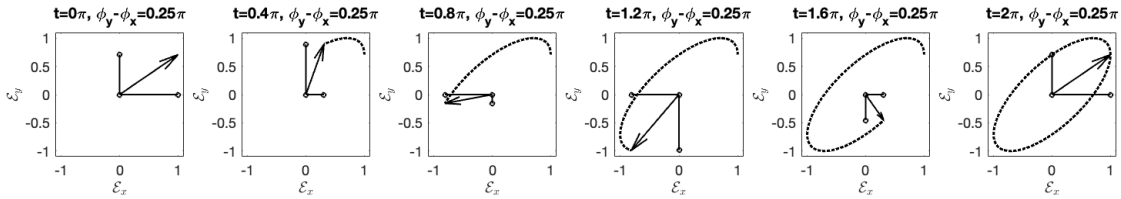
[2] Born and Wolf, *Principles of Optics*, Section 1.4.3.



(a) Linear polarisation, $\varphi_y - \varphi_x = 0$



(b) Circular polarisation, $\varphi_y - \varphi_x = \pi/2$



(c) Elliptical polarisation, $\varphi_y - \varphi_x = \pi/4$

Figure 4.1: Illustration of different types of polarisation. Top: linear polarisation; middle: circular polarisation; bottom: elliptical polarisation. The horizontal and vertical arrows indicate the momentary field components $\mathcal{E}_x, \mathcal{E}_y$. The thick arrow indicates the vector $\boldsymbol{\mathcal{E}}$. The black curve indicates the trajectory of $\boldsymbol{\mathcal{E}}(t)$.

We have seen that the polarisation state depends on the ratio of the amplitudes and on the phase difference $\varphi_y - \varphi_x$ of the orthogonal components $\mathcal{E}_y$ and $\mathcal{E}_x$ of the electric field. Thus, to change linearly polarised light to some other state of polarisation, a certain phase shift (say $\Delta\varphi_x$) must be introduced to one component (say $\mathcal{E}_x$), and another phase shift $\Delta\varphi_y$ to the orthogonal component $\mathcal{E}_y$. We can achieve this with a **birefringent crystal**, such as calcite. What is special about such a crystal is that it has two refractive indices: light polarised in a certain direction experiences a refractive index n_o, while light polarised perpendicular to it feels another refractive index n_e (the subscripts o and e stand for "ordinary" and "extraordinary", but for our purpose we do not need to understand this terminology). The direction for which the refractive index is smallest (which can be either n_o or n_e) is called the **fast axis** because its phase velocity is largest, and the other direction is the **slow axis**. Because there are two different refractive indices, one can see double images through a birefringent crystal[3]. The difference between the two refractive indices $\Delta n = n_e - n_o$ is called the **birefringence**.

Suppose $n_e > n_o$ and that the fast axis, which corresponds to n_o is aligned with $\mathcal{E}_x$, while the slow axis (which then has refractive index n_e) is aligned with $\mathcal{E}_y$. If the wave travels a distance d through the crystal, $\mathcal{E}_y$ will accumulate a phase $\Delta\varphi_y = \frac{2\pi n_e}{\lambda} d$, and $\mathcal{E}_x$ will accumulate a phase $\Delta\varphi_x = \frac{2\pi n_o}{\lambda} d$. Thus, after propagation through the crystal the phase difference $\varphi_y - \varphi_x$ has increased by

$$\Delta\varphi_y - \Delta\varphi_x = \frac{2\pi}{\lambda} d(n_e - n_o). \tag{4.15}$$

[3]Double Vision - Sixty Symbols: Demonstration of double refraction by a calcite crystal due to birefringence.

4.2.1 Jones Matrices

By letting light pass through crystals of different thicknesses d we can create different phase differences between the orthogonal field components and in this way we can create different states of polarisation. To be specific, let $\mathbf{J}$, as given by (4.4), be the Jones vector of the plane wave before the crystal. Then we have, for the Jones vector after the passage through the crystal:

$$\tilde{\mathbf{J}} = \mathcal{M}\mathbf{J}, \tag{4.16}$$

where

$$\mathcal{M} = \begin{pmatrix} e^{\frac{2\pi i}{\lambda}dn_o} & 0 \\ 0 & e^{\frac{2\pi i}{\lambda}dn_e} \end{pmatrix} = e^{\frac{2\pi i}{\lambda}dn_o} \begin{pmatrix} 1 & 0 \\ 0 & e^{\frac{2\pi i}{\lambda}d(n_e-n_o)} \end{pmatrix}. \tag{4.17}$$

A matrix such as $\mathcal{M}$, which transfers one state of polarisation of a plane wave in another, is called a **Jones matrix**. Depending on the phase difference which a wave accumulates by traveling through the crystal, these devices are called **quarter-wave plates** (phase difference $\pi/2$), **half-wave plates** (phase difference π), or **full-wave plates** (phase difference 2π). The applications of these wave plates will be discussed in later sections.

Consider as example the Jones matrix which describes the change of linear polarised light into circular polarisation. Assume that we have diagonally (linearly) polarised light, so that

$$J = \frac{1}{\sqrt{2}} \begin{pmatrix} 1 \\ 1 \end{pmatrix}. \tag{4.18}$$

We want to change it to circularly polarised light, for which

$$J = \frac{1}{\sqrt{2}} \begin{pmatrix} 1 \\ i \end{pmatrix}, \tag{4.19}$$

where one can check that indeed $\varphi_y - \varphi_x = \pi/2$. This can be done by passing the light through a crystal such that $\mathcal{E}_y$ accumulates a phase difference of $\pi/2$ with respect to $\mathcal{E}_x$. The transformation by which this is accomplished can be written as

$$\begin{pmatrix} 1 & 0 \\ 0 & i \end{pmatrix} \frac{1}{\sqrt{2}} \begin{pmatrix} 1 \\ 1 \end{pmatrix} = \frac{1}{\sqrt{2}} \begin{pmatrix} 1 \\ i \end{pmatrix}. \tag{4.20}$$

The matrix on the left is the Jones matrix describing the operation of a quarter-wave plate.

Another important Jones matrix is the **rotation matrix**. In the preceding discussion it was assumed that the fast and slow axes were aligned with the x- and y-direction (i.e. they were parallel to $\mathcal{E}_x$ and $\mathcal{E}_y$). Suppose now that the slow and fast axes of the wave plate no longer coincide with $\widehat{\mathbf{x}}$ and $\widehat{\mathbf{y}}$, but rather with some other $\widehat{\mathbf{x}}'$ and $\widehat{\mathbf{y}}'$ as in Fig. 4.2. In that case we apply a basis transformation: the electric field vector which is expressed in the $\widehat{\mathbf{x}}$, $\widehat{\mathbf{y}}$ basis should first be expressed in the $\widehat{\mathbf{x}}'$, $\widehat{\mathbf{y}}'$ basis before applying the Jones matrix of the wave plate to it. After applying the Jones matrix, the electric field has to be transformed back from the $\widehat{\mathbf{x}}'$, $\widehat{\mathbf{y}}'$ basis to the $\widehat{\mathbf{x}}$, $\widehat{\mathbf{y}}$ basis.

Let $\mathbf{E}$ be given in terms of its components on the $\hat{\mathbf{x}}$, $\hat{\mathbf{y}}$ basis:

$$\mathbf{E} = E_x\widehat{\mathbf{x}} + E_y\widehat{\mathbf{y}} \tag{4.21}$$

To find the components $E_{x'}$, $E_{y'}$ on the $\widehat{\mathbf{x}}'$, $\widehat{\mathbf{y}}'$ basis:

$$\mathbf{E} = E_{x'}\widehat{\mathbf{x}}' + E_{y'}\widehat{\mathbf{y}}' \tag{4.22}$$

we first write the unit vectors $\widehat{\mathbf{x}}'$ and $\widehat{\mathbf{y}}'$ in terms of the basis $\hat{\mathbf{x}}$, $\hat{\mathbf{y}}$ (see Fig. 4.2)

$$\widehat{\mathbf{x}}' = \cos\theta\,\widehat{\mathbf{x}} + \sin\theta\,\widehat{\mathbf{y}}, \tag{4.23}$$
$$\widehat{\mathbf{y}}' = -\sin\theta\,\widehat{\mathbf{x}} + \cos\theta\,\widehat{\mathbf{y}}, \tag{4.24}$$

By substituting (4.23) and (4.24) into (4.22) we find

$$\begin{aligned}\mathbf{E} &= E_{x'}\widehat{\mathbf{x}}' + E_{y'}\widehat{\mathbf{y}}' \\ &= E_{x'}(\cos\theta\,\widehat{\mathbf{x}} + \sin\theta\,\widehat{\mathbf{y}}) + E_{y'}(-\sin\theta\,\widehat{\mathbf{x}} + \cos\theta\,\widehat{\mathbf{y}}), \\ &= (\cos\theta E_{x'} - \sin\theta E_{y'})\widehat{\mathbf{x}} + (\sin\theta E_x + \cos\theta E_y)\widehat{\mathbf{y}}. \end{aligned} \tag{4.25}$$

Comparing with (4.21) implies

$$\begin{pmatrix} E_x \\ E_y \end{pmatrix} = \begin{pmatrix} E_{x'}\cos\theta - E_{y'}\sin\theta \\ E_{x'}\sin\theta + E_{y'}\cos\theta \end{pmatrix} = \mathcal{R}_\theta \begin{pmatrix} E_{x'} \\ E_{y'} \end{pmatrix}, \tag{4.26}$$

where $\mathcal{R}_\theta$ is the rotation matrix over an angle θ in the anti-clockwise direction: [4]

$$\mathcal{R}_\theta \equiv \begin{pmatrix} \cos\theta & -\sin\theta \\ \sin\theta & \cos\theta \end{pmatrix}. \tag{4.27}$$

That $\mathcal{R}(\theta)$ indeed is a rotation over angle θ in the anti-clockwise direction is easy to see by considering what happens when $\mathcal{R}_\theta$ is applied to the vector $(1,0)^T$. Since $\mathcal{R}_\theta^{-1} = \mathcal{R}_{-\theta}$ we get:

$$\begin{pmatrix} E_{x'} \\ E_{y'} \end{pmatrix} = \mathcal{R}_{-\theta} \begin{pmatrix} E_x \\ E_y \end{pmatrix}. \tag{4.28}$$

This relationship expresses the components $E_{x'}$, $E_{y'}$ of the Jones vector on the $\widehat{\mathbf{x}}'$, $\widehat{\mathbf{y}}'$ basis, which is aligned with the fast and slow axes of the crystal, in terms of the components E_x and E_y on the original basis $\widehat{\mathbf{x}}$, $\widehat{\mathbf{y}}$. If the matrix $\mathcal{M}$ describes the Jones matrix as defined in (4.17), then the matrix M_θ for the same wave plate but with x' as slow and y' as fast axis, is, with respect to the $\widehat{\mathbf{x}}$, $\widehat{\mathbf{y}}$ basis, given by:

$$\mathcal{M}_\theta = \mathcal{R}_\theta \mathcal{M} \mathcal{R}_{-\theta}. \tag{4.29}$$

For more information on basis transformations, see Appendix F.

4.2.2 Linear Polarisers

A polariser that only transmits horizontally polarised light is described by the Jones matrix:

$$\mathcal{M}_{LP} = \begin{pmatrix} 1 & 0 \\ 0 & 0 \end{pmatrix}. \tag{4.30}$$

[4] KhanAcademy - Linear transformation examples: Rotations

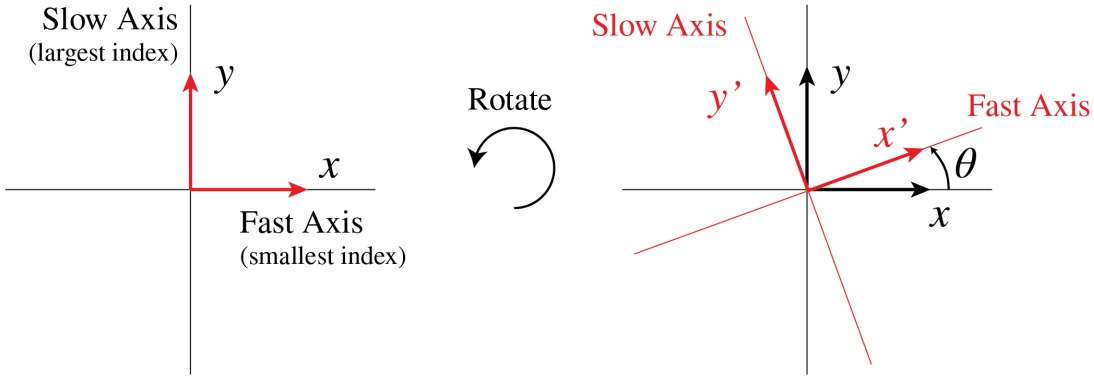


Figure 4.2: If the wave plate is rotated, the fast and slow axis no longer correspond to x and y. Instead, we have to introduce a new coordinate system (x', y').

Clearly, horizontally polarised light is completely transmitted, while vertically polarised light is not transmitted at all. More generally, for light that is polarised at an angle α, we get

$$\mathcal{M}_\alpha = \mathcal{M}_{LP} \begin{pmatrix} \cos\alpha \\ \sin\alpha \end{pmatrix} = \begin{pmatrix} 1 & 0 \\ 0 & 0 \end{pmatrix} \begin{pmatrix} \cos\alpha \\ \sin\alpha \end{pmatrix} = \begin{pmatrix} \cos\alpha \\ 0 \end{pmatrix}. \tag{4.31}$$

The amplitude of the transmitted field is reduced by the factor $\cos\alpha$, which implies that the intensity of the transmitted light is reduced by the factor $\cos^2\alpha$. This relation is known as **Malus' law**.

4.2.3 Degree of Polarisation

Natural light such as sun light is unpolarised. The instantaneous polarisation of unpolarised light fluctuates rapidly in a random manner. A linear polariser produces linear polarised light from unpolarised light. It follows from (4.31) that the intensity transmitted by a linear polariser when unpolarised light is incident, is the average value of $\cos^2\alpha$ namely $\frac{1}{2}$, times the incident intensity.

Light that is a mixture of polarised and unpolarised light is called partially polarised. The **degree of polarisation** is defined as the fraction of the total intensity that is polarised:

$$\text{degree of polarisation} = \frac{I_{pol}}{I_{pol} + I_{unpol}}. \tag{4.32}$$

4.2.4 Quarter-Wave Plates

A quarter-wave plate has already been introduced above. It introduces a phase shift of $\pi/2$, so its Jones matrix is

$$\mathcal{M}_{QWP} = \begin{pmatrix} 1 & 0 \\ 0 & i \end{pmatrix}, \tag{4.33}$$

because $\exp(i\pi/2) = i$. To describe the actual transmission through the quarter-wave plate, the matrix should be multiplied by some global phase factor, but because we only care about the **phase difference** between the field components, this global phase factor can be omitted without problem. The quarter-wave plate is typically used to **convert linearly polarised light to elliptically polarised light and vice-versa**[5]. If the incident light is linearly polarised at

[5] Demonstration of a Quarter-Wave Plate by Andrew Berger

angle α, the state of polarisation after the quarter-wave plate is

$$\begin{pmatrix} \cos\alpha \\ i\sin\alpha \end{pmatrix} = \begin{pmatrix} 1 & 0 \\ 0 & i \end{pmatrix} \begin{pmatrix} \cos\alpha \\ \sin\alpha \end{pmatrix}. \tag{4.34}$$

In particular, if incident light is linear polarised under 45°, or equivalently, if the quarter wave plate is rotated over this angle, it will transform linearly polarised light into circularly polarised light (and vice versa).

$$\frac{1}{\sqrt{2}} \begin{pmatrix} 1 \\ i \end{pmatrix} = \begin{pmatrix} 1 & 0 \\ 0 & i \end{pmatrix} \frac{1}{\sqrt{2}} \begin{pmatrix} 1 \\ 1 \end{pmatrix}. \tag{4.35}$$

A demonstration is shown in[6].

4.2.5 Half-Wave Plates

A half-wave plate introduces a phase shift of π, so its Jones matrix is

$$\mathcal{M}_{HWP} = \begin{pmatrix} 1 & 0 \\ 0 & -1 \end{pmatrix}, \tag{4.36}$$

because $\exp(i\pi) = -1$. An important application of the half-wave plate is to **change the orientation of linearly polarised light**. After all, what this matrix does is mirroring the polarisation state in the x-axis. Thus, if we choose our mirroring axis correctly (i.e. if we choose the orientation of the wave plate correctly), we can change the direction in which the light is linearly polarised arbitrarily[7][8]. To give an example: a wave with linear polarisation parallel to the x-direction, can be rotated over angle α by rotating the crystal such that the fast axis makes angle $\alpha/2$ with the x-axis. Upon propagation through the crystal, the slow axis gets an additional phase of π, due to which the electric vector makes angle α with the x-axis (see Fig. 4.3). It is not difficult to verify that when the fast and slow axis are interchanged, the same linear state of polarisation results.

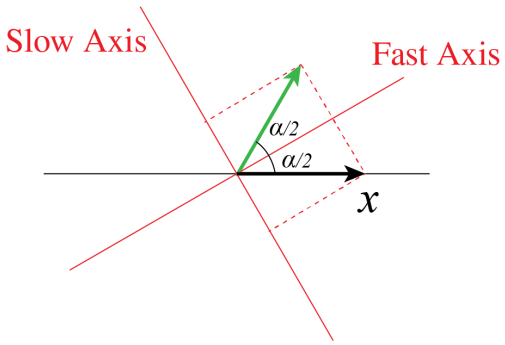


Figure 4.3: Rotation of horizontally polarised light over an angle α using a half-wave plate.

[6] MIT OCW - Quarter-wave Plate: Demonstration of the quarter-wave plate to create elliptical (in particular circular) polarisation.
[7] Demonstration of a Half-Wave Plate by Andrew Berger
[8] MIT OCW - Half-wave Plate: Demonstration of the half-wave plate.

4.2.6 Full-Wave Plates

A full-wave plate introduces a phase difference of 2π, which is the same as introducing no phase difference between the two field components. So what can possibly be an application for a full-wave plate? We recall from Eq. (4.15) that the phase difference is 2π only for a particular wavelength. If we send through linearly (say vertically) polarised light of other wavelengths, these will become elliptically polarised, while the light with the correct wavelength λ_0 will stay vertically polarised. If we then let all the light pass through a horizontal polariser, the light with wavelength λ_0 will be completely extinguished, while the light of other wavelengths will be able to pass through at least partially. Therefore, **full-wave plates can be used to filter out specific wavelengths of light**.

4.3 More on Jones matrices

If the direction of either the slow or fast axis is given and the ordinary and extra-ordinary refractive indices n_o and n_e, it is easy to write down the Jones matrix of a birefringent plate of given thickness d using the rotation matrices, see (4.29). Instead of using the rotation matrices, one can also write down a system of equations for the elements of the Jones matrix. Suppose that $\hat{\mathbf{v}}_\mathbf{o} = v_{o,x}\hat{\mathbf{x}} + v_{o,y}\hat{\mathbf{y}}$ and $\hat{\mathbf{v}}_\mathbf{e} = v_{e,x}\hat{\mathbf{x}} + v_{e,y}\hat{\mathbf{y}}$, are in the direction of the ordinary and the extra-ordinary axes, respectively. Then if the Jones matrix is

$$\mathcal{M} = \begin{pmatrix} a & b \\ c & d \end{pmatrix}, \tag{4.37}$$

then

$$\begin{aligned} \mathcal{M}\hat{\mathbf{v}}_o &= e^{ikn_o d}\,\hat{\mathbf{v}}_o, \\ \mathcal{M}\hat{\mathbf{v}}_e &= e^{ikn_e d}\,\hat{\mathbf{v}}_e \end{aligned}$$

which implies

$$\begin{aligned} av_{o,x} + bv_{o,y} &= e^{ikn_o d}v_{o,x}, \\ cv_{o,x} + dv_{o,y} &= e^{ikn_o d}v_{o,y}, \\ av_{e,x} + bv_{e,y} &= e^{ikn_e d}v_{e,x}, \\ cv_{e,x} + dv_{e,y} &= e^{ikn_e d}v_{e,x}. \end{aligned} \tag{4.38}$$

Similarly, for a linear polariser it is simple to write down the Jones matrix if one knows the direction in which the polariser absorbs or transmits all the light: use (4.30) in combination with the rotation matrices. Alternatively, if $\hat{\mathbf{v}}$ is in the direction of the linear polariser and $\hat{\mathbf{w}}$ is perpendicular to it, we have

$$\begin{aligned} \mathcal{M}\hat{\mathbf{v}} &= \hat{\mathbf{v}} \\ \mathcal{M}\hat{\mathbf{w}} &= \mathbf{0}, \end{aligned}$$

which is a system of equation of type (4.38) for the elements of the Jones matrix.

Suppose now that the complex (2,2)-matrix (4.37) is given. How can one verify whether this matrix corresponds to a linear polariser or to a wave plate? Note that the elements of a Jones matrix are in general complex.

1. **Linear Polariser**. The matrix corresponds to a linear polariser if there is a real vector which remains invariant under $\mathcal{M}$ and all vectors orthogonal to this vector are mapped to zero. In other words, there must be an orthogonal basis of **real** eigenvectors and one of the eigenvalues

must be 1 and the other 0. Hence, to check that a given matrix corresponds to a linear polariser, one should verify that one eigenvalue is 1 and the other is 0 and furthermore that the eigenvectors are **real** orthogonal vectors. It is important to check that the eigenvectors are real because if they are not, they do not correspond to particular linear polarisation directions and then the matrix does not correspond to a linear polariser.

2. **Wave plate**. To show that the matrix corresponds to a wave plate, there should exist two **real** orthogonal eigenvectors with, in general, complex eigenvalues of modulus 1. In fact, one of the eigenvectors corresponds to the ordinary axis with refractive index n_o, and the other to the extra-ordinary axis with refractive index n_e. The eigenvalues are then

$$e^{ikn_1d} \quad \text{and} \quad e^{ikn_2d},$$

where d is the thickness of the plate and k is the wave number. Hence to verify that a $(2,2)$-matrix corresponds to a wave plate, one has to compute the eigenvalues and check that these have modulus 1 and that the corresponding eigenvectors are real vectors and orthogonal.

3. **Jones matrix for propagation through sugars.** In sugars, left and right circular-polarised light propagate with their own refractive index. Therefore sugars are called **circular birefringent**. The matrix (4.37) corresponds to propagation through sugar when there are two real orthogonal unit vectors $\hat{\mathbf{v}}$ and $\hat{\mathbf{w}}$ such that the circular polarisation states

$$\hat{\mathbf{v}} + i\hat{\mathbf{w}}, \quad \hat{\mathbf{v}} - i\hat{\mathbf{w}} \tag{4.39}$$

are eigenstates of $\mathcal{M}$ with complex eigenvalues with modulus 1.

4.4 Decomposition of an Elliptical Polarisation state into sums of Linear & of Circular States

Any elliptical polarisation state can be written as the sum of two perpendicular linear polarised states:

$$J = \begin{pmatrix} \mathcal{A}_x e^{i\varphi_x} \\ \mathcal{A}_y e^{i\varphi_y} \end{pmatrix} = \mathcal{A}_x e^{i\varphi_x} \begin{pmatrix} 1 \\ 0 \end{pmatrix} + \mathcal{A}_y e^{i\varphi_y} \begin{pmatrix} 0 \\ 1 \end{pmatrix}. \tag{4.40}$$

Furthermore, any elliptical polarisation state can be written as the sum of two circular polarisation states, one right- and the other left-circular polarised:

$$J = \begin{pmatrix} \mathcal{A}_x e^{i\varphi_x} \\ \mathcal{A}_y e^{i\varphi_y} \end{pmatrix} = \frac{1}{2}(\mathcal{A}_x e^{i\varphi_x} - i\mathcal{A}_y e^{i\varphi_y}) \begin{pmatrix} 1 \\ i \end{pmatrix} + \frac{1}{2}(\mathcal{A}_x e^{i\varphi_x} + i\mathcal{A}_y e^{i\varphi}) \begin{pmatrix} 1 \\ -i \end{pmatrix}. \tag{4.41}$$

We conclude that to study what happens to elliptic polarisation, it suffices to consider two orthogonal linear polarisations, or, if that is more convenient, left- and right-circular polarised light. In a birefringent material each of two linear polarisations, namely parallel to the o-axis and parallel to the e-axis, propagate with their own refractive index. To predict what happens to an arbitrary linear polarisation state which is not aligned to either of these axes, or more generally what happens to an elliptical polarisation state, we write this polarisation state as a linear combination of o- and e-states, i.e. we expand the field on the o- and e-basis.

To see what happens to an arbitrary elliptical polarisation state in a circular birefringent material, the incident light is best written as linear combination of left-and right-circular polarisations.

External sources in recommended order

1. Double Vision - Sixty Symbols: Demonstration of double refraction by a calcite crystal due to birefringence.
2. MIT OCW - Linear polariser: Demonstration of linear polarisers and linear polarisation.
3. MIT OCW - Polarization Rotation Using polarisers: Demonstration of polarisation rotation using linear polarisers.
4. Demonstration of a QuarterWavePlate by Andrew Berger.
5. MIT OCW - Quarter-wave Plate: Demonstration of the quarter-wave plate to create elliptical (in particular circular) polarisation.
6. Demonstration of a HalfWavePlate by Andrew Berger.
7. MIT OCW - Half-wave Plate: Demonstration of the half-wave plate.

Problems

1. Consider a time-harmonic plane wave with real electric field which with respect to a Cartesian coordinate system (x, y, z) is given by:

$$\mathbf{E}(z,t) = A\sin(kz - \omega t + \pi/2)\,\hat{\mathbf{x}} + A\sin(kz - \omega t)\,\hat{\mathbf{y}} \tag{4.42}$$

where A is a positive real number.

a) Write this electric field as the real part of a complex field.

b) What is its corresponding Jones vector?

c) What is the polarisation of this electric field? Make a drawing of the electric field vector in the (x, y)-plane at $z = 0$ as function of time for an observer that is looking towards the source of the field.

d) The beam passes normally through a linear polariser whose transmission axis makes an angle of $45°$ with the positive x-axis. What is the Jones matrix of this linear polariser?

e) Derive the real electric field transmitted by the linear polariser as function of z and t.

f) What is the state of polarisation of the transmitted beam?

g) What is the intensity of the transmitted beam?

h) What happens to the difference in energy between the incident and transmitted beam?

2. **Partial linear polarisation.** Consider a light beam that is partially linear polarised. Show that the degree of polarisation is given by

$$\frac{I_{max} - I_{min}}{I_{max} + I_{min}}. \tag{4.43}$$

where I_{max} and I_{min} are the maximum and minimum of the light transmitted through a linear polariser when it is turned through $360°$.

3. **Optical isolator.** In this problem we consider an optical isolator as shown in Fig. 4.4. In the setup, light can pass in one direction, but it cannot go back. This can for example be used to prevent laser light from going back into the laser source, hereby preventing unwanted effects such as intensity and frequency instabilities.

a) Give the Jones matrix for a linear polariser $\mathcal{P}$ that polarises light in the vertical direction (i.e. the y-direction).

b) Now we rotate the linear polariser by $\theta = \pi/4$ anti-clockwise. Find the Jones matrix for the rotated polariser $\mathcal{P}_{\pi/4}$. Check your result by verifying that:

$$\mathcal{P}_{\pi/4}\begin{pmatrix}1\\-1\end{pmatrix} = \begin{pmatrix}1\\-1\end{pmatrix}, \quad \mathcal{P}_{\pi/4}\begin{pmatrix}1\\1\end{pmatrix} = \begin{pmatrix}0\\0\end{pmatrix}. \tag{4.44}$$

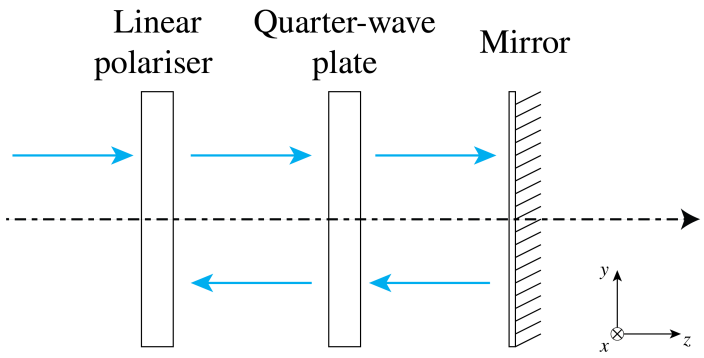


Figure 4.4: Schematic of a simple optical isolator.

c) Give the Jones matrix $\mathcal{Q}$ for the quarter-wave plate of which the slow axis points in the vertical direction (i.e. the y-direction).

d) Suppose we send light through the linear polariser and the quarter-wave plate. Then the light is partially transmitted and partially reflected by the mirror. The reflected light passes again through the quarter-wave plate and the polariser. Using Jones matrices calculate the state of the light that exits. A video demonstration of this optical isolator can be viewed at [9] (or search for "MIT optical isolator" on Youtube).

4. **Phase plates.** We consider a time-harmonic plane wave which propagates in the positive z-direction.

a) Suppose we have a linear polariser orientated such that the angle with the positive x-axis is $+45°$. Behind the linear polariser there is a half wave plate with fast axis orientated parallel to the y-axis. What is the orientation of the polarisation of the wave transmitted first by the linear polariser and then by the half wave plate when the incident wave is linear polarised parallel to the x-axis?

b) What is the intensity of the transmitted wave when the incident wave in a) has amplitude A?

c) Suppose now that the half wave plate behind the linear polariser with angle $45°$ with the x-axis, is replaced by a quarter wave plate with the fast axis parallel to the y-axis. What is the polarisation of the transmitted light when the incident wave is linearly polarised parallel to the x-axis?

d) What is the intensity of the transmitted wave when the incident wave in c) has amplitude A?

e) Suppose that an incident linear polarised wave which is polarised parallel to the x-axis light is first transmitted by a quarter wave plate of which the fast axis makes an angle of $+45°$ with the positive x-axis, and is then transmitted by a half wave plate with fast axis parallel to the y-axis. What is the polarisation of the transmitted light if the incident wave is polarised parallel to the x-axis?

5. **Jones Matrices.** Verify for each of the following matrices whether they correspond to a linear polariser, a wave plate or are neither. Also specify the direction of the linear polariser and the type of the wave plate.

a)

$$\begin{pmatrix} -1 & 1 \\ -\frac{2}{5}+i\frac{2}{5} & -\frac{1}{5}+i\frac{4}{5} \end{pmatrix}. \tag{4.45}$$

b)

$$\begin{pmatrix} 1 & -1 \\ -1 & 1 \end{pmatrix}. \tag{4.46}$$

c)

$$\begin{pmatrix} 1 & 0 \\ 0 & 3 \end{pmatrix} \tag{4.47}$$

[9] http://ocw.mit.edu/resources/res-6-006-video-demonstrations-in-lasers-and-optics-spring-2008/demonstrations-in-physical-optics/optical-isolator/

d) Determine the Jones matrix for the case of a wave plate of thickness equal to the wavelength, with fast axis parallel to the vector

$$\begin{pmatrix} 1 \\ -1 \end{pmatrix}, \tag{4.48}$$

and with refractive indices $n_1 = 1.5$ and $n_2 = 2$.

Chapter 5

Interference and Coherence

What you should know and be able to do after studying this chapter

- Understand time coherence and spatial coherence.
- Know how the degree of time coherence can be measured with a Michelson interferometer.
- Understand the connection between the time coherence and the frequency bandwidth.
- Know that the spatial coherence of the field in two points in space can be measured with Young's two-slit experiment.
- Understand that spatial coherence increases by propagation.
- Understand how the size of an incoherent source such as a star can be derived from measuring the spatial coherence at large distance from the source.
- Know the definition of fringe contrast.
- Know and understand the three Laws of Fresnel-Arago.

5.1 Introduction

Although the model of geometrical optics helps us to design optical systems and explains many phenomena, there are properties of light that require a more elaborate model. For example, interference fringes observed in Young's double-slit experiment or the Arago spot (Fig. 5.1) indicate that light is more accurately modelled as a wave.
In this chapter we will study the wave model of light. It will be shown that the extent to which light can show interference depends on a property called coherence. In the largest part of the discussion we will assume that all light has the same polarisation, so that we can treat the fields as scalar. In the last section we will look at how polarisation affects interference, as described by the Fresnel-Arago laws.
It is important to note that the concepts of interference and coherence are not just restricted to optics. Since quantum mechanics dictates that particles have a wave-like nature, interference and coherence also play a role in e.g. solid state physics and quantum information.

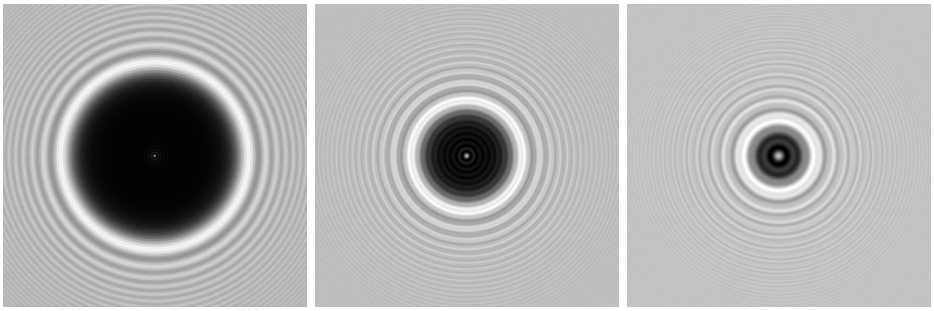


Figure 5.1: The Arago spot is the bright spot which occurs at the centre of the shadow of a circular disc and which is caused by diffraction. The disc has diameter 4 mm, 2 mm and 1 mm, from left to right, the wavelength is 633 nm and the intensity is simulated at 1 m behind a disc of 16 mm diameter (from Wikimedia Commons by Thomas Reisinger / CC BY-SA 3.0).

External sources in recommended order

- KhanAcademy - Interference of light waves: Playlist on wave interference at secondary school level.
- Yale Courses - 18. Wave Theory of Light

5.2 Interference of Monochromatic Fields of the Same Frequency

Let us first recall the basic concepts of interference. What causes interference is the fact that light is a wave, which means that it not only has an **amplitude** but also a **phase**. Suppose for example we evaluate a time-harmonic field in two points

$$\mathcal{U}_1(t) = \cos(\omega t), \quad \mathcal{U}_2(t) = \cos(\omega t + \varphi). \tag{5.1}$$

Here φ denotes the phase difference between the fields at the two points. If $\varphi = 0$, or φ is a multiple of 2π, the fields are **in phase**, and when they are added they interfere **constructively**

$$\mathcal{U}_1(t) + \mathcal{U}_2(t) = \cos(\omega t) + \cos(\omega t + 2m\pi) = 2\cos(\omega t). \tag{5.2}$$

However, when $\varphi = \pi$, or more generally $\varphi = \pi + 2m\pi$, for some integer m, then the waves are **out of phase**, and when they are superimposed, they interfere **destructively**.

$$\begin{aligned} \mathcal{U}_1(t) + \mathcal{U}_2(t) &= \cos(\omega t) + \cos(\omega t + \pi + 2m\pi) \\ &= \cos(\omega t) - \cos(\omega t) \\ &= 0. \end{aligned} \tag{5.3}$$

We can sum the two fields for arbitrary φ more conveniently using complex notation:

$$\mathcal{U}_1(t) = \mathrm{Re}[e^{-i\omega t}], \quad \mathcal{U}_2(t) = \mathrm{Re}[e^{-i\omega t}e^{-i\varphi}]. \tag{5.4}$$

Adding gives

$$\begin{aligned} \mathcal{U}_1(t) + \mathcal{U}_2(t) &= \mathrm{Re}[e^{-i\omega t}(1 + e^{-i\varphi})] \\ &= \mathrm{Re}[e^{-i\omega t}e^{-i\varphi/2}(e^{i\varphi/2} + e^{-i\varphi/2})] \\ &= \mathrm{Re}[e^{-i\omega t}e^{-i\varphi/2}2\cos(\varphi/2)] \\ &= 2\cos(\varphi/2)\cos(\omega t + \varphi/2). \end{aligned} \tag{5.5}$$

For $\varphi = 2m\pi$ and $\varphi = \pi + 2m\pi$ we retrieve the results obtained before. It is important to realize that what we see or detect physically (the 'brightness' of light) does not correspond to the quantities $\mathcal{U}_1$, $\mathcal{U}_2$. After all, $\mathcal{U}_1$ and $\mathcal{U}_2$ can attain negative values, while there is no such thing as 'negative brightness'. What $\mathcal{U}_1$ and $\mathcal{U}_2$ describe are the **fields**, which may be positive or negative. The 'brightness' or the **irradiance** or **intensity** is given by taking an average over a long time of $\mathcal{U}(t)^2$ (see (1.83), we shall omit the factor $\sqrt{\epsilon/\mu_0}$). As explained in Chapter 1, we see and measure only the long time-average of $\mathcal{U}(t)^2$, because at optical frequencies $\mathcal{U}(t)^2$ fluctuates very rapidly. We recall the definition of the time average over an interval of length T at a specific time t given in (1.88) in Chapter 1:

$$\langle f(t)\rangle = \frac{1}{T}\int_t^{t+T} f(t')\,\mathrm{d}t', \tag{5.6}$$

where T is a time interval that is the response time of a typical detector, i.e. $T \approx 10^{-6}\,\mathrm{s}$ which is extremely long compared to the period of visible light which is of the order of $10^{-14}\,\mathrm{s}$. For a time-harmonic function, the long-time average is equal to the average over one period of the field and hence **it is independent of the time t at which it is taken**. Indeed for (5.5) we get

$$\begin{aligned} I &= \langle(\mathcal{U}_1(t)+\mathcal{U}_2(t))^2\rangle \\ &= 4\cos^2(\varphi/2)\,\langle\cos^2(\omega t+\varphi/2)\rangle \\ &= 2(1+\cos\varphi)\,\langle\cos^2(\omega t+\varphi/2)\rangle \\ &= 1+\cos(\varphi) \end{aligned} \tag{5.7}$$

Using complex notation one can obtain this result more easily. Let

$$\mathcal{U}_1(t) = \mathrm{Re}[U_1 e^{-i\omega t}], \quad \mathcal{U}_2(t) = \mathrm{Re}[U_2 e^{-i\omega t}], \tag{5.8}$$

where

$$U_1 = 1, \quad U_2 = e^{-i\varphi}. \tag{5.9}$$

Then we find

$$\begin{aligned} |U_1+U_2|^2 &= |1+e^{-i\varphi}|^2 \\ &= (1+e^{i\varphi})(1+e^{-i\varphi}) \\ &= 1+1+e^{-i\varphi}+e^{i\varphi} \\ &= 2+2\cos(\varphi), \end{aligned} \tag{5.10}$$

hence

$$I = \frac{1}{2}|U_1+U_2|^2. \tag{5.11}$$

To see why this works, recall Eq. (1.89) and choose $A = B = U_1 + U_2$.

> **Remark.** To shorten the formulae, we will omit in this chapter the factor $1/2$ in front of the time-averaged intensity.

Hence we define $I_1 = |U_1|^2$ and $I_2 = |U_2|^2$, and we then find for the time-averaged intensity of the sum of U_1 and U_2:

$$\begin{aligned} I &= |U_1+U_2|^2 = (U_1+U_2)(U_1+U_2)^* \\ &= |U_1|^2+|U_2|^2+U_1U_2^*+U_1^*U_2 \\ &= I_1+I_2+2\mathrm{Re}[U_1U_2^*] \\ &= I_1+I_2+2\sqrt{I_1}\sqrt{I_2}\cos(\phi_1-\phi_2), \end{aligned} \tag{5.12}$$

where ϕ_1 and ϕ_2 are the arguments of U_1 and U_2 and $\phi_1 - \phi_2$ is the phase difference. The term $2\text{Re}[U_1^* U_2]$ is known as the **interference term**. In the famous double-slit experiment (which we will discuss in a later section), we can interpret the terms as follows: let us say U_1 is the field that comes from slit 1, and U_2 comes from slit 2. If only slit 1 is open, we measure on the screen intensity I_1, and if only slit 2 is open, we measure I_2. If both slits are open, we would not measure $I_1 + I_2$, but we would observe fringes due to the interference term $2\text{Re}[U_1^* U_2]$.

The intensity (5.12) varies when the phase difference varies. These variations are called fringes. The fringe contrast is defined by

$$\text{Fringe contrast} = \frac{I_{max} - I_{min}}{I_{max} + I_{min}}. \tag{5.13}$$

It is maximum and equal to 1 when the intensities of the interfering fields are the same. If these intensities are different the fringe contrast is less than 1.

More generally, the intensity of a sum of multiple time-harmonic fields U_j all having the same frequency is given by the **coherent sum**

$$I = \left| \sum_j U_j \right|^2 . \tag{5.14}$$

However, we will see in the next section that sometimes the fields are unable to interfere. In that case all the interference terms of the coherent sum vanish, and the intensity is given by the **incoherent sum**

$$I = \sum_j |U_j|^2. \tag{5.15}$$

5.3 Coherence

In the discussion so far we have only considered **monochromatic** light, which means that the spectrum of the light consists of only one frequency. Although light from a laser often has a very narrow band of frequencies and therefore can be considered to be monochromatic, purely monochromatic light does not exist. One reason that light can not be perfectly monochromatic is that any source must have been switched on a finite time ago. Hence, all light consists of multiple frequencies and therefore is **polychromatic**. Classical light sources such as incandescent lamps and also LEDs have relatively broad frequency bands. The question then arises how differently polychromatic light behaves compared to the idealised case of monochromatic light. To answer this question, we must study the topic of coherence. One distinguishes between two extremes: fully **coherent** and fully **incoherent** light, while the degree of coherence of practical light is somewhere in between. Generally speaking, the broader the frequency band of the source, the more incoherent the light is. It is a very important observation that no light is actually completely coherent or completely incoherent. All light is **partially coherent**, but some light is more coherent than others.

An intuitive way to think about these concepts is in terms of the ability to form interference fringes. For example, with laser light, which usually is almost monochromatic and hence coherent, one can form an interference pattern with clear maxima and minima in intensities using a double slit, while with sunlight (which is incoherent) this is much more difficult. Every frequency in the spectrum of sunlight gives its own interference pattern with its own frequency dependent fringe pattern. These fringe patterns wash out due to superposition and the total intensity therefore shows little fringe contrast, i.e. the coherence is less. However, it is not impossible to create interference fringes with natural light.[2] The trick is to let the two slits be so close together (of the

[2]See Veritasium - The original double-slit experiment, starting at 2:15 - Demonstration of an interference pattern obtained with sunlight.

order of 0.02 mm) that the *difference* in distances from the slits to the sun is so small for the fields in the slits to be sufficiently coherent to interfere. To understand the effect of polychromatic light, it is essential to understand that the degree to which the fields in two points are coherent, i.e. the ability to form fringes, is determined by the **difference in distances between these points and the source**. The distance itself to the source is **not** relevant. This will be made clear in this chapter.

5.3.1 Coherence of Light Sources

In a conventional light source such as a gas discharge lamp, photons are generated by **spontaneous emission** with energy equal to the energy difference between certain electronic states of the atoms of the gas. These transitions have a duration of the order of 10^{-8} to 10^{-9} s. Because the emitted wave trains are finite, the emitted light does not have a single frequency; instead, there is a band of frequencies around a centre frequency with width roughly equal to the reciprocal of the duration of the wave train. This spread of frequencies is called the **natural linewidth**. Random thermal motions of the molecules cause further broadening due to the Doppler effect. In addition, the atoms undergo collisions that interrupt the wave trains and therefore further broaden the frequency spectrum.

We first consider a **single emitting atom**. When collisions are the dominant broadening effect and these collisions are sufficiently brief such that any radiation emitted during the collision can be ignored, an accurate model for the emitted wave is a steady monochromatic wave train at frequency $\bar{\omega}$ at the centre of the frequency band, interrupted by random phase jumps each time that a collision occurs. The discontinuities in the phase due to the collisions cause a spread of frequencies around the centre frequency. An example is shown in Fig. 5.2. The average time τ_0 between the collisions is typically less than 10^{-10} s which implies that on average between two collisions roughly 10^6 harmonic oscillations occur and that during an atom transition of the order of hundred collisions may occur. The coherence time τ_c is defined as the maximum time interval over which the phase of the electric field can be predicted. In the case of collisions-dominated emission by a single atom, the coherence time is equal to the average time between subsequent collisions: $\Delta\tau_c \approx 10^{-10}$ s.

To understand coherence and incoherence it is helpful to use the model that the emission by a single atom consists of harmonic wave trains of many thousands of periods interrupted by roughly hundred random phase jumps. Due to the random phase jumps the interference term of the sum of harmonic wave trains emitted by two atoms when integrated of the relatively long integration time of a detector becomes a sum over integrals over time intervals of average length τ_0:

$$\sum_j \int_0^{\tau_0} \cos(\omega t)\cos(\omega t + \phi_j)\mathrm{d}t,$$

where the sum is over roughly one hundred random phase jumps during the total duration of the wave trains. The random phase jumps lead to cancellation of the integrals and hence the interference term vanishes. We conclude that for common integration times of typical detectors:

> light trains which have been spontaneously emitted by different atoms can not interfere.

The coherence time and the width $\Delta\omega$ of the frequency line are related as

$$\Delta\tau_c = \frac{2\pi}{\Delta\omega}. \tag{5.16}$$

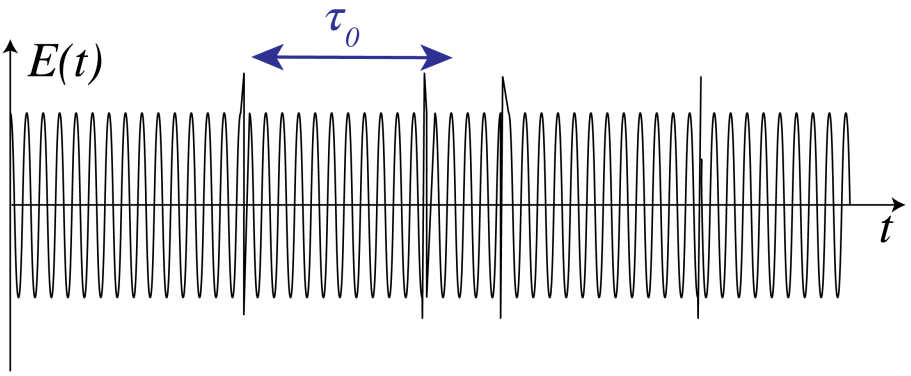


Figure 5.2: The electric field amplitude of the harmonic wave train radiated by a single atom at the centre frequency $\bar{\omega}$. The vertical lines are collisions separated by periods of free flight with mean duration $\Delta\tau_c$. The quantity $\bar{\omega}\tau_0$, which is the number of periods in a typical wave train, is chosen unrealistically small (namely 60, whereas a realistic value would be 10^5) to show the random phase changes.

The coherence length is defined by

$$\Delta\ell_c = c\Delta\tau_c. \tag{5.17}$$

Since $\lambda\omega = 2\pi c$, we have

$$\frac{\Delta\lambda}{\bar{\lambda}} = \frac{\Delta\omega}{\bar{\omega}}, \tag{5.18}$$

where $\bar{\lambda}$ and $\bar{\omega}$ are the wavelength and the frequency at the centre of the line. Hence,

$$\Delta\ell_c = c\frac{2\pi}{\Delta\omega} = 2\pi\frac{c}{\bar{\omega}}\frac{\bar{\omega}}{\Delta\omega} = \frac{\bar{\lambda}^2}{\Delta\lambda}. \tag{5.19}$$

The coherence length and coherence time of a number of sources are listed in Table 5.1. For a laser, the linewidth is extremely small and the coherence time very long. This is because the photons in a laser are not generated predominantly by spontaneous emission as classical sources, but instead by **stimulated emission**. Lasers are discussed in Chapter 7.

Source	Mean wavelength $\bar{\lambda}$	Linewidth $\Delta\lambda$	Coherence Length $\bar{\lambda}^2/\Delta\lambda$	Coherence Time $\Delta\tau_c$
Mid-IR (3-5 μm)	4.0 μm	2.0 μm	8.0 μm	2.66×10^{-14} s.
White light	550 nm	$\approx$ 300 nm	$\approx$ 900 nm	$\approx 3.0 \times 10^{-14}$s.
Mercury arc	546.1 nm	$\approx$ 1.0 nm	$\approx$ 0.3 mm	$\approx 1.0 \times 10^{-12}$s.
Kr^{86} discharge lamp	605.6 nm	1.2×10^{-3} nm	0.3 m	1.0×10^{-9}s.
Stabilised He-Ne laser	632.8 nm	$\approx 10^{-6}$ nm	400 m	1.33×10^{-6}s.

Table 5.1: Coherence time and coherence length of several sources

5.3.2 Polychromatic Light

When dealing with coherence one has to consider fields that consist of a range of different frequencies. Let $\mathcal{U}(\mathbf{r}, t)$ be the real-valued field component. It is always possible to write $\mathcal{U}(\mathbf{r}, t)$

as an integral over time-harmonic components:

$$\mathcal{U}(\mathbf{r},t) = \mathrm{Re}\int_0^\infty A_\omega(\mathbf{r})e^{-i\omega t}\,\mathrm{d}\omega, \tag{5.20}$$

where $A_\omega(r)$ is the complex amplitude of the time-harmonic field with frequency ω. When there is only a certain frequency band that contributes, then $A_\omega = 0$ for ω outside this band. We define the **complex time-dependent field** $U(\mathbf{r},t)$ by

$$U(\mathbf{r},t) = \int_0^\infty A_\omega(\mathbf{r})e^{-i\omega t}\,\mathrm{d}\omega. \tag{5.21}$$

Then

$$\mathcal{U}(\mathbf{r},t) = \mathrm{Re}\,U(\mathbf{r},t). \tag{5.22}$$

Remark. The complex field $U(\mathbf{r},t)$ contains now the time dependence in contrast to the notation used for a time-harmonic (i.e. single frequency) field introduced in Chapter 2, where the time-dependent $e^{-i\omega t}$ was a separate factor.

We now compute the intensity of polychromatic light. The instantaneous energy flux is (as for monochromatic light) proportional to the square of the instantaneous real field: $\mathcal{U}(\mathbf{r},t)^2$. We average the instantaneous intensity over the integration time T of common detectors which, as stated before, is very long compared to the period at the centre frequency $2\pi/\bar{\omega}$ of the field. Using definition (5.6) and

$$\mathcal{U}(\mathbf{r},t) = \mathrm{Re}\,U(\mathbf{r},t) = (U(\mathbf{r},t) + U^*(\mathbf{r},t))/2, \tag{5.23}$$

we get

$$\begin{aligned}
\langle \mathcal{U}(\mathbf{r},t)^2\rangle &= \frac{1}{4}\langle (U(\mathbf{r},t)+U^*(\mathbf{r},t))(U(\mathbf{r},t)+U^*(\mathbf{r},t))\rangle \\
&= \frac{1}{4}\left\{\langle U(\mathbf{r},t)^2\rangle + \langle (U^*(\mathbf{r},t))^2\rangle + 2\langle U^*(\mathbf{r},t)U(\mathbf{r},t)\rangle\right\} \\
&\approx \frac{1}{2}\langle U(\mathbf{r},t)U^*(\mathbf{r},t)\rangle \\
&= \frac{1}{2}\langle |U(\mathbf{r},t)|^2\rangle\,, \qquad (5.24)\\
& \qquad (5.25)
\end{aligned}$$

where the averages of $U(\mathbf{r},t)^2$ and $(U^*(\mathbf{r},t))^2$ are zero because they are fast-oscillating and go through many cycles during the integration time of the detector. In contrast, $|U(\mathbf{r},t)|^2 = U^*(\mathbf{r},t)U(\mathbf{r},t)$ has a DC-component which does not average to zero.

Remark. In contrast to the time-harmonic case, the long time average of polychromatic light depends on the time t at which the average is taken. However, we assume in this chapter that the fields are omitted by sources that are **stationary**. The property of stationarity implies that the average over the time interval of long length T does not depend on the time that the average is taken. Many light sources, in particular conventional lasers, are stationary. (However, a laser source which emits short high-power pulses cannot be considered as a stationary source). We furthermore assume that the fields are **ergodic**, which means that taking the time-average over a long time interval amounts to the same as taking the average over the ensemble of possible fields. It can be shown that this property implies that the limit $T \to \infty$ in (5.6) indeed exists[4].

We use for the intensity again the expression without the factor 1/2 in front, i.e.

$$I(\mathbf{r}) \quad = \quad \langle |U(\mathbf{r},t)|^2 \rangle \, . \tag{5.26}$$

The time-averaged intensity has hereby been expressed in terms of the **time-average of the squared modulus of the complex field**.

Quasi-monochromatic field. If the width $\Delta\omega$ of the frequency band is very narrow compared to the centre frequency $\bar{\omega}$, the field is called quasi-monochromatic field. In the propagation of quasi-monochromatic fields, we use the formula for time-harmonic fields at $\bar{\omega}$. The quasi-monochromatic assumption simplifies the computations considerably and will be used frequently.

5.4 Temporal Coherence and the Michelson Interferometer

To investigate the time coherence of a field in a certain point $\mathbf{r}$, we let the field in that point interfere with itself but delayed in time, i.e. we let $U(\mathbf{r},t)$ interfere with $U(\mathbf{r},t-\tau)$.

Because, when studying temporal coherence, the point $\mathbf{r}$ is always the same, we omit it from the formula. Furthermore, for easier understanding of the phenomena, we assume for the time being that the field considered is emitted by a single atom (i.e. a point source).

Temporal coherence is closely related to the spectral content of the light: if the light consists of fewer frequencies (think of monochromatic light), then it is more temporally coherent. To study the interference of $U(t)$ with $U(t-\tau)$, a Michelson interferometer, shown in Fig. 5.3, is a suitable setup. The light that goes through one arm takes time t to reach the detector, while the light that goes through the other (longer) arm takes time $t+\tau$ which means that it was radiated earlier. Therefore, the detector observes the time-averaged intensity $\langle |U(t)+U(t-\tau)|^2 \rangle$. As remarked before, this averaged intensity does not depend on the time the average is taken, it only depends on the time difference τ between the two beams. We have

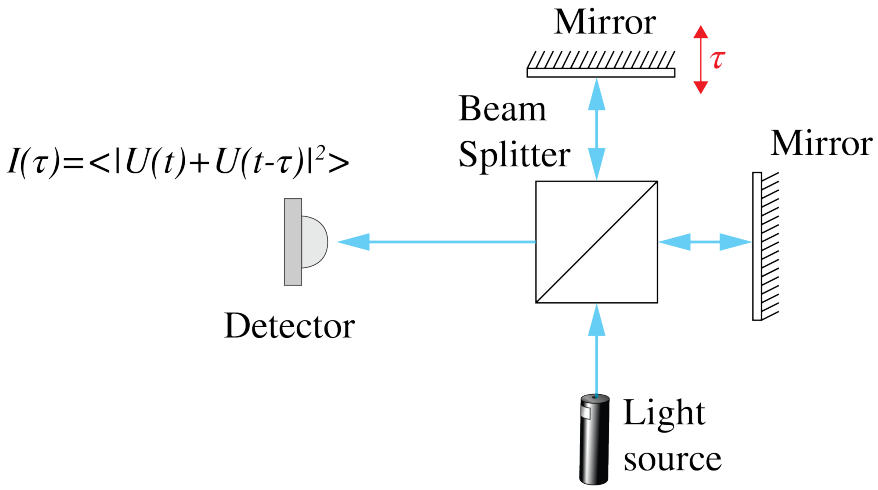


Figure 5.3: A Michelson interferometer to study the temporal coherence of a field. A beam is split in two by a beam splitter, and the two beams propagate over different distances which corresponds to a time difference τ and then interfere at the detector.

[4]For more details see J.W. Goodman, *Statistical Optics*

$$\begin{aligned} I(\tau) &= \langle |U(t) + U(t-\tau)|^2 \rangle \\ &= \langle |U(t)|^2 \rangle + \langle |U(t-\tau)|^2 \rangle + 2\mathrm{Re}\, \langle U(t)U^*(t-\tau) \rangle \\ &= 2\, \langle |U(t)|^2 \rangle + 2\mathrm{Re}\, \langle U(t)U^*(t-\tau) \rangle\,. \end{aligned} \tag{5.27}$$

The detected intensity varies with the difference in arm length.

So far we have considered a field that originates from a single atom. The total field emitted by an extended source is the sum of fields $U_i(t)$ corresponding to all atoms i. As has been explained already, the fields emitted by different atoms can not interfere. But the field emitted by an atom can interfere with the delayed field of that same atom and for every atom the interference is given by the same expression (5.27). The total intensity is simply that given by that of a single atom multiplied by the number of atoms. In particular, the ratio of the interference term and the other terms is the same for the entire source as for a single atom.

The **self coherence function** $\Gamma(\tau)$ is defined by

$$\Gamma(\tau) = \langle U(t)U^*(t-\tau) \rangle \qquad \textbf{self-coherence}. \tag{5.28}$$

The intensity of $U(t)$ is

$$I_0 = \langle |U(t)|^2 \rangle = \Gamma(0). \tag{5.29}$$

The **complex degree of self-coherence** is defined by:

$$\gamma(\tau) = \frac{\Gamma(\tau)}{\Gamma(0)}. \qquad \textbf{complex degree of self-coherence} \tag{5.30}$$

Using Bessel's inequality it can be shown that this is a complex number with modulus between 0 and 1:

$$0 \leq |\gamma(\tau)| \leq 1. \tag{5.31}$$

The observed intensity can then be written:

$$I(\tau) = 2I_0 \left\{1 + \mathrm{Re}\left[\gamma(\tau)\right]\right\}, \tag{5.32}$$

We consider two special cases.

1. Suppose $U(t)$ is a monochromatic wave

$$U(t) = e^{-i\omega t}. \tag{5.33}$$

In that case we get for the self-coherence

$$\Gamma(\tau) = \langle e^{-i\omega t} e^{i\omega(t-\tau)} \rangle = e^{-i\omega\tau}, \tag{5.34}$$

and

$$\gamma(\tau) = e^{-i\omega\tau}. \tag{5.35}$$

Hence the interference pattern is given by

$$I(\tau) = 2\left[1 + \cos\left(\omega\tau\right)\right]. \tag{5.36}$$

So for monochromatic light we expect to detect a cosine interference pattern, which shifts as we change the arm length of the interferometer (i.e. change τ). No matter how large the time delay

τ, a clear interference pattern should be observed.
2. Next we consider what happens when the light is a superposition of two frequencies:

$$U(t) = \frac{e^{-i(\bar{\omega}+\Delta\omega/2)t} + e^{-i(\bar{\omega}-\Delta\omega/2)t}}{2}, \tag{5.37}$$

where $(2\pi/T) \ll \Delta\omega \ll \bar{\omega}$, where T is the integration time of the detector. Then:

$$\begin{aligned} \Gamma(\tau) &= \frac{1}{4}\langle\left(e^{-i(\bar{\omega}+\Delta\omega/2)t} + e^{-i(\bar{\omega}-\Delta\omega/2)t}\right)\left(e^{i(\bar{\omega}+\Delta\omega/2)(t-\tau)} + e^{i(\bar{\omega}-\Delta\omega/2)(t-\tau)}\right)\rangle \\ &\approx \frac{e^{-i(\bar{\omega}+\Delta\omega/2)\tau} + e^{-i(\bar{\omega}-\Delta\omega/2)\tau}}{4} \\ &= \cos\left(\Delta\omega\,\tau/2\right)\frac{e^{-i\bar{\omega}\tau}}{2}, \end{aligned} \tag{5.38}$$

where in the second line the time average of terms that oscillate with time is set to zero because the averaging is done over time interval T satisfying $T\Delta\bar{\omega} \gg 1$. Hence, the complex degree of self-coherence is:

$$\gamma(\tau) = \cos\left(\Delta\omega\,\tau/2\right)e^{-i\bar{\omega}\tau} \tag{5.39}$$

and (5.32) becomes

$$I(\tau) = 2\left\{1 + \mathrm{Re}\left[\gamma(\tau)\right]\right\} = 2 + 2\cos\left(\Delta\omega\,\tau/2\right)\cos(\bar{\omega}\tau). \tag{5.40}$$

The interference term is the product of the function $\cos(\bar{\omega}\tau)$, which is a rapidly oscillating function of τ, and a slowly varying envelope $\cos\left(\Delta\omega\,\tau/2\right)$. It is interesting to note that the envelope, and hence $\gamma(\tau)$, vanishes for some periodically spaced τ, which means that for certain τ the degree of self-coherence vanishes and no interference fringes form [5,6]. Note that when $\Delta\omega$ is larger the intervals between the zeros of $\gamma(\tau)$ decrease. If more frequencies are added, the envelope function is not a cosine function but on average decreases with τ. The typical value of τ below which interferences are observed is roughly equal to half the first zero of the envelope function. This value is called the **coherence time** $\Delta\tau_c$. We conclude with some further interpretations of the degree of self-coherence $\gamma(\tau)$.

Remarks.

1. In stochastic signal analysis $\Gamma(\tau) = \langle U(t)U^*(t-\tau)\rangle$ is called the **autocorrelation** of $U(t)$. Informally, one can interpret the autocorrelation function as the ability to predict the field U at time t given the field at time $t-\tau$.

2. The Wiener-Khinchin theorem says that (under the assumptions of ergodicity and a stationary field) the **Fourier transform of the self coherence function is the spectral power density of** $U(t)$:

$$\hat{\Gamma}(\omega) = |\hat{U}(\omega)|^2, \tag{5.41}$$

'Using the uncertainty principle, we can see that the larger the spread of the frequencies of $U(t)$ (i.e. the larger the bandwidth), the more sharply peaked $\Gamma(\tau)$ is. Thus, the light gets temporally less coherent when it consists of a broader range of frequencies. Measuring the spectral power density with a spectroscope and applying a back Fourier transform is an alternative method to obtain the complex self-coherence function.

[5] MIT OCW - Fringe Contrast - Path Difference: Demonstration of how fringe contrast varies with propagation distance.

[6] MIT OCW - Coherence Length and Source Spectrum: Demonstration of how the coherence length depends on the spectrum of the laser light.

5.5 Spatial Coherence and Young's Experiment

Temporal coherence concerns the coherence of the field in one point. The absolute value of the degree of self coherence (5.30) quantifies how strong the interference is of the field in the point of interest with the field in that same point at a later time. In contrast, spatial coherence is concerned with determining how coherent the fields in two different points are. This is done by letting the fields interfere using a mask with two small holes at the positions of the points of interest and observing the fringe contrast at a distant screen (Young's experiment).

While for temporal coherence we used a **Michelson interferometer**, the natural choice to characterize spatial coherence is **Young's experiment**, because it allows the fields in two points P_1, P_2 which are separated in space to interfere with each other. Let $\mathbf{r}_1$ and $\mathbf{r}_2$ be the position

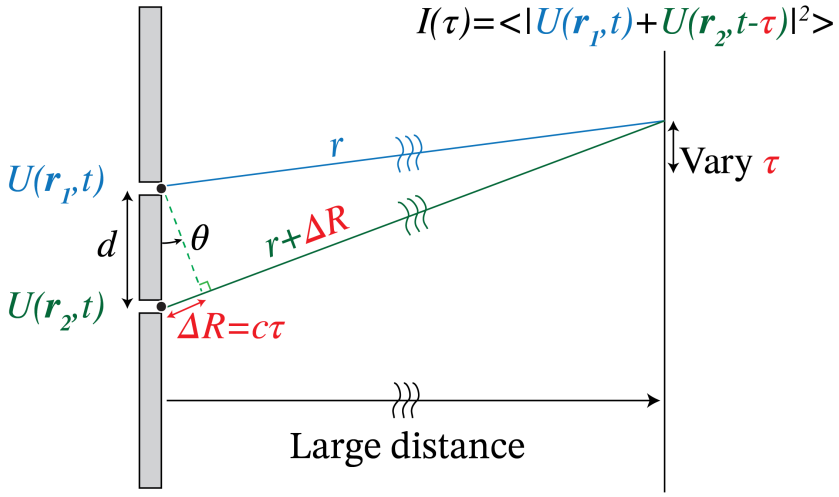


Figure 5.4: Young's experiment to evaluate the spatial coherence of two points. A mask with two holes at the two points of interest, $\mathbf{r}_1$ and $\mathbf{r}_2$, is used to let the fields in these points interfere with on a screen at a large distance. Because the light propagates over different distances from the two holes to the points of observation, $U(\mathbf{r}_1, t)$ interferes with $U(\mathbf{r}_2, t+\tau)$, where τ is the difference in propagation time.

vectors of the points P_1 and P_2, respectively. We write the complex field in P_1 as a superposition of monochromatic fields as in (5.21):

$$U(\mathbf{r}_1, t) = \int A_\omega(\mathbf{r}_1) e^{-i\omega t} \, \mathrm{d}\omega. \tag{5.42}$$

The reason for doing this is that for a monochromatic field in $\mathbf{r}_1$ in the pinhole, i.e. for a field with a well defined frequency, we can derive from the Huygens-Fresnel Principle that the disturbance in a point $\mathbf{r}$ behind the mask is given by the spherical wave:

$$A_\omega(\mathbf{r}_1) \; S \frac{\omega}{2\pi c} \frac{e^{-i\omega(t-|\mathbf{r}-\mathbf{r}_1|/c)}}{|\mathbf{r}-\mathbf{r}_1|} \, \mathrm{d}\omega, \tag{5.43}$$

where S is the surface area of the pinhole. The total field $U_1(\mathbf{r}, t)$ in $\mathbf{r}$ due to the pinhole at P_1

is obtained by integrating over frequency:

$$\begin{aligned} U_1(\mathbf{r},t) &= \int A_\omega(\mathbf{r}_1)\; S\frac{\omega}{2\pi c}\,\frac{e^{-i\omega(t-|\mathbf{r}-\mathbf{r}_1|/c)}}{|\mathbf{r}-\mathbf{r}_1|}\,\mathrm{d}\omega \\ &\approx S\,\frac{\bar\omega}{2\pi c}\int A_\omega(\mathbf{r}_1)\,\frac{e^{-i\omega(t-|\mathbf{r}-\mathbf{r}_1|/c)}}{|\mathbf{r}-\mathbf{r}_1|}\,\mathrm{d}\omega \\ &\approx S\,\frac{\bar\omega}{2\pi c}\,\frac{U(\mathbf{r}_1,t-|\mathbf{r}-\mathbf{r}_1|/c)}{|\mathbf{r}-\mathbf{r}_1|} \end{aligned} \tag{5.44}$$

where we assumed that the frequency band is so small that the factor ω/c in the integrand may be replaced by $\bar\omega/c$ at the centre frequency $\bar\omega$ of the band. Note that in the exponential factor and in A_ω, the frequency is not replaced by $\bar\omega$. In words:

> The field in $\mathbf{r}$ at time t due to the pinhole at $\mathbf{r}_1$ is proportional to the field at $\mathbf{r}_1$ at the earlier time $= |\mathbf{r}-\mathbf{r}_1|/c$ that it takes for the light to propagate form $\mathbf{r}_1$ to $\mathbf{r}$. The proportionality factor scales with the reciprocal distance between $\mathbf{r}$ and $\mathbf{r}_1$.

For the field in $\mathbf{r}$ due to pinhole 2 we have similarly

$$U_2(\mathbf{r},t) = S\,\frac{\bar\omega}{2\pi c}\,\frac{U(\mathbf{r}_2,t-|\mathbf{r}-\mathbf{r}_2|/c)}{|\mathbf{r}-\mathbf{r}_2|}. \tag{5.45}$$

The total field in $\mathbf{r}$ is the sum $U_1(\mathbf{r},t)+U_2(\mathbf{r},t)$. Because of the difference in propagation distance $\Delta R = |\mathbf{r}-\mathbf{r}_2| - |\mathbf{r}-\mathbf{r}_1|$, there is a time difference τ between when the two fields have been emitted by the two pinholes when they arrive at a given time T in point $\mathbf{r}$ on the screen in Fig. 5.4. This time difference is given by

$$\tau = \frac{\Delta R}{c}. \tag{5.46}$$

Furthermore, the amplitudes are reduced by a factor proportional to the reciprocal distance which is different for the two fields. But if the distance of the screen to the mask is large enough, we may assumne these factors to be the same and then omit them. Using (5.46), the interference pattern on the screen is then, apart from a constant factor, given by

$$\begin{aligned} I(\tau) &= \langle\, |U_1(\mathbf{r},t)+U_2(\mathbf{r},t)|^2 \,\rangle \\ &= \langle\, |U(\mathbf{r}_1,t-|\mathbf{r}-\mathbf{r}_1|/c)+U(\mathbf{r}_2,t-|\mathbf{r}-\mathbf{r}_2|/c)|^2 \,\rangle \\ &= \langle\, |U(\mathbf{r}_1,t)+U(\mathbf{r}_2,t-\tau)|^2 \,\rangle \\ &= \langle\, |U(\mathbf{r}_1,t)|^2\rangle + \langle |U(\mathbf{r}_2,t-\tau)|^2 \,\rangle + 2\mathrm{Re}\,\langle\, U(\mathbf{r}_1,t)U^*(\mathbf{r}_2,t-\tau)\,\rangle \\ &= \langle\, |U(\mathbf{r}_1,t)|^2 \,\rangle + \langle\, |U(\mathbf{r}_2,t)|^2 \,\rangle + 2\mathrm{Re}\,\langle\, U(\mathbf{r}_1,t)U^*(\mathbf{r}_2,t-\tau)\,\rangle\,, \end{aligned} \tag{5.47}$$

where in the third and last line we used that the time average does not depend on the time it is taken because the light source is assumed to be stationary. We define the **mutual coherence function** by:

$$\Gamma_{12}(\tau) = \langle\, U(\mathbf{r}_1,t)U^*(\mathbf{r}_2,t-\tau\,\rangle\,, \qquad \textbf{mutual coherence.} \tag{5.48}$$

With the intensities

$$\begin{aligned} I_1 &= \langle\, |U(\mathbf{r}_1,t)|^2 \,\rangle = \Gamma_{11}(0), \\ I_2 &= \langle\, |U(\mathbf{r}_2,t)|^2 \,\rangle = \Gamma_{22}(0). \end{aligned} \tag{5.49}$$

the **complex degree of mutual coherence** is defined by

$$\gamma_{12}(\tau) = \frac{\Gamma_{12}(\tau)}{\sqrt{\Gamma_{11}(0)}\sqrt{\Gamma_{22}(0)}}, \qquad \textbf{complex degree of mutual coherence.} \tag{5.50}$$

It can be proved using Bessel's inequality that

$$|\gamma_{12}(\tau)| \leq 1. \tag{5.51}$$

We can now write (5.47) as

$$I(\tau) = I_1 + I_2 + 2\sqrt{I_1}\sqrt{I_2}\,\mathrm{Re}\,\gamma_{12}(\tau). \tag{5.52}$$

By varying the point $\mathbf{r}$ over the screen we can vary τ and by measuring the intensities we can determine the real part of $\gamma_{12}(\tau)$ and hence the fringe contrast observed on the screen.

As an example, consider what happens when $U(\mathbf{r}, t)$ is a monochromatic field

$$U(\mathbf{r}, t) = A(\mathbf{r})e^{-i\omega t}. \tag{5.53}$$

In that case

$$\begin{aligned} \Gamma_{12}(\tau) &= \langle A(\mathbf{r}_1)A^*(\mathbf{r}_2)e^{-i\omega t}e^{i\omega(t-\tau)}\rangle \\ &= A(\mathbf{r}_1)A^*(\mathbf{r}_2)e^{-i\omega\tau}. \end{aligned} \tag{5.54}$$

and

$$\Gamma_{11}(0) = |A(\mathbf{r}_1)|^2, \qquad \Gamma_{22}(0) = |A(\mathbf{r}_2)|^2. \tag{5.55}$$

So we get

$$\gamma_{12}(\tau) = \frac{\Gamma_{12}(\tau)}{|A(\mathbf{r}_1)||A(\mathbf{r}_2)|} = e^{-i\omega\tau + i\varphi}, \tag{5.56}$$

where φ is the phase difference of $A(\mathbf{r}_2)$ and $A(\mathbf{r}_1)$. In this case γ_{12} has modulus 1, as expected for a monochromatic field. The intensity on the screen becomes

$$I(\tau) = |A(\mathbf{r}_1)|^2 + |A(\mathbf{r}_2)|^2 + 2|A(\mathbf{r}_1)||A(\mathbf{r}_2)|\cos(\omega\tau - \varphi). \tag{5.57}$$

So indeed we see interference fringes with maximum contrast 1 and hence the fields in P_1 and P_2 are fully coherent as one would expect for a monochromatic wave. If $\varphi = 0$, then interference maxima occur for

$$\omega\tau = 0, \pm 2\pi, \pm 4\pi, \pm 6\pi, \ldots \tag{5.58}$$

Because $\omega = c\frac{2\pi}{\lambda}$, and $\Delta R = c\tau$, we find that maxima occur when

$$\Delta R = 0, \pm\lambda, \pm 2\lambda, \pm 3\lambda, \ldots \tag{5.59}$$

For large distance between the screen and the mask (in the Fraunhofer limit), these path length differences correspond to directions of the maxima given by the angles θ_m (see Fig. 5.4):

$$\theta_m = \frac{\Delta R}{d} = m\frac{\lambda}{d}, \tag{5.60}$$

where d is the distance between the slits and m is an integer[8].

[8] KhanAcademy - Young's Double slit part 1

Remarks.

1. The mutual coherence $\Gamma_{12}(\tau) = \langle U(\mathbf{r}_1, t)U^*(\mathbf{r}_2, t-\tau)\rangle$ is the **cross-correlation** of the two signals $U(\mathbf{r}_1, t)$ and $U(\mathbf{r}_2, t)$.

2. As remarked above, by moving the point of observation $\mathbf{r}$ over the screen one can obtain the real part of the complex degree of mutual coherence. To derive also the imaginary part, one can put a piece of glass behind one of the pinholes with thickness such that for the centre frequency $\bar{\omega}$ an additional phase difference of $\pi/2$ is obtained of the fields in $\mathbf{r}_1$ and $\mathbf{r}_2$. If the frequency band $\Delta\omega$ is sufficiently narrow this phase difference applies in good approximations to all frequencies in the band.

5.6 More on Spatial Coherence

We first consider the case that the source is so small (e.g. a single emitting atom) that it can be considered to be a point source S. In that case it is the fields in two points P_1, P_2 somewhere in space are coherent if and only if the difference in time that it takes for light to propagate from S to P_1 and from S to P_2 is less than the coherence time $\Delta\tau_c$. Equivalently, for coherence the difference between the distances SP_1 and SP_2 must be less than the coherence length Δl_c.

An extended classical light source consists of a large set of emitting point sources that emit by spontaneous emission. As we have explained in Section 5.3.1, the wave trains emitted by different atoms (point sources) in the source suffer random phase jumps due to e.g. collisions and therefore the fields emitted by different point sources in an extended classical light source can not interfere. Such a light source is called **spatially incoherent**. For a spatially incoherent light source, the spatial coherence in any two points P_1 and P_2 is determined by measuring the fringe contrast on a distance screen when a mask is used that is perpendicular to the mean direction of propagation of the light and which contains pinholes at P_1 and P_2. The fringe contrast and hence the mutual coherence at P_1 and P_2 is determined by two effects:

1. First of all it is determined by how coherent the contributions to the total field in P_1 and P_2 are of the individual point sources S in the extended source. This coherence is determined by the extent to which the difference between the distance of S to P_1 and of S to P_2 is smaller than the coherence length. If these differences in distances are for all point sources larger than the coherence length, the fringe contrast on the screen in Young's experiment will be very low and hence the mutual coherence at P_1 and P_2 is very low.

2. The second effect is the size of the extended source. Even if for all point sources in the source the fields in P_1 and P_2 are coherent, the coherence of the total fields at P_1 and P_2 due to the entire source can be small. As we know, the contributions of different point sources can not interfere. Hence the intensity observed in Young's experiment is the sum of the intensities due to the individual point sources in the extended source. The reason that the coherence of the total fields in P_1 and P_2 due to the entire extended source can be low even though for all point sources individually the mutual coherence in P_1 and P_2 is high, is that the fringe patterns due to the point sources are shifted with respect to each other which reduces the fringe contrast and hence the mutual coherence. The shift of the fringe patterns is due to the different positions in the extended source of the point sources which cause that the phase difference between the fields in P_1 and P_2 varies with the point sources.

We will show that when P_1 and P_2 have a large distance to the extended source, the two conditions mentioned above for the fields in P_1 and P_2 to be spatially mutually coherent are equivalently to the requirement that:

The product of the angle subtended by the extended source at the midpoint of P_1P_2 and the distance between P_1 and P_2 should be smaller than the coherence length $\Delta l_c = c\Delta\tau_c$.

To show this we consider two mutually incoherent point sources S_1 and S_2 in the $z = 0$ plane. Their mutual coherence function satisfies:

$$\Gamma_{S_1S_2}(\tau) = 0, \text{ for all } \tau, \tag{5.61}$$
$$\Gamma_{S_1S_1}(\tau) = \Gamma_{S_2S_2}(\tau) = \Gamma_0(\tau), \tag{5.62}$$

where Γ_0 is the self-coherence which we assume to be the same for both point sources. $\Gamma_0(\tau)$ has width given by the coherence time $\Delta\tau_c$ of the source and on average decreases with τ (although not always monotonically). Eq. (5.61) expresses the fact that two point sources are mutually incoherent. Using that the long-time average does not depend on the moment the average is taken we find:

$$\Gamma_0(-\tau) =< U(S_1,t)U^*(S_1,t+\tau) >=< U(S_1,t-\tau)U^*(S_1,t) >= \Gamma_0^*(\tau). \tag{5.63}$$

Furthermore, for $\tau = 0$: $\Gamma_0(0) = I_0$, which is the intensity of either source.

We assume for convenience that the two points P_1, P_2 are at a large distance z from the two point sources and that the line P_1P_2 is parallel to the extended source as shown in Fig. 5.5. We will compute the mutual coherence $\Gamma_{P_1P_2}(0)$ for zero time delay $\tau = 0$ (we can also compute the mutual coherence for more general time delays $\tau > 0$, i.e. $\Gamma_{P_1P_2}(\tau)$, but it will suffice for our purpose to take $\tau = 0$). The fields in P_1 and P_2 are the sum of the fields emitted by S_1 and S_2. Since S_1 and S_2 are point sources they emit spherical waves. Therefore, similarly to (5.44) we find that the field in P_1 is proportional to

$$U(P_1,t) \propto \frac{U(S_1,t-|S_1P_1|/c)}{|S_1P_1|} + \frac{U(S_2,t-|S_2P_1|/c)}{|S_2P_1|}, \tag{5.64}$$

and

$$U(P_2,t) \propto \frac{U(S_1,t-|S_1P_2|/c)}{|S_1P_2|} + \frac{U(S_2,t-|S_2P_2|/c)}{|S_2P_2|}, \tag{5.65}$$

where we omitted the constant factors in front of (5.44). For z sufficiently large all distances

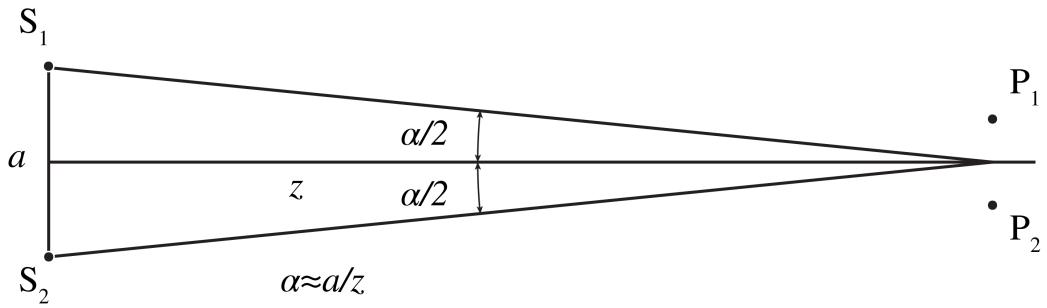


Figure 5.5: Two incoherent point sources S_1, S_2 at a distance a from each other and two points P_1, P_2 in a plane at large distance z from the point sources.

$|S_iP_j|$ in the denominators may be replaced by z and then these equal distances can be omitted. By substituting (5.64) and (5.65) into (5.48) with $\tau = 0$, we find for the mutual coherence of P_1

and P_2:

$$\begin{aligned}\Gamma_{P_1P_2}(0) &= \langle U(P_1,t)U^*(P_2,t)\rangle \\ &= \Gamma_{S_1S_1}\left(\frac{|S_1P_2|-|S_1P_1|}{c}\right)+\Gamma_{S_1S_2}\left(\frac{|S_2P_2|-|S_1P_1|}{c}\right) \\ &\quad +\Gamma_{S_2S_1}\left(\frac{|S_1P_2|-|S_2P_1|}{c}\right)+\Gamma_{S_2S_2}\left(\frac{|S_2P_2|-|S_2P_1|}{c}\right). \end{aligned} \tag{5.66}$$

Now we use (5.61) and (5.62) to get

$$\Gamma_{P_1P_2}(0) = \Gamma_0\left(\frac{|S_1P_2|-|S_1P_1|}{c}\right)+\Gamma_0\left(\frac{|S_2P_2|-|S_2P_1|}{c}\right). \tag{5.67}$$

Similarly,

$$\Gamma_{P_1P_1}(0)=\Gamma_{P_2P_2}(0)=2\Gamma_0(0)=2I_0. \tag{5.68}$$

Since the width of the self coherence function Γ_0 is the coherence time $\Delta\tau_c$, result (5.67) confirms that for the fields in P_1 and P_2 to be coherent, the **difference in distance** of each of the source points to points P_1 and P_2 should be smaller than the coherence length $\Delta l_c = c\Delta\tau_c$. To express the result in the angle α subtended by the source at the midpoint of P_1P_2 we choose coordinates such that $P_j=(x_j,0,z)$ for $j=1,2$. If the distance to the source is so large that S_1P_1 and S_1P_2 are almost parallel, we see from Fig. 5.6 that

$$|S_1P_2|-|S_1P_1|\approx|QP_2|=\frac{\alpha}{2}|x_1-x_2|. \tag{5.69}$$

Similarly,

$$|S_2P_1|-|S_2P_2|\approx\frac{\alpha}{2}|x_1-x_2|. \tag{5.70}$$

Hence, with $\Gamma_0(-\tau)=\Gamma_0^*(\tau)$, (5.67) becomes

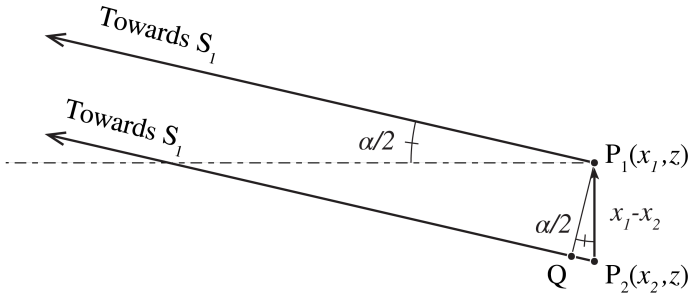


Figure 5.6: For z very large, S_1P_1 and S_1P_2 are almost parallel and $|S_1P_2|-|S_1P_1|\approx|QP_2|=|x_1-x_2|\alpha/2$.

$$\Gamma_{P_1P_2}(0)=2\mathrm{Re}\,\Gamma_0\left(\frac{\alpha}{2}\frac{(x_1-x_2)}{c}\right). \tag{5.71}$$

We conclude that for the fields in P_1 and P_2 to be coherent, the product of the angle α which the source subtends at the midpoint of P_1P_2 and the distance of P_1P_2 should be smaller than the coherence length $\Delta l_c = c\Delta\tau_c$. The smaller this product is the higher the degree of spatial coherence of P_1 and P_2.

The angle α decreases when the distance to the sources is increased and/or when the size of the source is decreased. Loosely speaking one can say that as the light propagates, it becomes

more coherent. When the distance to the source increases and/or when the size of the source is decreased the **difference in distance of all point sources to P_1 and P_2** decreases and will ultimately become smaller than the coherence length. Furthermore, for smaller α the fringe patterns on the distant screen in Young's experiment due to different point sources more strongly overlap which leads to a stronger overall fringe contrast.

As example consider quasi-monochromatic light for which (see (5.34)):

$$\Gamma_0(\tau) = I_0 e^{-i\bar{\omega}\tau}, \text{ for all } \tau. \tag{5.72}$$

where $\bar{\omega}$ is the centre frequency. In this case the coherence length Δl_c of the source is so large that the contributions to the total field of all individual point sources are coherent. Hence the only remaining criterion for coherence of the total fields in P_1 and P_2 is that the fringe patterns due to the different point sources in Young's experiment sufficiently overlap. Indeed, in this case of very long coherence time $\Delta\tau_c$ we have

$$\Gamma_{P_1P_2}(0) = 2I_0 \cos\left[\frac{\alpha}{2}\frac{\bar{\omega}|x_1 - x_2|}{c}\right], \tag{5.73}$$

and hence the degree of mutual coherence is:

$$\begin{aligned} \gamma_{P_1P_2}(0) &= \frac{\Gamma_{P_1P_2}(0)}{\sqrt{\Gamma_{P_1P_1}(0)}\sqrt{\Gamma_{P_2P_2}(0)}} \\ &= \cos\left[\frac{\alpha}{2}\frac{\bar{\omega}|x_1 - x_2|}{c}\right]. \end{aligned} \tag{5.74}$$

We see that when

$$|x_1 - x_2| < \bar{\lambda}/(2\alpha), \tag{5.75}$$

the fields in P_1 and P_2 are at least partially mutually coherent.

Example. We determine the maximum distance d between two points on earth for which sun light is coherent. The sun subtends on earth the angle:

$$\alpha = \frac{2R_\circ}{\text{AU}} \approx 0.015, \tag{5.76}$$

where AU and $R_\circ$ are the distance of the sun to the earth and the radius of the sun. Hence, for green light $\lambda = 550$nm and by requiring

$$d < \frac{\bar{\lambda}}{4\alpha}$$

for appreciable mutual coherence, we find $d_{\max} \approx 20\mu$m.

5.7 Stellar Interferometry

The property that the spatial coherence of two points decreases for increasing angle which the source subtends halfway between the two points, is used in **stellar interferometry**. It works as follows: we want to know the size of a certain star. The size of the star, being an extended spatially incoherent source, determines the spatial coherence of the light we receive on earth. Thus, by measuring the interference of the light collected by two transversely separated telescopes, one can effectively create a double-slit experiment, with which the degree of spatial coherence of the star light on earth can be measured, and thereby the angle which the star subtends on earth. The resolution in retrieving the angle from the spatial coherence is larger when the distance between

the telescopes is larger (see (5.74)). Then, if we know the distance of the star by independent means, e.g. from its spectral brightness, we can deduce its size from its angular size.

The method can also be used to derive the intensity distribution at the surface of the star. It can be shown that the degree of spatial coherence as function of the relative position of the telescopes is the Fourier transform of this intensity distribution. Hence, by moving the telescopes around and measuring the spatial coherence for many positions, the intensity distribution at the surface of the star can be derived from a back Fourier transform.

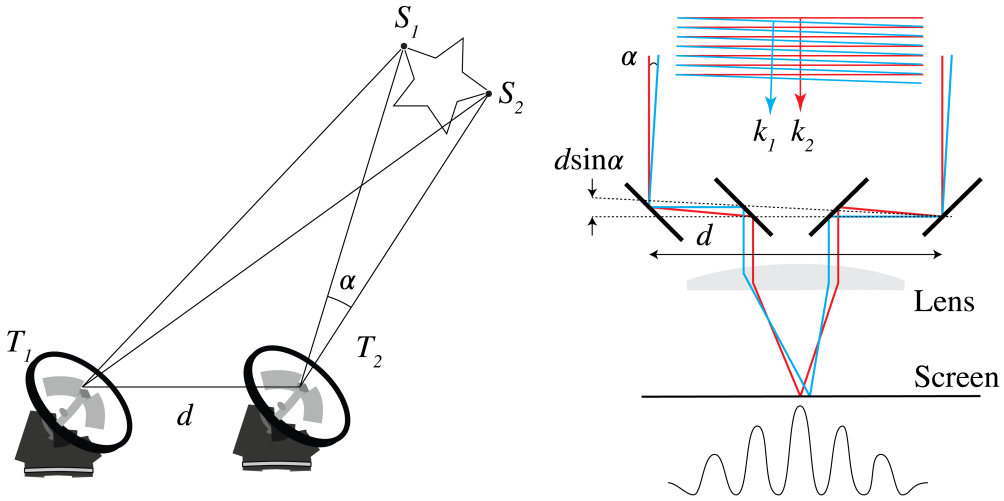


Figure 5.7: Left: a stellar interferometer with two telescopes that can be moved around to measure the interference at many relative positions. Right: single telescope with two outer movable mirrors. The telescope can move around it axis. The larger the distance d the higher the resolution.

5.8 Fringe contrast

We have seen that when the interference term $\mathrm{Re}\,\langle U_1 U_2^* \rangle$ vanishes, no fringes form, while when this term is nonzero, there are fringes. The **fringe contrast** is expressed directly in measurable intensities. Given some interference intensity pattern $I(x)$ as in Fig. 5.8, the fringe contrast is defined as

$$\mathcal{V} = \frac{I_{\max} - I_{\min}}{I_{\max} + I_{\min}}. \qquad \textbf{fringe contrast.} \tag{5.77}$$

For example, if we have two perfectly coherent, monochromatic point sources emitting the fields U_1, U_2 with intensities $I_1 = |U_1|^2$, $I_2 = |U_2|^2$, then the interference pattern is with (5.57):

$$I(\tau) = I_1 + I_2 + 2\sqrt{I_1 I_2}\cos(\omega\tau + \varphi). \tag{5.78}$$

We then get

$$I_{\max} = I_1 + I_2 + 2\sqrt{I_1 I_2}, \quad I_{\min} = I_1 + I_2 - 2\sqrt{I_1 I_2}, \tag{5.79}$$

so

$$\mathcal{V} = \frac{2\sqrt{I_1 I_2}}{I_1 + I_2}. \tag{5.80}$$

In case $I_1 = I_2$, we find $\mathcal{V} = 1$.

In contrast, when U_1 and U_2 are completely incoherent, we find

$$I(\tau) = I_1 + I_2, \tag{5.81}$$

from which follows

$$I_{\max} = I_{\min} = I_1 + I_2, \tag{5.82}$$

which gives $\mathcal{V} = 0$.

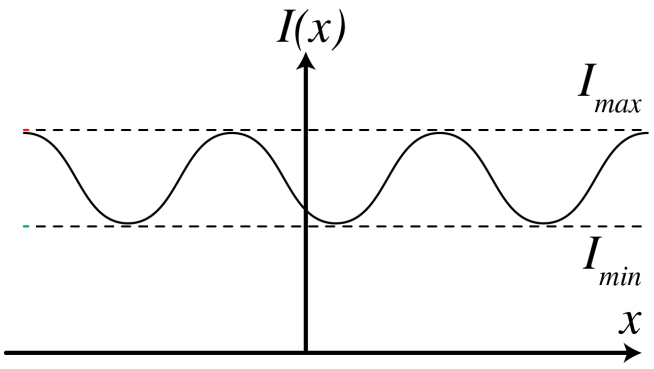


Figure 5.8: Illustration of $I_{\max}$ and $I_{\min}$ of an interference pattern $I(x)$ that determines the fringe contrast$\mathcal{V}$.

5.9 Fabry-Perot resonator

In interferometry two mutually coherent waves are added and the intensity of the sum of the two fields is measured. This intensity contains information about the phase difference of the waves from which for example a path length difference can be deduced. One distinguishes between two types of interferometers: **wavefront splitting interferometers** and **amplitude splitting interferometers**. Examples of the first type are Young's two slit experiment and Lloyd's mirror (Fig. (5.9)). Examples of amplitude splitting interferometers are the Michelson interferometer and the Fabry-Perot interferometer. The latter is not only a spectrometer of extremely high resolution but is also the resonance cavity in a laser.

A Fabry-Perot interferometer consists of two parallel highly reflecting surfaces with vacuum or a dielectric in between. These surfaces can be optical flats which have been coated by a metal like silver on one side. Consider a coordinate system as in Fig. 5.10 such that the reflecting surfaces are at $z = 0$ and $z = d$. The refractive indices of the half spaces $z < 0$ and $z > d$ are n_1 and n_3, respectively, and the refractive index of the medium between the surfaces is n_2. We will first assume that all refractive indices are real.

Let there be a plane wave **with unit amplitude** incident from $z < 0$ under angle θ_1 with the normal as shown in Fig. 5.10. The incident wave is assumed to be either s- or p-polarised. There are a reflected plane wave in $z < 0$, two plane waves in medium 2 one propagating in the positive z-direction and the other in the negative z-direction and there is a transmitted plane wave in $z > d$. It follows from the boundary conditions that the tangential component of the electric and magnetic field are continuous across the interfaces, that the tangential components of the wave vectors of all these plane waves are identical.

Let r_{ij} and t_{ij} be the reflection and transmission coefficient for a wave that is incident from medium i on the interface with medium j. When the wave is s-polarised, r_{12} and t_{12} are given by Fresnel coefficients (1.139),(1.140), whereas if the wave is p-polarised, they are given by (1.141), (1.142).

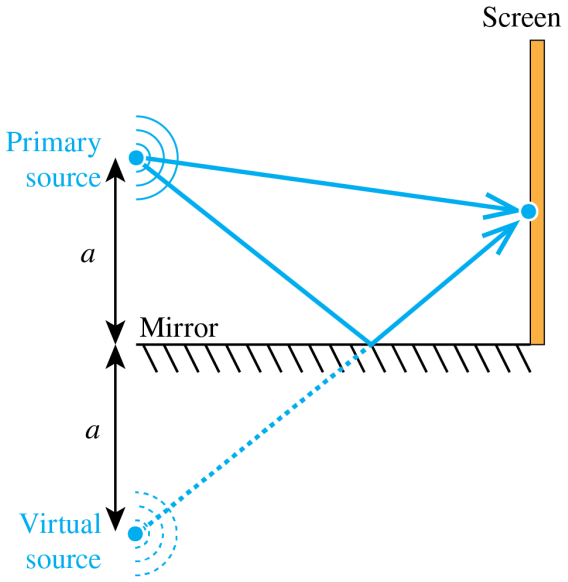


Figure 5.9: Lloyd's mirror as example of wavefront splitting interferometry.

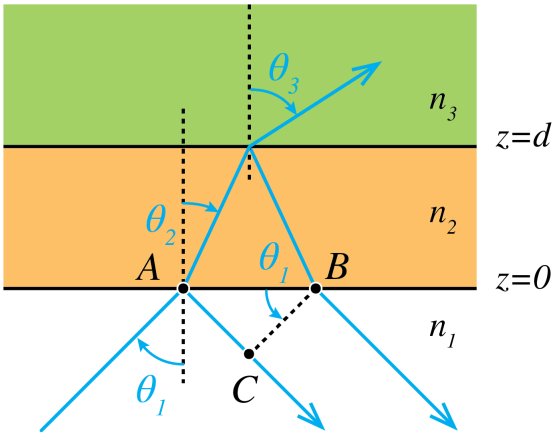


Figure 5.10: Fabry-Perot with 3 layers.The light comes from the bottom and is reflected by each interface.

The incident wave, which has amplitude 1 in point A, is partially reflected and partially transmitted by the interface $z = 0$. The reflected wave gets amplitude r_{12}. The transmitted field propagates in medium $0 < z < d$ to the interface at $z = d$ and is then partially reflected with reflection coefficient r_{23} back to the interface $z = 0$. Because the path length inside medium 2 is $2d/\cos\theta_2$, the complex amplitude B of this wave in point B after transmission by the interface $z = 0$ is

$$t_{21}r_{23}t_{21}e^{2ik_0n_2\frac{d}{\cos\theta_2}}, \tag{5.83}$$

where k_0 is the wave number in vacuum. To compute the interference of the directly reflected wave and the wave that has made one round trip in medium 2, the two fields should be evaluated at the same wavefront such as wavefront CB in Fig. 5.10. The directly reflected field in C is obtained by propagating from B over the distance

$$\begin{aligned} \mathrm{AC} &= \mathrm{AB}\sin\theta_1 \\ &= 2d\tan\theta_2\sin\theta_1 \\ &= 2d\frac{n_2}{n_1}\frac{\sin^2\theta_2}{\cos\theta_1}. \end{aligned} \tag{5.84}$$

where Snell's law: $n_1\sin\theta_1 = n_2\sin\theta_2$ has been used. Hence the total field due to the direct reflection at $z = 0$ and one round trip (5.83)

$$\begin{aligned} &r_{12}e^{i2k_0n_2\frac{\sin^2\theta_2}{cos\theta_2}} + t_{21}r_{23}t_{21}e^{2ik_0n_2\frac{d}{\cos\theta_2}} \\ &= e^{i2k_0n_2d\frac{\sin^2\theta_2}{\cos\theta_2}}\left(r_{12} + t_{21}r_{23}t_{12}e^{2ik_0n_2d\cos\theta_2}\right). \end{aligned} \tag{5.85}$$

The common phase factor in front of the brackets may be omitted since it does not influence the reflected intensity. We then obtain

$$r_{12} + t_{21}r_{23}t_{12}e^{2ik_z^{(2)}d}, \tag{5.86}$$

where,

$$k_z^{(2)} = k_0n_2\cos\theta_2,$$

is the z-component of the wave vector in medium 2 of the wave that propagates in the postive z-direction.

Incorporating the contributions of waves having made two or more round trips in the slab leads to the reflection coefficient of the Fabry-Perot when the field is incident from medium 1:

$$\begin{aligned} r &= r_{12} + t_{21}r_{13}t_{12}e^{2ik_z^{(2)}d}\left[1 + r_{23}r_{21}e^{2ik_z^{(2)}d} + (r_{23}r_{21}e^{2ik_z^{(2)}d})^2 + \ldots\right] \\ &= r_{12} + t_{21}r_{13}t_{12}e^{2ik_z^{(2)}d}\frac{1}{1 - r_{23}r_{21}e^{2ik_z^{(2)}d}} \\ &= \frac{r_{12} - r_{23}e^{2ik_z^{(2)}d}}{1 - r_{23}r_{21}e^{2ik_z^{(2)}d}}, \end{aligned} \tag{5.87}$$

where in the last step we used

$$\begin{aligned} t_{21} &= 1 + r_{21}, \\ t_{12} &= 1 + r_{12}, \\ r_{12} &= -r_{21} \end{aligned}$$

Similarly, the amplitude of the transmitted field in $z = d$ gives the transmission coefficient of the Fabry-Perot when the field is incident from medium 1:

$$\begin{aligned} t &= t_{12}t_{23}e^{ik_z^{(2)}d}\left[1 + r_{21}r_{23}e^{2k_z^{(2)}d} + (r_{21}r_{23}e^{ik_z^{(2)}d})^2 + \ldots\right] \\ &= \frac{t_{12}t_{23}e^{ik_z^{(2)}d}}{1 - r_{21}r_{23}e^{2ik_z^{(2)}d}}. \end{aligned} \tag{5.88}$$

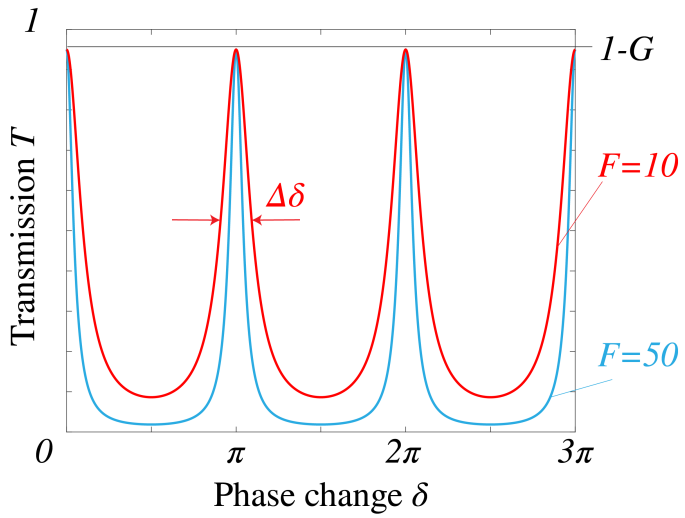


Figure 5.11: Transmission coefficient versus the phase change δ due to the Fabry-Perot. One can see the resonances occurring at every multiple of π.

Finally, the electric field between the reflectors is given by

$$\begin{aligned} U(z) &= t_{12}e^{ik_z^{(2)}z}\left[1 + r_{21}r_{23}e^{2ik_z^{(2)}d} + (r_{21}r_{23}e^{2ik_z^{(2)}d})^2 + \ldots +\right] \\ &\quad + t_{12}e^{ik_z^{(2)}(d-z)}\left[1 + r_{21}r_{23}e^{2ik_z^{(2)}d} + (r_{21}r_{23}e^{2ik_z^{(2)}d})^2 + \ldots +\right] \\ &= t_{12}\frac{e^{ik_z^{(2)}z} + r_{23}e^{ik_z^{(2)}(d-z)}}{1 - r_{21}r_{23}e^{2ik_z^{(2)}d}}, \end{aligned} \tag{5.89}$$

where the factor $\exp[i(k_x x + k_y y)]$ which gives the dependence on (x, y) has been omitted.

Define

$$G = \frac{(|r_{12}| - |r_{23}|)^2}{(1 - |r_{23}||r_{21}|)^2}, \tag{5.90}$$

$$F = \frac{4|r_{23}||r_{21}|}{(1 - |r_{23}||r_{21}|)^2}. \tag{5.91}$$

F is called the **coefficient of Finesse** of the Fabry-Perot. It is large when the mirrors are very good reflectors. The reflected and transmitted powers, relative to the incident power are then

$$R = |r|^2 = \frac{G + F\sin^2(k_z^{(2)}d)}{1 + F\sin^2(k_z^{(2)}d)}, \tag{5.92}$$

and

$$\begin{aligned} T &= |t|^2 = 1 - |R|^2 \\ &= \frac{1 - G}{1 + F\sin^2(k_z^{(2)}d)}. \end{aligned} \tag{5.93}$$

We define

$$\delta = k_z^{(2)}d, \tag{5.94}$$

which is the phase change due to one pass through the middle layer of the Fabry-Perot. Then (5.92) and (5.93) become

$$R = \frac{G + F\sin^2(k_z^{(2)}d)}{1 + F\sin^2\delta}. \tag{5.95}$$

$$T = \frac{1-G}{1+F\sin^2\delta}. \tag{5.96}$$

If the reflection by the mirrors is high: $|r_{21}| \approx 1$, $|r_{23}| \approx 1$, then F is large. This implies

$$R \approx 1, \quad T \approx 0, \tag{5.97}$$

for all δ except when $\sin(\delta) = 0$, i.e. when

$$\delta = m\pi, \tag{5.98}$$

for some positive integer m. With $k_0 = 2\pi/\lambda_0$ this becomes in terms of wavelength:

$$\frac{2d}{\lambda_0} n_2 \cos\theta_2 = m. \tag{5.99}$$

The wavelengths correspond to the maximum values of the transmission:

$$T_{max} = 1 - G. \tag{5.100}$$

and they are therefore called resonances. The width $\Delta\delta$ at a resonance is defined as the full width at half maximum (FWHM) of the transmission, i.e.

$$\frac{1-G}{1+\sin^2(m\pi + \Delta\delta/2)} = \frac{1}{2}(1-G), \tag{5.101}$$

which implies with $\sin^2(m\pi + \Delta\delta/2) \approx (\Delta\delta/2)^2$:

$$\Delta\delta = \frac{2}{\sqrt{F}}. \tag{5.102}$$

Using again $k_0 = 2\pi/\lambda_0$ and the fact that the width in terms of wavelength is small:

$$\begin{aligned} \frac{|\Delta\lambda_0|}{\lambda_0} &\approx \lambda_0 \Delta\left(\frac{1}{\lambda_0}\right) \\ &= = \lambda_0 \frac{\Delta\delta}{2\pi n_2 d\cos\theta_2} \\ &= \frac{\Delta\delta}{m\pi} \\ &= \frac{2}{m\pi\sqrt{F}} \end{aligned} \tag{5.103}$$

where (5.99) has been used. The resolution is defined as

$$\text{Resolution} = \frac{\lambda_0}{|\Delta\lambda_0|} = \frac{m\pi\sqrt{r_{23}||r_{21}|}}{1-|r_{23}||r_{21}|}. \tag{5.104}$$

The free spectral range is the distance between adjacent resonances:

$$\Delta\delta_{free} = \pi \tag{5.105}$$

With a similar derivation as for (5.103)

$$\begin{aligned} \frac{|(\Delta\lambda_0)_{free}|}{\lambda_0} &\approx -\lambda_0 \Delta\left(\frac{1}{\lambda_0}\right)_{free} \\ &= \frac{\Delta\delta_{free}}{m\pi} \\ &= \frac{1}{m}. \end{aligned} \tag{5.106}$$

A Fabry-Perot can be used as a high resolution spectrometer. Eq. (5.104) implies that the resolution increases for higher order m. However, M can not be made arbitrary large because increasing m means according to (5.106) that the free spectral range decreases. The ratio

$$\frac{(\Delta\lambda_0)_{free}}{(\Delta\lambda_0) = \frac{\pi}{2}\sqrt{F}}, \tag{5.107}$$

should therefore be large.

Example.
For a wavelength of $\lambda_0 = 600$nm and $n_f d = 12$mm we have for normal incidence $m = 40000$. Then, if the reflection coefficients satisfy $|r_{12}|^2 = |r_{23}|^2 = 0.9$, we have $F = 360$ and $G = 0$. The resolution is more than one million which is better than the grating spectrometers, which will be discussed in Section 6.4.3.

Remark. Although in the derivation we have assumed that all refractive indices are real, the final formulae also apply to the case that n_2 is complex. In that case $k_z^{(2)}$ and the reflection coefficients are complex.

5.10 Interference and polarisation

In the study of interference we have so far ignored the vectorial nature of light by assuming that all the fields have the same polarisation. Suppose now that we have two real vector fields $\boldsymbol{\mathcal{E}}_1$, $\boldsymbol{\mathcal{E}}_2$. The (instantaneous) intensity of each field is (apart from a constant factor) given by

$$\boldsymbol{\mathcal{E}}_1 \cdot \boldsymbol{\mathcal{E}}_1, \quad \boldsymbol{\mathcal{E}}_2 \cdot \boldsymbol{\mathcal{E}}_2. \tag{5.108}$$

If the two fields interfere, the instantaneous intensity is given by

$$(\boldsymbol{\mathcal{E}}_1 + \boldsymbol{\mathcal{E}}_2) \cdot (\boldsymbol{\mathcal{E}}_1 + \boldsymbol{\mathcal{E}}_2) = \boldsymbol{\mathcal{E}}_1 \cdot \boldsymbol{\mathcal{E}}_1 + \boldsymbol{\mathcal{E}}_2 \cdot \boldsymbol{\mathcal{E}}_2 + 2\boldsymbol{\mathcal{E}}_1 \cdot \boldsymbol{\mathcal{E}}_2, \tag{5.109}$$

where $2\boldsymbol{\mathcal{E}}_1 \cdot \boldsymbol{\mathcal{E}}_2$ is the interference term. Suppose the polarisation of $\boldsymbol{\mathcal{E}}_1$ is orthogonal to the polarisation of $\boldsymbol{\mathcal{E}}_2$, e.g.

$$\boldsymbol{\mathcal{E}}_1 = \begin{pmatrix} \mathcal{E}_{1x} \\ 0 \\ 0 \end{pmatrix}, \quad \boldsymbol{\mathcal{E}}_2 = \begin{pmatrix} 0 \\ \mathcal{E}_{2y} \\ 0 \end{pmatrix}. \tag{5.110}$$

Then $\boldsymbol{\mathcal{E}}_1 \cdot \boldsymbol{\mathcal{E}}_2 = 0$, which means the two fields can not interfere. This observation is the

First Fresnel-Arago Law: fields with orthogonal polarisation cannot interfere.

Next we write the fields in terms of orthogonal components

$$\boldsymbol{\mathcal{E}}_1 = \begin{pmatrix} \mathcal{E}_{1\perp} \\ \mathcal{E}_{1\parallel} \end{pmatrix}, \quad \boldsymbol{\mathcal{E}}_2 = \begin{pmatrix} \mathcal{E}_{2\perp} \\ \mathcal{E}_{2\parallel} \end{pmatrix}. \tag{5.111}$$

This is always possible, whether the fields are polarised or randomly polarised. Then (5.109) becomes

$$\boldsymbol{\mathcal{E}}_1 \cdot \boldsymbol{\mathcal{E}}_1 + \boldsymbol{\mathcal{E}}_2 \cdot \boldsymbol{\mathcal{E}}_2 + 2\boldsymbol{\mathcal{E}}_1 \cdot \boldsymbol{\mathcal{E}}_2 = \mathcal{E}_{1\perp}^2 + \mathcal{E}_{2\perp}^2 + 2\mathcal{E}_{1\perp}\mathcal{E}_{2\perp} + \mathcal{E}_{1\parallel}^2 + \mathcal{E}_{2\parallel}^2 + 2\mathcal{E}_{1\parallel}\mathcal{E}_{2\parallel}. \tag{5.112}$$

If the fields are randomly polarised, the time average of the $\perp$-part will equal the average of the $\parallel$-part, so the time-averaged intensity becomes

$$\begin{aligned} I &= 2\left\langle \mathcal{E}_{1\perp}^2 + \mathcal{E}_{2\perp}^2 + 2\mathcal{E}_{1\perp}\mathcal{E}_{2\perp} \right\rangle \\ &= 2\left\langle \mathcal{E}_{1\parallel}^2 + \mathcal{E}_{2\parallel}^2 + 2\mathcal{E}_{1\parallel}\mathcal{E}_{2\parallel} \right\rangle . \end{aligned} \tag{5.113}$$

This is qualitatively the same as what we would get if the fields had parallel polarisation, e.g.

$$\boldsymbol{\mathcal{E}}_1 = \begin{pmatrix} \mathcal{E}_{1\perp} \\ 0 \end{pmatrix}, \quad \boldsymbol{\mathcal{E}}_2 = \begin{pmatrix} \mathcal{E}_{2\perp} \\ 0 \end{pmatrix}. \tag{5.114}$$

This leads to the

Second Fresnel-Arago Law: two fields with parallel polarisation interfere the same way as two fields that are randomly polarised.

This indicates that our initial assumption in the previous sections that all our fields have parallel polarisation is not as limiting as it may have appeared at first.

Suppose now that we have some field

$$\boldsymbol{\mathcal{E}} = \begin{pmatrix} \mathcal{E}_{\perp} \\ \mathcal{E}_{\parallel} \end{pmatrix}, \tag{5.115}$$

which is **randomly polarised**. Suppose we separate the two polarisations, and rotate one so that the two resulting fields are aligned, e.g.

$$\boldsymbol{\mathcal{E}}_1 = \begin{pmatrix} \mathcal{E}_{\perp} \\ 0 \end{pmatrix}, \quad \boldsymbol{\mathcal{E}}_2 = \begin{pmatrix} \mathcal{E}_{\parallel} \\ 0 \end{pmatrix}. \tag{5.116}$$

These fields can not interfere because $\mathcal{E}_{\perp}$ and $\mathcal{E}_{\parallel}$ are incoherent. This leads to the

Third Fresnel-Arago Law: the two constituent orthogonal linearly polarised states of natural light cannot interfere to form a readily observable interference pattern, even if rotated into alignment.

External sources in recommended order

1. Veritasium - The original double-slit experiment, starting at 2:15 - Demonstration of an interference pattern obtained with sunlight.
2. MIT OCW - Two-beam Interference - Collimated Beams: Interference of laser light in a Michelson interferometer.
3. MIT OCW - Fringe Contrast - Path Difference: Demonstration of how fringe contrast varies with propagation distance.
4. MIT OCW - Coherence Length and Source Spectrum: Demonstration of how the coherence length depends on the spectrum of the laser light.
5. Lecture - 18 Coherence: Lecture Series on Physics - I: Oscillations and Waves by Prof. S. Bharadwaj, Department of Physics and Meteorology, IIT Kharagpur.
6. Lecture - 19 Coherence: Lecture Series on Physics - I: Oscillations and Waves by Prof. S. Bharadwaj, Department of Physics and Meteorology, IIT Kharagpur.

Problems

1. **Michelson interferometer.**
   a) A Michelson interferometer is illuminated with monochromatic light. One of its mirrors is moved 2.53×10^{-5} m, and it is observed that 92 fringe-pairs, bright and dark, pass by the screen during the process. Determine the wavelength of the incident beam.
   b) Suppose that for the wavelength determined under a), only 23 fringes can be distinguished when one of the mirrors in moved over 2.53×10^{-5} m. What is the coherence length and coherence time of the source?
2. **Two sources.**
   a) Suppose the two sources S_1 and S_2 are coherent and emit radio waves with a wavelength of 3 m. The two sources are in phase, and they are separated by 3 m. How far should an observer be directly in front of either source (along a perpendicular to $\overline{S_1 S_2}$, see Fig. 5.12), to encounter a minimum of irradiance?

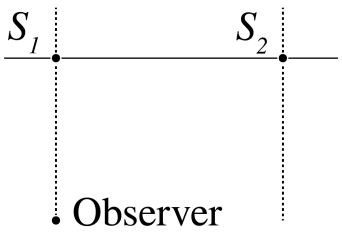


Figure 5.12

   b) Suppose that the sources are mutually incoherent. Their distance is again 3 m and the centre wavelength is 3 m. What should be the perpendicular distance to the two sources of two points that have distance of 6 m when the degree of mutual coherence is 0.866. You may use the formula for quasi-monochromatic light.
3. **Reflection coating.** A thin planar film with an index of refraction of $n_2 = 1.5$ is immersed in air with $n_1 = 1$ as shown in Fig 5.13. A plane wave with a wavelength of $\lambda = 632$ nm hits the film at an angle of incidence of $\theta_1 = 30°$ with respect to the normal on the surface. Some of the light will reflect directly at the air-film interface, and some of the light will make one or several round trips through the film and then adds to the directly reflected light. In this exercise we only consider the directly reflected light at the air-film interface and the light that makes one round trip inside the film.

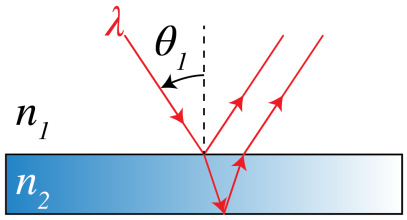


Figure 5.13: Thin film illuminated by a plane wave.

a) What is the smallest film thickness for which we get a maximum reflectance of the film? We recall that the light that is reflected directly at the air-glass interface gets a phase shift of π.

b) Describe what happens to the reflected field when the film is 237 nm thick?

4. **Point source and mirror.** Let a point source P be at $\mathbf{r}_p = (0, 0, d)$ where $d > 0$ is the distance to a mirror in the $z = 0$ plane (Fig. 5.14).

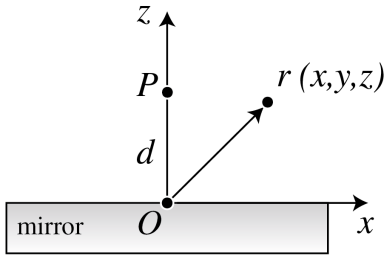


Figure 5.14: A point source P above a perfect mirror.

The point source emits a time-harmonic field with complex amplitude in a point $\mathbf{r} = (x, y, z)$ given by

$$U_p(\mathbf{r}) = \frac{e^{ik\sqrt{x^2+y^2+(z-d)^2}}}{\sqrt{x^2+y^2+(z-d)^2}}.$$

Assume that the mirror is perfect, i.e. the total field on the mirror surface vanishes: $U_{total}(x, y, 0) = 0$.

a) Derive the formula for the reflected and the total field in an arbitrary point $\mathbf{r} = (x, y, z)$ with $z > 0$.

b) What is the total intensity in an arbitrary point $\mathbf{r}$?

c) Compute the intensity on the z-axis for $0 \leq z \leq d$. What is the period of the fringes? For which z-value does the intensity vanish?

d) Derive the intensity for $x = y = 0$ and $z > d$. Show that for very large z the intensity is zero when $d = (2m + 1)\lambda/4$ for $m = 0, 1, 2, \ldots$.

e) Suppose that the coherence time of the field radiated by the point source is τ_c. For which distances d does there occur no interference anywhere in $z > 2d$ between the field directly radiated by the point source and the reflected field? What is the intensity in this case?

5. **Two sources and two pinholes.** Two independently radiating small sources S_1 and S_2 emit light with centre frequency ω_c and bandwidth $\Delta\omega \ll \omega_c$. (see the figure below). The coherence time of the sources is thus $\tau_c = \Delta\omega$. At a distance z_1 a first screen with pinholes P_1 and P_2 is placed. Far away, at (Fraunhofer) distance z_2 from the first screen a second screen is placed. Which of the following statements are true

a) The interference fringes disappear if the differences between distances: $|P_1S_1 - P_2S_1|$ and $|P_1S_2 - P_2SA_2|$ are larger than $l_c = \tau_c c$.

b) There are no fringes on the second screen if one of the sources S_1 or S_2 is switched off.

c) There can only be fringes on the second screen when there is only one source.

d) The interference fringe contrast on the second screen decreases when z_2 is decreased.

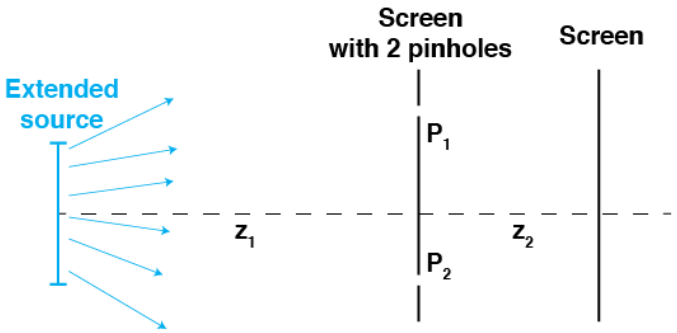


Figure 5.15: Two independent small sources S_1 and S_2 with 2 pinholes and a screen (Exercise 4).

e) The interference fringe contrast on the second screen decreases when z_1 is increased.

f) There are no fringes when the pinholes are of the order of a wavelength and one of the pinholes is closed.

g) There are interference fringes on the screen when the distance z_1 is large enough and the pinholes have width of many wavelength and one of them is closed.

h) If more pinholes are added between P_1 and P_2 the interference fringes become broader.

Chapter 6

Scalar Diffraction Optics

What you should know and be able to do after studying this chapter

- Be able to derive the angular spectrum decomposition, also known as the plane wave expansion, and understand its physical interpretation.
- Know the Rayleigh-Sommerfeld formula; in particular be able to write down the integral over spherical waves with amplitudes proportional to the field in the starting plane.
- Know how to deduce the Fresnel and Fraunhofer approximation of the Rayleigh-Sommerfeld integral and understand their relation to the Fourier transformation.
- Understand intuitively in what sense the Fourier transform is linked to resolution.
- Understand why propagation of light leads to loss of resolution (i.e. the evanescent waves disappear).
- Understand why propagation to the focal plane of a lens corresponds to taking the Fourier transform.
- Understand how the Numerical Aperture (NA) of a lens ultimately determines the resolution of images.
- Understand how a lens can be used for Fourier filtering.

6.1 Introduction

In this chapter we will study how light propagates as a wave. In the study of the double-slit experiment we concluded from the interference pattern observed on a screen that light is a wave. To demonstrate more convincingly that light is indeed a wave, we require a detailed quantitative model of the propagation of light, which gives experimentally verifiable predictions.

But a precise description of the propagation of light is not only important for fundamental science, it also has many practical applications. For example, if a sample must be analysed by illuminating it and measuring the scattered light, the fact that the detected light has not only been affected by the sample, but by both the sample and propagation has to be taken into account. Another example is lithography. If a pattern has to be printed onto a substrate using a mask that is illuminated and there is a certain distance between the mask and the photoresist, the light which reaches the resist does not have the exact shape of the mask due to propagation effects. Therefore the mask needs to be designed to compensate for these effects.

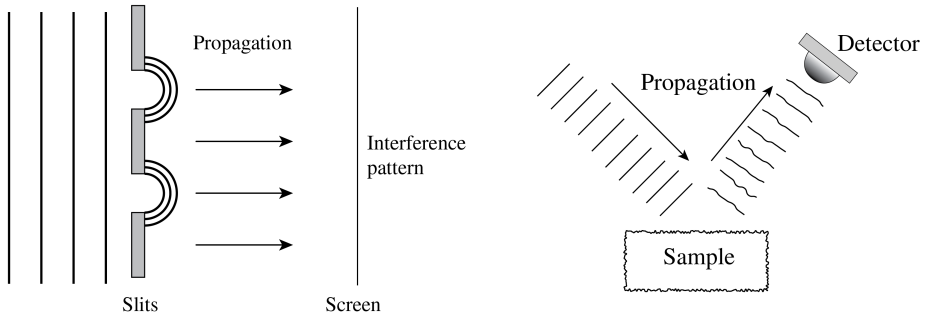


Figure 6.1: A quantitative model of the propagation of light is required to predict the properties of propagation and to apply it in sample analyses and lithography.

In Section 1.4 we have derived that in homogeneous matter (i.e. the permittivity is independent of position), every component U of a time-harmonic electromagnetic field satisfies the scalar Helmholtz equation (1.46):

$$\left(\nabla^2 + k^2\right) U(\mathbf{r}) = 0, \tag{6.1}$$

where $k = \omega\sqrt{\epsilon\mu_0}$ is the wave number of the light in matter with permittivity ϵ and refractive index $n = \sqrt{\epsilon/\epsilon_0}$.

When the refractive index is not independent of position, Maxwell's equations are no longer equivalent to the wave equation for the individual electromagnetic field components and there is then coupling between the components due to the curl operators in Maxwell's equation. When the variation of the refractive index is slow on the scale of the wavelength, the scalar wave equation may still be a good approximation, but for structures that vary on the scale of the wavelength (i.e. on the scale of ten microns or less), the scalar wave equation is not sufficiently accurate.

6.2 Propagation of light through a homogeneous medium

We will describe two equivalent methods to compute the propagation of a time-harmonic field through homogeneous matter, namely the angular spectrum method and the Rayleigh-Sommerfeld diffraction formula. Our goal is to derive the field in some point (x, y, z) with $z > 0$, given the field in the plane $z = 0$, as illustrated in Fig. 6.2. The sources of the field are assumed to be in the half space $z < 0$. Although both methods in the end describe the same, they give physical insight into different aspects of propagation. As usual for time-harmonic fields, we will omit the implicit time dependence $\exp(-i\omega t)$ from all formulae.

6.2.1 Angular Spectrum Method

One way to see how light propagates from one plane to another is by using the **angular spectrum method**. We decompose the field in plane waves by taking the two-dimensional Fourier transform. Since we know how each plane wave propagates, we can propagate each Fourier component separately and then add them all together by taking the inverse Fourier transform. Mathematically this is described as follows: we know the field $U(x, y, 0)$. We will write $U_0(x, y) = U(x, y, 0)$ for convenience and apply a two-dimensional Fourier transform to U_0:

$$\mathcal{F}(U_0)(\xi, \eta) = \int\int U_0(x, y) e^{-2\pi i(\xi x + \eta y)} \, \mathrm{d}x\mathrm{d}y, \tag{6.2}$$

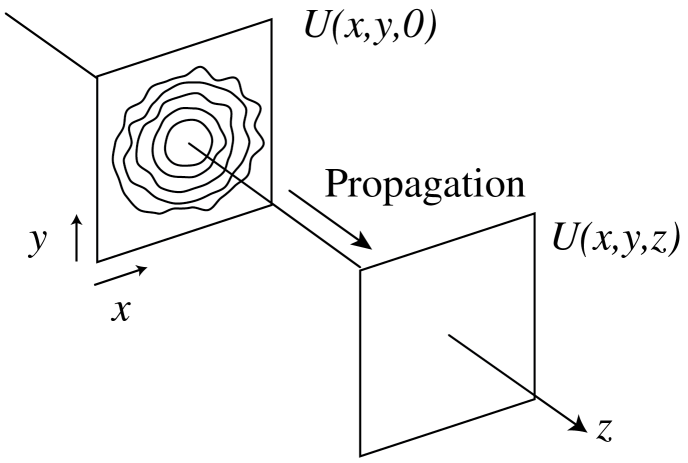


Figure 6.2: Given the field $U(x, y, 0)$, we want to find U in a point (x, y, z) with $z > 0$. It is assumed that the field propagates in the positive z-direction and that all sources are in the region $z < 0$.

The inverse Fourier transform implies:

$$U_0(x,y) = \int\int \mathcal{F}(U_0)(\xi,\eta) e^{2\pi i(\xi x+\eta y)}\, \mathrm{d}\xi \mathrm{d}\eta \tag{6.3}$$

$$= \mathcal{F}^{-1}\{\mathcal{F}(U_0)\}(x,y). \tag{6.4}$$

Important properties of the Fourier transform are listed in Appendix E. By defining $k_x = 2\pi\xi$, $k_y = 2\pi\eta$, (6.3) can be written as

$$U_0(x,y) = \frac{1}{4\pi^2} \int\int \mathcal{F}(U_0)\left(\frac{k_x}{2\pi}, \frac{k_y}{2\pi}\right) e^{i(k_x x+k_y y)}\, \mathrm{d}k_x \mathrm{d}k_y. \tag{6.5}$$

The variables in the Fourier plane: (ξ, η) and (k_x, k_y) are called **spatial frequencies**.

Eq. (6.5) says that we can write $U_0(x, y) = U(x, y, z = 0)$ as an integral (a sum) of plane waves[1] with wave vector $\mathbf{k} = (k_x, k_y, k_z)^T$, each with its own weight (i.e. complex amplitude) $\mathcal{F}(U_0)\left(\frac{k_x}{2\pi}, \frac{k_y}{2\pi}\right)$. We know how each plane wave with complex amplitude $\mathcal{F}(U_0)\left(\frac{k_x}{2\pi}, \frac{k_y}{2\pi}\right)$ and wave vector $\mathbf{k} = (k_x, k_y, k_z)^T$ propagates over a distance $z > 0$

$$\mathcal{F}(U_0)\left(\frac{k_x}{2\pi}, \frac{k_y}{2\pi}\right) e^{i(k_x x+k_y y)} \to \mathcal{F}(U_0)\left(\frac{k_x}{2\pi}, \frac{k_y}{2\pi}\right) e^{i(k_x x+k_y y+k_z z)}, \tag{6.6}$$

Therefore, the field $U(x, y, z)$ in a plane $z > 0$ is given by

$$U(x,y,z) = \frac{1}{4\pi^2} \int\int \mathcal{F}(U_0)\left(\frac{k_x}{2\pi}, \frac{k_y}{2\pi}\right) e^{i(k_x x+k_y y+k_z z)}\, \mathrm{d}k_x\, \mathrm{d}k_y, \tag{6.7}$$

where

$$k_z = \sqrt{\left(\frac{2\pi}{\lambda}\right)^2 - k_x^2 - k_y^2}, \tag{6.8}$$

[1] Every picture is made of waves - Sixty Symbols, 3:33 to 7:15: Basic explanation of Fourier transforms. Also see Section 6.3.

with λ the wavelength of the light as measured **in the material** (hence, $\lambda = \lambda_0/n$, with λ_0 the wavelength in vacuum). The sign in front of the square root in (6.8) could in principle be chosen negative: one would then also obtain a solution of the Helmholtz equation. The choice of the sign of k_z is determined by the direction in which the light propagates, which in turn depends on the location of the sources **and** on the convention chosen for the time dependence. We have to choose here the + sign in front of the square root because the sources are in $z < 0$ and the time dependence of time-harmonic fields is (as always in this book) given by $e^{-i\omega t}$ with $\omega > 0$.

Eq. (6.7) can be written alternatively as

$$U(x, y, z) = \mathcal{F}^{-1}\{\mathcal{F}(U_0)(\xi, \eta)e^{ik_z z}\}(x, y), \tag{6.9}$$

where now k_z has to be considered as a function of (ξ, η):

$$k_z = 2\pi\sqrt{\left(\frac{1}{\lambda}\right)^2 - \xi^2 - \eta^2}. \tag{6.10}$$

Note that one can interpret this as a diagonalisation of the propagation operator, as explained in Appendix F.

We can observe something interesting: if $k_x^2 + k_y^2 > \left(\frac{2\pi}{\lambda}\right)^2$, then k_z becomes imaginary, and $\exp(ik_z z)$ decays exponentially for increasing z:

$$\exp\left\{i\left[k_x x + k_y y + z\sqrt{\left(\frac{2\pi n}{\lambda}\right)^2 - k_x^2 - k_y^2}\right]\right\} = e^{i(k_x x + k_y y)}e^{-z\sqrt{k_x^2+k_y^2-\left(\frac{2\pi}{\lambda}\right)^2}}. \tag{6.11}$$

These exponentially decaying waves are called **evanescent in the positive z-direction**. We have met evanescent waves already in the context of total internal reflection discussed in Section 1.9.5. The physical consequences of evanescent waves in the angular spectrum decomposition will be explained in Section 6.3.

The waves for which k_z is real have constant amplitude: only their phase changes due to propagation. These waves therefore are called **propagating waves**.

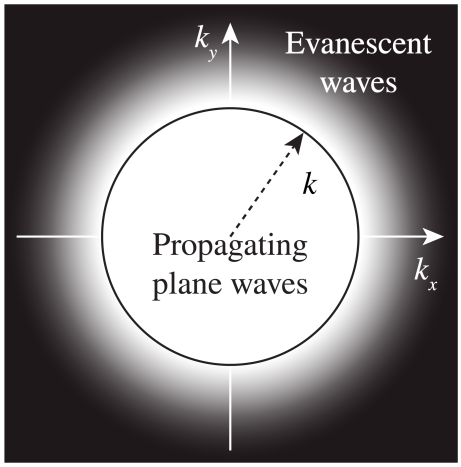


Figure 6.3: The spatial frequencies k_x, k_y of the plane waves in the angular spectrum of a time-harmonic field which propagates in the z-direction. There are two types of waves: the propagating waves with spatial frequencies inside the circle $\sqrt{k_x^2 + k_y^2} < k = 2\pi/\lambda$ and which have phase depending on the propagation distance z but constant amplitude, and the evanescent waves for which $\sqrt{k_x^2 + k_y^2} > k$ and of which the amplitude decreases exponentially during propagation.

Remark. In homogeneous space, the scalar Helmholtz equation for every electric field component is equivalent to Maxwell's equations and hence we may propagate each component E_x, E_y and E_z individually using the angular spectrum method. If the data in the plane $z = 0$ of these field components are physically consistent, the electric field thus obtained will automatically satisfy the condition that the electric field is free of divergence, i.e.

$$\nabla \cdot \mathbf{E} = 0, \tag{6.12}$$

everywhere in $z > 0$. This is equivalent to the statement that the electric vectors of the plane waves in the angular spectrum are perpendicular to their wave vectors. Alternatively, one can propagate only the E_x- and E_y-components and afterwards determine E_z from the condition that (6.12) must be satisfied.

6.2.2 Rayleigh-Sommerfeld Diffraction Integral

Another method to propagate a wave field is by using the **Rayleigh-Sommerfeld** integral. A very good approximation of this integral states that each point in the plane $z = 0$ emits spherical waves with amplitude proportional to the field in the plane $z = 0$. To find the field in a point (x, y, z), we have to add the contributions from all these point sources together. This corresponds to the Huygens-Fresnel principle postulated earlier in Section 5.5. Because a more rigorous derivation starting from the Helmholtz equation[3] would be rather lengthy, we will just give the final result:

$$\begin{aligned} U(x,y,z) &= \frac{1}{i\lambda}\int\int U_0(x',y')\frac{z\,e^{ik\sqrt{(x-x')^2+(y-y')^2+z^2}}}{(x-x')^2+(y-y')^2+z^2}\,\mathrm{d}x'\,\mathrm{d}y' \\ &= \frac{1}{i\lambda}\int\int U_0(x',y')\frac{z}{r}\frac{e^{ikr}}{r}\,\mathrm{d}x'\,\mathrm{d}y', \end{aligned} \tag{6.13}$$

where we wrote again $U_0(x, y) = U(x, y, 0)$ and where

$$r = \sqrt{(x-x')^2+(y-y')^2+z^2}. \tag{6.14}$$

Remarks.

1. The formula (6.13) is not completely rigorous because a term that is a factor $1/(kr)$ smaller (and which in practice therefore is very much smaller) has been omitted.

2. In (6.13) there is an additional factor z/r that has been omitted in the time-harmonic spherical wave as given in (1.53) and at the right-hand side of (5.43). This factor means that the amplitudes of the spherical waves in the Rayleigh-Sommerfeld diffraction integral depend on direction (although their wave fronts are spherical), the amplitudes being largest in the forward direction.

3. The angular spectrum method amounts to a multiplication by $\exp(izk_z)$ in Fourier space, while the Rayleigh-Sommerfeld integral is a convolution with respect to (x, y). It is a property of the Fourier transform that a multiplication in Fourier space corresponds to a convolution in real space and vice versa. Indeed a mathematical result called **Weyl's identity**

[3] For a rigorous derivation see e.g. J. Goodman, *Introduction to Fourier Optics*, §3.3, §3.4, §3.5 - and *Lecture Notes of Advanced Photonics*, Delft University of Technology.

implies that the rigorous version of (6.13) and the plane wave expansion (i.e. the angular spectrum method) give identical results.

6.3 Intuition for the Spatial Fourier Transform in Optics

Since spatial Fourier transformations play an important role in our discussion of the propagation of light, it is important to understand them not just mathematically, but also intuitively.

What happens when an object is illuminated and the reflected or transmitted light is detected at some distance from the object? Let us look at transmission for example. When the object is much larger than the wavelength, a transmission function $\tau(x, y)$ is often defined and the field transmitted by the object is then assumed to be simply the product of the incident field and the function $\tau(x, y)$. For example, for a hole in a metallic screen with diameter large compared to the wavelength, the transmission function would be 1 inside the hole and 0 outside. However, if the object has features of the size of the order of the wavelength, this simple model of multiplying by a transmission function breaks down and the transmitted field must instead be determined by solving Maxwell's equations. This is not easy, but some software packages can do it.

Now suppose that the transmitted electric field has been obtained in a plane $z = 0$ very close to the object (a distance within a fraction of a wavelength). This field is called the **transmitted near field** and it may have been obtained by simply multiplying the incident field with a transmission function $\tau(x, y)$ or by solving Maxwell's equations. This transmitted near field is a kind of footprint of the object. But it should be clear that, although it is quite common in optics to speak in terms of "imaging an object", strictly speaking we do not image an object as such, but we image the transmitted or reflected near field which is a kind of copy of the object. After the transmitted near field has been obtained, we apply the angular spectrum method to propagate the individual plane waves through homogeneous matter (e.g. air) from the object to the detector plane or to an optical element like a lens.

Let $U_0(x, y) = U(x, y, 0)$ be a component of the transmitted near field. The first step is to Fourier transform it, by which the field component is decomposed in plane waves. To each plane wave, characterised by the wave numbers k_x and k_y, the Fourier transform assigns a complex amplitude $\mathcal{F}(U_0)\left(\frac{k_x}{2\pi}, \frac{k_y}{2\pi}\right)$, the magnitude of which indicates how important the role is which this particular wave plays in the formation of the near field. So what can be said about the object field $U_0(x, y)$, by looking at the magnitude of its spatial Fourier transform $|\mathcal{F}(U_0)\left(\frac{k_x}{2\pi}, \frac{k_y}{2\pi}\right)|$?

Suppose $U_0(x, y)$ has sharp features, i.e. there are regions where $U_0(x, y)$ varies rapidly as a function of x and y. To describe these features as a combination of plane waves, these waves must also vary rapidly as a function of x and y, which means that the length of their wave vectors $\sqrt{k_x^2 + k_y^2}$ must be large. Thus, the sharper the features that $U_0(x, y)$ has, the larger we can expect $|\mathcal{F}(U_0)\left(\frac{k_x}{2\pi}, \frac{k_y}{2\pi}\right)|$ to be for large $\sqrt{k_x^2 + k_y^2}$, i.e. high spatial frequencies can be expected to have large amplitude. Similarly, the slowly varying, broad features of $U_0(x, y)$ are described by slowly fluctuating waves, i.e. by $\mathcal{F}(U_0)\left(\frac{k_x}{2\pi}, \frac{k_y}{2\pi}\right)$ for small $\sqrt{k_x^2 + k_y^2}$, i.e. for low spatial frequencies. This is illustrated in Fig. 6.4.

To investigate these concepts further we choose a certain field, take its Fourier transform, remove the higher spatial frequencies and then invert the Fourier transform. We then expect that the resulting field has lost its sharp features and only retains its broad features, i.e. the image is blurred. Conversely, if we remove the lower spatial frequencies but retain the higher, then the result will only show its sharp features, i.e. its contours. These effects are shown in Fig. 6.5. Recall that when $k_x^2 + k_y^2 > \left(\frac{2\pi}{\lambda}\right)^2$, the plane wave decays exponentially as the field propagates. Because by propagation through homogeneous space, the information contained in the high spatial frequencies corresponding to evanescent waves is lost (only exponentially small amplitudes of the evanescent waves remain), perfect imaging is impossible, no matter how

well-designed an optical system is.

> Propagation of light leads to irrecoverable loss of resolution.

It is this fact that motivates near-field microscopy, which tries to detect these evanescent waves by scanning close to the sample, thus obtaining subwavelength resolution.

So we have seen how we can guess properties of some object field $U_0(x, y)$ given the amplitude of its spatial Fourier transform $|\mathcal{F}(U_0)\left(\frac{k_x}{2\pi}, \frac{k_y}{2\pi}\right)|$. But what about the phase of $\mathcal{F}(U_0)\left(\frac{k_x}{2\pi}, \frac{k_y}{2\pi}\right)$? Although one cannot really guess properties of $U_0(x, y)$ by looking at the phase of $\mathcal{F}(U_0)\left(\frac{k_x}{2\pi}, \frac{k_y}{2\pi}\right)$ the same way as we can by looking at its amplitude, it is in fact the phase that plays a larger role in defining $U_0(x, y)$. This is illustrated in Fig. 6.6: if the amplitude information of $\mathcal{F}(U_0)\left(\frac{k_x}{2\pi}, \frac{k_y}{2\pi}\right)$ is removed, features of the original $U_0(x, y)$ may still be retrieved. However, if we only know the amplitude $|\mathcal{F}(U_0)(k_x, k_y)|$ but not the phase, then the original object is completely lost. Thus, the phase of a field $\mathcal{F}(U_0)$ is very important, arguably often more important than its amplitude. However, we cannot measure the phase of a field directly, only its intensity $I = |\mathcal{F}(U_0)|^2$ from which we can calculate the amplitude $|\mathcal{F}(U_0)|$. It is this fact that makes **phase retrieval** an entire field of study on its own: how can we find the phase of a field, given that we can only perform intensity measurements? This question is related to a new field of optics called "lensless imaging", where amplitudes and phases are retrieved from intensity measurements and the image is reconstructed **computationally**. Interesting as this topic may be, we will not treat it in these notes and refer instead to master courses in optics [5].

Remark. The importance of the phase for the field can also be seen by looking at the plane wave expansion (6.7). We have seen that the field in a plane $z =$ constant can be obtained by propagating the plane waves by multiplying their amplitudes by the phase factors $\exp(izk_z)$, which depends on the propagation distance z. If one leaves the evanescent waves out of consideration (since after some distance they hardly contribute to the field anyway), it follows that only the phases of the plane waves change upon propagation, while their amplitudes (the moduli of their complex amplitudes) do not change. Yet, depending on the propagation distance z, widely differing light patterns are obtained (see e.g. Fig. 6.10).

Another aspect of the Fourier transform is the **uncertainty principle**. It states that many waves of different frequencies have to be added to get a function that is confined to a small space[7]. Stated differently, if $U(x, y)$ is confined to a very small region, then $\mathcal{F}(U)(k_x, k_y)$ must be very spread out. This can also be illustrated by the scaling property of the Fourier transform:

$$\text{if} \quad h(x) = f(ax) \quad \text{then} \quad \mathcal{F}(h)\left(\frac{k_x}{2\pi}\right) = \frac{1}{|a|}\mathcal{F}(f)\left(\frac{k_x}{2\pi a}\right), \tag{6.15}$$

which simply states that the more $h(x)$ is squeezed by increasing a, the more its Fourier transform $\mathcal{F}(h)$ spreads out. This principle is illustrated in Fig. 6.7. The uncertainty principle is familiar from quantum physics where it is stated that a particle cannot have both a definite momentum and a definite position. In fact, this is just one particular manifestation of the uncertainty principle just described. A quantum state $|\psi\rangle$ can be described in the position basis $\psi_x(x)$ as well as in the momentum basis $\psi_p(p)$. The basis transformation that links these two expressions is the Fourier transform

$$\psi_p(p) = \mathcal{F}\{\psi_x(x)\}(p). \tag{6.16}$$

[5] See the course Advanced Photonics given at TU Delft.

[7] Heisenberg's Microscope - Sixty Symbols, 0:20 to 2:38: Basic explanation of the uncertainty principle (though in the context of quantum physics)

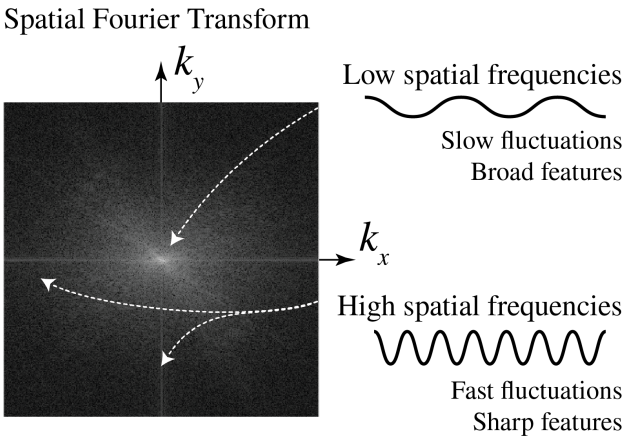


Figure 6.4: A qualitative interpretation of spatial Fourier transforms. The low spatial frequencies (i.e. small $\sqrt{k_x^2 + k_y^2}$) represent slow fluctuations, and therefore contribute to the broad features of the real-space object. The high spatial frequencies (i.e. large $\sqrt{k_x^2 + k_y^2}$) fluctuate rapidly, and can therefore form sharp features in the real-space object.

Hence, the two are obviously subject to the uncertainty principle! In fact, any two quantum observables which are related by a Fourier transform (also called conjugate variables), such as position and momentum, obey this uncertainty relation. The **uncertainty relation** states:

If a function $f(x)$ has width Δx, its Fourier transform has a width $\Delta k_x \approx 2\pi/\Delta x$.

Since after propagation over a distance z larger than the wavelength the contribution of the evanescent waves to the Fourier transform of the field is negligible, it follows that this Fourier transform has maximum width $\Delta k_x = k$. By the uncertainty principle it follows that after propagation, the minimum width of the field is $\Delta x, \Delta y \approx 2\pi/k = \lambda$.

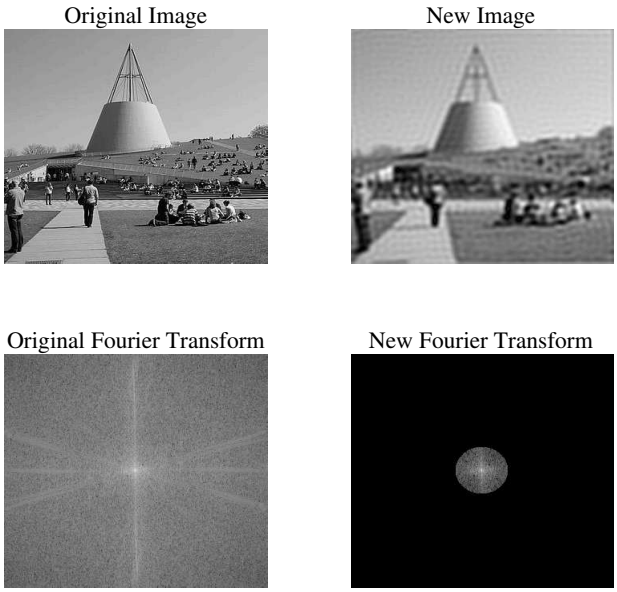
The minimum feature size of a field after propagation is of the order of the wavelength.

This poses a fundamental limit to resolution given by the wavelength of the light.

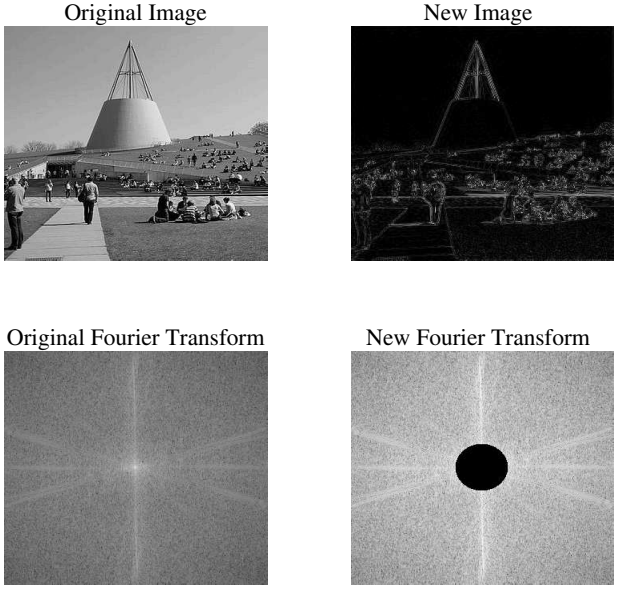
6.4 Fresnel and Fraunhofer Approximations

The Fresnel and Fraunhofer approximations are two approximations of the Rayleigh-Sommerfeld integral (6.13). The approximations are accurate provided the propagation distance z is sufficiently large. In the Fraunhofer approximation, z has to be *quite* large, i.e. larger than for the Fresnel approximation, which is already accurate for typical distances occuring in optical imaging systems. Putting it differently: in order of most accurate to least accurate (i.e. only valid for large propagation distances), the diffraction integrals would rank as:

[Most accurate] Rayleigh-Sommerfeld → Fresnel → Fraunhofer **[Least accurate]**.

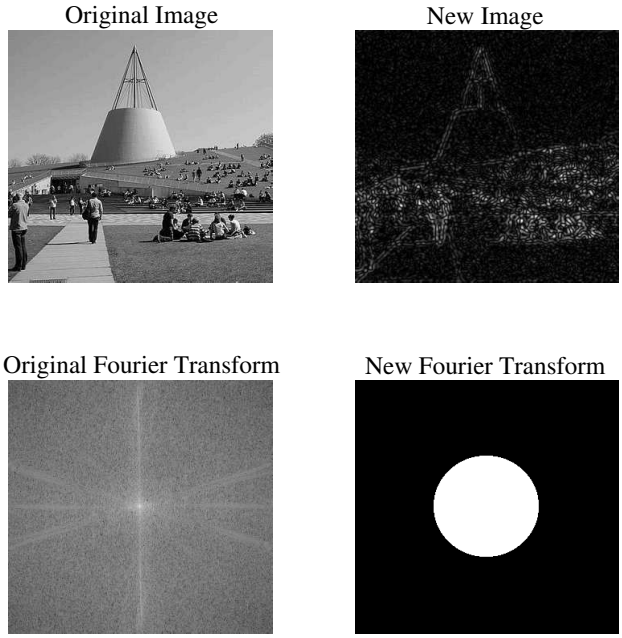


(a) Removing the high spatial frequencies

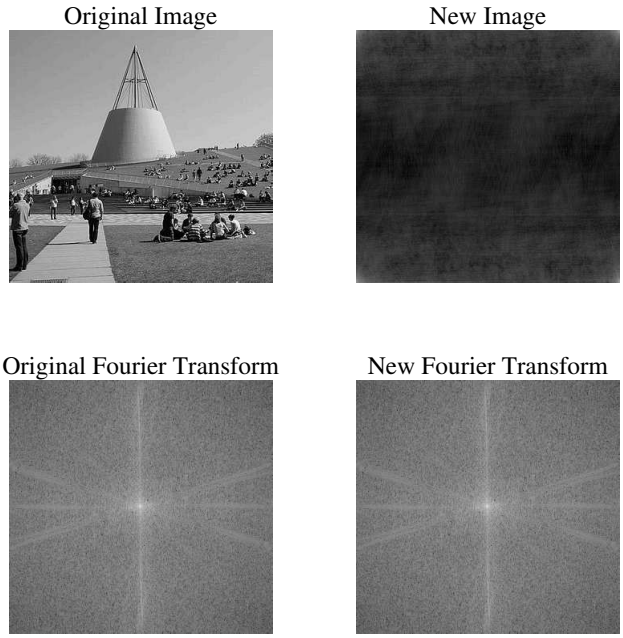


(b) Removing the low spatial frequencies

Figure 6.5: Demonstration of the roles of different spatial frequencies. By removing the high spatial frequencies, only the broad features of the image remain and resolution s lost. If the low spatial frequencies are removed, only the sharp features (i.e. the contours) remain.



(a) Removing the amplitude information by setting the amplitude of propagating and evanescent waves to 1 and 0, respectively.



(b) Removing the phase information by setting the phase equal to 0.

Figure 6.6: Demonstration of the role of the phase of the spatial Fourier transform. If the amplitude information is removed, but phase information is kept, some features of the original image are still recognizable. However, if the phase information is removed but amplitude information is kept, the original image is completely lost.

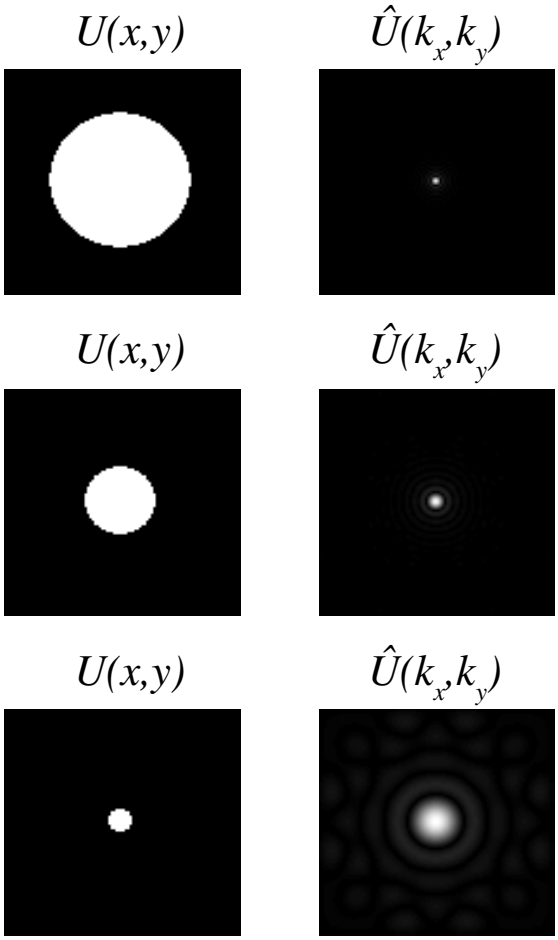


Figure 6.7: Demonstration of the uncertainty principle. The more confined $U(x, y)$ is, the larger the spread of $\hat{U}(k_x, k_y) = \mathcal{F}(U)\left(\frac{k_x}{2\pi}, \frac{k_y}{2\pi}\right)$.

6.4.1 Fresnel Approximation

We assume that z in Eq. (6.13) is so large that in the denominator we can approximate r by z:

$$U(x,y,z) = \frac{1}{i\lambda}\int\int U_0(x',y')\frac{z}{r}\frac{e^{ikr}}{r}\,\mathrm{d}x'\,\mathrm{d}y' \tag{6.17}$$

$$\approx \frac{1}{i\lambda z}\int\int U_0(x',y')e^{ikr}\,\mathrm{d}x'\,\mathrm{d}y'. \tag{6.18}$$

The reason why we can not apply the same approximation for r in the exponent, is that in the exponent r is multiplied by $k = 2\pi/\lambda$, which is a very large number at optical frequencies, so any error introduced by approximating r would be drastically magnified by multiplying by k which can easily lead to a completely different value of $\exp(ikr) = \cos(kr) + i\sin(kr)$. To approximate r in $\exp(ikr)$ we must be more careful and apply a Taylor expansion. Recall that

$$r = \sqrt{(x-x')^2+(y-y')^2+z^2}$$

$$= z\sqrt{\frac{(x-x')^2+(y-y')^2}{z^2}+1}. \tag{6.19}$$

We know that the Taylor expansion around $s = 0$ implies:

$$\sqrt{s+1} = 1 + \frac{s}{2} - \frac{s^2}{8} + \ldots. \tag{6.20}$$

Since we assume that z is large, $\frac{(x-x')^2+(y-y')^2}{z^2}$ is small (compare to 1), so we have

$$r = z\sqrt{\frac{(x-x')^2+(y-y')^2}{z^2}+1}$$

$$\approx z\left[1+\frac{(x-x')^2+(y-y')^2}{2z^2}\right]$$

$$= z + \frac{(x-x')^2+(y-y')^2}{2z}, \qquad \textbf{Fresnel approximation.} \tag{6.21}$$

With this approximation, we arrive at the **Fresnel diffraction integral**, which can be written in the following equivalent forms:

$$U(x,y,z) \approx \frac{e^{ikz}}{i\lambda z}\int\int U_0(x',y')e^{\frac{ik}{2z}\left[(x-x')^2+(y-y')^2\right]}\,\mathrm{d}x'\,\mathrm{d}y'$$

$$= \frac{e^{ikz}e^{\frac{ik(x^2+y^2)}{2z}}}{i\lambda z}\int\int U_0(x',y')e^{\frac{ik(x'^2+y'^2)}{2z}}e^{-ik\left(\frac{x}{z}x'+\frac{y}{z}y'\right)}\,\mathrm{d}x'\,\mathrm{d}y' \tag{6.22}$$

$$= \frac{e^{ikz}e^{\frac{ik(x^2+y^2)}{2z}}}{i\lambda z}\mathcal{F}\left\{U_0(x',y')e^{\frac{ik(x'^2+y'^2)}{2z}}\right\}\left(\frac{x}{\lambda z},\frac{y}{\lambda z}\right).$$

Especially the last expression is interesting, because it shows that

> The Fresnel approximation is proportional to the Fourier transform of the field $U_0(x',y')$ multiplied by the Fresnel propagator $\exp\left[\frac{ik(x'^2+y'^2)}{2z}\right]$.

Note that this propagator depends on the distance of propagation z.

Remark. The so-called paraxial wave equation is an approximation to the wave equation which is valid for fields that propagate predominantly in the z-direction, i.e. of which the plane waves with wave vectors that make a small angle with the z-axis have dominant amplitudes. The paraxial wave equation is often used to describe the propagation of laser beams. It can be proved that the Fresnel approximation satisfies the paraxial wave equation and that conversely every solution of the paraxial wave equation can be written as a Fresnel diffraction integral[8].

6.4.2 Fraunhofer Approximation

To obtain the Fraunhofer approximation, we will make one further approximation to r in $\exp(ikr)$ in addition to the Fresnel approximation:

$$r \approx z + \frac{(x-x')^2 + (y-y')^2}{2z} \quad \textbf{Fresnel approximation} \tag{6.23}$$

$$\approx z + \frac{x^2 + y^2 - 2xx' - 2yy'}{2z} \quad \textbf{Fraunhofer approximation.} \tag{6.24}$$

Hence we omit the quadratic terms $x'^2 + y'^2$ and by this the Fresnel diffraction integral becomes the **Fraunhofer diffraction integral**:

$$U(x,y,z) \approx \frac{e^{ikz} e^{\frac{ik(x^2+y^2)}{2z}}}{i\lambda z} \mathcal{F}(U_0)\left(\frac{x}{\lambda z}, \frac{y}{\lambda z}\right). \tag{6.25}$$

This leads to the following important observation:

> The Fraunhofer far field of $U_0(x', y')$ is proportional to the Fourier transform of U_0.

Note that to obtain the Fraunhofer field in (x, y, z), the Fourier transform has to be evaluated at spatial frequencies $x/(\lambda z)$ and $y/(\lambda z)$. These spatial frequencies scale with $1/z$ and the overall field $U(x, y, z)$ is proportional to $1/z$. This implies that when z is increased the field pattern spreads out without changing its shape while its amplitude goes down so that the total energy is preserved. Stated differently, apart from the factor $1/z$ in front of the integral, the Fraunhofer field depends on the angles x/z and y/z. Therefore for large propagation distances z for which the Fraunhofer approximation is accurate, the field becomes broader (it diverges) when the propagation distance increases.

> Eventually, for sufficiently large propagation distances, i.e. in the Fraunhofer limit, light always spreads out without change of shape of the light distribution.

Remarks.

1. The Fresnel approximation is, like the Fraunhofer approximation, a Fourier transform of the field in the starting plane ($z = 0$), evaluated in spatial frequencies which depend on the point of observation:

$$\xi = \frac{x}{\lambda z}, \quad \eta = \frac{y}{\lambda z}. \tag{6.26}$$

[8] For a proof see A.E. Siegman, *Lasers*

However, in contrast to the Fraunhofer approximation, the Fresnel approximation depends additionally in a different way on the propagation distance z, namely through the exponent of the Fresnel propagator in the integrand. Therefore the Fresnel approximation gives quite diverse patterns depending on the propagation distance z, as is shown in Fig. 6.10.

2. In the Rayleigh-Sommerfeld diffraction integral, the field is written as a superposition of spherical waves. In the Fresnel approximation the spherical waves are approximated by parabolic waves. Finally, in the Fraunhofer approximation the propagation distance is so large that the parabolic waves are approximately plane waves.

3. Let $f_{a,b}(x,y) = f(x-a, y-b)$ be the function obtained from f by translation. From the general property of the Fourier transform:

$$\mathcal{F}(f_{a,b})(\xi,\eta) = e^{-2\pi i(\xi a+\eta b)}\mathcal{F}(f)(\xi,\eta), \tag{6.27}$$

it follows that when the field U_0 is translated, the intensity in the Fraunhofer far field is not changed. In contrast, due to the additional quadratic phase factor in the integrand of the Fresnel integral, the intensity of the Fresnel field in general changes when U_0 is translated.

4. Suppose that U_0 is the field immediately behind an aperture $\mathcal{A}$ with diameter D in an opaque screen. It can then be shown that points (x,y,z) of observation, for which the Fresnel and Fraunhofer diffraction integrals are sufficiently accurate, satisfy:

$$\frac{z}{\lambda} \gg \left(\frac{\max_{(x',y')\in\mathcal{A}}\sqrt{(x-x')^2+(y-y')^2}}{\lambda}\right)^{4/3}, \quad \textbf{Fresnel} \tag{6.28}$$

$$\frac{z}{\lambda} \gg \left(\frac{D}{\lambda}\right)^2, \quad \textbf{Fraunhofer} \tag{6.29}$$

5. The Fresnel number is defined by

$$N_F = \frac{D^2}{\lambda z}, \quad \textbf{Fresnel number}. \tag{6.30}$$

When $N_F < 0.1$ the Fraunhofer approximation is accurate, while for $N_F > 0.1$ it is better to use the Fresnel approximation (see Fig. 6.10. Suppose that $D = 1$ mm and the wavelength is that of green light: $\lambda = 550$ nm, then Fraunhofer's approximation is accurate if $z > 20$ m.

6. The points of observation where the Fraunhofer approximation can be used must in any case satisfy:

$$\frac{x}{z} < 1, \quad \frac{y}{z} < 1. \tag{6.31}$$

When $x/z > 1$, the spatial frequency $k_x = \frac{2\pi x}{z\lambda} > k$ associated with this point corresponds to an evanescent wave. An evanescent wave obviously cannot contribute to the Fraunhofer far field because it exponentially decreases with distance z. In practice the Fresnel and Fraunhofer approximations are used only when x/z and y/z are smaller than 0.3.

7. In any expression for an optical field, one may always omit factors of constant phase, i.e. an overall phase which does not depend on position. If one is only interested in the field in certain planes $z =$ constant, then a factor like $\exp(ikz)$ may also be omitted. Further, in some cases also a position dependent phase factor in front of the Fresnel and Fraunhofer

diffraction integrals is omitted, namely when only the intensity is of interest. In exercises it is usually mentioned that this factor may be omitted: if this is not stated, it should be retained in the formulae.

6.4.3 Examples of Fresnel and Fraunhofer approximations

6.4.3.1 Fresnel approximation of the field of two point sources.

Consider two mutual coherent time-harmonic point sources in $\mathbf{r}_s^+ = (a/2, 0, 0)$ and $\mathbf{r}_s^- = (-a/2, 0, 0)$. The fields in $\mathbf{r} = (x, y, z)$ emitted are according to (5.43) proportional to

$$U_\pm(\mathbf{r}) = \frac{e^{ik|\mathbf{r}-\mathbf{r}_s^\pm|}}{|\mathbf{r}-\mathbf{r}_s^\pm|}. \tag{6.32}$$

We apply the Fresnel approximation for large z:

$$\begin{aligned} |\mathbf{r}-\mathbf{r}_s^\pm| &= z\sqrt{1+\frac{(x\mp a/2)^2+y^2}{z^2}} \\ &\approx z+\frac{(x\mp a/2)^2+y^2}{2z} \\ &= z+\frac{x^2+y^2+a^2/4}{2z}\mp\frac{ax}{2z}. \end{aligned} \tag{6.33}$$

Hence,

$$U_\pm(\mathbf{r}) \approx \frac{e^{ikz}}{z} e^{ik\frac{x^2+y^2}{2z}} e^{ik\frac{a^2}{8z}} e^{\mp ik\frac{ax}{2z}}, \tag{6.34}$$

where in the denominator we replaced $|\mathbf{r}-\mathbf{r}_s^\pm|$ by z. Note that the Fraunhofer approximation amounts to $e^{ika^2/(8z)} \approx 1$ while the phase factor $e^{ik\frac{x^2+y^2}{2z}}$ remains. The intensity on a screen $z =$ constant of the sum of the two fields for the case that the sources have equal strength and emit in phase is:

$$\begin{aligned} I_{tot}(\mathbf{r}) &= |U_+(\mathbf{r})+U_-(\mathbf{r})|^2 = \frac{1}{z^2}|e^{-ik\frac{ax}{2z}}+e^{ik\frac{ax}{2z}}|^2 \\ &= \frac{2}{z^2}\left[1+\cos\left(2\pi\frac{ax}{\lambda z}\right)\right]. \end{aligned} \tag{6.35}$$

It is seen that the intensity results from the interference of two plane waves: $\exp[\pm ikax/(\lambda z)]$ and is given by a cosine function (see Fig. 6.8). Note that for two point sources, the intensity pattern is the same in the Fresnel and the Fraunhofer approximation. However, this is special for two point sources: when more than two point sources are considered, the Fresnel and Fraunhofer patterns are different. The intensity pattern is independent of y, and vanishes on lines

$$\frac{x}{z} = (2m+1)\frac{\lambda}{2a}, \tag{6.36}$$

and has maxima on lines

$$\frac{x}{z} = m\frac{\lambda}{a}, \tag{6.37}$$

for integer m.

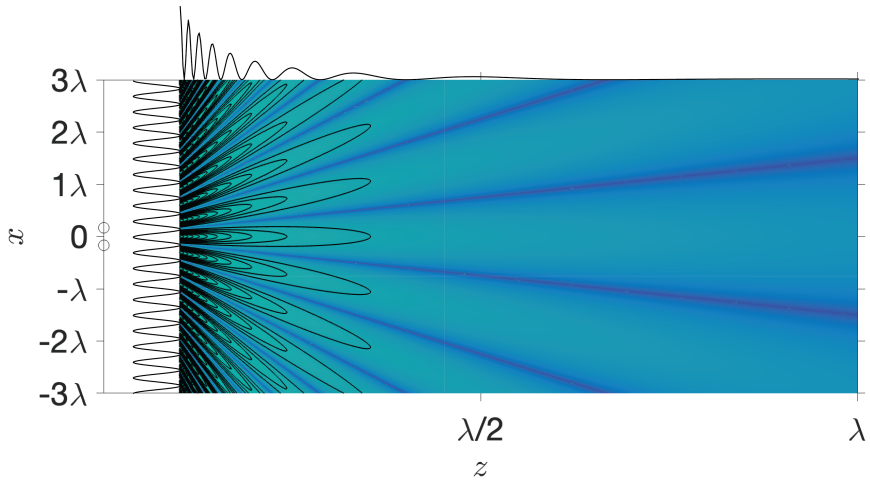


Figure 6.8: Intensity pattern (6.35) of two mutually coherent point sources of equal strength and emitting in phase. The distance between the point source is $\lambda/3$. On top the intensity is shown as function of z for $x = 3\lambda$.

6.4.3.2 Fraunhofer approximation of a rectangular aperture in a screen.

Let the screen be $z = 0$ and the aperture be given by $-a/2 < x < a/2$, $-b/2 < y < b/2$. The transmission function $\tau(x, y)$ is:

$$\tau(x, y) = 1_{[-a/2,a/2]}(x)1_{[-b/2,b/2]}(y), \tag{6.38}$$

where

$$1_{[-a/2,a/2]}(x) = \begin{cases} 1, \text{ if } -\frac{a}{2} \le x \le \frac{a}{2}, \\ 0, \text{ otherwise,} \end{cases} \tag{6.39}$$

and similarly for $1_{[-b/2,b/2]}(y)$. Let the aperture be illuminated by a perpendicular incident plane wave with unit amplitude. Then the field immediately behind the screen is:

$$U_0(x, y) = \tau(x, y) = 1_{[-a/2,a/2]}(x)1_{[-b/2,b/2]}(y), \tag{6.40}$$

We have

$$\begin{aligned} \mathcal{F}\left(1_{[-a/2,a/2]}\right)(\xi) &= \int_{-a/2}^{a/2} e^{-2\pi i\xi x}\,\mathrm{d}x \\ &= \frac{e^{\pi ia\xi} - e^{-\pi ia\xi}}{2\pi i\xi} \\ &= a\,\mathrm{sinc}(\pi a\xi), \end{aligned} \tag{6.41}$$

where $\mathrm{sinc}(u) = \sin(u)/u$. Hence,

$$\mathcal{F}(U_0)\left(\frac{x}{\lambda z}, \frac{y}{\lambda z}\right) = ab\,\mathrm{sinc}\left(\frac{\pi ax}{\lambda z}\right)\mathrm{sinc}\left(\frac{\pi by}{\lambda z}\right). \tag{6.42}$$

The Fraunhofer far field at large distance z from a rectangular aperture in mask is obtained by substituting (6.42) into (6.25).

Remarks.

1. The first zero along the x-direction from the centre $x = 0$ occurs for

$$x = \pm \frac{\lambda z}{a}. \tag{6.43}$$

The distance between the first two zeros along the x-axis is $2\lambda z/a$, which increases when the width along the x-direction of the aperture is decreased.

2. The inequalities (6.31) imply that when $a < \lambda$, the far field pattern does not have any zeros as function of x. When a is further decreased it becomes more and more difficult to deduce the width a from the Fraunhofer intensity. This is an illustration of the fact that information about features that are smaller than the wavelength cannot propagate to the far field.

3. As illustrated in Fig. 6.9, the Fraunhofer diffraction pattern as function of diffraction angle is narrowest in the direction in which the aperture is widest.

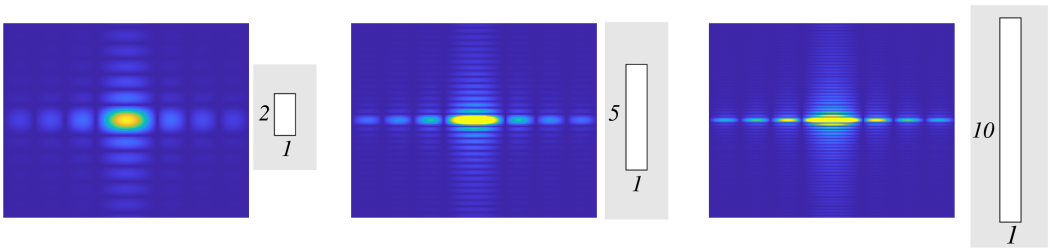


Figure 6.9: Fraunhofer diffraction pattern of a rectangular aperture in an opaque screen. Left: the width of the aperture in the y-direction is twice that in the x-direction; middle: the width in the y-direction is 5 times that in the x-direction; right: the width in the y-direction is 10 times that in the x-direction.

6.4.3.3 Fresnel approximation of a rectangular aperture in a mask

The integral in the Fresnel approximation for the field of a rectangular aperture in a mask can be computed analytically (and leads to special functions that are known under the name "Fresnel integrals" and which can be studied using the Cornu spirals). We will not go deeper in this matter but simply show the results of the simulations in Fig. 6.10. The distance to the mask increases (N_F decreases), from very close to the mask at the bottom right, to further from the mask at the bottom left, to rather far from the mask in the upper right, to the Fraunhofer distance in the upper left figures. Note the change in scale along the axis in the figures and the decrease of intensity with propagation distance. It is seen that the pattern changes and broadens drastically with distance from what close to the aperture is more or less a copy of the aperture, to a broad pattern equal to the Fourier transform of the aperture at large distances. Once the Fraunhofer approximation is accurate, a further increase of distance only results in a widening of the pattern and a decrease of overall amplitude without change of shape. In contrast, in the region where the Fresnel approximation is accurate, the shape of the pattern is seen to change a lot with distance to the mask.

6.4.3.4 Fraunhofer approximation of a periodic array of slits

We can now predict what is the diffraction pattern of an array of slits of finite width. It follows from the Fraunhofer pattern of a single rectangular aperture that when the sides parallel to the y-direction are very much longer than the sides parallel to the x-direction, the Fraunhofer

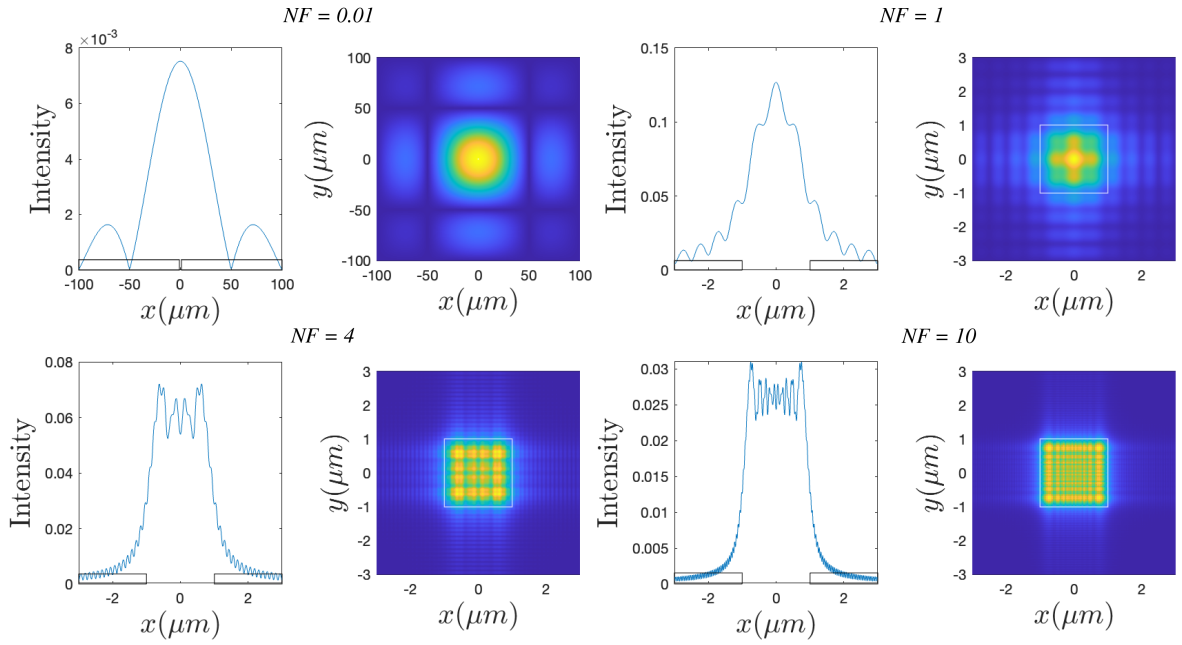


Figure 6.10: Diffraction patterns of a square opening in a mask with corresponding cross-sections along the x-axis, showing the transition from Fresnel to Fraunhofer approximations. The distance to the mask increases when the Fresnel number N_F decreases from the near field pattern close to the mask in the right bottom figures to the Fraunhofer diffraction pattern in the upper left. Note the different scales along the axis in the figures.

diffraction pattern as function of angle in the y-direction is very narrow compared to that in the x-direction. In Fig. 6.9c the Fraunhofer diffraction pattern of a rectangular aperture is shown, of which the width in the y-direction is 10 times that in the x-direction. The diffraction pattern is then strongly concentrated along the x-axis. If we only consider the Fraunhofer pattern for $y/z = 0$ while still considering it as a function of x/z, it suffices to compute the Fourier transform only with respect to x. The problem then becomes a diffraction problem for a one-dimensional slit.

We consider now an array of such slits of which the long sides are all parallel to the y-axis and we neglect from now on the y-variable. Suppose $W_{\text{slit}}(x)$ is the function that describes the transmission of a single slit. Then the transmission function of M equidistant slits is

$$\tau(x) = \sum_{m=1}^{M} W_{\text{slit}}\left(x + (M+1)\frac{p}{2} - mp\right), \tag{6.44}$$

where p is the distance of neighbouring slits, i.e. p is the period of the row. If the illumination is by a perpendicular incident plane wave with unit amplitude, the transmitted near field $U_0(x)$ is simply $\tau(x)$. Then

$$\mathcal{F}(U_0)(\xi) = \mathcal{F}(\tau)(\xi) = \sum_{m=1}^{M} \mathcal{F}(W_{slit})(\xi)\, e^{\pi i(M+1)p\xi} e^{-2\pi imp\,\xi}, \tag{6.45}$$

where for a slit with width a we have according to (6.41):

$$\mathcal{F}(W_{slit})(\xi) = a\frac{\sin(\pi a\xi)}{\pi a\xi}.$$

The slit width a must of course be smaller than the period: $a < p$. Using

$$\begin{aligned}\sum_{m=1}^{M} e^{-2\pi imp\xi} &= e^{-2\pi ip\xi}\sum_{m=0}^{M-1} e^{2\pi mp\xi} \\ &= e^{-2\pi ip\xi}\frac{1-e^{-2\pi iMp\xi}}{1-e^{-2\pi ip\xi}} \\ &= e^{-\pi i(M+1)p\xi}\frac{e^{i\pi Mp\xi}-e^{-i\pi Mp\xi}}{e^{i\pi p\xi}-e^{-i\pi p\xi}} \\ &= e^{-\pi i(M+1)p\xi}\frac{\sin(\pi Mp\xi)}{\sin(\pi p\xi)},\end{aligned} \tag{6.46}$$

we get

$$\mathcal{F}(U_0)(\xi) = \mathcal{F}(W_{slit})(\xi)\frac{\sin(\pi Mp\xi)}{\sin(\pi p\xi)}. \tag{6.47}$$

The intensity of the Fraunhofer far field is:

$$I(x,z) = \left|\frac{1}{\lambda z}\mathcal{F}(U_0)\left(\frac{x}{\lambda z}\right)\right|^2 = \frac{1}{\lambda^2 z^2}\left|\mathcal{F}(W_{slit})\left(\frac{\theta}{\lambda}\right)\right|^2 \frac{\sin^2\left(\pi M\frac{p}{\lambda}\theta\right)}{\sin^2\left(\pi\frac{p}{\lambda}\theta\right)}. \tag{6.48}$$

where $\theta = x/z$ is the diffraction angle. For large M the ratio

$$\frac{\sin^2\left(\pi M\frac{p}{\lambda}\theta\right)}{\sin^2\left(\pi\frac{p}{\lambda}\theta\right)}, \tag{6.49}$$

is a fast oscillating function of θ. In contrast, $|\mathcal{F}(W_{slit})(\theta/\lambda)|^2$ is a relatively slowly varying envelope. This is a manifestation of the property of the Fourier transform that small details of a structure (e.g. the size of a single slit) cause large scale features of the far field pattern, whereas large scale properties such as the length Mp of the total structure, cause quickly changing features. This is illustrated in Fig. 6.11.

The diffraction amplitude is maximum for angles where both the denominator and numerator of (6.49)) vanish:

$$\theta_m = \frac{m\lambda}{p}, \quad m = 0, \pm 1, \pm 2, \ldots, \qquad \textbf{diffraction orders.} \tag{6.50}$$

These directions are called diffraction orders and since

$$\frac{\sin^2\left(\pi M\frac{p}{\lambda}\theta_m\right)}{\sin^2\left(\pi\frac{p}{\lambda}\theta_m\right)} = M^2, \tag{6.51}$$

which follows by applying l'Hôpital's rule, the intensity of the mth order is

$$\frac{M^2}{\lambda^2 z^2}\left|\mathcal{F}(W_{slit})\left(\frac{m}{p}\right)\right|^2, \tag{6.52}$$

hence it is proportional to the square of the number of periods and to the squared modulus of the envelope in θ_m.

Between two adjacent diffraction orders, (6.49) has $M-1$ zeros and $M-2$ secondary maxima (see Fig. 6.11). The angular width of a diffraction order is half the angular distance to the nearest zeros adjacent to the order, i.e.

$$\Delta\theta = \frac{\lambda}{Mp}, \qquad \textbf{angular width of a diffraction order.} \tag{6.53}$$

If there are more slits, the diffraction orders into which the energy is diffracted are narrower and their peaks are higher.

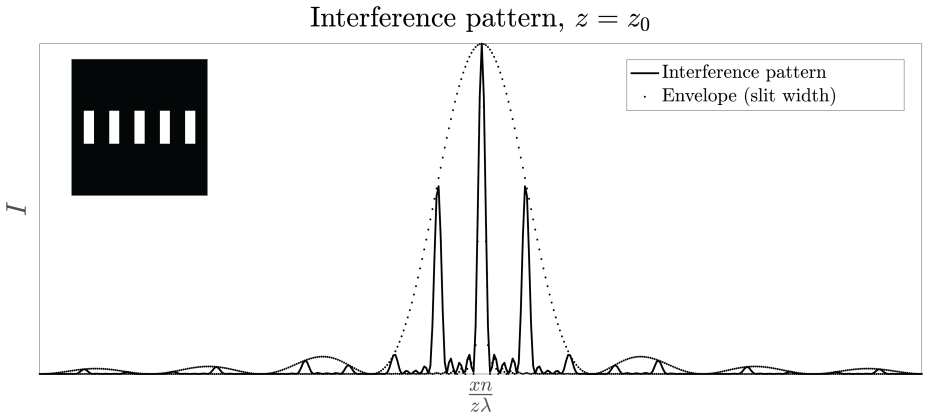


Figure 6.11: An illustration of a diffraction pattern of a series of five slits. The peak width is inversely proportional to the number of slits.

As explained above, there holds in the Fraunhofer far field: $\theta = x/z < 1$. This sets a limit to the number of diffracted orders:

$$|m| \leq p/\lambda. \tag{6.54}$$

Hence, the larger the ratio of the period and the wavelength, the more diffraction orders.

The property (6.50) that the diffraction orders $m \neq 0$ depend on wavelength is used to separate wavelengths. **Grating spectrometers** use periodic structures such as an array of slits to very accurately separate and measure wavelengths. The mth diffraction order of two wavelengths $\lambda_2 > \lambda_1$ are just separated if

$$m\frac{\lambda_2}{p} > m\frac{\lambda_1}{p} + \Delta\theta = m\frac{\lambda_1}{p} + \frac{\lambda_1}{Mp},$$

which implies with $\Delta\lambda = \lambda_2 - \lambda_1$ and $\lambda = \lambda_1$ that

$$\frac{\Delta\lambda}{\lambda} > \frac{1}{mM}. \tag{6.55}$$

It follows that the resolution is higher when there are more slits and for larger diffraction order. However, the disadvantage of using higer diffraction orders is that often their intensity is less. For a grating with 1000 periods (M=1000) one can obtain a resolution of $\Delta\lambda/\lambda = 10^{-3}$ in the first order.

It should be remarked that a grating is obtained for any periodic variation of the refractive index. If the proper transmission function for the unit cell of the grating is substituted for W_{slit}, the formulae above also give the Fraunhofer far field of such more general diffraction gratings. By changing the unit cell, the envelope of the diffraction pattern can be changed and a certain order can be given more intensity. In Fig. 6.12 a so-called blazed grating is shown which is used in reflection and which (in the case shown) has a strong first diffracted order for a certain angle of incidence.

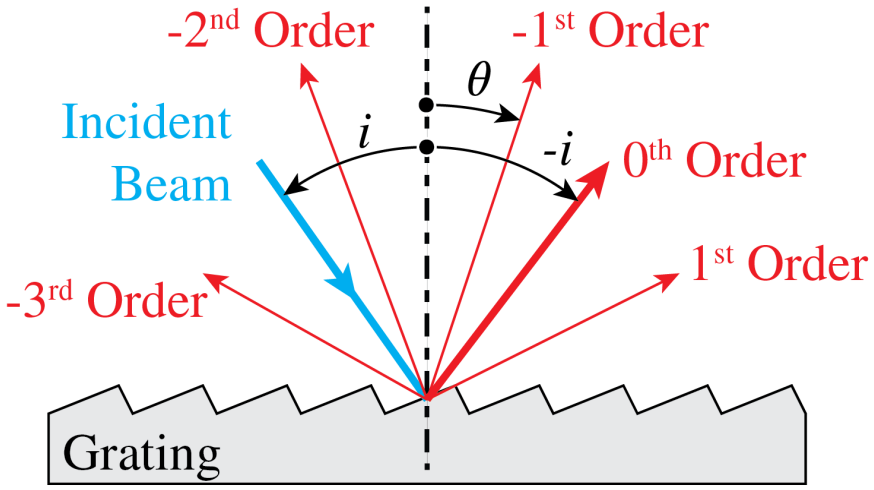


Figure 6.12: Diffraction grating used in reflection with a so-called blazed unit cell. The 0th order is also the direction of the spuriously reflected beam when the structure is flat.

Remark. Structures can be periodic in one, two and three directions. A crystal acts as a three-dimensional grating whose period is the period of the crystal, which typically is a few Angstrom. Electromagnetic waves with wavelength less than one Angstrom are called x-rays. When a beam of x-rays illuminates a crystal, a detector in the far field measures the Fraunhofer diffraction pattern given by the intensity of the Fourier transform of the refracted near field. These diffraction orders of crystals for x-rays where discovered by M. von Laue et al. [11]. They are used to study the atomic structure of crystals.

6.5 Fraunhofer Diffraction Revisited

Fraunhofer diffraction patterns can qualitatively be explained by considering directions in which destructive and constructive interferences occur. Consider two mutually coherent point sources S_1, S_2 at distance a on the x-axis as shown in Fig. 6.13. We assume that these point sources have the same strengths and are in phase. On a screen at large distance z an interference pattern is observed. If the distance z of the screen is very large, the spherical wave fronts emitted by the point sources are almost plane at the screen and the field is the Fraunhofer far field of the two point sources. In point P on the screen at a distance x above the z-axis the optical path differences of the waves emitted by the two sources is approximately given by $S_2Q = a\theta$, where $\theta = x/z$ is assumed small. Hence constructive interference occurs for angles θ such that $S_2Q = m\lambda$ for some integer m, i.e. when

$$\theta = m\frac{\lambda}{a}, \qquad \text{constructive interference.} \tag{6.56}$$

Destructive interference occurs when the path length difference satisfies $S_2Q = \lambda/2 + m\lambda$ for some integer m, hence for angles

$$\theta = (1/2 + m)\frac{\lambda}{a} \qquad \text{destructive interference.} \tag{6.57}$$

If the point sources have the same strength, their fields perfectly cancel for these angles.

[11] Friedrich, W., P. Knipping, and M. von Laue. "Sitzungsberichte der Math. Phys. Klasse (Kgl.), Bayerische Akademie der Wissenschaften." (1912): 303-322

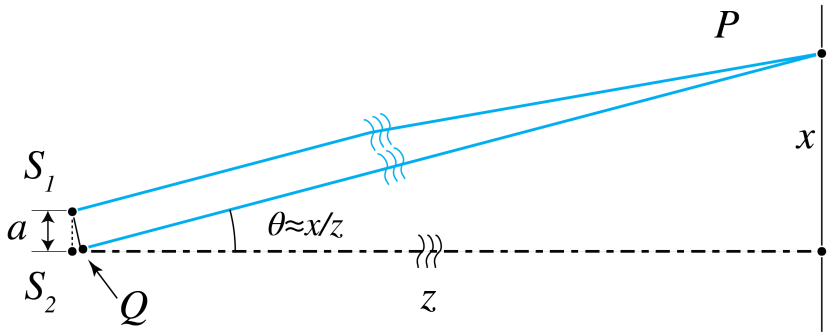


Figure 6.13: Interference of two mutually coherent point sources. For z very large, the points P where constructive or destructive interference occurs are such that for some integer m: $S_2Q = m\lambda$ or $S_2Q = (1/2 + m)\lambda$, respectively.

Now consider a slit as shown in Fig. 6.14 which is illuminated by a perpendicular incident plane wave. By the Huygens-Fresnel principle, the field at a screen far from the slit is the sum of the fields of point sources in the aperture, with strengths proportional to the field in the slit at the position of the point sources. When the slit is illuminated by a plane wave at perpendicular incidence, all point sources are in phase and have equal strengths. Divide the slit in two equal halves as shown in Fig. 6.14. The point sources in the slit can be arranged into pairs, of which one point source is in the upper half of the slit and the other is at the equivalent position in the lower half of the slit (at distance $a/2$ from the other point source). Let θ be an angle for which the two point sources of a pair cancel each other i.e.

$$\theta = (1/2 + m)\frac{\lambda}{a/2} = (1 + 2m)\frac{\lambda}{a}, \tag{6.58}$$

since the distance between the point sources is $a/2$. By translating the pair of point sources through the slits, it follows that both half slits perfectly cancel each other for these angles. In this way we have found the angles $\theta = m\lambda/a$ with m odd for which destructive interference occurs. Destructive interference for m even can be derived by further subdivisions of the aperture.

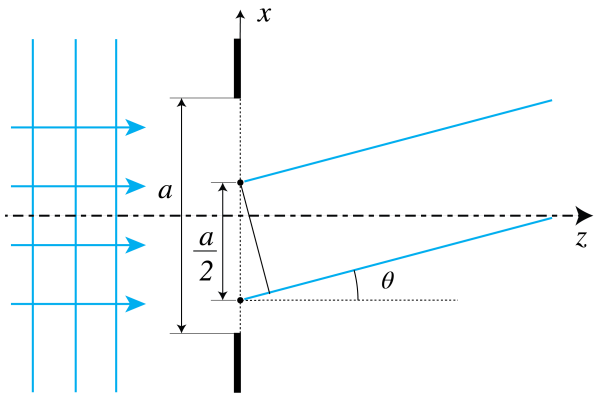


Figure 6.14: By dividing the slit into two slits of size $a/2$ each and considering pairs of point sources of which one is in the upper half of the slit and the other is at the corresponding position in the lower half, angles where destructive interference occurs between these point sources lead to minima in the diffraction pattern. Note that the point sources have corresponding positions in the two parts of the slit if their distance is $a/2$.

In general it is easier to find the angles for which the far field vanishes than to find (local) maxima of the field. An exception is the case of a diffraction grating. It follows from Fig. 6.15

that there will be constructive interference between adjacent periods, and hence for the entire grating, for angles for which the distance SQ in Fig. 6.15 is a multiple of the wavelength, i.e. for

$$\theta = m\frac{\lambda}{p}, \tag{6.59}$$

which corresponds to the direction of the diffraction orders. For other angles the phases of the fields transmitted by the different periods differ widely and therefore the fields almost cancel at these angles when there are many periods. This explains that for a diffraction grating of many periods, the far field intensity is highly concentrated in particular directions given by the orders (6.59) which depend only on the ratio of the wavelength and the period.

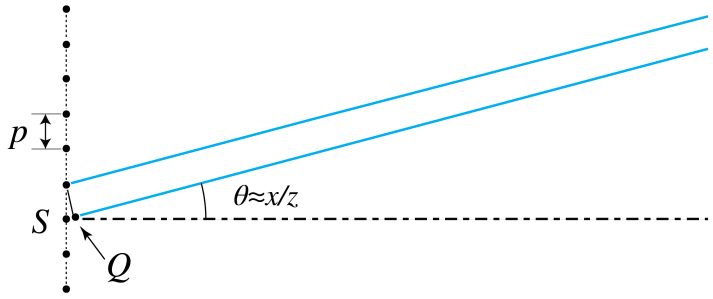


Figure 6.15: If the angle θ is such that SQ is a multiple of the wavelength, two adjacent periods, and hence all periods of the grating, constructively interfere. These angles correspond to the diffraction orders.

6.6 Fourier Optics

In this section we apply diffraction theory to a lens. We consider in particular the focusing of a parallel beam and the imaging of an object.

6.6.1 Focusing of a Parallel Beam

A lens induces a local phase change to an incident field in proportion to the local thickness of the lens. Let a plane wave which propagates parallel to the optical axis be incident on a positive lens with radius a. In Gaussian geometrical optics all incident rays are focused into the Gaussian image focal point. According to the Principle of Fermat, all rays have travelled the **same optical distance** when they intersect in the image focal point where they constructively interfere and cause an intensity maximum. The wave fronts are surfaces on which the phase is constant, i.e. all points of the wave fronts have the optical path length to the source. In the focal region the wave fronts therefore are **spheres with common centre the focal point**, cut off by the cone with the focal point as top and opening angle $2a/f_i$, as shown in Fig. 6.16. Behind the focal point, there is a second cone with again spherical wave fronts, but there the light is propagating away from the focal point. According to Gaussian geometrical optics it is in image space completely dark outside of the two cones in Fig. 6.16. However, as we will see in diffraction optics this is not true.

We assume that the lens is thin and positive. We choose as origin of our coordinate system the centre of the thin lens with the positive z-axis along the optical axis. Then $(0, 0, f_i)$ is the image focal point. Let (x, y, z) be a point between the lens and this focal point. The spherical wave in this point, which according to Gaussian geometrical optics converges to the focal point,

is mathematically described by

$$\begin{cases} \frac{e^{-ik\sqrt{x^2+y^2+(z-f_i)^2}-i\omega t}}{\sqrt{x^2+y^2+(z-f_i)^2}}, & \text{if } (x,y,z) \text{ is inside the cone,} \\ 0, & \text{if } (x,y,z) \text{ is outside the cone,} \end{cases} \tag{6.60}$$

where we have included the time-dependence. The surfaces of constant phase:

$$-\sqrt{x^2+y^2+(z-f_i)^2}-\omega t = \text{constant},$$

are indeed spheres with centre the focal point. For increasing time, these spheres converge to the focal point, while the amplitude in (6.60) increases as the distance to the focal point decreases such that energy is preserved.

Remark. For a point (x,y,z) to the **right** of the focal point, i.e. for $z > f_i$, the spherical wave fronts propagate away from the focal point and therefore the wave is there proportional to (6.60) with in the exponent $-ik$ replaced by $+ik$.

Because the exit pupil of the lens is in the plane $z = 0$ and the radius of the lens is a, it follows from (6.60) that the field in the plane $z = 0$ is given by

$$1_{\odot_a}(x,y)\frac{e^{-ik\sqrt{x^2+y^2+f_i^2}}}{\sqrt{x^2+y^2+f_i^2}}, \tag{6.61}$$

where the time dependence has been omitted and

$$1_{\odot_a}(x,y) = \begin{cases} 1 & \text{if } x^2+y^2 < a^2, \\ 0 & \text{otherwise,} \end{cases} \tag{6.62}$$

i.e. $1_{\odot_a}(x,y) = 1$ for (x,y) in the exit pupil of the lens and $= 0$ otherwise. If a/f_i is sufficiently small, we may replace the distance $\sqrt{x^2+y^2+f_i^2}$ between a point in the exit pupil and the image focal point in the denominator of (6.61) by f_i. This is not a sufficiently accurate approximation to be used in the exponent because of the multiplication by the large wave number k. In the exponent we therefore use instead the first two terms of the Taylor series (6.20):

$$\sqrt{x^2+y^2+f_i^2} = f_i\sqrt{1+\frac{x^2+y^2}{f_i^2}} \approx f_i + \frac{x^2+y^2}{2f_i}, \tag{6.63}$$

which is valid for a/f_i sufficiently small. Then (6.61) becomes:

$$1_{\odot_a}(x,y)e^{-ik\frac{x^2+y^2}{2f_i}}, \tag{6.64}$$

where we dropped the constant factors e^{ikf_i} and $1/f_i$. For a general field $U_i(x,y)$ incident on the lens, i.e. in the entrance pupil, the lens applies a transformation such that the field in the exit plane becomes:

$$U_i(x,y) \to U_i(x,y)1_{\odot_a}(x,y)e^{-ik\frac{x^2+y^2}{2f_i}}, \tag{6.65}$$

transformation applied by a lens between its entrance and exit plane.

The function that multiplies $U_i(x,y)$ is the **transmission function of the lens**:

$$\tau_{\text{lens}}(x,y) = 1_{\odot_a}(x,y)e^{-ik\frac{x^2+y^2}{2f_i}}. \tag{6.66}$$

This result makes sense: in the centre $(x,y)=0$ the lens is thickest, so the phase is shifted the most (but we can define this phase shift to be zero because only phase *differences* matter, not absolute phase). As is indicated by the minus-sign in the exponent, the further you move away from the centre of the lens, the less the phase is shifted. For shorter f_i, the lens focuses more strongly, so the phase shift changes more rapidly as a function of the radial coordinate. Note that transmission function (6.66) has modulus 1 so that energy is conserved.

In diffraction optics the field at the right of (6.65) is the field in the exit pupil of the lens. It is propagated to any point (x,y,z) of interest behind the lens using the Fresnel diffraction integral (6.22):

$$U(x,y,z) = \frac{e^{ikz}e^{\frac{ik(x^2+y^2)}{2z}}}{i\lambda z}\mathcal{F}\left\{U_i(x',y')1_{\odot_a}(x',y')e^{ik\frac{x'^2+y'^2}{2}\left(\frac{1}{z}-\frac{1}{f_i}\right)}\right\}\left(\frac{x}{\lambda z},\frac{y}{\lambda z}\right). \tag{6.67}$$

For points in the image focal plane of the lens, i.e. for $z=f_i$, we have in particular:

$$U(x,y,f_i) = \frac{e^{ikf_i}e^{\frac{ik(x^2+y^2)}{2f_i}}}{i\lambda f_i}\mathcal{F}\left\{U_i(x',y')1_{\odot_a}(x',y')\right\}\left(\frac{x}{\lambda f_i},\frac{y}{\lambda f_i}\right), \tag{6.68}$$

which is the same as the **Fraunhofer integral** for propagation over the distance f_i! Note that it is the field in the **entrance pupil**, i.e. $U_i(x,y)1_{\odot_a}(x',y')$ which is propagated as a Fraunhofer integral.

> The field in the **entrance pupil** of the lens and the field in the focal plane are related by a Fourier transform (apart from a quadratic phase factor in front of the integral).

It can furthermore be shown that the fields in the front focal plane $U(x,y,-f_i)$ and the back focal plane $U(x,y,f_i)$ are related **exactly** by a Fourier transform, i.e. without the quadratic phase, but we will not consider this special case.

The intensity $I=|U|^2$ in the focal region is shown at the bottom left of Fig. 6.16 for the case that $U_i=1$, i.e. for the focusing of a plane wave. It is seen that the intensity does not monotonically increase for decreasing distance to the focal point. Instead, secondary maxima occur along the optical axis. Also the boundary of the light cone is not sharp, as predicted by geometrical optics, but blurred. The bottom right of Fig. 6.16 shows the phase in the focal region. The wave fronts are almost but not exactly spherical inside the cones. factor[13].

So a lens performs a Fourier transform between the **entrance pupil** and the focal plane. Let us see if that agrees with some of the facts we know from geometrical optics.

1. We know from Gaussian geometrical optics that if we illuminate a positive lens with rays parallel to the optical axis, these rays all intersect in the image focal point. This corresponds with the fact that for $U_i(x,y)=1$ (i.e. plane wave illumination, neglecting the finite aperture of the lens, i.e. neglecting diffraction due to the finite size of the pupil), the Fourier transform of the pupil field is a delta peak:

$$\mathcal{F}(U_0)\left(\frac{x}{\lambda f_i},\frac{y}{\lambda f_i}\right) = \delta\left(\frac{x}{\lambda f_i}\right)\delta\left(\frac{y}{\lambda f_i}\right), \tag{6.69}$$

   which represents the perfect focused spot (without diffraction).

[13] J.W. Goodman, *Introduction to Fourier Optics*, §5.2.2 - Several calculations on the Fourier transforming properties of lenses.

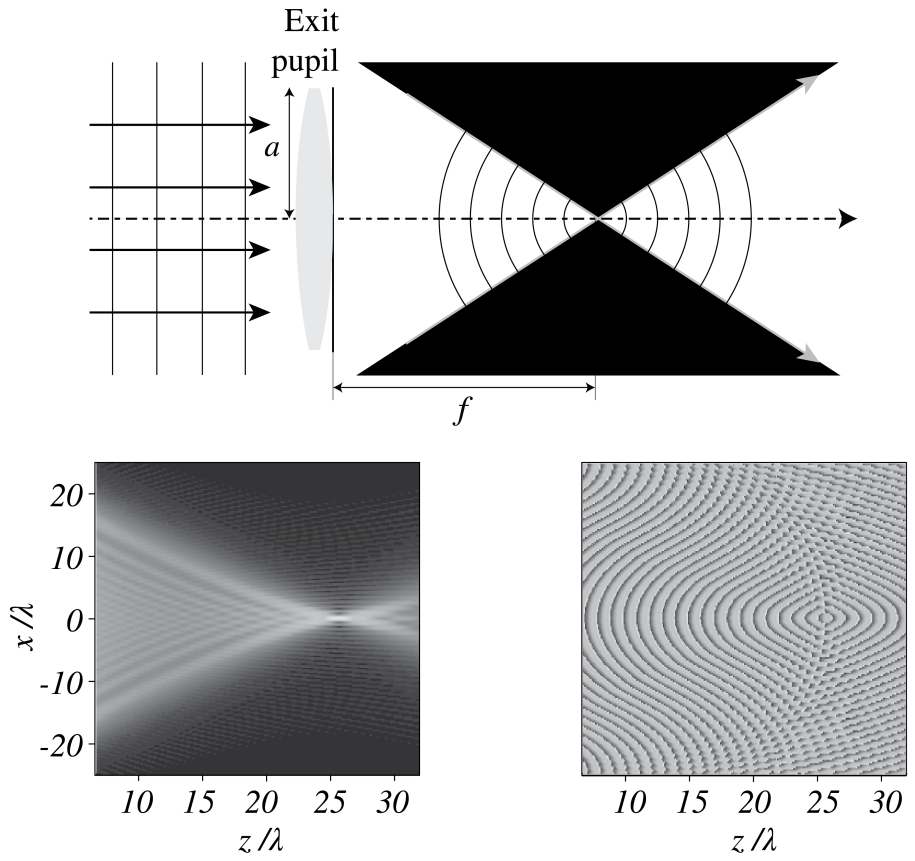


Figure 6.16: Top: wave fronts of the incident plane wave and the focused field according to Gaussian geometrical optics. There is no light outside of the two cones. Bottom left: amplitude as predicted by diffraction optics. The boundary of the cones is blurred and it is not absolutely dark outside of the cones. Furthermore, the intensity does not increase monotonically with decreasing distance to the focal point, as predicted by geometrical optics. Bottom right: phase of the focused field as predicted by diffraction optics.

2. If in Gaussian geometrical optics we illuminate a lens with tilted parallel rays of light (a plane wave propagating in an oblique direction), then the point in the back focal plane where the rays intersect is laterally displaced. A tilted plane wave is described by $U_i(\mathbf{r}) = \exp(i\mathbf{k}_0 \cdot \mathbf{r})$, and its Fourier transform with respect to (x, y) is given by

$$\mathcal{F}\{U_0\}\left(\frac{x}{\lambda f_i}, \frac{y}{\lambda f_i}\right) = \delta\left(\frac{x}{\lambda f_i} - \frac{k_{0,x}}{2\pi}\right)\delta\left(\frac{y}{\lambda f_i} - \frac{k_{0,y}}{2\pi}\right),$$

which is indeed a shifted delta peak (i.e. a shifted focal spot).

It seems that the diffraction model of light confirms what we know from geometrical optics. But in the previous two examples we discarded the influence of the finite size of the pupil, i.e. we have left out of consideration the function $1_{\odot_a}$ in calculating the Fourier transform. If $U_i(x, y) = 1$ in the entrance pupil and we take the finite size of the pupil properly into account, the δ-peaks become blurred: the focused field is then given by the Fourier transform of the circular disc with radius a, evaluated at spatial frequencies $\xi = \frac{x}{\lambda f_i}$, $\eta = \frac{y}{\lambda f_i}$. This field is called the **Airy spot** and is given by (See Appendix E.17):

$$U(x, y, z) = \frac{\pi a^2}{\lambda f_i} \frac{2J_1\left(2\pi \frac{a}{\lambda f_i}\sqrt{x^2 + y^2}\right)}{\frac{2\pi a}{\lambda f_i}\sqrt{x^2 + y^2}}, \qquad \textbf{Airy pattern for focusing}, \tag{6.70}$$

where J_1 is the Bessel function of the first kind and where the phase factors in front of the Fourier transform have been omitted. The pattern is shown in Fig. 6.17. It is circular symmetric and consists of a central maximum surrounded by concentric rings of alternating zeros and secondary maxima with decreasing amplitudes. In cross-section, as function of $r = \sqrt{x^2 + y^2}$, the Airy pattern is similar (but not identical) to the sinc-function. From the uncertainty principle illustrated in Fig. 6.7 it follows that the size of the focal spot decreases as a increases, and from (6.70) we see that the Airy function is a function of the dimensionless variable $ar/(\lambda f_i)$. Hence the focal spot becomes narrower as $a/(\lambda f_i)$ increases. The Numerical Aperture (NA) is defined by

$$\mathrm{NA} = \frac{a}{f_i}, \qquad \textbf{numerical aperture}. \tag{6.71}$$

Since the first zero of the Airy pattern occurs for $ar/(\lambda f_i) = 0.61$, the width of the focal spot can be estimated by

$$\textbf{Size of focal spot} \approx 0.61\frac{\lambda}{\mathrm{NA}} \tag{6.72}$$

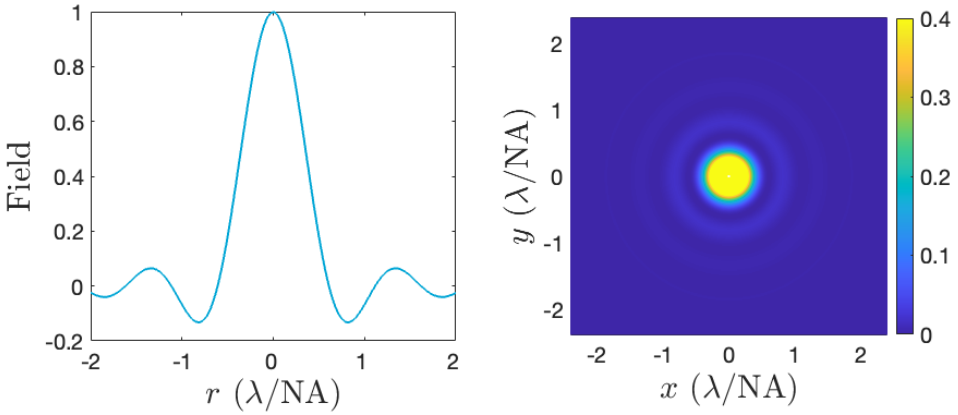


Figure 6.17: Left: cross-section of the rotational symmetric field of the Airy pattern as function of the radial coordinate. Right: intensity of the Airy pattern.

Remarks.

1. In the simple case of a single thin lens, the entrance and exit pupils coincide with the lens itself. As has been explained in Section 2.5.9, the exit pupil in systems consisting of several lenses is the real or virtual image of the aperture stop under all optical lenses to the right of the stop. To model the effect of diffraction in such more complicated systems, diffraction is assumed to take place only in the exit pupil. The field in the exit pupil is first determined by non-paraxial ray tracing and is then integrated over the exit pupil using the Fresnel diffraction integral.

2. Derivation of the Airy spot suggests that it is valid only in the paraxial approximation and that therefore it is only valid for sufficiently small NA. Indeed, we have replaced the spherical wave converging to the focal point by a parabolic wave using (6.63). It can be shown however that for points (x, y, f_i) in the focal plane that are close to the Gaussian geometrical focal point $(0, 0, f_i)$, the Airy spot is valid also for higher NA. However, when NA > 0.6 the rotation of the polarisation state of the light in the exit pupil by the lens can becomes important and then the scalar Airy spot (6.70) is not accurate anymore[14].

3. The focusing system that we have considered did not have aberrations. The finite size of the focused spot was entirely due to diffraction. Such as system is called **diffraction limited**.

6.6.2 Imaging by a lens

It follows from the derivations in the previous section that the Airy pattern is the image of a point source infinitely far in front of a lens. In this section we study the imaging of a general object at finite distance to the lens. Consider first a real point object on the optical axis with coordinate $z = s_o < f_o$ to the left of the object focal point of a positive lens with image focal coordinate $f_i > 0$. This lens will form a real image with positive coordinate $s_i > 0$.

The field in image space is derived similar to the focused field in the previous section. We postulate that the lens transforms the field radiated by the point object into a spherical wave in the exit pupil which converges to the ideal image point of Gaussian geometrical optics. This wave in the exit pupil is propagated to the image space using the Fresnel diffraction integral. Then for an object point on the optical axis we find the same Airy pattern as in Fig. 6.17, except that the variable $ar/(\lambda f_i)$ is replaced by $ar/(\lambda s_i)$, where s_i is the ideal image coordinate as given by the Lensmaker's Formula. This Airy pattern is called the Point Spread Function (PSF):

[14] J.Braat et al. Imaging Optics, Cambridge University Press, 2019

$$\mathrm{PSF}(x,y) = \frac{\pi a^2}{\lambda s_i} \frac{J_1\left(2\pi \frac{a}{\lambda s_i}\sqrt{x^2+y^2}\right)}{\frac{2\pi a}{\lambda s_i}\sqrt{x^2+y^2}}, \qquad \textbf{Airy pattern for imaging.} \tag{6.73}$$

For object points that are not on the optical axis, the PSF is translated such that it remains centred on the ideal Gaussian image point.

A general object field $U_o(x,y)$ can be considered a superposition of point objects and the images of these points are given by translated PSFs:

$$\mathrm{PSF}(x - x_i, y - y_i),$$

where (x_i, y_i) are the transverse coordinates of the image point according to Gaussian geometrical optics. The total image field is obtained by summing (integrating) over these PSFs, weighted by the field at the object points:

$$U_i(x,y,s_i) = \int\int \mathrm{PSF}\,(x - Mx_o, x - My_o)\, U_o(x_o, y_o, s_o)\,\mathrm{d}x_o\mathrm{d}y_o. \tag{6.74}$$

where $x_o = x_i/M$, $y_o = y_i/M$ is the image point and M is the magnification. The integral can be made into a convolution by using the coordinates x_i, y_i as integration variables.

It is clear from (6.73) that larger radius a of the lens and smaller wavelength λ imply a narrower PSF. This in turn implies that the kernel in the convolution is more sharply peaked and hence that the resolution of the image is higher [15].

Remarks.

1. If laser light is used to illuminate the object, the object field may be considered perfectly coherent. This implies that a detector in the image plane would measure the squared modulus of the complex field (6.74):

$$I_i(x,y,s_i) = \left|\int\int \mathrm{PSF}\,(x - Mx_o, y - My_o)\, U_o(x_o, y_o, s_o)\,\mathrm{d}x_o\mathrm{d}y_o\right|^2. \tag{6.75}$$

In this case the system is called a **coherent imaging system**.

2. If the object is a spatially incoherent extended source, the fields emitted by the point sources of which extended source consists cannot interfere in the image plane. Therefore, in this case the intensity in the image plane is given by the incoherent sum:

$$I_i(x,y,s_i) = \int\int |\mathrm{PSF}\,(x - Mx_o, y - Mx_o)|^2\; I_o(x_o, y_o, s_o)\,\mathrm{d}x_o\mathrm{d}y_o, \tag{6.76}$$

where $I_o = |U_o|^2$ is the intensity distribution of the extended source. Hence the image intensity is expressed in the intensity of the source by a convolution with the intensity of the PSF. This system is called an **incoherent imaging system**.

3. An object is often illuminated by a spatially incoherent extended light source and then imaged. According to the discussion in Section 5.6, the field that illuminates the object is then **partially coherent**. It is more coherent when the angle that the source extends at the object is smaller. The intensity in the image plane can be computed by splitting the spatially incoherent source into sufficiently many mutually incoherent point sources and computing the intensities in the image plane due to the illumination of the object by each individual point source. The total intensity in the image plane is then the sum of these intensities.

[15] Hecht §10.2.6 '*Resolution of imaging systems*'.

4. We have considered only scalar diffraction theory. However, for a lens with numerical aperture larger than 0.6, the change of polarisation can be important. Then a more general diffraction theory is needed [16].

6.6.3 Spatial Light Modulators and Optical Fourier Filtering

- **SLM.** The field in the entrance pupil of a lens, in particular its phase can be changed spatially by a so-called **spatial light modulator** (SLM). A SLM has thousands of pixels by which very general focused fields can be made. An example is a focused fields with only a longitudinal component in the focal point (i.e. only the E_z-component is nonzero at the focal point)[17].

- **Fourier filtering.** Suppose we have the setup as shown in Fig. 6.18. With one lens we can create the Fourier transform of some field $U(x, y)$. Let a mask be put in the focal plane and a second lens be used to refocus the light. This implies that the amplitude and the phase of the plane waves in the angular spectrum of the field are manipulated. The procedure is called Fourier filtering using lenses. An application of this idea is the phase contrast microscope.

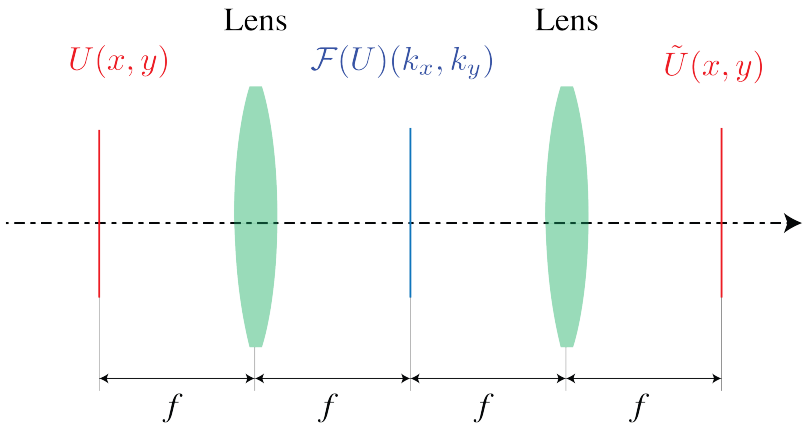


Figure 6.18: Set-up for Fourier filtering. The first lens creates a Fourier transform of $U(x, y)$, to which we can apply some operation (e.g. applying different phase shifts to different parts of the field). The second lens then applies another Fourier transform (which is the same as the inverse Fourier transform and a mirror transformation).

6.7 Super-resolution

We have emphasised that evanescent waves set the ultimate limit to resolution in optics. In Chapter 2 it was explained that, although within geometrical optics one can image a single point perfectly using conical surfaces, planes can in general not be imaged perfectly. It was furthermore explained that when only paraxial rays are considered, i.e. within Gaussian geometrical optics, perfect imaging of extended objects *is* achieved by spherical lenses. However, non-paraxial rays cause aberrations. But even when perfect imaging would be possible in geometrical optics, a real image can never be perfect due to the fact that information contained in the amplitudes and phase of the evanescent waves cannot propagate. The resolution that can be obtained with an optical system consisting of lenses is less than follows from considering the loss of information due to evanescent waves, because propagating waves with spatial frequencies that are too large

[16] J.Braat et al. Imaging Optics, Cambridge University Press, 2019
[17] See Phys. Rev. Lett. 100, 123904, 2008

to be captured by the optical system (i.e. waves of which the angles with the optical axis are larger than the numerical aperture) cannot contribute to the image. Therefore the image of a point object has the size

$$0.61\lambda/NA_i, \tag{6.77}$$

where $NA_i = a/s_i$ is the numerical aperture in image space, i.e. it is the sinus of half the opening angle of the cone extended by the exit pupil at the Gaussian image point on the optical axis. This resolution limit is called the diffraction limit.

The size of the image of a point as given by the PSF in (6.73) is influenced by the magnification of the system. To characterise the resolution of a diffraction-limited system, it is therefore better to consider the numerical aperture on the object side: $NA_o = NA_i|M| = a/s_o$. The value of NA_o is the sinus of the half angle of the cone subtended by the entrance pupil of the system on the object point on the optical axis. This is the cone of wave vectors emitted by this object point that can contribute to the image (they are "accepted" by the optical system). The larger the half angle of this cone, the more spatial frequencies can contribute to the image and hence the larger the information about finer details of the object that can reach the image plane. The spatial frequencies that contribute to the image are inside the circular base of the cone in object space.

It should be clear by now that beating the diffraction limit is extremely difficult. Nevertheless, a lot of research in optics is directed towards realising this goal. Many attempts have been made, some successful others not, but whether successful or not, most were based on very ingenious ideas. To close this chapter on diffraction theory, we will give examples of attempts to achieve what is called super-resolution.

- **Confocal microscopy.** A focused spot is used to scan the object and the reflected field is imaged onto a small detector ("point detector"). The resolution is roughly a factor 1.5 better than for normal imaging with full field of view using the same objective. The higher resolution is achieved thanks to the illumination by oblique plane waves that are present in the spatial Fourier transform of the illuminating spot. By illumination with plane waves with large angles of incidence, higher spatial frequencies of the object which under normal incidence are not accepted by the objective, are now "folded back" into the cone of plane waves accepted by the objective. The higher resolution comes at the prize of longer imaging time because of scanning. The confocal microscope was invented by Marvin Minsky in 1957.

- **The Perfect Lens based on negative refraction.** It can be shown that a slab of a material with **negative permittivity** and **negative permeability** which are opposite to the permittivity and permeability of the surrounding medium, there is no reflection at the interfaces. Furthermore, the phase velocity in a material with negative permittivity and negative permeability is opposite to the direction of the flow of energy and plane waves are refracted at the interface as if the refractive index in Snell's Law is negative. Therefore these media are called negative index media. Because the phase velocity is opposite to the energy velocity, it is as if time is reversed inside the slab. The change of phase of propagating waves of the field of point source due to propagating in the surrounding medium is reversed inside the slab and both some where inside the slab and at some distance on the other side of it there is an image point where all propagating waves are in phase, as illustrated in Fig. 6.19. Furthermore, evanescent waves **gain** amplitude inside the slab and it turns out they have the same amplitude in the image point as in the source, hence the image point is perfect. Note that the increase of amplitude of an evanescent wave does not violate the conservation of energy, because an evanescent wave does not propagate energy in the direction in which it is evanescent.

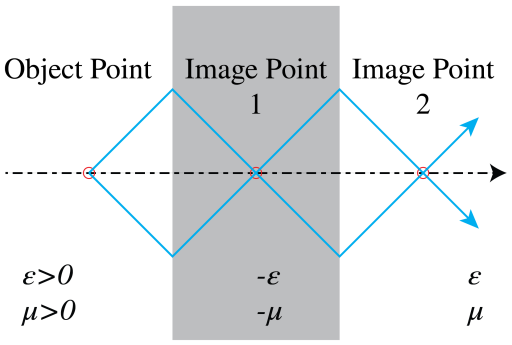


Figure 6.19: Pendry's perfect lens consists of a slab of a material with negative permittivity and negative permeability such that its absolute values are equal to the positive permittivity and positive permeability of the surrounding medium. Points outside the slab are imaged perfectly in two planes: one inside the slab and the other on the opposite side of the slab.

The simple slab geometry seen in Fig. 6.19 which acts as a perfect lens was proposed by John Pendry in 2000 [18]. Unfortunately, a material with negative permittivity and negative permeability has not been found in nature. Therefore, many researchers have attempted to mimic such a material by mixing metals and dielectrics on a sub-wavelength scale. It seems that a negative index without absorption would violate causality. But when there is absorption, the image is not anymore perfect.

- **Hyperbolic materials.** Hyperbolic materials are anisotropic, i.e. the phase velocity of a plane wave depends on the polarisation and on the direction of the wave vector. The permittivity of an anisotropic material is a tensor (loosely speaking a (3,3)-matrix). Normally the eigenvalues of the permittivity matrix are positive. However, in a hyperbolic material two eigenvalues are of equal sign and the third has opposite sign. Therefore an hyperbolic medium behaves partially as a dielectric and partially as a metal. In=t can be shown that all waves with the so-called extraordinary state of polarisation propagate, no matter how high the spatial frequencies are. Hence, for the extraordinary state of polarisation evanescent waves do not exist and therefore super-resolution and perfect imaging should be possible in such a medium.

[18] J.B. Pendry, PRL 18, 2000

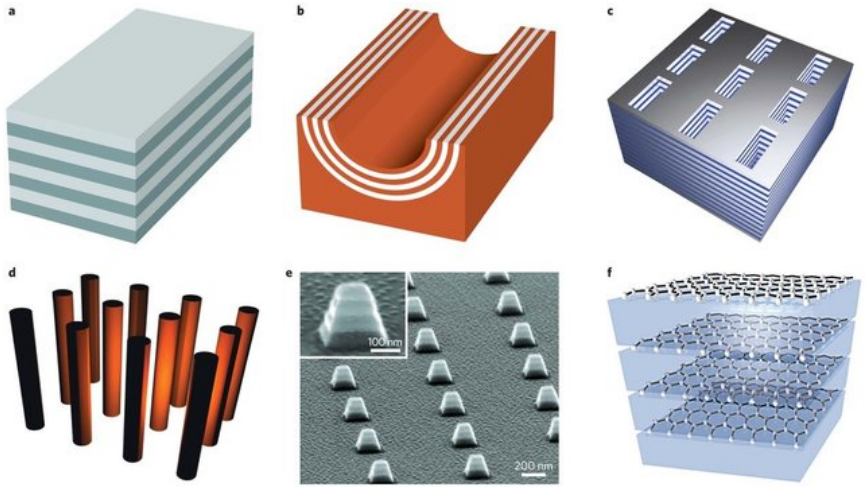


Figure 6.20: Examples of composite materials consisting of thin (sub-wavelength) layers of metals and dielectrics. These artificial materials are called metamaterials. (A. Poddubny, I. Iorsh, P. Belov, & Y. Kivshar, *Hyperbolic Metamaterials*, Nat. Photon., 7(12), 948-957 (2013)).

A few natural hyperbolic media exist for visible frequencies, but there are more in the mid-infrared. Researchers try to approximate hyperbolic media by metamaterials, made e.g. multi-layers consisting of alternating thin metallic and dielectric layers, so that the effective permittivity has the desired hyperbolic property. Also metallic nanopilars embedded in a dielectric are used.

- **Nonlinear effects.** When the refractive index of a material depends on the local electric field, the material is nonlinear. At optical frequencies nonlinear effects are in general very small, but with a strong laser they can become significant. One effect is self-focusing, where the refractive index is proportional to the local light intensity. The locally higher intensity causes an increase of the refractive index, leading to a waveguiding effect due to which the beam focuses even more strongly. Hence the focused beam becomes more and more narrow while propagating, until finally the material breaks down.

- **Stimulated Emission Depletion Microscopy (STED).** This technique was invented by V. A. Okhonin in 1986 in the USSR and was further developed by Stefan Hell and his co-workers in the nineties. Hell received the Nobel Prize in chemistry for his work in 2014. STED is a non-linear technique with which super-resolution in fluorescence microscopy can be achieved. Images made with a fluorescence microscope are blurred when the fluorescent molecules are very close together. In the STED microscope a special trick is used to ensure that molecules which fluoresce at the same time are sufficiently far from each other. To achieve this two focused spots are used: the first spot excites the molecules to a higher level. The second spot is slightly red-shifted and has a doughnut shape (see Fig. 6.21). It causes decay of the excited molecules to the lower level by stimulated emission (the excited state is depleted). Because of the doughnut shape of the second spot, the molecule in the centre of the spot is not affected and will still fluoresce. Crucial is that that the doughnut spot has a central dark region which is very narrow. A region where the field is almost zero can indeed be much smaller than the Airy spot and this is the reason for the super-resolution.

External sources in recommended order

1. Every picture is made of waves - Sixty Symbols, 3:33 to 7:15: Basic explanation of Fourier transforms.
2. Heisenberg's Microscope - Sixty Symbols, 0:20 to 2:38: Basic explanation of the uncertainty principle (though in the context of quantum physics).
3. E. Hecht, *Optics*, §7.4.4, subsection '*Fourier Analysis and Diffraction*'.
4. J. Goodman, *Introduction to Fourier Optics*, §5.2.2: Several calculations on the Fourier transforming properties of lenses.
5. E. Hecht, *Optics*, §10.2.6, subsection '*Resolution of imaging systems*'.

Problems

1. **Radiating point source.** Consider a radiating time-harmonic point source in $\mathbf{r}_1 = (x_1, 0, 0)$. The complex field in the point of observation $\mathbf{r} = (x, y, z)$, where $z > 0$, is given by:

$$U_1(x, y, z) = Q_1 \frac{e^{ik\sqrt{(x-x_1)^2+y^2+z^2}}}{\sqrt{(x-x_1)^2+y^2+z^2}}.$$

where Q_1 is a given complex number of which the modulus is proportional to the source strength.

   a) Derive that for fixed z_1 and for sufficiently large $z > 0$ the field can be approximated by

$$U_{1,far}(x, y, z) = Q_1 \frac{e^{ikz}}{z} e^{ik\frac{x^2+y^2}{2z}} e^{-i\frac{kx_1 x}{z}}. \tag{6.78}$$

   b) Let there be a second point source at $\mathbf{r}_2 = (x_2, 0, 0)$, with complex source strength Q_2 with $|Q_2| = |Q_1|$. We assume that both point sources are coherent. This means that there is ϕ such that $Q_2 = Q_1 e^{i\phi}$. Show that the field in (x, y, z) for $z > 0$ large due to the two point sources can be written as

$$U(x, y, z) \approx U_{1,far}(x, y, z) \left(1 + e^{i\phi} e^{i\frac{k\Delta x x}{z}}\right), \tag{6.79}$$

   where $\Delta x = x_1 - x_2$.

   c) For which angles $\theta = x/z$ does the intensity in the far field vanish? Show that the distance between the point sources Δx can be determined from the angular separation of the zeros of the intensity. Does the angular separation depend on the phase difference ϕ?

   d) What should be the phase difference between the point sources such that for $x/z = 0$ on the screen at large distance z the intensity vanishes?

2. **Two slits.** Consider two slits of equal width a in a non-transparent screen of thickness d in the plane $z = 0$ as shown in Fig. 6.22. The screen is illuminated by a plane wave with unit amplitude and propagating in the positive z-direction. In the second slit there is a piece of glass with refractive index n and thickness d. In the first slit there is vacuum.

   a) If the field immediately behind slit 1 has complex amplitude equal to 1, explain that the field immediately after behind 2 is given by

$$e^{i\phi}$$

   with $\phi = k(n-1)d$.

   b) Derive (using (6.78) or in another way) that the Fraunhofer intensity pattern on a screen along the line $y = 0$ at large distance z is given by (upto factors that do not depend on x/z).

$$I_{far}(x, 0, z) = 2\frac{a^2}{z^2} \left[\frac{\sin\left(\frac{kax}{2z}\right)}{\frac{kax}{2z}}\right]^2 \left[1 + \cos\left(\frac{kbx}{z} + \phi\right)\right]. \tag{6.80}$$

   In deriving this result you may omit all factors that are independent of x/z. 5and y/z. If you use (6.79) you may take $Q_1 = 1$, $Q_2 = e^{i\phi}$.

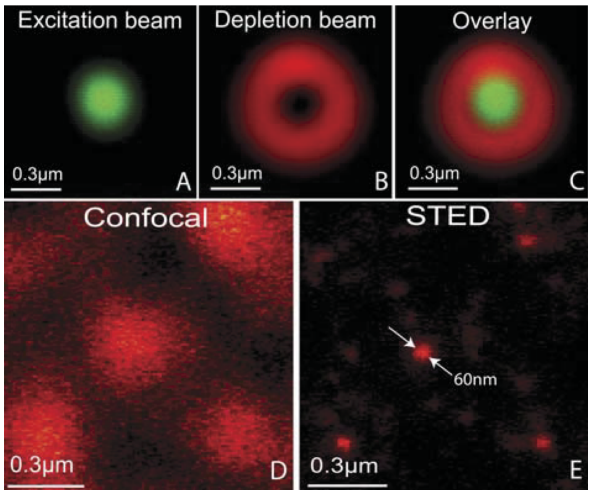


Figure 6.21: Spot used for excitation (top left) and for depletion (top middle). Fluorescence signal top right. In the lower figure the confocal image is compared to the STED image. (P.F. Rodriguez and al., *Building a fast scanning stimulated emission depletion microscope*, Materials Science (2012))

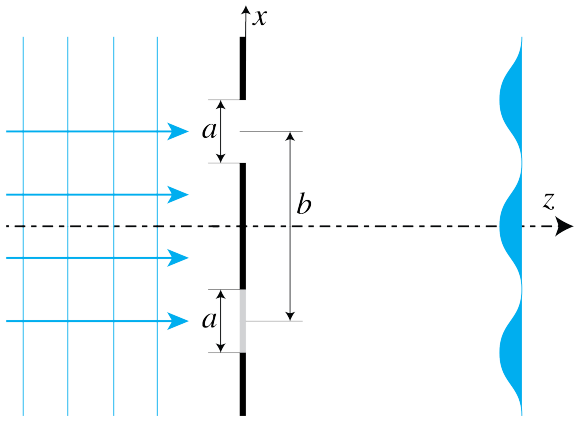


Figure 6.22: Two slits centred at $y = 0$ and very long in the y-direction in a dark screen of thickness d. The lower slit is filled with glass, the upper is in vacuum.

c) Make a sketch of this intensity pattern, showing the zeros and maxima as function of $\theta = x/z$ when $a = 2\lambda$, $b = 4\lambda$ and $\phi = -\pi/2$. Explain where the the envelope and the other factor that depends on x/z are caused by.

3. **Point source, aperture and mirror.** We consider the optical set-up shown at the left of Fig. 6.23 where a point source at point $\mathbf{r}_s = (a, 0, 0)$ is above a plane mirror in the plane $x = 0$. The time-harmonic field emitted by the point source **without the mirror being present** is in complex notation given by:

$$U_s(x, y, z, t) = \frac{e^{ik\sqrt{(x-a)^2+y^2+z^2}-i\omega t}}{\sqrt{(x-a)^2+y^2+z^2}}.$$

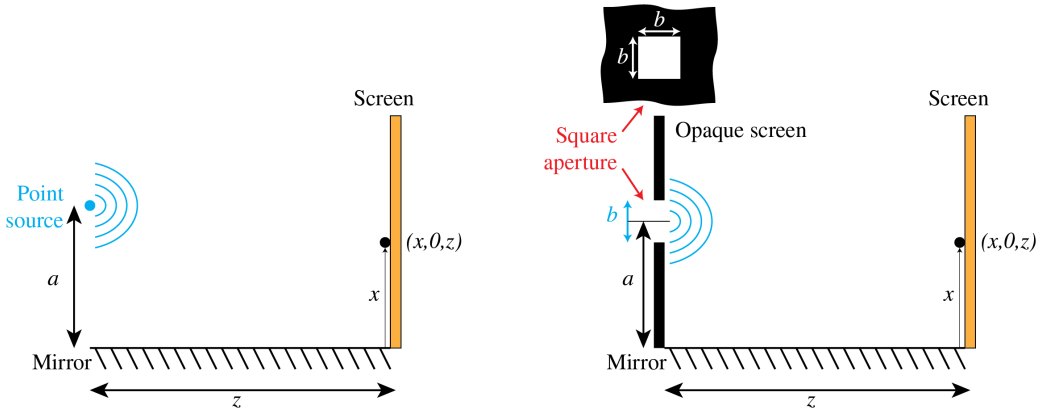


Figure 6.23: Lloyd mirror configuration with a point source (left) and a rectangular aperture in a dark screen (right), above a mirror and with a screen at distance z where the field is observed.

a) Let U_r be the field reflected by the mirror. Assume that the mirror is perfect so that the total field $U_s(x, y, z) + U_r(x, y, z)$ is zero on the surface of the mirror, i.e. when $x = 0$. Show that the reflected field U_r can be considered to be emitted by a point source in $(-a, 0, 0)$, which is the image of the original point source by the mirror, and which is **out of phase** with the original point source and has the **same strength**.

b) Consider the field on a screen at $z > 0$. According to (a) the field in the presence of the mirror can be considered to be radiated by two point sources, namely at $(a, 0, 0)$ and $(-a, 0, 0)$, that are of equal strength and out of phase with each other. Assume that z is so large that the spherical waves emitted by these point sources and arriving at the screen can both be considered to be plane waves. Derive that the point on the screen $(x, 0, z)$ with smallest $x > 0$ where the field is zero is given by

$$x = \frac{\lambda}{2a} z, \tag{6.81}$$

where λ is the wavelength. In your derivation use path length differences of interfering rays and make a drawing.

c) What happens with this zero and with the fringe patten on the screen when the perfect mirror is replaced by a dielectric such as a piece of glass?

d) Suppose now that there is a second point source at $(2a, 0, 0)$ above the mirror and suppose that it has the same strength and is in phase with the point source in $(a, 0, 0)$. Assume again that the mirror is perfectly reflecting and derive (again by considering path length differences and using a drawing) that the smallest $x > 0$ for which a zero occurs in point $(x, 0, z)$ on the screen is given by

$$x = \frac{\lambda}{3a} z$$

e) Derive the smallest $x > 0$ for which the field is zero in $(x, 0, z)$ when the two point sources at $(a, 0, 0)$ and $(2a, 0, 0)$ are mutually incoherent. Use again path length differences and make a drawing.

f) Next suppose that there is a square aperture with centre at $(a, 0, 0)$ and sides of length $b < a$ parallel to the x- and y-directions in an opaque (i.e. dark) screen above the mirror as shown at the right of Fig. 6.23. The aperture is illuminated by a plane wave that propagates parallel to the z-axis, hence the field in the aperture has constant phase and amplitude. Compute the smallest positive x for which a zero occurs at $(x, 0, z)$ on the screen at large distance $z > 0$. Use again path length differences and a drawing in your derivation.

4. **Diffraction without calculations.**
Note: to answer the following questions it is **NOT** necessary to compute diffraction integrals.

a) Consider two equally strong point sources which with respect to a coordinate system (x, y, z) are at $(-a/2, 0, 0)$ and $(a/2, 0, 0)$, where the z-axis is the optical axis. Suppose the point sources are mutually coherent and suppose that they emit in phase. The maximum intensity on a screen at large (i.e. Fraunhofer) distance is then on the optical axis. Show that the smallest angle with the optical axis at which there is a zero on this screen is given by $\lambda/(2a)$.

b) What is the smallest angle with the optical axis at which there is a zero on the screen when the two point sources emit with phase difference $\pi/2$?

c) Are there any zeros on the screen when the two point sources are mutually incoherent?

d) Consider now two identical apertures in an opaque screen at $z = 0$. One aperture has its centre at $(-a/2, 0, 0)$ and the other has its centre at $(a/2, 0, 0)$. The apertures are illuminated by a time-harmonic plane wave at perpendicular incidence to the screen (i.e. propagating parallel to the z-axis). Explain that whatever the shape of these apertures, the smallest angle for which a zero occurs in the far field intensity is at $\lambda/(2a)$.

e) Suppose that the plane wave is incident at some angle different from 90°. Let its complex field be given by

$$U(x, z) = e^{i(k_x x + k_z z)}$$

where $\sqrt{k_x^2 + k_z^2} = k$. Suppose that $k_x a = \pi/2$ (modulo 2π). What is now the smallest angle where a zero occurs on the screen in the far field? Explain your answer.

f) Now imagine that both (identical) apertures are filled with glass plates with thickness that varies with position. The two glass plates are identical and they are identically positioned in each of the two apertures. Imagine that we illuminate the apertures with a plane wave at perpendicular incidence. The field transmitted by each aperture is now a rather complicated function of position, however the transmitted fields behind both apertures are identical. Does the far field intensity still vanish for angle $\lambda/(2a)$ or will it be modified by the presence of the glass plates? Explain your answer.

5. **Bessel beams.** Suppose there is a mask in the entrance pupil of radius a of a positive thin lens with image focal length f_i with a thin ring-shaped aperture at $r = b$ with width Δr. If a plane wave with amplitude A is at perpendicular incidence on the mask, the field immediately behind the mask is given by

$$U_{Bessel}(x, y) = \begin{cases} A, & \text{if } b - \Delta r < \sqrt{x^2 + y^2} < b, \\ 0, & \text{otherwise} \end{cases}$$

a) Use the integral

$$\int_0^{2\pi} e^{i\zeta \cos\psi} \, \mathrm{d}\psi = 2\pi J_0(\zeta).$$

to derive that for sufficiently small Δr, the field in the focal plane is in good approximation given by

$$U_{Bessel}(x, y, f_i) = 2\pi A b \Delta r J_0\left(k \frac{br}{f}\right).$$

b) The beam obtained this way is called a Bessel beam. Explain why this beam has a very long focal depth.

c) Suppose that the Airy spot obtained by focussing of a unit amplitude plane wave and the Bessel beam carry the same amount of energy. Show that then the amplitude of the Bessel beam is given by

$$A = \frac{a}{\sqrt{2b\Delta r}}$$

d) Derive that the ratio of the field amplitudes in the focal point of the Bessel beam i: $U_{Bessel}(0,0,f_i)$ and the Airy spot: $U_{Airy}(0,0,f_i)$ is given by

$$\frac{U_{Bessel}}{U_{Airy}} = \frac{\sqrt{2b\Delta r}}{a}.$$

If $b = a$ and $\Delta r = 0.1a$ this becomes

$$\frac{U_{Bessel}}{U_{Airy}} = \sqrt{\frac{2\Delta r}{a}} \approx 0.44,$$

which is the case shown in Fig. 6.24.

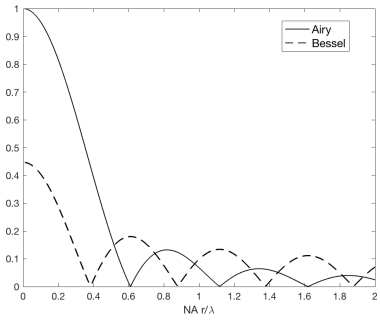


Figure 6.24: Amplitude in the focal plane of a Bessel beam and of an Airy spot with the same total energy. The lens pupil has diameter $a = 10000\lambda$, the ring aperture of the Bessel beam case is at the outer edge of the pupil ($b = a$) and has width $\Delta r = 0.1a$ and the NA $= 0.1$.

e) The Bessel beam has stronger side lobes than the Airy spot. Explain the reason.

6. * **Stellar interferometry.** We consider the emission by a star of light of a narrow frequency band with centre frequency $\bar{\omega}$ and corresponding wavelength $\bar{\lambda} = c2\pi/\bar{\omega}$ The star is an extended spatially incoherent source. Let $I(x,y)$ be the intensity on the star's surface orientated towards the earth. The aim of the exercise is to determine $I(x,y)$ by stellar interferometry.
Let $U_0(x,y,t)$ be the field emitted at the surface of the star. Then the mutual coherence function at points $S_1 = (x_1, y_1)$, $S_2 = (x_2, y_2)$ on the surface of the star is:

$$\begin{aligned} \Gamma(S_1, S_2, \tau) &= \langle U_0^*(S_1, t) U_0(S_2, t+\tau) \rangle \\ &= I(x_1, y_1) e^{i\omega\tau} \delta(x_1 - x_2)\delta(y_1 - y_2) \quad \text{for all } \tau. \end{aligned}$$

a) Let z_e be the distance of the star from earth. Use the quasi-monochromatic approximation to derive the field in a point $P_e = (x_e, y_e)$ on earth.

b) Show that the mutual coherence function in two points $P_e = (x_e, y_e)$ and $\tilde{P}_2 = (\tilde{x}_e, \tilde{y}_e)$ on earth is for $\tau = 0$ given by

$$\Gamma(P_e, \tilde{P}_e, \tau = 0) = \int\int I(x_1, y_1) e^{2\pi i \left(\frac{x_e - \tilde{x}_e}{\lambda z_e} x_1 + \frac{y_e - \tilde{y}_e}{\lambda z_e} y_1 \right)} dx_1 dy_1.$$

i.e. the mutual coherence function between points on earth for time delay $\tau = 0$ can be expressed in the Fourier transform of the intensity $I(x,y)$ emitted by the star, evaluated at spatial frequencies $\xi = \frac{x_e - \tilde{x}_e}{\lambda z_e}$ and $\eta = \frac{y_e - \tilde{y}_e}{\lambda z_e}$.

c) Explain how the mutual coherence for time delay $\tau = 0$ can be measured on earth using interferometry and how this can lead to retrieving the intensity of the star.

d) What determines the resolution that can be achieved?

Chapter 7

Lasers

What you should know and be able to do after studying this chapter

- Know the special properties of laser sources.
- Understand the optical resonator and why it is needed.
- Understand the role of the amplifier and explain what the gain curve is.
- Explain the principle of population inversion and how it can be achieved.
- Explain how single frequency operation can be obtained.
- Understand what transverse modes are and how they can be prevented.

In the early 1950s a new source of microwave radiation, **the maser**, was invented by C.H. Townes in the USA and A.M. Prokhorov and N.G. Basov in the USSR. Maser stands for "Microwave Amplification by Stimulated Emission of Radiation". In 1958, A.L. Schawlow and Townes formulated the physical constraint to realise a similar device for visible light. This resulted in 1960 in the first optical maser by T.H. Maiman in the USA. This device was since then called **L**ight **A**mplification by **S**timulated **E**mission of **R**adiation or **laser**. It has revolutionised science and engineering and has many applications, e.g.

- bar code readers,
- compact discs,
- computer printers,
- fiber optic communication,
- sensors,
- material processing,
- non-destructive testing,
- position and motion control,
- medical applications, such as treatment of retina detachment,
- nuclear fusion,
- holography.

7.1 Unique Properties of Lasers

The broad application of lasers is made possible by the unique properties which distinguishes lasers from all other light sources. We discuss these unique properties below.

7.1.1 Narrow Spectral Width; High Temporal Coherence

These properties are equivalent. A spectral lamp, like a gas discharge lamp based on Mercury vapour, can have a spectral width of $\Delta\nu = 10$ GHz. Visible frequencies are around 2×10^{14} Hz, hence the spectral width of the lamp is roughly 0.02%. The line width measured in wavelengths satisfies

$$\frac{\Delta\lambda}{\lambda} = \frac{\Delta\nu}{\nu}, \tag{7.1}$$

and hence for $\lambda = 550$ nm, $\Delta\lambda$ of a spectral lamp is of the order of 0.1 nm. A laser can however easily have a frequency band that is a factor of 100 smaller, i.e. less than 10 MHz=10^7 Hz in the visible. For a wavelength of 550 nm this means that the linewidth is only 0.001 nm. As has been explained in Chapter 7, the coherence time τ_c of the emitted light is the reciprocal of the frequency bandwidth:

$$\Delta\tau_c = 1/\Delta\nu. \tag{7.2}$$

Light is emitted by atoms in bursts of harmonic (cosine) waves consisting of a great but finite number of periods. As will be explained in this chapter, due to the special configuration of the laser, the wave trains in laser light can be extremely long, corresponding to a very long coherence time.

7.1.2 Highly Collimated Beam

Consider a discharge lamp as shown in Fig. 7.1. To collimate the light, the lamp can be positioned

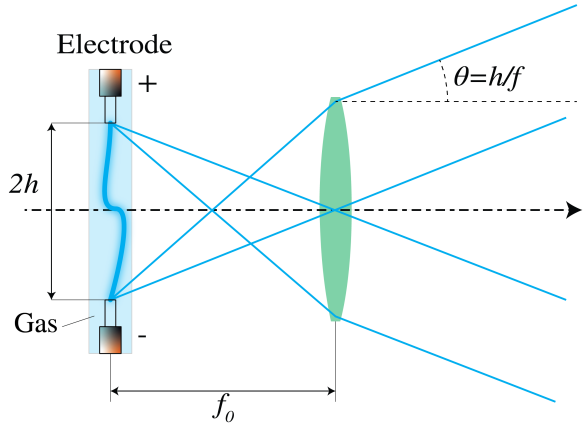


Figure 7.1: A discharge lamp in the focal plane of a converging lens. Every atom in the lamp emits a spherical wave during a burst of radiation, lasting on average a coherence time $\Delta\tau_c$. The overall divergence of the beam is determined by the atoms at the extreme positions of the source.

in the focal plane of a lens. The spherical waves emitted by the atoms (point sources) in the lamp are collimated into plane waves whose direction depends on the position of the atoms in the source. The atoms at the edges of the source determine the overall divergence angle θ, which is given by

$$\theta = h/f, \tag{7.3}$$

where $2h$ is the size of the source and f is the focal length of the lens as shown in Fig. 7.1. Hence the light can be collimated by either choosing a lens with large focal length or by reducing the size of the source, or both. Both methods lead, however, to weak intensities. Due to the special

configuration of the laser source, which consists of a Fabry-Perot resonator in which the light bounces up and down in the z-direction many times before being emitted, the atomic sources are effectively all at very large distance and hence the effective size of the source is very small. The divergence of the laser beam is therefore not limited by the size of the source but by the size of its emitting surface through the inevitable effect of diffraction. As follows from Chapter 6, a parallel beam of diameter D and wavelength λ has a diffraction limited divergence given by:

$$\theta = \frac{2\lambda}{D}. \tag{7.4}$$

The diffraction-limited divergence thus depends on the wavelength and decreases when the diameter of the emitting surface increases. With a laser source, the diffraction-limited convergence angle can almost be reached and therefore a collimated beam with very high intensity can be realised (Fig. 7.2).

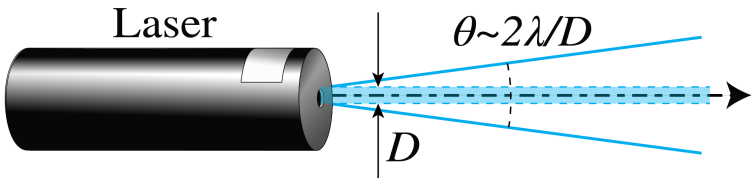


Figure 7.2: A laser beam can almost reach diffraction-limited collimation.

7.1.3 Diffraction-Limited Focused Spot; High Spatial Coherence

If a perfectly collimated beam is focused with a lens with very small aberrations and with numerical aperture NA, the lateral size of the focused spot is, according to Chapter 6, diffraction-limited and given by

$$\text{diffraction-limited spot size} = 0.61\frac{f}{D}\lambda = 0.61\frac{\lambda}{NA}. \tag{7.5}$$

With a laser one can achieve a diffraction-limited spot with a very high intensity.

As has been explained in Chapter 5, a light wave has **high spatial coherence** if at any given time, its amplitude and phase in different points can be predicted. The spherical waves emitted by a point source have this property. But when there are many point sources (atoms) that each emit bursts of harmonic waves that start at random times, as is the case in a classical light source, the amplitude and phase of the total emitted field at any position in space cannot be predicted. The only way to make the light spatially coherent is by making the light source very small, but then the intensity is low. As will be explained below, by the design of the laser, the emissions by the atoms of the amplifying medium in a laser are phase-correlated, which leads to a very high temporal and spatial coherence. The property of a small spot size with high intensity is essential for many applications, such as high resolution imaging, material processing with cutting, welding and drilling spots with very high power and in retina surgery, where a very small, high-intensity spot is applied to weld the retina without damaging the surrounding healthy tissue.

7.1.4 High Power

There are two types of lasers namely continuous wave (CW) lasers, which produce a continuous output, and pulsed lasers which emit a train of pulses. These pulses can be very short: from nanoseconds to even femtoseconds (10^{-15} s). A relatively low-power CW laser is the HeNe laser which emits roughly 1 mW at the wavelength 632 nm. Other lasers can emit up to a megawatt

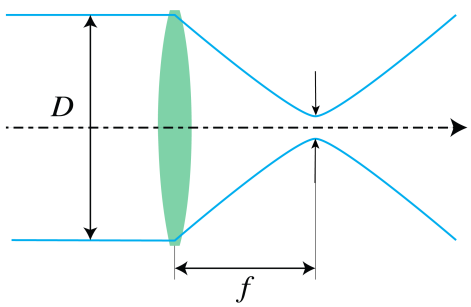


Figure 7.3: Diffraction-limited spot obtained by focusing a collimated beam.

of continuous power. Pulsed lasers can emit enormous peak intensities (i.e. at the maximum of a pulse), of more than 10^9 Watt.

There are many applications of high-power lasers such as for cutting and welding materials. To obtain EUV light with sufficient high intensity for use in photolithography for manufacturing ICs, extremely powerful CO_2 lasers are used to excite a plasma. Extremely high-power lasers are also applied to initiate fusion and in many nonlinear optics applications. Lasers with very short pulses are used to study very fast phenomena with short decay times.

7.1.5 Wide Tuning Range

For a wide range of wavelengths, from the vacuum ultra-violet (VUV), the ultra-violet (UV), the visible, the infrared (IR), the mid-infrared (MIR) up into the far infrared (FIR), lasers are available. For some type of lasers, the tuning range can be quite broad. The gaps in the electromagnetic spectrum that are not directly addressed by laser emission can be covered by techniques such as higher harmonic generation and frequency differencing.

7.2 Optical Resonator

We now explain the working of lasers. A laser consists of

1. an optical resonator;

2. an amplifying medium.

In this section we consider the resonator. Its function is to obtain a high light energy density and to gain control over the emission wavelengths.

A resonator, whether it is mechanical like a pendulum, a spring or a string, or electrical like an LRC circuit, has one or multiple resonance frequencies ν_{res}. Every resonator has losses due to which the oscillation gradually dies out when no energy is supplied. The losses cause an exponential decrease of the amplitude of the oscillation, as shown in Fig. 7.4. The oscillation is therefore not purely monochromatic but has a finite bandwidth of order $\Delta\nu \approx 1/\Delta\tau$ as shown in Fig. 7.4, where $\Delta\tau$ is the time at which the amplitude of the oscillation has reduced to half the initial value.

The optical resonator is a Fabry-Perot resonator filled with some material with refractive index n bounded by two aligned, highly reflective mirrors at a distance L. The Fabry-Perot resonator is discussed extensively in Section 5.9 but to understand this chapter a detailed analysis of the Fabry-Perot is not needed.

Let the z-axis be chosen along the axis of the cavity as shown in Fig. 7.5, and assume that the transverse directions are so large that the light can be considered a plane wave bouncing back and forth along the z-axis between the two mirrors. Let ω be the frequency and $k_0 = \omega/c$

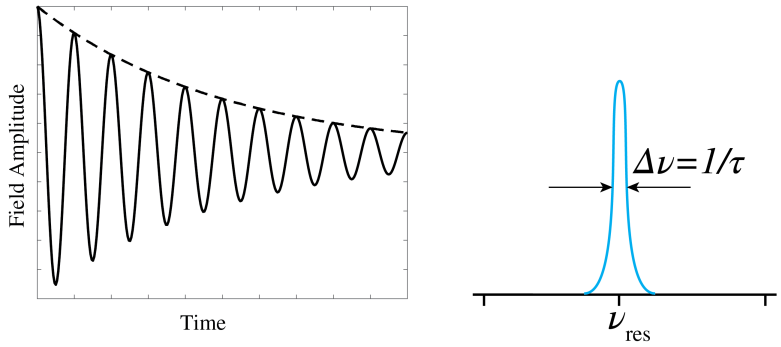


Figure 7.4: Damped oscillation (left) and frequency spectrum of a damped oscillation (right) with resonance wavelength and frequency width equal to the reciprocal of the decay time.

the wave number in vacuum. The plane wave that propagates in the positive z-direction is given by:

$$E(z) = Ae^{ik_0 nz}, \tag{7.6}$$

For very good mirrors, the amplitude remains unchanged after a reflection, while the phase

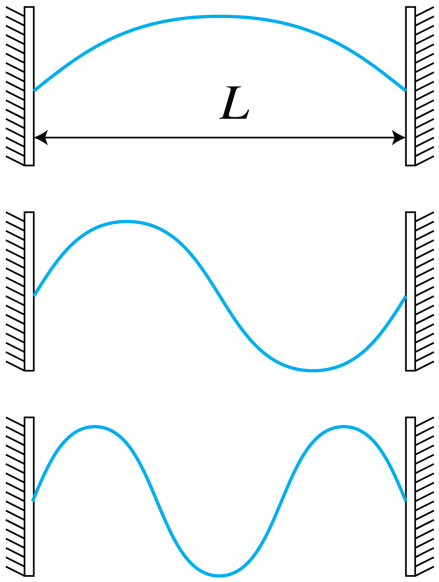


Figure 7.5: Fabry-Perot resonances.

typically changes by π. After one round trip (i.e. two reflections) the phase changes at the mirrors add up to 2π and hence have no effect) and the field is:

$$E(z) = Ae^{2ik_0 nL}e^{ik_0 nz}. \tag{7.7}$$

A high field builds up when this wave constructively interferes with (7.6), i.e. when

$$k_0 = \frac{2\pi m}{2nL}, \quad \text{or} \quad \nu = \frac{kc}{2\pi} = m\frac{c}{2nL}, \tag{7.8}$$

for $m = 1, 2, \ldots$. Hence, provided dispersion of the medium can be neglected (n is independent of the frequency), the resonance frequencies are separated by

$$\Delta\nu_f = c/(2nL), \tag{7.9}$$

which is the so-called **free spectral range**. For a gas laser of length 1 m, the free spectral range is approximately 150 MHz.

Example.
Suppose that the cavity is 100 cm long and is filled with a material with refractive index $n = 1$. Light with visible wavelength of $\lambda = 500$ nm corresponds to mode number $m = 2L/\lambda = 4 \times 10^6$ and the free spectral range is $\Delta\nu_f = c/(2L) = 150$ MHz.

The multiple reflections inside the resonator make the optical path length very large. For an observer, the atomic sources seem to be at a very large distance and the light that is exiting the cavity resembles a plane wave. As explained above, the divergence of the beam is therefore not limited by the size of the source, but by diffraction due to the aperture of the exit mirror.

Because of losses caused by the mirrors (which never reflect perfectly) and by the absorption and scattering of the light, the resonances have a certain frequency width $\Delta\nu$. When a resonator is used as a laser, one of the mirrors is given a small transmission to couple the laser light out and this also contributes to the loss of the resonator. To compensate for all losses, the cavity must contain an amplifying medium. Due to the amplification, the resonance line widths inside the bandwidth of the amplifier are reduced to very sharp lines as shown in Fig. 7.6.

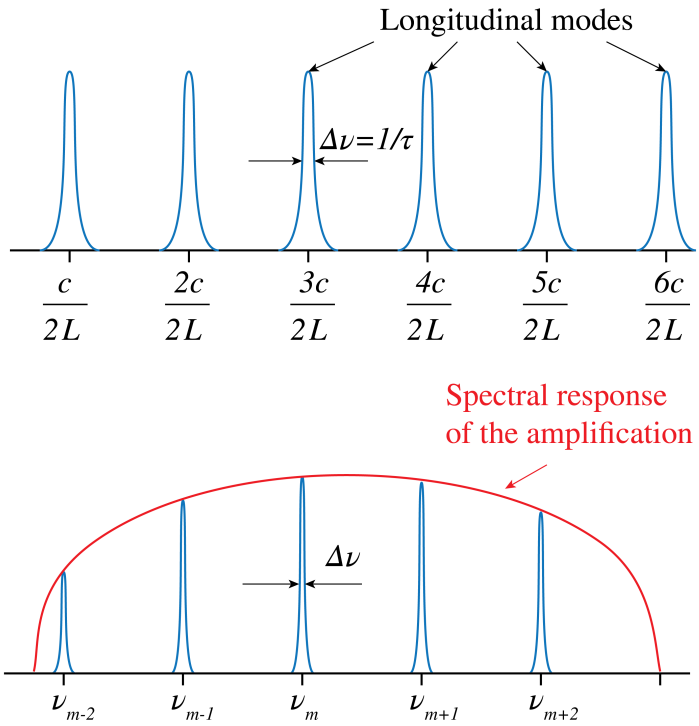


Figure 7.6: Resonant frequencies of a cavity of length L when the refractive index $n = 1$. With an amplifier inside the cavity, the line widths of the resonances within the bandwidth of the amplifier are reduced. The envelope is the spectral function of the amplification.

7.3 Amplification

Amplification can be achieved by a medium with atomic resonances that are at or close to one of the resonances of the resonator. We first recall the simple theory developed by Einstein in 1916 of the dynamic equilibrium of a material in the presence of electromagnetic radiation.

7.3.1 The Einstein Coefficients

We consider two atomic energy levels $E_2 > E_1$. By absorbing a photon of energy

$$\hbar\omega = E_2 - E_1, \tag{7.10}$$

an atom that is initially in the lower energy state 1 can be excited to state 2. Here $\hbar$ is Planck's constant:

$$\hbar = \frac{6.626070040}{2\pi} \times 10^{-34} \quad \text{Js} . \tag{7.11}$$

Suppose $W(\omega)$ is the time-averaged electromagnetic energy density *per unit of frequency interval* around frequency ω. Hence W has dimension $\text{Js}\,\text{m}^3$. Let N_1 and N_2 be the number of atoms in state 1 and 2, respectively, where

$$N_1 + N_2 = N, \tag{7.12}$$

is the total number of atoms which is constant. The rate of absorption is the rate of decrease of N_1 and is proportional to the energy density and the number of atoms in state 1:

$$\frac{dN_1}{dt} = -B_{12}N_1W(\omega), \qquad \textbf{absorption}, \tag{7.13}$$

where the constant $B_{12} > 0$ has dimension $\text{m}^3\text{J}^{-1}\text{s}^{-2}$. Without any external influence, an atom that is in the excited state will usually transfer to state 1 within 1 ns or so, while emitting a photon of energy (7.10). This process is called **spontaneous emission**, since it happens also without an electromagnetic field present. The rate of spontaneous emission is given by:

$$\frac{dN_2}{dt} = -A_{21}N_2, \qquad \textbf{spontaneous emission}, \tag{7.14}$$

where A_{21} has dimension s^{-1}. The lifetime of spontaneous transmission is $\tau_{sp} = 1/A_{21}$. It is important to note that the spontaneously emitted photon is emitted in a **random direction**. Furthermore, since the radiation occurs at a random time, there is no phase relation between the spontaneously emitted field and the field that excites the atom.

It is less obvious that in the presence of an electromagnetic field of frequency close to the atomic resonance, an atom in the excited state can also be **stimulated** by that field to emit a photon and transfer to the lower energy state. The rate of **stimulated emission** is proportional to the number of excited atoms and to the energy density of the field:

$$\frac{dN_2}{dt} = -B_{21}N_2W(\omega), \qquad \textbf{stimulated emission}, \tag{7.15}$$

where B_{21} has the same dimension as B_{12}. It is very important to remark that stimulated emission occurs in the **same electromagnetic mode** (e.g. a plane wave) as the mode of the field that excites the transmission and that the phase of the radiated field is **identical** to that of the exciting field. This implies that stimulated emission enhances the electromagnetic field by constructive interference. This property is crucial for the operation of the laser.

7.3.2 Relation Between the Einstein Coefficients

The Einstein coefficients A_{21}, B_{12} and B_{21} are related. Consider a black body, such as a closed empty box. Because no radiation is entering nor leaving the box, after a certain time the electromagnetic energy density is the thermal density $W_T(\omega)$, which, according to Planck's Law, is independent of the material of which the box is made and is given by:

$$W_T(\omega) = \frac{\hbar\omega^3}{\pi^2c^3}\frac{1}{\exp\left(\frac{\hbar\omega}{k_BT}\right) - 1}, \tag{7.16}$$

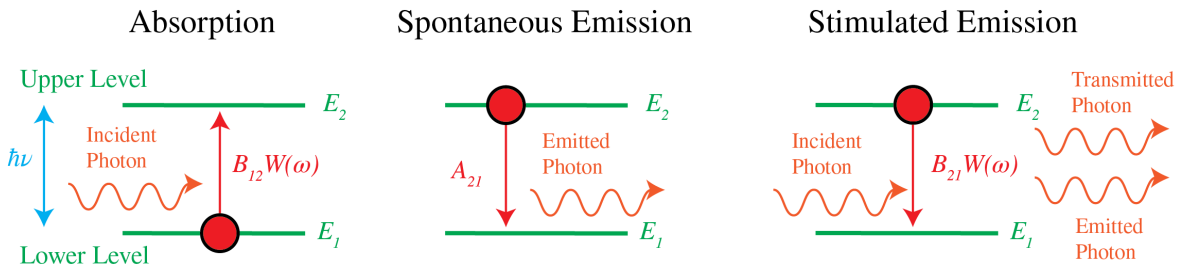


Figure 7.7: Absorption, spontaneous emission and stimulated emission.

where k_B is Boltzmann's constant:

$$k_B = 1.38064852 \times 10^{-23} \mathrm{m}^2\,\mathrm{kg}\,\mathrm{s}^{-2}\mathrm{K}^{-1}. \tag{7.17}$$

The rates of upward and downward transitions of the atoms in the wall of the box must be identical:

$$B_{12}N_1W_T(\omega) = A_{21}N_2 + B_{21}N_2W_T(\omega). \tag{7.18}$$

Hence,

$$W_T(\omega) = \frac{A_{21}}{B_{12}N_1/N_2 - B_{21}}. \tag{7.19}$$

But in thermal equilibrium:

$$\frac{N_2}{N_1} = \exp\left(-\frac{E_2 - E_1}{k_BT}\right) = \exp\left(-\frac{\hbar\omega}{k_BT}\right). \tag{7.20}$$

By substituting (7.20) into (7.19), and comparing the result with (7.16), it follows that both expressions for $W_T(\omega)$ are identical for all temperatures only if

$$B_{12} = B_{21}, \quad A_{21} = \frac{\hbar\omega^3}{\pi^2c^3}B_{21}. \tag{7.21}$$

Example.
For green light of $\lambda = 550$ nm, we have $\omega/c = 2\pi/\lambda = 2.8560 \times 10^6\mathrm{m}^{-1}$ and thus

$$\frac{A_{21}}{B_{21}} = 1.5640 \times 10^{-15}\mathrm{J\ s\ m}^{-3}. \tag{7.22}$$

Hence the spontaneous and stimulated emission rates are equal if $W(\omega) = 1.5640 \times 10^{-15}$ Js m^{-3}.

For a (narrow) frequency band $\mathrm{d}\omega$ the time-averaged energy density is $W(\omega)\,\mathrm{d}\omega$ and for a plane wave the energy density is related to the intensity I (i.e. the length of the time-averaged Poynting vector) by:

$$W(\omega)\,\mathrm{d}\omega = I/c. \tag{7.23}$$

A typical value for the frequency width of a narrow emission line of an ordinary light source is: 10^{10} Hz, i.e. $\mathrm{d}\omega = 2\pi \times 10^{10}$ Hz. The spontaneous and stimulated emission rates are then identical if the intensity is $I = 2.95 \times 10^4$ W/m^2. As seen from Table 7.1, only for laser light stimulated emission is larger than spontaneous emission. For classical light sources the spontaneous emission rate is much larger than the stimulated emission rate.

	I (W m^{-2})
Mercury lamp	10^4
Continuous laser	10^5
Pulsed laser	10^{13}

Table 7.1: Typical intensities of light sources.

If a beam with frequency width $\mathrm{d}\omega$ and energy density $W(\omega)\,\mathrm{d}\omega$ propagates through a material, the rate of loss of energy is proportional to:

$$(N_1 - N_2)B_{12}W(\omega). \tag{7.24}$$

According to (7.18) this is equal to the spontaneous emission rate. Indeed, the spontaneously emitted light corresponds to a loss of intensity of the beam, because it is emitted in random directions and with random phase.

When $N_2 > N_1$, the light is **amplified**. This state is called **population inversion** and it is essential for the operation of the laser. Note that the ratio of the spontaneous and stimulated emission rates is, according to (7.21), proportional to ω^3. Hence for shorter wavelengths such as x-rays, it is much more difficult to make lasers than for visible light.

7.3.3 Population Inversion

For electromagnetic energy density $W(\omega)$ per unit of frequency interval, the rate equations are

$$\frac{dN_2}{dt} = -A_{21}N_2 + (N_1 - N_2)B_{12}W(\omega), \tag{7.25}$$

$$\frac{dN_1}{dt} = A_{21}N_2 - (N_1 - N_2)B_{12}W(\omega). \tag{7.26}$$

Hence, for $\Delta N = N_2 - N_1$:

$$\frac{d\Delta N}{dt} = -A_{21}\Delta N - 2\Delta N B_{12}W(\omega) - A_{21}N, \tag{7.27}$$

where as before: $N = N_1 + N_2$ is constant. If at $t = 0$ all atoms are in the lowest state: $\Delta N(t = 0) = -N$, then it follows from (7.27):

$$\Delta N(t) = -N\left[\frac{A_{21}}{A_{21} + 2B_{12}W(\omega)} + \left(1 - \frac{A_{21}}{A_{21} + 2B_{12}W(\omega)}\right)e^{-(A_{21}+2B_{12}W(\omega))t}\right]. \tag{7.28}$$

An example where $A_{21}/B_{12}W(\omega) = 0.5$ is shown in Fig. 7.8. We always have $\Delta N < 0$, hence $N_2(t) < N_1(r)$ for all times t. Therefore, a system with only two levels cannot have population inversion.

A way to achieve population inversion of levels 1 and 2 and hence amplification of the radiation with frequency ω with $\hbar\omega = E_2 - E_1$ is to use more atomic levels, for example three. In Fig. 7.9 the ground state is state 1 with two upper levels 2 and 3 such that $E_1 < E_2 < E_3$. The transition of interest is still that from level 2 to level 1. Initially almost all atoms are in the ground state 1. Then atoms are pumped with rate R from level 1 directly to level 3. The transition $3 \to 2$ is non-radiative and has a high rate A_{32} so that level 3 is quickly emptied and therefore N_3 remains small. State 2 is called a metastable state, because the residence time in this state is for every atom relatively long. Therefore its population tends to increase, leading to population inversion between the metastable state 2 and the lower ground state 1 (which is continuously being depopulated by pumping to the highest level). Note that A_{31} has to be small, because

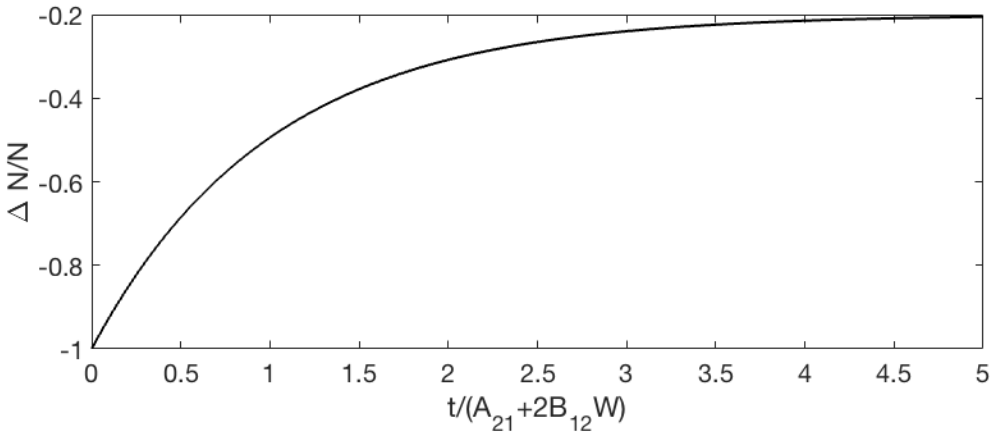


Figure 7.8: $\Delta N/N$ as function of $t/(A_{21}+2B_{12}W)$ when all atoms are in the ground state at $t = 0$, i.e. $\Delta N(0) = -N$.

otherwise level 1 will quickly be filled, by which population inversion will be stopped. This effect can be utilised to obtain a series of laser pulses as output, but is undesirable for a continuous output power.

Pumping may be done optically as described, but the energy to transfer atoms from level 1 to level 3 can also be supplied by an electrical discharge in a gas or by an electric current. After the pumping has achieved population inversion, initially no light is emitted. So how does the laser actually start? Lasing starts by spontaneous emission. The spontaneously emitted photons stimulate emission of the atoms in level 2 to decay to level 1, while emitting a photon of energy $\hbar\omega$. The **stimulated emission occurs in phase with the exciting light** and hence the light continuously builds up coherently, while it is bouncing back and forth between the mirrors of the resonator. Because one of the mirrors is slightly transparent a certain laser power is emitted.

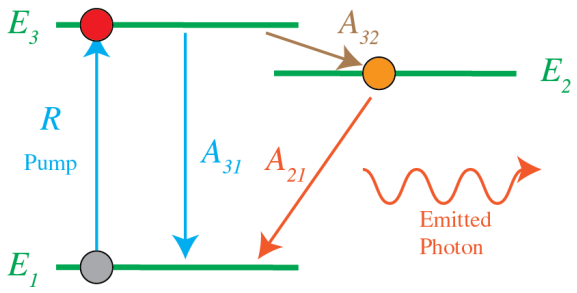


Figure 7.9: The three Einstein transitions and the pump. The rate A_{32} is large while A_{31} is small.

7.4 Cavities

The amplifying medium can completely fill the space between the mirrors as at the top of Fig. 7.10, or there can be space between the amplifier and the mirrors. For example, if the amplifier is a gas, it may be enclosed by a glass cylinder. The end faces of the cylinder are positioned under the Brewster angle with respect to the axis, as shown in the middle figure of Fig. 7.10, to minimise reflections. This type of resonator is called a resonator with external mirrors.

Usually one or both mirrors are convex, as shown in the third figure of Fig. 7.10. We state

without proof that in that case the distance L between the mirrors and the radii of curvature R_1 and R_2 of the mirrors has to satisfy

$$0 < \left(1 - \frac{L}{R_1}\right)\left(1 - \frac{L}{R_2}\right) < 1, \tag{7.29}$$

or else the laser light will ultimately leave the cavity laterally, i.e. it will escape sideways. This condition is called the **stability condition**. The curvature of a convex mirror is positive and that of a concave mirror is negative. Clearly, when both mirrors are concave, the laser is always unstable.

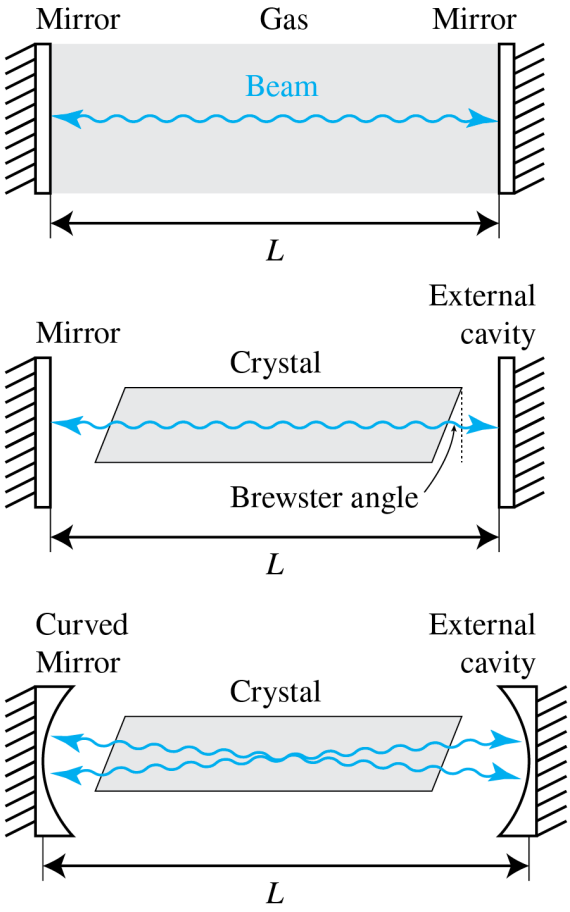


Figure 7.10: Three types of laser cavity. The shaded region is the amplifier. The second and third is called a laser with external cavity.

7.5 Problems with Laser Operation

In this section we consider some problems that occur with lasers and discuss what can be done to solve them.

1. **Multiple Resonance Frequencies**
   In many applications such as laser communication and interferometry one needs a single wavelength. Consider a cavity of length L as shown in Fig. 7.11 and suppose that the amplifier has a gain curve covering many resonances of the resonator. One way to achieve single-frequency output is by taking care that there is only one frequency for which the gain is larger than the losses. One then says that the laser is above threshold for only one frequency. This

can be done by choosing the length L of the cavity to be so small that there is only one mode under the gain curve for which the gain is higher than the losses. However, a small length of the amplifier means less output power and a less collimated output beam. Another method would be to reduce the pumping so that for only one mode the gain compensates the losses. But this implies again that the laser output power is relatively small. A better solution is to add a Fabry-Perot cavity inside the laser cavity as shown in Fig. 7.12. The cavity consists e.g. of a piece of glass of a certain thickness a. By choosing a sufficiently small, the distance in frequency $c/(2a)$ between the resonances of the Fabry-Perot cavity becomes so large that there is only one Fabry-Perot resonance under the gain curve of the amplifier. Furthermore, by choosing the proper angle for the Fabry-Perot cavity with respect to the axis of the laser cavity, the Fabry-Perot resonance can be coupled to the desired resonance frequency.

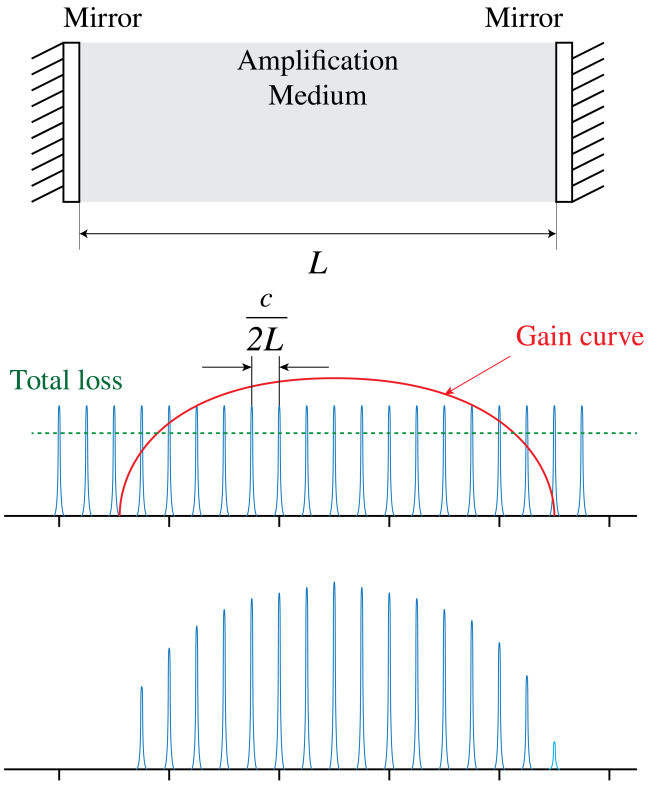


Figure 7.11: Laser with cavity of length L and broad amplifier gain curve. Many resonance frequencies of the resonances are above threshold to compensate the losses.

2. **Multiple Transverse Modes**
The best-known laser mode has transverse Gaussian intensity. We call a mode with Gaussian transverse shape a **longitudinal mode** and when its frequency satisfies $\nu = mc/(2L)$, it is called the mth longitudinal mode. However, inside the laser cavity other modes with different transverse patterns can also resonate. An example is shown in Fig. 7.13 where mode (1,0) consists of two maxima. There exist many more transverse modes, as shown in Fig. 7.14. The transverse modes all have slightly different frequencies. So even when there is only one Gaussian mode above threshold (i.e. modes occur for only one value of m), there can be many transverse modes with frequencies very close to the frequency of the Gaussian mode, which are also above threshold. This is illustrated in Fig. 7.15 where the frequencies of modes (0,0), (1,0) and (1,1) all are above threshold. Usually one prefers the Gaussian mode and the transverse modes are undesired. Because the Gaussian mode has smallest transverse width, the other transverse modes can be eliminated by inserting an aperture in the laser cavity.

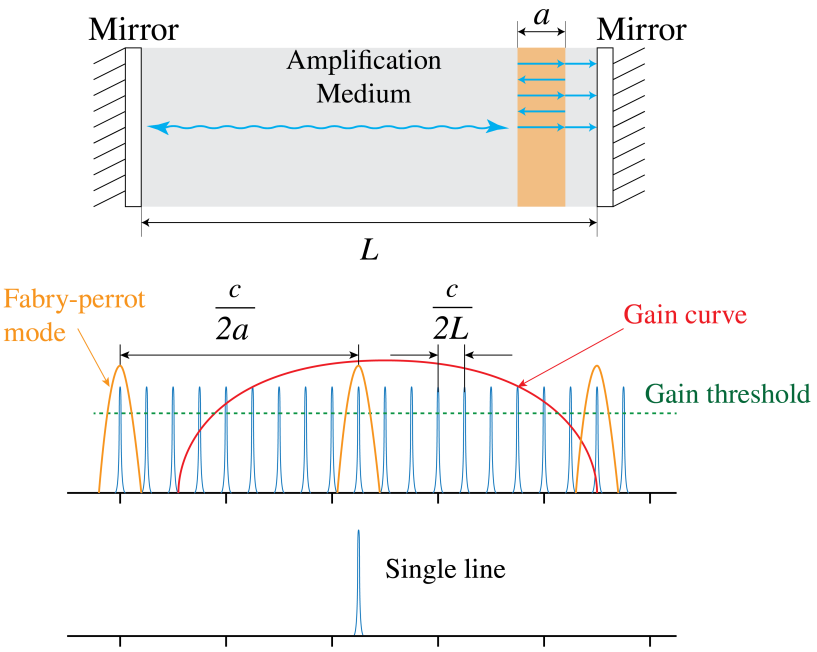


Figure 7.12: Laser with cavity of length L, a broad amplifier gain curve and an added Fabry-Perot cavity. The FP resonances act as an extra filter to select only one mode of the laser.

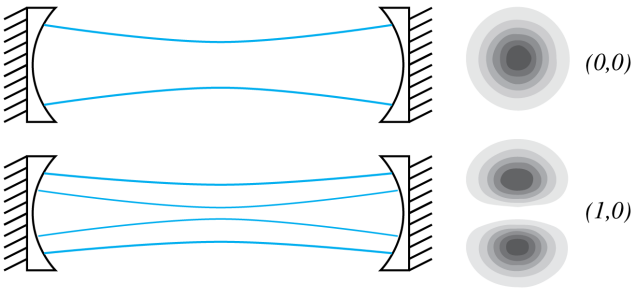


Figure 7.13: Laser cavity with (0,0) and (1,0) modes.

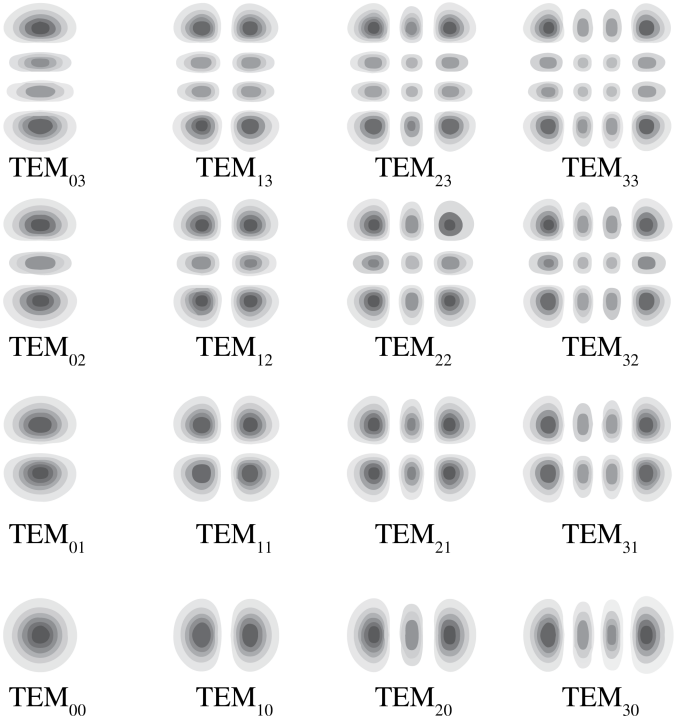


Figure 7.14: Intensity pattern of several transverse modes.

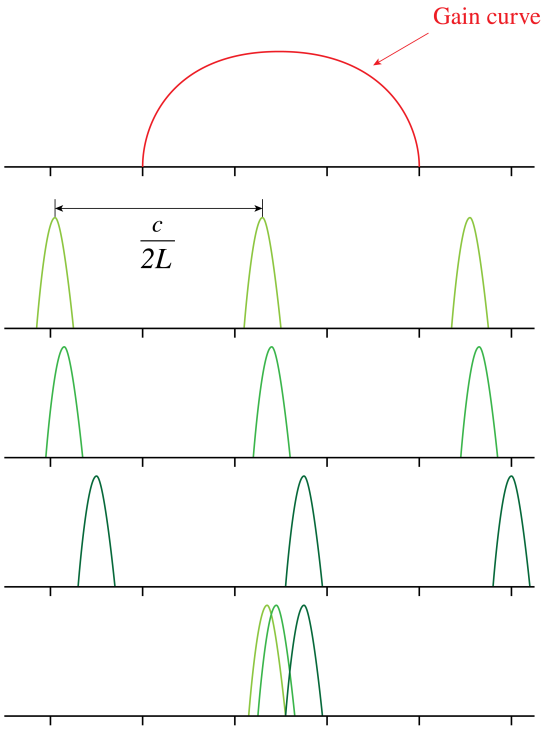


Figure 7.15: Resonance frequencies of transverse modes that have sufficient gain to compensate the losses.

7.6 Types of Lasers

There are many types of lasers: gas, solid, liquid, semiconductor, chemical, excimer, e-beam, free electron, fiber and even waveguide lasers. We classify them according to the pumping mechanism.

7.6.1 Optical Pumping

The energy to transfer the atom A from the ground state to the excited state is provided by light. The source could be another laser or an incoherent light source, such as a discharge lamp. If A is the atom in the ground state and A^* is the excited atom, we have

$$\hbar\omega_{13} + A \rightarrow A^*, \tag{7.30}$$

where ω_{13} is the frequency for the transition $1 \rightarrow 3$ as seen in Fig. 7.18. The Ruby laser, of which the amplifying medium consists of Al_2O_3 with 0.05 weight percent Cr_2O_3, was the first laser, invented in 1960. It emits pulses of light of wavelength 694.3 nm and is optically pumped with a gas discharge lamp. Other optically pumped lasers are the YAG, glass, fiber, semiconductor and dye laser. In the dye laser the amplifier is a liquid (e.g. Rhodamine6G). It is optically

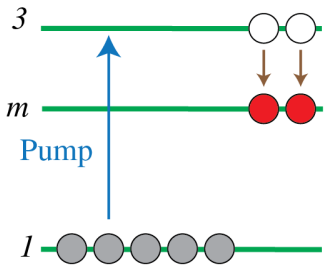


Figure 7.16: Optical pumping.

pumped by an argon laser and has a huge gain width, which covers almost the complete visible wavelength range. We can select a certain wavelength by inserting a dispersive element like the Fabry-Perot cavity inside the laser cavity and rotating it at the right angle to select the desired wavelength, as explained above.

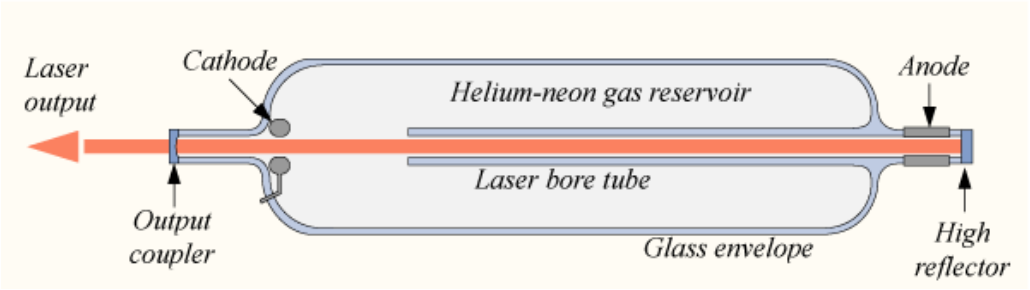


Figure 7.17: HeNe laser with spherical external mirrors, a discharge tube with faces at the Brewster angle to minimise reflections, and an anode and cathode for the discharge pumping(from Wikimedia Commons by DrBob / CC BY-SA 3.0).

7.6.2 Electron-Collision Pump

Energetic electrons are used to collide with the atoms of the amplifier, thereby transferring some of their energy:

$$A + e(\mathcal{E}_3) \rightarrow A^* + e(\mathcal{E}_1), \tag{7.31}$$

where $e(\mathcal{E}_3)$ means an electron with energy $\mathcal{E}_3$ and where $\mathcal{E}_3 - \mathcal{E}_1$ is equal to $\hbar\omega_{13}$ so that the atom is transferred from the ground state 1 to state 3 to obtain population inversion. Examples are the HeNe, Argon, Krypton, Xenon, Nitrogen and Copper lasers. Electrons can be created by a discharge or by an electron beam.

7.6.3 Atomic Collision

Let B^m be atom B in an excited, so-called metastable state. This means that B^m, although unstable, has a very long relaxation time, i.e. longer than 1 ms or so. If B^m collides with atom A, it transfers energy to A:

$$B^m + A \rightarrow B + A^*, \tag{7.32}$$

where A^* is the excited state used for the stimulated emission. The relaxation time τ_{m1} of metastable state B^m is very large and hence the spontaneous emission rate is very small. This implies that the number of metastable atoms as function of time t is given by a slowly decaying exponential function $\exp(-t/\tau_{m1})$. To get metastable atoms, one can for example pump atom B

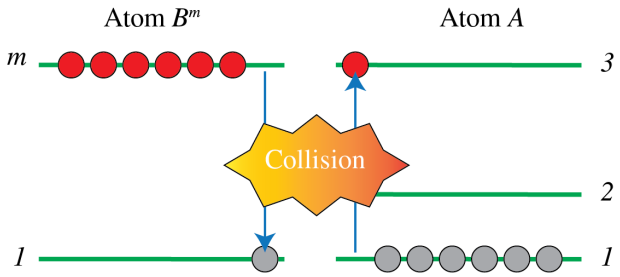


Figure 7.18: Pumping atoms A to state 2 by collision with metastable atoms B^m.

from its ground state 1 to an excited state 3 above state m such that the spontaneous emission rate $3 \rightarrow m$ is large. The pumping can be done electrically or by any other means. If it is done electrically, then we have

$$B + e(\mathcal{E}_3) \rightarrow B^m + e(\mathcal{E}_1), \tag{7.33}$$

Examples of these types of laser are HeNe lasers, which emits in the red at 632 nm, N_2CO_2 and HeCd lasers. All of these depend on atom or molecule collisions, where the atom or molecule that is mentioned as first in the name is brought into the metastable state and lasing occurs at a wavelength corresponding to a level difference of the second mentioned atom or molecule. The CO_2 laser emits at 10 μm and can achieve huge power.

7.6.4 Chemical Pump

In some chemical reactions, a molecule is created in an excited state with population inversion. An example is:

$$A + B_2 \rightarrow (AB)^* + B. \tag{7.34}$$

So in this case the lasing will take place for a transfer between states of molecule AB. The HF, ArCl lasers are all chemically pumped.

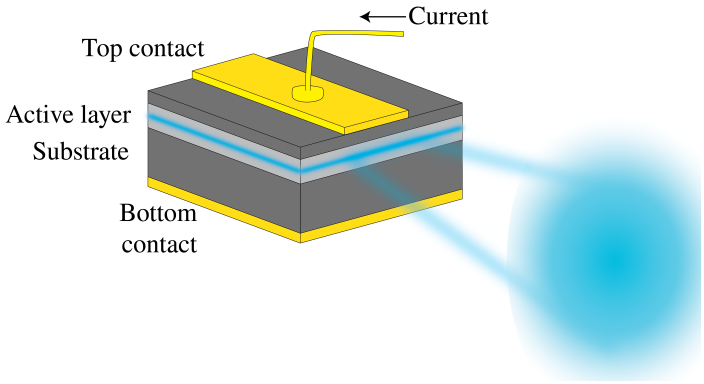


Figure 7.19: Semiconductor laser with active p-n junction, polished end faces and current supply for pumping.

7.6.5 Semiconductor Laser

In a semiconductor laser as shown in Fig. 7.19, the pumping is done by electron current injection. It is one of the most compact lasers and yet it typically emits 20 mW of power. Transitions occur between the conduction and valence bands close to the p-n junction. Electrons from the n-layer conduction band will recombine with the holes in the p-layer. A cavity is obtained by polishing the end faces that are perpendicular to the junction to make them highly reflecting. Semiconductor lasers are produced for wavelengths from 700 nm to 30 μm and give continuous (CW) output.

Problems

1. **Short Question on Laser.**

   a) A ring laser is composed of 4 identical mirrors with a reflection coefficient of 0.99. Give the value of the gain that is necessary in the amplifier medium to obtain lasing.

   b) Give the frequency difference between two longitudinal modes in a linear cavity whose optical length is L = 300mm.

   c) Imagine that one of the mirrors in a two mirror cavity is not perfect and has a complex index of refraction (such as gold for example with n=0.25+3i for 600 nm). How does it affect the mode in the laser?

   d) The neon helium gain medium has a spectral band of amplification of 1 GHz at 633 nm. It is assumed that the spectral profile is rectangular to simplify. The linear cavity of the laser has a length of 30 cm. Give the number of longitudinal modes that can oscillate in this cavity.

   e) A pulsed laser produces pulses of 10 μJ with a duration of 1 ns. The pulse repetition frequency is 10 kHz. Give the peak power of the pulses and the average output power of the laser.

About the authors

Sander Konijnenberg studied Applied Physics at Delft University of Technology. At the same university, he obtained his PhD (cum laude) in the Optics Group on the topic of ptychography and phase retrieval. He currently works at ASML Research in Veldhoven (NL).

Aurèle J.L. Adam is an Assistant Professor at Delft University of Technology. He is an Engineer from CentraleSupelec (promo 2000) and got his PhD from the University of Paris VI. His expertise lies in the Terahertz field and he enjoys scattering problems and free form optics.

H. Paul Urbach is emeritus professor of Optics at Delft University of Technology. His research interests are optical imaging and diffraction theory. After his PhD at Groningen University, he has been principle scientist of Philips Research Laboratories in Eindhoven. From 2014-2016 and again in 2018 he was president of the European Optical Society.

References

Chapter 1

Software

Free software for practicing geometrical optics
https://www.geogebra.org/m/X8RuneVy

Videos

Faraday's Law Introduction by KhanAcademy
https://www.khanacademy.org/science/physics/magnetic-flux-and-faradays-law/magnetic-flux-faradays-law/v/faradays-law-introduction
Magnetic field created by a current carrying wire (Ampere's Law Introduction) by KhanAcademy
https://www.khanacademy.org/science/physics/magnetic-forces-and-magnetic-fields/magnetic-field-current-carrying-wire/v/magnetism-6-magnetic-field-due-to-current
Lecture 18: Index of Refraction, Reflection, Fresnel Equations, Brewster Angle by Walter Lewin
https://www.youtube.com/watch?v=_D1z6t2z168
Demonstration of reflection of polarised light and the Brewster angle by MIT OCW
http://ocw.mit.edu/resources/res-6-006-video-demonstrations-in-lasers-and-optics-spring-2008/demonstrations-in-physical-optics/reflection-at-the-air-glass-boundary/
Playlist on elementary geometrical optics by KhanAcademy
https://www.khanacademy.org/science/physics/geometric-optics
Yale Courses - 16. Ray or Geometrical Optics I - Lecture by Ramamurti Shankar
https://www.youtube.com/watch?v=bxGgcgSbQBA
Yale Courses - 17. Ray or Geometrical Optics II - Lecture by Ramamurti Shankar
https://www.youtube.com/watch?v=qm4QR_ycRhY

Figures

Fig. 1.1 is from *Wikimedia Commons* by NASA / CC BY-SA
https://commons.wikimedia.org/wiki/File:EM_Spectrum_Properties_edit.svg
Fig. 1.8 is from *Wikimedia Commons*, original JPG due to Averse, SVG by Maschen., CC0
Wikimedia Commons

Fig. 1.13-left is from *Wikimedia Commons* by Keerthi / CC BY
https://commons.wikimedia.org/wiki/File:Demostration_of_Total-Internal-Reflection(TIR)_in_a_wine_glass.jpg
Fig. 1.13 down-right is a courtesy of Schott
Fig. 1.6 is from *Wikimedia Commons* by Geek3 / CC BY-SA
https://commons.wikimedia.org/wiki/File:Mplwp_dispersion_curves.svg

Literature

A.A. Van Heel, *New Method of transporting Optical Images without Aberrations*, Nature 173, 39 (1954) https://doi.org/10.1038/173039a0
R.K. Luneburg, *Mathematical Theory of Optics*, University of California Press, Berkeley and Los Angeles (1964)
M. Born & E. Wolf, *Principles of Optics*, Cambridge University Press (2013)
https://doi.org/10.1017/CBO9781139644181

Chapter 2

Figures

Fig. 2.2 is from *Wikimedia Commons* in Popular Science Monthly, Volume 5 / Public Domain
https://commons.wikimedia.org/w/index.php?curid=10770493
Fig. 2.24 is the EUV stepper TWINSCAN NXE:3400B by ASML
https://www.asml.com/en/news/media-library

Literature

J. Braat, P. Török, *Imaging Optics*, Cambridge University Press (2019)
https://doi.org/10.1017/9781108552264

Chapter 3

Videos

Polarisation of light, linear and circular: Explanation of different polarisation states and their applications by KhanAcademy
https://www.khanacademy.org/science/physics/light-waves/introduction-to-light-waves/v/polarization-of-light-linear-and-circular
Linear transformation examples: rotations by KhanAcademy
https://www.khanacademy.org/math/linear-algebra/matrix_transformations/lin_trans_examples/v/linear-transformation-examples-rotations-in-r2
Demonstration of the quarter-wave plate to create elliptical polarisation from MIT
http://ocw.mit.edu/resources/res-6-006-video-demonstrations-in-lasers-and-optics-spring-2008/demonstrations-in-physical-optics/quarter-wave-plate/

Demonstration of an Optical isolator from MIT
http://ocw.mit.edu/resources/res-6-006-video-demonstrations-in-lasers-and-optics-spring-2008/demonstrations-in-physical-optics/optical-isolator/
Demonstration of double refraction by a calcite crystal due to birefringence from Sixty Symbols
https://www.youtube.com/watch?v=k1oh3lXR5P
Demonstration of a Half WavePlate from Andrew Berger
https://www.youtube.com/watch?v=HriBBJ-6gd8
Demonstration of a Quarter WavePlate by Andrew Berger
https://www.youtube.com/watch?v=ZhkcKlksV1g

Figures

Fig. 3.1 is from *Wikimedia Commons* in Fizyka z (1910) / Public Domain
https://commons.wikimedia.org/wiki/File:Camera_obscura_1.jpg
Fig. 3.2 is from *Wikimedia Commons* by Jean François Witz / CC BY-SA 3.0
https://commons.wikimedia.org/wiki/File:Reflex_camera_numeric.svg
Fig. 3.4 is by A.J.L. Adam (author) / CC BY-SA 4.0
Fig. 3.5 is from *Wikimedia Commons* by Holly Fischer / CC BY
https://commons.wikimedia.org/wiki/File:Three_Internal_chambers_of_the_Eye.png
Fig. 3.6 left is adapted from *Wikimedia Commons* by Erin Silversmith / CC BY-SA 2.5 Generic
https://commons.wikimedia.org/wiki/File:Focus_in_an_eye.svg
Fig. 3.6 right is adapted from Sjaastad O.V., Sand O. and Hove K., *Physiology of domestic animals*, 2nd edn., Oslo: Scandinavian Veterinary Press (2010)
Fig. 3.7 is adapted from *Wikimedia Commons* by Gumenyuk I.S. / CC BY-SA 4.0
https://en.wikipedia.org/wiki/File:Myopia_and_lens_correction.svg
Fig. 3.8 is a picture taken by A.J.L. Adam (author) / CC BY-SA 4.0
Fig. 3.10 is from *Wikimedia Commons* by Tamas-flex / CC BY-SA 3.0
https://commons.wikimedia.org/wiki/File:Exitpupil.png

Links

Collections of pictures taken using a camera obscura in Pinterest
https://www.pinterest.com/bonfoton/camera-obscura-photographs/

Chapter 4

Videos

Yale Courses - Wave Theory of Light
https://www.youtube.com/watch?v=5tKPLfZ9JVQ
Demonstration of an interference pattern obtained with sunlight by Veritasium
https://www.youtube.com/watch?v=Iuv6hY6zsd0
Demonstration of laser light in a Michelson interferometer for collimated beams by MIT OCW
http://ocw.mit.edu/resources/res-6-006-video-demonstrations-in-lasers-and-optics-spring-2008/demonstrations-in-physical-optics/two-beam-interference-2014-collimated-beams/
Demonstration of beam interference by MIT OCW
http://ocw.mit.edu/resources/res-6-006-video-demonstrations-in-lasers-and-optics-spring-2008/demonstrations-in-physical-optics/two-beam-interference-2014-diverging-beams/

Demonstration of how fringe contrast varies with propagation distance by MIT OCW
http://ocw.mit.edu/resources/res-6-006-video-demonstrations-in-lasers-and-optics-spring-2008/demonstrations-in-physical-optics/fringe-contrast-2014-path-difference/
Demonstration of how the coherence length depends on the spectrum of the laser light by MIT OCW
http://ocw.mit.edu/resources/res-6-006-video-demonstrations-in-lasers-and-optics-spring-2008/demonstrations-in-physical-optics/coherence-length-and-source-spectrum/
Lecture Series on Physics - I: Oscillations and Waves - Lecture 19 Coherence by Prof. S. Bharadwaj, Department of Physics and Meteorology, IIT Kharagpur.
https://www.youtube.com/watch?v=fwRFaZnr2WU
Lecture Series on Physics - I: Oscillations and Waves - Lecture 19 Coherence by Prof. S. Bharadwaj, Department of Physics and Meteorology, IIT Kharagpur.
https://www.youtube.com/watch?v=jnQFMdMSRAE
Interference of light waves by KhanAcademy
https://www.khanacademy.org/science/physics/light-waves/interference-of-light-waves/v/wave-interference
Young's Double Slit by KhanAcademy
https://www.khanacademy.org/science/physics/light-waves/interference-of-light-waves/v/youngs-double-split-part-1
Playlist on wave interference at secondary school level by KhanAcademy
https://www.khanacademy.org/science/physics/light-waves/interference-of-light-waves/v/wave-interference

---

Chapter 5

Videos

Basic explanation of Fourier transforms from Every picture is made of waves (3:33 to 7:15) by Sixty Symbols
https://www.youtube.com/watch?v=mEN7DTdHbAU
Basic explanation of the uncertainty principle (though in the context of quantum physics from Heisenberg's Microscope (0:20 to 2:38)) by Sixty Symbols
https://www.youtube.com/watch?v=dgoA_jmGIcA

Literature

E. Hecht, *Optics*, Pearson (2016)

J.W. Goodman, *Introduction to Fourier Optics*, Macmillan (2017)

Figures

Fig. 5.1 is from *Wikimedia Commons* by Thomas Reisinger / CC BY-SA 3.0
https://commons.wikimedia.org/w/index.php?curid=116648035

Chapter 6

Figures

Fig. 6.20 is from A. Poddubny, I. Iorsh, P. Belov, & Y. Kivshar, *Hyperbolic metamaterials.* Nat. Photon., 7(12), 948-957 (2013)
https://doi.org/10.1038/nphoton.2013.243
Fig. 6.21 is from P.F. Rodriguez and al., *Building a fast scanning stimulated emission depletion microscope*, Materials Science (2012)
https://www.semanticscholar.org/paper/Building-a-fast-scanning-stimulated-emission-a-step-Rodriguez-Wu/46d8c4148e93f30cf11e1ae4356620bd5fcd0475

Chapter 7

Figure

Fig. 7.17 is from *Wikimedia Commons* by DrBob / CC BY-SA 3.0
https://commons.wikimedia.org/wiki/File:Hene-1.png

Appendix A

Vector Calculus

Below, $\mathbf{A}$, $\mathbf{B}$ $\mathbf{C}$, and $\mathbf{D}$ are vector fields (or constant vectors) and ϕ and ψ are scalar functions. Then:

$$\mathbf{A} \cdot (\mathbf{B} \times \mathbf{C}) = \mathbf{B} \cdot (\mathbf{C} \times \mathbf{A}) = \mathbf{C} \cdot (\mathbf{A} \times \mathbf{B}). \tag{A.1}$$

$$\mathbf{A} \times (\mathbf{B} \times \mathbf{C}) = (\mathbf{A} \cdot \mathbf{C})\mathbf{B} - (\mathbf{A} \cdot \mathbf{B})\mathbf{C}. \tag{A.2}$$

$$(\mathbf{A} \times \mathbf{B}) \cdot (\mathbf{C} \times \mathbf{D}) = (\mathbf{A} \cdot \mathbf{C})(\mathbf{B} \cdot \mathbf{D}) - (\mathbf{A} \cdot \mathbf{D})(\mathbf{B} \cdot \mathbf{C}) \tag{A.3}$$

$$\nabla \cdot (\phi \mathbf{A}) = \phi \nabla \cdot \mathbf{A} + \nabla \phi \cdot \mathbf{A}. \tag{A.4}$$

$$\nabla \times (\phi \mathbf{A}) = \phi \nabla \times \mathbf{A} + \nabla \phi \times \mathbf{A}. \tag{A.5}$$

$$\nabla \cdot (\mathbf{A} \times \mathbf{B}) = -\mathbf{A} \cdot \nabla \times \mathbf{B} + \mathbf{B} \cdot \nabla \times \mathbf{A}. \tag{A.6}$$

$$\nabla \times (\mathbf{A} \times \mathbf{B}) = -(\mathbf{A} \cdot \nabla)\mathbf{B} + \mathbf{A}\nabla \cdot \mathbf{B} + (\mathbf{B} \cdot \nabla)\mathbf{A} - \mathbf{B}\nabla \cdot \mathbf{A}. \tag{A.7}$$

$$\nabla(\mathbf{A} \cdot \mathbf{B}) = (\mathbf{A} \cdot \nabla)\mathbf{B} + \mathbf{A} \times \nabla \times \mathbf{B} + (\mathbf{B} \cdot \nabla)\mathbf{A} + \mathbf{B} \times \nabla \times \mathbf{A}. \tag{A.8}$$

$$\nabla \cdot \nabla \phi = \Delta \phi, \tag{A.9}$$

where $\Delta = \partial^2/\partial x^2 + \partial^2/\partial y^2 + \partial^2/\partial z^2$ provided that (x, y, z) is an orthonormal basis.

$$\nabla \times \nabla \times \mathbf{A} = -\Delta \mathbf{A} + \nabla \nabla \cdot \mathbf{A}. \tag{A.10}$$

Remark: The last formula is only valid in a Cartesian coordinate system. This means that the vector field $\mathbf{A}$ must be decomposed on the Cartesian basis and the derivatives must be computed with respect to the corresponding Cartesian coordinates and then $\Delta\mathbf{A}$ must be interpreted component-by-component: $\Delta\mathbf{A}= (\Delta A_x,\ \Delta A_y,\ \Delta A_z)^T$, where A_x, A_y, A_z are components with respect to the Cartesian basis. The formula does *not* hold in cylindrical or spherical coordinates!

$$\nabla \times \nabla \phi = 0. \tag{A.11}$$

$$\nabla \cdot (\nabla \times \mathbf{A}) = 0. \tag{A.12}$$

In addition, the following integral theorems apply (V is a volume with surface area S and *outward* unit normal $\mathbf{n}$.
Gauss's Theorem (or divergence theorem):

$$\iiint_V \nabla \cdot \mathbf{A}\, dV = \iint_S \mathbf{A} \cdot \mathbf{n}\, dS. \tag{A.13}$$

Apply this to the vector field $\mathbf{A} = \phi\nabla\psi$. Because of (A.4) and (A.9) holds $\nabla\cdot\mathbf{A} = \phi\Delta\psi + \nabla\cdot\nabla\psi$ and thus (*Green's Theorem*):

$$\iiint_V \phi\Delta\psi + \nabla\phi\cdot\nabla\psi\, dV = \iint_S \phi\frac{\partial\psi}{\partial n}\, dS. \tag{A.14}$$

By subtracting the analogous relation from (A.14) with ϕ and ψ interchanged, one gets:

$$\iiint_V \phi\Delta\psi - \psi\Delta\phi\, dV = \iint_S \phi\frac{\partial\psi}{\partial n} - \psi\frac{\partial\phi}{\partial n}\, dS. \tag{A.15}$$

By using (A.6) and Gauss's theorem it follows furthermore that

$$\begin{aligned} \iiint_V \mathbf{B}\cdot\nabla\times\mathbf{A}dV - \iiint_V \mathbf{A}\cdot\nabla\times\mathbf{B}dV &= \iint_S \mathbf{n}\dot{(}\mathbf{A}\times\mathbf{B})\, dS \\ &= \iint_S (\mathbf{n}\times\mathbf{A})\cdot\mathbf{B})\, dS \\ &= \iint_S \mathbf{A}\cdot(\mathbf{n}\times\mathbf{B})\, dS, \end{aligned} \tag{A.16}$$

where in the right-hand side we used (A.1).
Stokes' Theorem (S is a possibly curved surface with contour C):

$$\iint_S \nabla\times\mathbf{A}\cdot\mathbf{n}\, dS = \int_C \mathbf{A}\cdot d\mathbf{s}, \tag{A.17}$$

where $\mathbf{n}$ is the unit vector field that is perpendicular to S, which is in the direction to which a right-handed corkscrew points if it is rotated in the positive direction of the line integral along C.

There is also an analogue of Green's Theorem for the curl operator:

$$\iiint_V \nabla\times\mathbf{A}\cdot\mathbf{B}\, dS - \iiint_V \mathbf{A}\cdot\nabla\times\mathbf{B}\, dS = \iint_S (\mathbf{n}\times\mathbf{A})\cdot\mathbf{B}\, dS = -\iint_S \mathbf{A}\cdot(\mathbf{n}\times\mathbf{B})\, dS. \tag{A.18}$$

Appendix B

The Lorentz Model for Material Dispersion

The Lorentz model, which we already mentioned in Section 1.3, leads to a dispersion relation for the susceptibility and hence for the permittivity given by

$$\epsilon(\omega) = \frac{1+2q}{1-q}, \tag{B.1}$$

with

$$q = \frac{Nq_e^2}{3\epsilon_0 m_e} \sum_j \frac{f_j}{\omega_j^2 - \omega^2 + i\gamma_j\omega}, \tag{B.2}$$

where N is the number density of electrons, q_e and m_e are the charge and mass of the electron, ω_j are resonance frequencies of atoms or molecules of the material, $\gamma_j > 0$ is a damping term and f_j are weighting factors (so-called oscillator strengths) satisfying: $\sum_j f_j = 1$. The refractive index is the square root of the permittivity: $n = \sqrt{\epsilon}$ and its real part is shown in Fig. B.1.

For dilute gases, N is small and hence q is small compared to 1. Then the permittivity becomes equal to

$$\epsilon(\omega) \approx 1 + q = 1 + \frac{Nq_e^2}{3\epsilon_0 m_e} \sum_j \frac{f_j}{\omega_j^2 - \omega^2 + i\gamma_j\omega}, \tag{B.3}$$

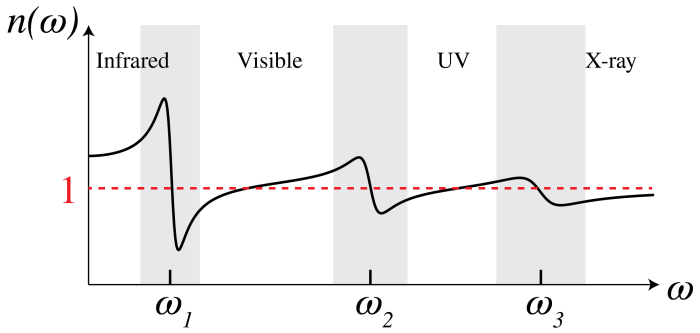


Figure B.1: Refractive index as function of frequency.

The resonances corresponding to transitions from a lower to a higher energy level of electrons that are in the inner shells of an atom, typically are in the x-ray region, whereas transitions of valence electrons can be in the ultra-violet to the visible. Resonances of relative motions of

atoms inside a molecule are often in the infrared. At a resonance, the atom absorbs a photon of energy $\hbar\omega$ equal to the difference between the energy levels. The material is then absorbing and this corresponds to a permittivity with positive imaginary part. In between the resonances, the absorption is low so that the imaginary part of the permittivity is almost zero while its real part is slowly increasing with frequency (this is called "normal" dispersion). Close to a resonance, the real part of the permittivity is quickly *decreasing* with frequency (abnormal dispersion).

Appendix C

About the Conservation of Electromagnetic Energy

We consider a time harmonic electric field that is more general than a plane wave (i.e. it is not necessarily a single plane wave but a superposition of plane waves with wave vectors with different directions). Let V be a bounded volume with closed boundary A. The time averaged flux of electromagnetic energy through the boundary A outwards from the volume is given by the surface integral

$$F = \int\int \mathbf{S}(\mathbf{r}) \cdot \hat{\mathbf{n}} dA, \tag{C.1}$$

where $\hat{\mathbf{n}}$ is the outwards pointing unit normal. We assume that there are no sources inside V. There are then two possibilities:

1. $F < 0$. In this case there is a nonzero net flux into the volume. Because all fields are time harmonic, there can only be a net influx if electromagnetic energy is absorbed inside the volume. Hence the imaginary part of the permittivity must be positive. It can be shown that the time average of the absorbed power is given by

$$\text{Absorbed e.m. energy} = \frac{\omega}{2}\text{Im}(\epsilon)|\mathbf{E}(\mathbf{r})|^2 dV, \tag{C.2}$$

   where $\mathbf{E}(\mathbf{r})$ is the complex amplitude of the electric field at position $\mathbf{r}$.

2. $F = 0$. In this case the net energy flow through the boundary is zero and hence the matter in the volume does not absorb.

Appendix D

Electromagnetic Momentum

We consider a time harmonic electromagnetic field in vacuum or in a dielectric without absorption. An electromagnetic field not only transports energy but also momentum. The instantaneous momentum, also called radiation pressure, points in the same direction as the flow of energy and is given by

$$\boldsymbol{\mathcal{P}}(\mathbf{r},t) = \frac{\boldsymbol{\mathcal{S}}(\mathbf{r},t)}{c}, \tag{D.1}$$

with c being the speed of light in the medium. The time averaged momentum per unit of area caried by the field is thus

$$< \boldsymbol{\mathcal{P}} >_{av} = \frac{\mathbf{S}(\mathbf{r})}{c}. \tag{D.2}$$

Appendix E

The Fourier Transform

E.1 Definitions

$$\mathcal{F}(h)(\xi,\eta) = \iint e^{-2\pi i(x\xi+y\eta)}h(x,y)dx\,dy. \tag{E.1}$$

$$\mathcal{F}^{-1}(H)(x,y) = \iint e^{2\pi i(x\xi+y\eta)}H(\xi,\eta)d\xi\,df_y. \tag{E.2}$$

E.2 General Equations

$$\mathcal{F}^{-1}\mathcal{F}(h)(x,y) = h(x,y), \tag{E.3}$$

$$\mathcal{F}(h)(\xi,\eta)^* = \mathcal{F}(h^*)(-\xi,-\eta), \tag{E.4}$$

(z^* is the complex conjugate of z).

$$\iint |h(x,y)|^2dx\,dy = \iint |\mathcal{F}(h)(\xi,\eta)|^2d\xi\,df_y, \text{ Parseval's formula,} \tag{E.5}$$

$$\mathcal{F}(g*h) = \mathcal{F}(g)\mathcal{F}(h), \tag{E.6}$$

$$\mathcal{F}(gh) = \mathcal{F}(g)*\mathcal{F}(h), \tag{E.7}$$

where

$$(g*h)(x,y) = \iint g(x-x',y-y')h(x',y')dx'\,dy'. \tag{E.8}$$

If $h(x)$ is a p-periodical function then

$$\mathcal{F}(h)(\xi) = \sum_{n=-\infty}^{+\infty} \hat{h}(n)\,\delta\left(\xi-\frac{n}{p}\right), \tag{E.9}$$

where

$$\hat{h}(n) = \frac{1}{p}\int_0^p h(x)e^{-2\pi nx}\,dx. \tag{E.10}$$

E.3 Some Fourier transforms

$$\mathcal{F}\left[1_{[-a,a]}(x)1_{[-b,b]}\right](\xi,\eta) = 4ab\,\mathrm{sinc}(2a\xi)\mathrm{sinc}(2bf_y), \tag{E.11}$$

where

$$\operatorname{sinc}(x) = \frac{\sin(\pi x)}{\pi x}. \tag{E.12}$$

$$\mathcal{F}\left[\delta(x/a)\delta(y/b)\right] = ab. \tag{E.13}$$

$$\mathcal{F}\left[1\right](\xi,\eta) = \delta(\xi)\delta(\eta). \tag{E.14}$$

$$\mathcal{F}\left[e^{-\pi(a^2x^2+b^2y^2)}\right](\xi,\eta) = \frac{1}{|ab|}e^{-\pi\left(\xi^2/a^2+\eta^2/b^2\right)}. \tag{E.15}$$

Let

$$1_{\bigcirc_a}(x,y) = \begin{cases} 1, & \text{als } \sqrt{x^2+y^2} \leq a, \\ 0, & \text{als } \sqrt{x^2+y^2} > a. \end{cases} \tag{E.16}$$

Then

$$\mathcal{F}(1_{\bigcirc_a})(\xi,\eta) = a\frac{J_1\left(2\pi a\sqrt{\xi^2+\eta^2}\right)}{\sqrt{\xi^2+\eta^2}}. \tag{E.17}$$

$$\mathcal{F}\left[e^{i\pi\left(a^2x^2+b^2y^2\right)}\right](\xi,\eta) = \frac{i}{|ab|}e^{-i\pi\left(\xi^2/a^2+\eta^2/b^2\right)} \tag{E.18}$$

Appendix F

Basis transformations

In this section, we discuss the relevance of basis transformations and how to apply them. So what are basis transformations essentially? It comes down to the following: if we have some physical object $\mathbf{\Psi}$, we can describe it with a vector (which can in principle be a continuous function). The form of the vector with which we represent $\mathbf{\Psi}$ depends on the basis that we choose. For example, we could represent a position vector $\mathbf{R}$ in Cartesian coordinates (x, y, z), or in spherical coordinates (ρ, ϕ, θ), or in cylindrical coordinates (r, ϕ, z). It is important to note that **the physical object** remains unchanged, it is only the **coefficients with which the object is represented** that change. The formulas that describe how the coefficients for one basis transform to the coefficients in the other basis constitute the **basis transformation**. In case these formulas can be described as a matrix operation, we have a **linear basis transformation**. This concept is extensively treated in Linear Algebra courses.

Basis transforms are ubiquitous, so it is important to be familiar with them also outside the context of optics. For example, if you have some signal $\mathbf{\Psi}$, you can either express it in the **time domain** or in the **frequency domain**. These are two different representations of the same physical object, and the basis transformation that relates the two is the **Fourier transform**. In the discrete case it would read

$$X_k = \sum_{n=0}^{N-1} x_n e^{-2\pi i k n/N}, \tag{F.1}$$

where x_n are the coefficients representing the signal in the time domain, and X_k are the coefficients representing the signal in the frequency domain. Note that this basis transformation can be described as a matrix operation

$$\begin{pmatrix} X_0 \\ X_1 \\ \vdots \end{pmatrix} = \begin{pmatrix} 1 & 1 & 1 & \dots \\ 1 & e^{-2\pi i/N} & e^{-4\pi i/N} & \dots \\ 1 & e^{-4\pi i/N} & e^{-8\pi i/N} & \dots \\ \vdots & \vdots & \vdots & \ddots \end{pmatrix} \begin{pmatrix} x_0 \\ x_1 \\ \vdots \end{pmatrix}, \tag{F.2}$$

so the Fourier transform is a linear basis transformation. The benefit of applying such a basis transformation is obvious: in different bases, there is different information that becomes apparent more obviously. In the time domain one can see how the signal progresses in time, but it is difficult to identify different frequency components, whereas in the frequency domain it is very easy to see how much each frequency contributes to the signal, but it is difficult to see how the signal changes in time. Also, sometimes it is more efficient to describe a signal in one basis than in the other. For example, if the signal is a sine wave in the time domain, it takes infinitely many nonzero coefficients (each coefficient being a point in time) to describe it in the time domain, while it takes only two nonzero coefficients to describe it in the frequency domain. We say that

a signal can be **sparse in a certain basis** (sparse meaning that it be represented with few non-zero coefficients). This sparsity can help in compressing data, or it can be used as a constraint in reconstruction algorithms (this field is known as **compressed sensing**).

A similar observation holds for the different representations of a quantum state. One can represent a quantum state $|\psi\rangle$ in the position basis (i.e. in terms of the eigenvectors of the position operator $\hat{x}$), or in the momentum basis (i.e. in terms of the eigenvectors of the position operator $\hat{p}$). Again, the physical object remains unchanged, but by representing it in different bases, different parts of information become more apparent. In the position basis it becomes easier to see where a particle may be located, while in the momentum basis it is easier to see what momentum it may have. The basis transformation that relates the position representation to the momentum representation is the Fourier transform. One can also represent a quantum state $|\psi\rangle$ in the energy basis (i.e. in terms of the eigenvectors of the energy operator $\hat{H}$, also called the Hamiltonian), in which case it is easier to see what energy a particle may have, and which makes it easier to calculate the time-evolution of the wave function (because the time evolution is determined by the Schrödinger equation, which is a differential equation involving $\hat{H}$).

So basis transformations can help in making certain properties of a vector $\mathbf{\Psi}$ become more apparent, or make its description simpler (i.e. more sparse). Another advantage that a basis transformation can have is that **applying operators can be easier in a certain basis**. In particular, applying a linear operator A to some vector $\mathbf{\Psi}$ is much easier if $\mathbf{\Psi}$ is expressed in the eigenbasis of A. Suppose we can write

$$\mathbf{\Psi} = \sum_k a_k \mathbf{v}_k, \tag{F.3}$$

where $\mathbf{v}_k$ are eigenvectors of A with eigenvalues λ_k, then applying A to $\mathbf{\Psi}$ will give

$$A\mathbf{\Psi} = \sum_k \lambda_k a_k \mathbf{v}_k. \tag{F.4}$$

In matrix notation, this is written as

$$\begin{aligned} A\mathbf{\Psi} &= \begin{pmatrix} \lambda_1 a_1 \\ \lambda_2 a_2 \\ \vdots \end{pmatrix} \\ &= \begin{pmatrix} \lambda_1 & 0 & \dots \\ 0 & \lambda_2 & \dots \\ \vdots & \vdots & \ddots \end{pmatrix} \begin{pmatrix} a_1 \\ a_2 \\ \vdots \end{pmatrix}. \end{aligned} \tag{F.5}$$

Thus, we see that **if $\mathbf{\Psi}$ is represented in terms of eigenvectors of the linear operator A (i.e. in the eigenbasis of A), then the matrix representation of A is a diagonal matrix, and on its diagonal are its eigenvalues**.

Expressing $\mathbf{\Psi}$ in terms of eigenvectors of A is thus very useful. But if $\mathbf{\Psi}$ is given in some arbitrary basis, how do we find the coefficients that represent it in the eigenbasis of A? To do this, let us consider a simple example. Suppose $\mathbf{\Psi}$ has the following representation in the $\hat{\mathbf{x}}, \hat{\mathbf{y}}$ basis

$$\mathbf{\Psi} = 4\hat{\mathbf{x}} + 7\hat{\mathbf{y}}. \tag{F.6}$$

Or in vector notation

$$\mathbf{\Psi}_{xy} = \begin{pmatrix} 4 \\ 7 \end{pmatrix}. \tag{F.7}$$

Keep in mind that this is not **the** vector corresponding to $\mathbf{\Psi}$. Rather, it is **a** representation of $\mathbf{\Psi}$ which holds in the $\hat{\mathbf{x}}, \hat{\mathbf{y}}$ basis (i.e. it should be understood that the first entry in the vector is the coefficient corresponding to $\hat{\mathbf{x}}$, and the second entry is the coefficient corresponding to $\hat{\mathbf{y}}$). Now, let us suppose that the linear operator A has eigenvectors

$$\begin{aligned} \mathbf{v}_1 &= 1\hat{\mathbf{x}} + 3\hat{\mathbf{y}}, \\ \mathbf{v}_2 &= 2\hat{\mathbf{x}} + 1\hat{\mathbf{y}}, \end{aligned} \tag{F.8}$$

or in vector notation (in the $\hat{\mathbf{x}}, \hat{\mathbf{y}}$ basis)

$$\mathbf{v}_1 = \begin{pmatrix} 1 \\ 3 \end{pmatrix}, \quad \mathbf{v}_2 = \begin{pmatrix} 2 \\ 1 \end{pmatrix}. \tag{F.9}$$

Suppose we want to write $\mathbf{\Psi}$ in the $\mathbf{v}_1, \mathbf{v}_2$ basis. We need to find $\Psi[v_1], \Psi[v_2]$ such that

$$\mathbf{\Psi} = \Psi[v_1]\mathbf{v}_1 + \Psi[v_2]\mathbf{v}_2, \tag{F.10}$$

Obviously

$$\mathbf{\Psi} = 2\mathbf{v}_1 + 1\mathbf{v}_2, \tag{F.11}$$

because in the $\hat{\mathbf{x}}, \hat{\mathbf{y}}$ basis this gives

$$\begin{pmatrix} 4 \\ 7 \end{pmatrix} = 2\begin{pmatrix} 1 \\ 3 \end{pmatrix} + \begin{pmatrix} 2 \\ 1 \end{pmatrix}. \tag{F.12}$$

Thus in the $\mathbf{v}_1, \mathbf{v}_2$ basis the vector representation of $\mathbf{\Psi}$ would read

$$\mathbf{\Psi}_A = \begin{pmatrix} 2 \\ 1 \end{pmatrix}. \tag{F.13}$$

Once again, we emphasize that although $\mathbf{\Psi}$ is represented with different numbers, the object itself has not changed.

Let us put our previous calculations in more general terms. We know representations of $\mathbf{\Psi}$, $\mathbf{v}_1, \mathbf{v}_2$ in the $\hat{\mathbf{x}}, \hat{\mathbf{y}}$ basis

$$\mathbf{\Psi} = \begin{pmatrix} \Psi[x] \\ \Psi[y] \end{pmatrix}, \quad \mathbf{v}_1 = \begin{pmatrix} v_1[x] \\ v_1[y] \end{pmatrix}, \mathbf{v}_2 = \begin{pmatrix} v_2[x] \\ v_2[y] \end{pmatrix}, \tag{F.14}$$

we want to find $\Psi[v_1], \Psi[v_2]$ such that

$$\begin{aligned} \begin{pmatrix} \Psi[x] \\ \Psi[y] \end{pmatrix} &= \Psi[v_1]\begin{pmatrix} v_1[x] \\ v_1[y] \end{pmatrix} + \Psi[v_2]\begin{pmatrix} v_2[x] \\ v_2[y] \end{pmatrix} \\ &= \begin{pmatrix} v_1[x] & v_2[x] \\ v_1[y] & v_2[y] \end{pmatrix}\begin{pmatrix} \Psi[v_1] \\ \Psi[v_2] \end{pmatrix}. \end{aligned} \tag{F.15}$$

Here, $\Psi[x], \Psi[y]$ represent $\mathbf{\Psi}$ in the $\hat{\mathbf{x}}, \hat{\mathbf{y}}$ basis, and $\Psi[v_1], \Psi[v_2]$ represent $\mathbf{\Psi}$ in the $\mathbf{v}_1, \mathbf{v}_2$ basis. Thus, defining the matrix

$$B = \begin{pmatrix} v_1[x] & v_2[x] \\ v_1[y] & v_2[y] \end{pmatrix}, \tag{F.16}$$

to go from the $\mathbf{v}_1, \mathbf{v}_2$ representation of $\mathbf{\Psi}$ to the $\hat{\mathbf{x}}, \hat{\mathbf{y}}$ representation of $\mathbf{\Psi}$, we must calculate

$$\begin{pmatrix} \Psi[x] \\ \Psi[y] \end{pmatrix} = B \begin{pmatrix} \Psi[v_1] \\ \Psi[v_2] \end{pmatrix}. \tag{F.17}$$

Conversely, to go from the $\hat{\mathbf{x}}, \hat{\mathbf{y}}$ representation to the $\mathbf{v}_1, \mathbf{v}_2$ representation, we must calculate

$$\begin{pmatrix} \Psi[v_1] \\ \Psi[v_2] \end{pmatrix} = B^{-1} \begin{pmatrix} \Psi[x] \\ \Psi[y] \end{pmatrix}. \tag{F.18}$$

So now we know how to go from one basis representation to another and back. We have seen previously that it can be convenient to change to the eigenbasis of a linear operator A, because in that representation A is diagonal. Thus we can **diagonalize** A as

$$A = B \begin{pmatrix} \lambda_1 & 0 \\ 0 & \lambda_2 \end{pmatrix} B^{-1}. \tag{F.19}$$

To summarize, with B^{-1} we go from some $\hat{\mathbf{x}}, \hat{\mathbf{y}}$ basis to the eigenbasis of A. The columns of B contain the eigenvectors of B in the $\hat{\mathbf{x}}, \hat{\mathbf{y}}$ basis. Then we apply the operator A, which in its eigenbasis is a diagonal matrix with its eigenvalues along the diagonal. Then, to go back from the eigenbasis to the $\hat{\mathbf{x}}, \hat{\mathbf{y}}$ basis, we apply B. This is in particular useful when one has to apply A many times, because in that case

$$A^N = B \begin{pmatrix} \lambda_1^N & 0 \\ 0 & \lambda_2^N \end{pmatrix} B^{-1}. \tag{F.20}$$

Or, it could be useful when we want to exponentiate A

$$\begin{aligned} e^A &= \sum_{k=0}^{\infty} \frac{A^k}{k!} \\ &= B \left(\sum_{k=0}^{\infty} \frac{\begin{pmatrix} \lambda_1 & 0 \\ 0 & \lambda_2 \end{pmatrix}^k}{k!} \right) B^{-1} \\ &= B \begin{pmatrix} e^{\lambda_1} & 0 \\ 0 & e^{\lambda_2} \end{pmatrix} B^{-1}. \end{aligned} \tag{F.21}$$

This is for example used in the solution of the Schrödinger equation

$$\begin{aligned} &\hat{H}\psi = i\hbar \frac{\mathrm{d}}{\mathrm{d}t}\psi \\ &\Rightarrow \\ &\psi(t) = e^{-i\hat{H}t/\hbar}\psi(0), \end{aligned} \tag{F.22}$$

which indicates why it's useful to describe $\psi(0)$ in the energy basis if we want to find its time evolution.

There are many applications of basis transformations and eigenvalue decompositions in Optics. Suppose we know the transmission axis of a linear polariser and let it be in the direction of the vector

$$\begin{pmatrix} a \\ b \end{pmatrix}$$

Then all light polarised in this direction will be transmitted completely, so this vector is an eigenvector of the polariser operator with eigenvalue 1. We know that all light polarised in the direction of the vector

$$\begin{pmatrix} b \\ -a \end{pmatrix}$$

(i.e. perpendicular to the transmission axis) will be completely blocked, so this is an eigenvector with eigenvalue 0. Thus, given the transmission axis of a linear polariser, we can immediately write down its Jones matrix

$$J = \begin{pmatrix} a & b \\ b & -a \end{pmatrix} \begin{pmatrix} 1 & 0 \\ 0 & 0 \end{pmatrix} \begin{pmatrix} a & b \\ b & -a \end{pmatrix}^{-1}. \tag{F.23}$$

Conversely, from the eigenvalue decomposition of a Jones matrix we can immediately see what its principal axes are, and how it acts on the components along those axes, i.e. whether it is a linear polariser, half-wave plate, quarter-wave plate, or something else.

Also, basis transformations can be used to describe **optical activity**. In optically active media, there are different refractive indices for left-circularly and right-circularly polarised light, so it is more convenient to represent the Jones vector in the basis of left-circularly and right-circularly polarised light, rather than in the basis of two linear orthogonal polarisations.

It is also interesting to note the equivalence between the Jones vector and the quantum states of photons that are used as qubits: the polarization of a photon is a two-state quantum-mechanical system. This qubit can be represented as

$$|\psi\rangle = \alpha\,|0\rangle + \beta\,|1\rangle\,, \tag{F.24}$$

where α and β are analogous to the entries of the Jones vector. Indeed, in experiments on quantum information with photons as qubits, wave plates are ubiquitous[1]. Also in quantum information, it is important to be familiar with basis transformations.

Another application of basis transformations and eigenvalue decompositions in optics is in the **Angular Spectrum Method**. This method is used to propagate a field U_0, and it is explained in the chapter on Diffraction Optics. The operation we want to apply in this case is the propagation operator $P_{\Delta z}$ which denotes the propagation over a distance z. To do this, we decompose the field U_0 in eigenfunctions of $P_{\Delta z}$, which are plane waves $e^{i\mathbf{k}\cdot\mathbf{r}}$ because

$$\begin{aligned} P_{\Delta z} e^{i(k_x x + k_y y + k_z z)} &= e^{i(k_x x + k_y y + k_z (z+\Delta z))} \\ &= e^{ik_z \Delta z} e^{i(k_x x + k_y y + k_z z)}. \end{aligned} \tag{F.25}$$

So indeed, $e^{i\mathbf{k}\cdot\mathbf{r}}$ is an eigenfunction of $P_{\Delta z}$, with eigenvalue $e^{ik_z\Delta z}$. The basis transformation we need to apply in order to decompose U_0 into eigenfunctions of $P_{\Delta z}$ is the Fourier transform. So similarly as in Eq. (F.19), to apply the propagation operator we Fourier transform U_0 to decompose it into eigenfunctions of $P_{\Delta z}$, we multiply each component with the eigenvalue $e^{ik_z\Delta z}$, and then we inverse Fourier transform to go back to the original basis

$$P_{\Delta z} U_0 = \mathcal{F}^{-1}\{\mathcal{F}\{U_0\} e^{ik_z \Delta z}\}. \tag{F.26}$$

In this framework, it can be easily understood how this method should be altered for propagation in non-homogeneous media. In that case the plane waves $e^{i\mathbf{k}\cdot\mathbf{r}}$ are no longer eigenfunctions of the propagation operator, and instead we must find the appropriate eigenfunctions and eigenvalues for propagation through such a medium.

For other explanations of basis transformations see Khan Academy - Alternate coordinate systems (bases), and Khan Academy - Showing that an eigenbasis is a useful coordinate systems.

[1] See e.g. Experimental Demonstration of Blind Quantum Computing, S. Barz et al. (2011).

Appendix G

Algebraic Distance in Geometrical Optics

There exists a method to deal with the sign convention in geometrical optics which uses so-called algebraic distances. It is a matter of taste but this method which is mostly taught in France may be an interesting alternative to the convention used in Chapter 2.

G.1 Definition

Let there be two points A and B in an affine space through which passes a directed line (a line with a direction, i.e. generated by a nonzero vector $\vec{v}$). We introduce the algebraic distance $\overline{AB}$ from A to B to be the real number such that :

1. its absolute value is the distance between A and B
2. if the value is non-zero:
   - $\overline{AB}$ is positive in the case the vector $\overrightarrow{\mathrm{AB}}$ has the same direction as $\vec{v}$, i.e. $\overrightarrow{\mathrm{AB}} = k\vec{v}$ with $k > 0$;
   - $\overline{AB}$ is negative otherwise.

It follows that

$$\overline{AB} = \frac{\overrightarrow{\mathrm{AB}} \cdot \vec{v}}{\|\vec{v}\|} \tag{G.1}$$

Note that to define the algebraic distance, no choice for the origin is needed, only a vector that defines the direction of the line.

G.2 Properties

The algebraic distance has the following properties:

- $\overline{AA} = 0$,
- $\overline{AB} = -\overline{BA}$,
- for three points A, B and C all on the same line:

$$\overline{AC} = \overline{AB} + \overline{BC} \tag{G.2}$$

  irrespective of the position of B relative to A and C on the line.

The last point can can be shown using the analogous equality for vectors:

$$\overrightarrow{\mathrm{AC}} = \overrightarrow{\mathrm{AB}} + \overrightarrow{\mathrm{BC}} \tag{G.3}$$

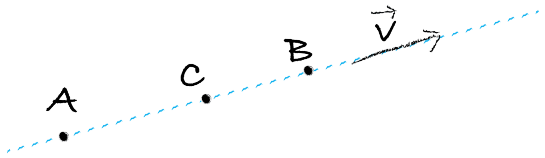


Figure G.1: Definition the different points in an optical system.

G.3 Algebraic distance in Optics

When we use the algebraic distance in optics, we use the following conventions:

1. Light propagates from left to right;
2. The optical axis is positively oriented towards the right (i.e. in the direction the light propagates);
3. the vertical axis, perpendicular to the optical axis is positively oriented upwards.

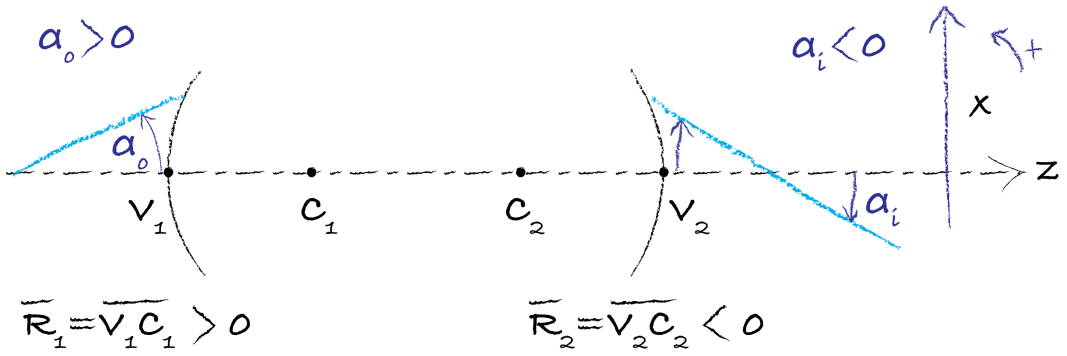


Figure G.2: Definition the different points in an optical system.

In Fig. G.2, the definition of positive ray angle and positive radii of curvature are defined:

$$\overline{R_1} \equiv \overline{V_1C_1} > 0, \text{ and } \overline{R_2} = \overline{V_2C_2} < 0. \tag{G.4}$$

G.4 One Spherical Surface

Let us consider a spherical interface between two media with different index of refraction n_1 and n_2 as shown in Fig. G.3. Let C be the centre of the sphere and let V be the vertex, i.e. the point of intersection of the sphere and the optical axis. One can show that for the image point A_2 of point A_1:

$$\frac{n_2}{\overline{VA_2}} - \frac{n_1}{\overline{VA_1}} = \frac{n_2 - n_1}{\overline{VC}} = V, \tag{G.5}$$

and that the transverse magnification can be written as:

$$M = \frac{\overline{VA_2}}{n_2} \cdot \frac{n_1}{\overline{VA_1}}. \tag{G.6}$$

If the object is at infinity $A_2 = F_2$ is the image focal point and

$$\frac{n_2}{\overline{VF_2}} = \frac{n_2 - n_1}{\overline{VC}} = P, \tag{G.7}$$

where P is the power of the surface. If the image is at the infinity, $A_1 = F_1$ is the object focal point and

$$\frac{n_1}{\overline{VF_1}} = -\frac{n_2 - n_1}{\overline{VC}} = -P \tag{G.8}$$

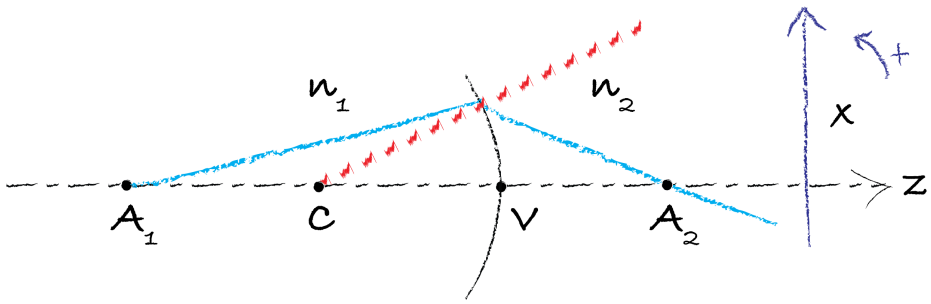


Figure G.3: Spherical surface separating two different media.

When the interface is flat: $\overline{VC} \to \infty$, we get

$$\frac{n_2}{\overline{VA_2}} = \frac{n_1}{\overline{VA_1}} \tag{G.9}$$

We can easily rewrite the Eq. G.5 as function of the centre instead of the summit by exchanging V with C and n_1 with n_2:

$$\frac{n_1}{\overline{CA_2}} - \frac{n_2}{\overline{CA_1}} = \frac{n_1 - n_2}{\overline{CV}} \tag{G.10}$$

and for the transverse magnification:

$$M = \frac{\overline{CA_2}}{\overline{CA_1}} \tag{G.11}$$

The last relation is usually called the relation of Descartes and put in relation F_1 and F_2 with the vertex:

$$\frac{\overline{VF_2}}{\overline{VA_2}} + \frac{\overline{VF_1}}{\overline{VA_1}} = 1 \tag{G.12}$$

The relation of Newton is an other way to link the position of the object and the one of the image via the focal points:

$$\overline{F_2A_2} \cdot \overline{F_1A_1} = \overline{VF_2} \cdot \overline{VF_1} \tag{G.13}$$

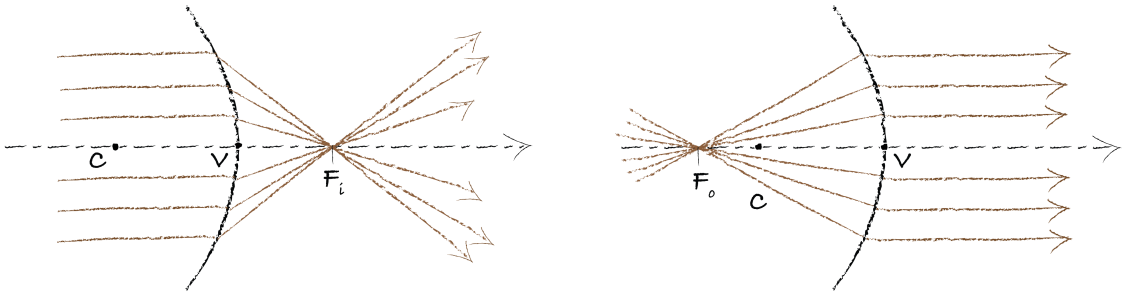


Figure G.4: Dioptre sphérique: position of the image focal point and the object focal point

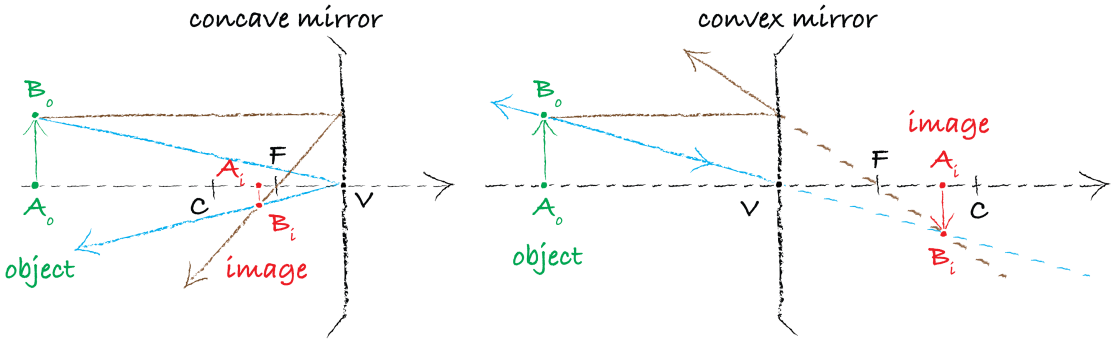


Figure G.5: Definition of O, F_o and F_i for a concave (left) and a convex (right) mirror.

G.5 Mirror

For the mirror, we define V as the vertex (the meeting point between the mirror and the optical axis), C the centre of the curvature and F the focal point as show in Fig. G.5. For a concave mirror $\overline{VC} = 2\overline{VF} < 0$ and for the convex mirror, $\overline{VC} = 2\overline{VF} > 0$.

If a point A is placed on the right of the mirror, i.e. $\overline{VA} > 0$, the point is consider virtual. Be aware that if you look at the mirror yourself, you will be able to "image" this virtual point. To convince yourself, just use a spoon.

We can derive the law of conjugation that works for any spherical mirror independent on its curvature:

$$\frac{1}{\overline{VA_i}} + \frac{1}{\overline{VA_o}} = \frac{2}{\overline{VC}} \tag{G.14}$$

The magnification can also be derived:

$$M \equiv \frac{\overline{A_iB_i}}{\overline{A_oB_o}} \tag{G.15}$$

$$= \frac{\overline{FV}}{\overline{FA_o}} = \frac{\overline{FA_i}}{\overline{FV}} = -\frac{\overline{VA_i}}{\overline{VA_o}} \tag{G.16}$$

As we have done earlier, we can rewrite these equations with centre instead of the summit:

$$\frac{1}{\overline{CA_i}} + \frac{1}{\overline{CA_o}} = \frac{2}{\overline{CV}} \tag{G.17}$$

The magnification can also be derived with C as origin:

$$M \equiv \frac{\overline{A_i B_i}}{\overline{A_o B_o}} \tag{G.18}$$

$$= \frac{\overline{CA_i}}{\overline{CA_o}} \tag{G.19}$$

G.6 Spherical lens

Spherical lenses are made of glass and are bounded by two spherical surfaces of curvature $\overline{R_1} = \overline{C_1V_1}$ and $\overline{R_2} = \overline{C_2V_2}$, with centres C_1 and C_2 and vertices V_1 and V_2 respectively. When $\overline{R_1} > 0$ and $\overline{R_2} < 0$, the lens is biconvex; when $\overline{R_2} > 0$ and $\overline{R_1} < 0$ it is biconcave. They are thin when the distance (V_1V_2) is very small compared to the radii of curvature R_1 and R_2.

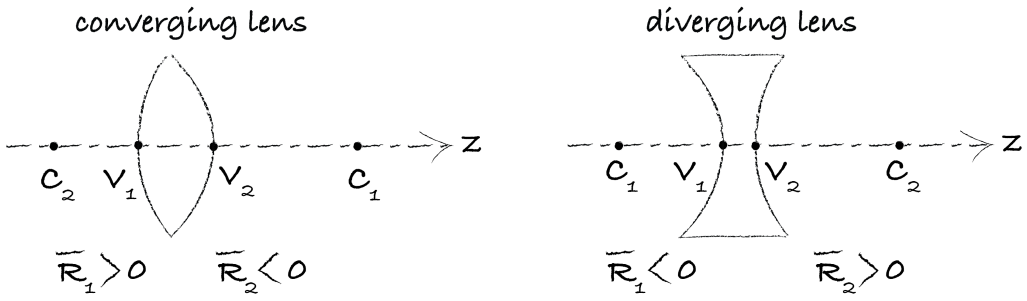


Figure G.6: Converging and diverging lens depending on the curvatures.

G.7 Thin spherical lens

When considering a thin spherical lens, we define 3 points O, F_o and F_i, respectively the center of the lens, the focal object point and focal image point. As shown in Fig. G.7, we can say:

- F_o is the point of origin of all the rays that hand up parallel to the optical axis when exiting the lens;

- F_i is the point of convergence of all the rays parallel to the optical axis coming towards the lens .

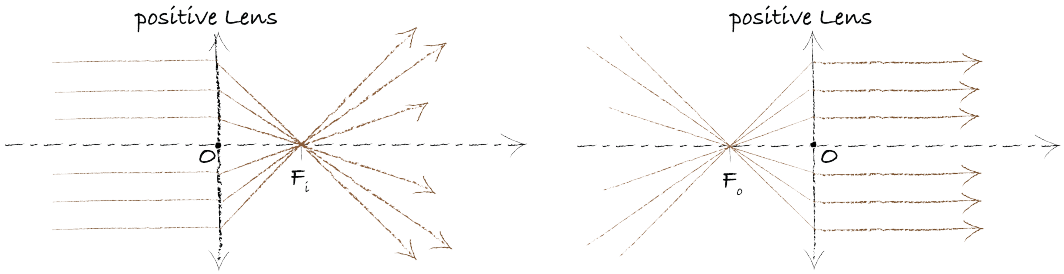


Figure G.7: Definition of O, F_o and F_i for a positive lens.

The **image focal length** f_i of a lens is defined as the algebraic quantity :

$$f_i \equiv \overline{OF_i} = -\overline{OF_o} = f_o \tag{G.20}$$

while we also introduce the **object focal length** f_o.

- In the case of a positive lens, the image focal distance f_i is positive, i.e. $\overline{OF_i} > 0$ and $\overline{OF_o} < 0$.
- In the case of a negative lens, the image focal distance f_i is negative, i.e. $\overline{OF_i} > 0$

The algebraic quantity called the **diopter** $\mathcal{D}$ of a thin lens is:

$$\mathcal{D} \equiv \frac{1}{\overline{OF_i}} = (1-n)\left(\frac{1}{\overline{V_2C_2}} - \frac{1}{\overline{V_1C_1}}\right) \tag{G.21}$$

where n is the index of refraction of the glass.
For any lens system defined with F_i as the image focal point, we now only have one equation which is always valid:

$$\frac{1}{\overline{OF_i}} = \frac{1}{\overline{OA_i}} - \frac{1}{\overline{OA_o}} \tag{G.22}$$

where the point A_i is image of the point A_o through the lens. Notice that we do not need to know where A_o is with regards to the lens to write the formula nor if we deal with a positive lens. If in your calculation you find for example that $\overline{OA_i} < 0$ then you know that the image is virtual.

We can also define the magnification as:

$$M \equiv \frac{\overline{A_iB_i}}{\overline{A_oB_o}} = \frac{\overline{OA_i}}{\overline{OA_o}} \tag{G.23}$$

where the point B_i is the image of the object point B_o. The sign of M will automatically give you if the image is inverted or not.

Fig. G.8 shows the case where the image is inverted compare to the object where $\overline{OA_i}$ is positive and $\overline{OA_o}$ is negative.

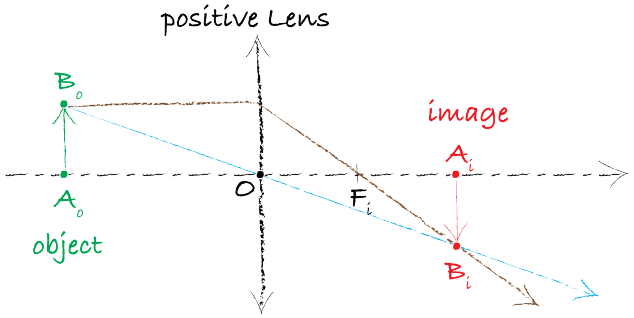


Figure G.8: Image of an object from a positive lens.

Index

Aberrations, 66
    distortion, 66
    spherical, 66
AFOV, *see* Angular field of view
Airy Spot, 68
Angular field of view, 78
Aperture stop, 65

Boundary conditions, 26
Brewster angle, 33

Coherence
    Length, 112
    partial, 110
    Time, 111
Complex notation, 15
Cones, 82
Critical angle, 29

Depth of focus, 79
Diffraction, 67
diopter, 220

Einstein Coefficients, 179
Energy
    flow, 22
    in a electromagnetic field, 22
    Poynting's vector, 22
    time averaged, 25
Entrance pupil, 65
Exit Pupil, 65
Eyepiece, 86

f-number, 65
Far point, 82
Fresnel-Arago laws, 130, 131
Fringes, 110
    visibility, 124
Full-wave plates, 98, 102

Half-wave plates, 98, 101
Hyperopia, 83

Jones Matrices, 98

Laser
    coherence, 175
    CW, 175
    dye laser, 187
    population inversion, 181
    pulsed, 175
    resonator, 176
    spontaneous emission, 179
    stimulated emission, 179
    transverse mode, 184
Lens
    aberrations, 66
    Magnifying power, 86
    thick, 63
lensmaker's formula, 57

Maxwell Equations
    in vacuum, 9
Myopia, 82

Near point, 82
numerical aperture, 88

Ocular, *see* Ocular
OPL, *see* optical path length
optical path length, 41

Polarisation
    circular, 95
    elliptical, 95
    linear, 94
Polariser
    linear, 99
Poynting's vector, *see* Energy

Quarter-wave plates, 98, 100

Reflection
    total internal, 29, 35
Refractive index, 12
Rods, 82
Rotation matrix, 98

Snell's Law, 43
Speed of light, 12

Telescope, 88

Wave
evanescent, 35
intensity, 25
plane wave, 13, 20
spherical, 16
Wave equation
scalar, 12
vector, 12
Wave number, 12
Wavelength, 12

BSc Optics - 2nd edition

Sander Konijnenberg, Aurèle J.L. Adam & H. Paul Urbach

Synopsis: This book treats optics at the level of students in the later stage of their achelor or the beginning of their master. It is assumed that the student is familiar with Maxwell's equations. Although the book takes account of the fact that optics is part of electromagnetism, special emphasis is put on the usefulness of approximate models of optics, their hierarchy and limits of validity.



Sander Konijnenberg
TU Delft | Optics Research Group at Applied Physics

Sander Konijnenberg studied Applied Physics at Delft University of Technology. At the same university, he obtained his PhD (cum laude) in the Optics Group on the topic of ptychography and phase retrieval. He currently works at ASML research in Veldhoven (NL).



Aurèle J.L. Adam
TU Delft | Optics Research Group at Applied Physics

Aurèle J.L. Adam is an Assistant Professor at Delft University of Technology. He is an Engineer from CentraleSupelec (promo 2000) and got his PhD from the University of Paris VI. His expertise lies in the Terahertz field and he enjoys scattering problems and free form optics.



H. Paul Urbach
TU Delft | Optics Research Group at Applied Physics

H. Paul Urbach is Professor of Optics at Delft University of Technology and scientific director of the Dutch Optics Centre, joint initiative of Delft University and the Dutch Organisation for Applied Scientific Research (TNO). Previously he has been with Philips Research Laboratories in Eindhoven. His research interests are optical imaging and diffraction theory.

© 2024 TU Delft Open
ISBN 978-94-6366-846-0
DOI: https://doi.org/10.59490/tb.91

textbooks.open.tudelft.nl

Cover image: Inside of a femto-laser taken by Roland Horsten, Delft University of Technology is licensed under CC-BY